Chair of Thermal Processing Technology

Doctoral Thesis

Investigation of the phenomena occurring in an inductively heated packed bed reactor for the pyrometallurgical recovery of valuable metals from lithium-ion batteries

Dipl.-Ing. Alexandra Holzer, BSc

February 2023

MONTANUNIVERSITÄT LEOBEN
www.unileoben.ac.at

AFFIDAVIT

I declare on oath that I wrote this thesis independently, did not use other than the specified sources and aids, and did not otherwise use any unauthorized aids.

I declare that I have read, understood, and complied with the guidelines of the senate of the Montanuniversität Leoben for "Good Scientific Practice".

Furthermore, I declare that the electronic and printed version of the submitted thesis are identical, both, formally and with regard to content.

Date 06.02.2023

Signature Author
Alexandra Holzer

Abstract

Global warming is one of the most significant challenges of our generation. An essential element in mitigating this is the drastic reduction of anthropogenic greenhouse gas emissions. In this respect, the political authorities' efforts are directed towards expanding the use of renewable energy. For example, essential targets and objectives have been set in the Paris Climate Agreement or the European Green Deal [1]. This transformation requires massive regulatory and, above all, technological change in all sectors. Lithium-ion batteries (LIB) play a crucial role in achieving these goals, as they are largely used in electromobility and energy supply. Due to the resulting growing demand for the raw materials required, such as lithium, phosphorus, nickel, and cobalt, sustainable materials management through a comprehensive circular economy is essential.

Within the scope of the presented doctoral thesis, a novel pyrometallurgical recycling approach, the so-called InduRed reactor concept, was further developed and optimized by researching the underlying processes and phenomena. Initially, the pre-pilot plant InduMelt, operated in batch mode, was improved, and currently commercially used cathode materials were investigated in this reducing process. In the experiments carried out, a promising recovery rate of the valuable metals into a metal alloy was demonstrated, as well as the transfer of lithium and phosphorus into the gas phase. The latter makes it easier to utilize these elements, which are declared as critical raw materials and represent an absolutely unique selling point in pyrometallurgy. Furthermore, it could be shown that the revised reactor design allows a better reproducible test performance. However, neither the originally used crucible material made of Al_2O_3 nor the new one made of MgO is suitable for continuous operation. In order to drive this technology towards industrial maturity, further research efforts must be made to find an optimum refractory material.

However, the waste stream resulting from LIB is composed not only of the cathode material but also of the anode material and other components of the battery assembly incompletely separated in the pretreatment. For this reason, the next step was to investigate the influence of copper and aluminum from the electrode conductor foils and graphite from the anode on the high-temperature behavior under reducing conditions. In the process, a contour model was created, enabling a more straightforward and less experimental application in the InduRed reactor concept in the future. This provides a basis for communication with the pretreatment process operators and is also essential for efficiently developing an overall recycling process.

Based on this, a possible process combination of hydromechanical pretreatment, flotation, and pyrometallurgical treatment in the InduMelt plant of a LIB waste stream was investigated. Even if the productivity has to be increased further with optimization measures, a remarkable lithium removal rate of more than 98% and a high product quality of the metal alloy could also be demonstrated in this application. This research activity thus confirms that the InduRed reactor concept is a promising technology for valuable metal recovery from spent lithium-ion batteries. Profound R&D activities in basic research, plant construction, or pre- and post-treatment of the products still have to be carried out to enable a rapid and efficient upscaling of the reactor concept to an industrial application, the execution of which concludes this thesis.

Kurzfassung

Die globale Erwärmung ist eine der zentralsten Herausforderungen unserer Generation. Wesentliches Element zur Eindämmung dieser ist die drastische Reduktion von anthropogen verursachten Treibhausgasemissionen. Dahingehend sind die Bestrebungen der politischen Instanzen ganz klar in Richtung dem Ausbau der Nutzung an erneuerbarer Energie zu verzeichnen. Wichtige Vorgaben und Zielsetzungen wurden beispielweise im Pariser Klimaabkommen oder dem Europäischen Green Deal festgelegt. Für diese Transformation ist in allen Sektoren ein massiver regulatorischer, aber vor allem auch technologischer Wandel notwendig. Lithium-Ionen Batterien (LIB) spielen eine entscheidende Rolle bei der Erreichung dieser Ziele, da sie weitgehend in der Elektromobilität aber auch in der Energieversorgung Anwendung finden. Durch den dadurch entstehenden wachsenden Bedarf an den darin enthaltenen Rohstoffen, wie Lithium, Phosphor, Nickel und Kobalt, ist ein nachhaltiges Materialmanagement durch eine vollständige Kreislaufwirtschaft unverzichtbar.

Im Rahmen der vorliegenden Doktorarbeit wurde ein neuartiges pyrometallurgisches Recyclingverfahren, das sogenannte InduRed Reaktorkonzept, durch die Erforschung der zugrunde liegenden Prozesse und Phänomene weiterentwickelt. Dabei wurde die im Batch-Betrieb geführte Vorpilotanlage InduMelt optimiert und aktuell kommerziell verwendete Kathodenmaterialien in diesem reduzierenden Prozess untersucht. Im Zuge der durchgeführten Versuche konnte eine vielversprechende Rückgewinnungsrate der Wertmetalle in eine Metalllegierung, wie auch die Überführung von Lithium und Phosphor in die Gasphase nachgewiesen werden. Zweiteres ermöglicht nicht nur die einfachere Nutzbarmachung dieser als kritische Rohstoffe deklarierten Elemente, sondern stellt auch ein absolutes Alleinstellungsmerkmal in der Pyrometallurgie dar. Darüber hinaus konnte gezeigt werden, dass das überarbeitete Reaktordesign eine bessere Reproduzierbarkeit der Versuchsdurchführung ermöglicht. Allerdings ist weder das ursprünglich verwendete Tiegelmaterial aus Al_2O_3, noch das neue aus MgO für einen kontinuierlichen Einsatz geeignet. Um diese Technologie zur Industriereife zu führen, müssen weitere Forschungsanstrengungen zur Findung eines optimalen Feuerfestmaterials unternommen werden.

Ein tatsächlicher Abfallstrom aus LIB setzt sich jedoch nicht nur aus dem Kathodenmaterial zusammen. Auch Anodenmaterial und in der Vorbehandlung unvollständig abgetrennte weitere Bestandteile des Batterieaufbaues sind darin vorzufinden. Aus diesem Grund wurde auch der Einfluss von Kupfer und Aluminium aus den Elektrodenableiterfolien, wie auch

Graphit aus der Anode auf das Hochtemperaturverhalten unter reduzierenden Bedingungen untersucht. Dabei wurde ein Höhenschichtmodell erstellt, welches eine zukünftig einfachere und versuchsärmere Einsatzfähigkeit im InduRed Reaktorkonzept ermöglicht. Dies stellt nicht nur eine Kommunikationsbasis mit den Betreibern der Vorbehandlungsverfahren dar, sondern ist auch ein wichtiges Werkzeug für eine effiziente Entwicklung eines Gesamtrecyclingverfahrens.

Darauf aufbauend wurde folglich eine mögliche Prozesskombination von hydromechanischer Vorbehandlung, Flotation und der pyrometallurgischen Behandlung in der InduMelt Anlage eines LIB Abfallstroms untersucht. Auch wenn die Produktivität durch weitere Optimierungsmaßnahmen gesteigert werden muss, so konnte auch in diesem Anwendungsfall eine hohe Entfernungsrate an Lithium von über 98% und eine hohe Produktqualität der Metalllegierung nachgewiesen werden. Diese Forschungsaktivität bestätigt somit, dass das InduRed Reaktorkonzept eine vielversprechende Technologie für die Wertmetallrückgewinnung aus verbrauchten Lithium-Ionen Batterien darstellt. Zur Ermöglichung einer raschen und effizienten Hochskalierung des Reaktorkonzeptes auf eine industrielle Anwendung müssen noch tiefgehende Forschungs- und Entwicklungstätigkeiten im Bereich der Grundlagenforschung, des Anlagenbaus und der Vor- und Nachbehandlung der Produkte durchgeführt werden, deren Ausführung diese Doktorarbeit beschließen.

Danksagung

Ein Abschluss bietet stets auch eine gute Gelegenheit sich bei allen Unterstützern und Wegbegleitern in einem würdigen Rahmen bedanken zu können.

An erster Stelle möchte ich meinen Doktorvater, Univ.-Prof. Dipl.-Ing. Dr.techn. Harald Raupenstrauch, nennen. Lieber Harald, vielen Dank dass du mich bereits seit meiner Bachelorarbeit unter deine Fittiche genommen und mich stets bei meiner fachlichen Weiterentwicklung und Umsetzung meiner Ideen unterstützt hast. Besonders erwähnen möchte ich dabei aber vor allem deine herzliche Art. Diese hat wesentlich dazu beigetragen, dass der Lehrstuhl nicht nur ein Arbeitsplatz, sondern mit allen Kollegen eine große TPT Familie war. Danke dem gesamten TPT Team für die großartige Zeit, vor allem Klaus, Christoph, Gregor, Wolfgang, Karin, Steffi, Slady und den „jungen Wilden“ Lukas, Christoph, Anna und Thomas (x2). Ein besonderer Weggefährte daraus ist Stefan Windisch-Kern, fixer Bestandteil der Winzer-Holdisch Crew. Herzlichen Dank für die zahllosen gemeinsamen Stunden in denen wir uns den Kopf über unerklärliches Hochtemperaturverhalten vom LIB Material zerbrochen haben, die gemeinsame Bewältigung purer Verzweiflung, aber vor allem auch für die unfassbar lustigen Momente bei Dienstreisen oder den legendären Biersprechungen – einfach ein Buddy für gute und schlechte Zeiten.

Eine großartige emotionale Stütze waren mir während der gesamten Studienzeit all meine Freunde und die gesamte Familie. Seien es die „Fahrt ins Blaue“-Partie, die „Mädels“, die „Musi“ oder die „Zaumgwürfelten Verwandten“ – ohne euch alle wären viele Stunden viel schwieriger gewesen.

Das Wort Emotionen ist auch zentral für die nächste Person, der unendlicher Dank gebührt – meinem Partner, besten Freund, Therapeuten und Lebensmenschen Patric. Du warst und bist stets die erste Anlaufstelle für all meine Gefühlslagen und schaffst es auf artistische Weise mir immer wieder ein Lächeln ins Gesicht zu zaubern. Vielen Dank mein Schützi für die wunderbare gemeinsame Zeit, deine Geduld und vor allem den gemeinsamen Spaß!

Zu guter Letzt gilt ein riesengroßer Dank meinen Eltern. Papa, Mama und Mandi, ich kann meine Dankbarkeit für eure bedingungslose Liebe und Unterstützung während meines ganzen Lebens nicht in Worte fassen. Vielen Dank für euren Rückhalt bei der Verwirklichung all meiner Träume, dass ihr immer bei allen möglichen Plänen hinter mir gestanden seid, mich aber auch in schwierigen Zeiten aufgefangen habt. Zusammengefasst: Danke, dass ihr mich zu dieser Frau geformt habt, die ich heute bin!

Content

Glossary

Al	Aluminum
Al_2O_3	Aluminum oxid
AM	Active material
Ar	Argon
BEV	Battery electric vehicle
BM	Black matter
C	Carbon
CH_4	Methane
Co	Cobalt
CO	Carbon monoxide
CO_2	Carbon dioxide
$CO_{2,eq}$	Carbon dioxide equivalent
COP	Conference of the Parties
CRM	Critical raw materials
CSA	Cross sectional area
Cu	Copper
ENVI	European Parliament's Committee on Environment, Public Health and Food Safety
EoL	End-of-Life
EU	European Union
EV	Electric vehicles
Fe	Iron
GHG	Greenhouse gases
Gt	Gigatons
HTPT	High-temperature processing technology

LCO	Lithium cobalt oxide
LFP	Lithium iron phosphate
Li	Lithium
LIB	Lithium-ion battery
$LiMeO_2$	Lithium metal oxide
Me or M	Metal
MgO	Magnesium oxid
Mn	Manganese
MUL	Montanuniversitaet Leoben
N_2O	Nitrous oxide
NCA	Lithium nickel cobalt aluminum oxide
Ni	Nickel
P	Phosphorus
PHEV	Plug-in hybrid electric vehicle
SD	Sustainable Development Scenario
SDG	Sustainable Deveoplment Goals
STEP	Stated Policies Scenario
TPT	Chair of Thermal Processing Technology
TRL	Technology readiness level

List of Figures and Tables

1 Introduction

Global warming and its impact on the entire ecosystem has become increasingly evident in recent decades. An average global temperature increase of 1.07°C compared to 1850-1900 was watched over the 2010-2019 observation period. This, in turn, can be directly linked to an increased emission of well-mixed greenhouse gases (GHG), with particular emphasis on CO_2, CH_4, and N_2O [2]. Based on this observed development, the effects are becoming more and more noticeable in form of weather and climate extremes in regions all over the world [3]. To curb global warming, the Paris Climate Agreement, the legally binding international treaty for climate change, was signed during COP21 in December 2015. It was determined that the average global temperature increase should be kept below 2°C compared to pre-industrial levels, and the corresponding efforts should focus on limiting an increase to 1.5°C [4–6].

Apart from reducing energy demand through improving energy efficiency, the transition to renewable energy supply technologies is of immense importance to meet these ambitious goals and achieve a net zero emission society [7–9]. From a technical view, the highest potential contribution to net emission reduction (Gt $CO_{2,eq}$ yr^{-1}) by 2030 is supposed to be solar and wind energy [3]. However, these renewable technologies are highly volatile compared to commercially used fossil fuels, which is why storage technologies are an indispensable part of an overall concept [10], therefore. In electricity, a significant expansion of battery capacity is crucial [7, 9].

With a projected growth of 14 times by 2030 with an annual increase of 25% in battery capacity, the vast bulk of the market growth is expected to be driven by lithium-ion battery (LIB) technology [11, 12]. In the sense of a circular economy and in consideration of the "zero-waste" approach, the life cycle of such a LIB, i.e., from the extraction of raw materials to complete recycling, must be taken into account. In battery recycling, legal frameworks have been

implemented over the past years to avoid illegal trafficking, landfilling or unfavorable incineration of batteries. Therefore, the legislation Directive 2006/66/EC [13] of the European Parliament and its revised version No. 2019/1020 regulates how to deal with end-of-life (EoL) batteries. This directive stipulates general specifications for battery producers, such as collection and treatment behavior and specific recovery rates for LIB. A current proposal [14] of the EU Commission to amend and extend the directive mentioned above goes even further. In a nutshell, batteries' full lifecycle rules are covered. Stronger sustainability, performance, labeling requirements, and due diligence policy to address social and environmental risks are claimed. Furthermore, the targets for waste collection, recycling efficiency, and material recovery have been strengthened. At a closer look at LIB requirements, specific recovery rates for the containing valuable metals of 95% for cobalt (Co), copper (Cu), and nickel (Ni) as well as 70% for lithium (Li) would be mandatory by 2030. After the assessment and adoption of the report by the European Parliament's Committee on Environment, Public Health and Food Safety (ENVI) [15], the requirements were tightened even further. For Li, recovery rates of 70% should be achieved by early 2026 (instead of the original 35%) and 90% by early 2030.

These material-specific recycling rates place a particular demand on the entire recycling industry since the various state-of-the-art technologies are subject to a multitude of different advantages and disadvantages from a technical and/or economic point of view [16]. This makes it all the more important to develop highly efficient, holistic recycling concepts that meet the requirements. The recycling chain can basically be divided into physical and chemical processes. Mechanical pretreatment, i.e., stripping and discharging, can be assigned to the former. The chemical step consists of a pyrometallurgical or hydrometallurgical process or a combination of both. In this process, the fine material extracted from the pretreatment step, commonly known as black matter, is treated metallurgically, and the metals, some of which are declared as critical raw materials (CRM), are recovered.

In this doctoral thesis, four peer-reviewed articles show the research on the underlying processes and phenomena for developing and optimizing a novel pyrometallurgical approach to recover valuable metals from LIB. Chapter 2 explains the motivation, basic principles, and the current state of the art in more detail. Chapter 3 deals with the research objectives and methodology. The results of the underlying publications are consequently presented in chapter 4 and discussed based on the research objectives. Finally, a conclusion is given in chapter 5, and an outlook on further questions with a critical review of the thesis and possible solution approaches are given in chapter 6.

Appendix A contains all four peer-reviewed articles in full length, and Appendix B concludes the thesis with a list of further publications with the author's participation.

2 Outline and Fundamentals

For a better understanding of the peer-reviewed articles integrated with the appendix, basic knowledge about the topic of lithium-ion batteries is presented in this chapter. Initially, this work's current market situation and motivation are discussed. Subsequently, an overview of the structure and functioning of LIB is provided. The current state of the art in the field of LIB recycling is then discussed, and the chapter concludes with a detailed explanation of the reactor concept on which this thesis is based.

2.1 Research Relevance

In order to achieve the goal mentioned earlier of curbing global warming and the necessary associated reduction in greenhouse gas (GHG) emissions, the origin of these gases must first be determined. The global GHGs are broken down into their sectorial origin in **Figure 1**. Comparing this data from 2016 with the figures from 2019 [17], it can be seen that the breakdown between sectors has changed only slightly. The illustration in **Figure 1** not only shows the high percentage of the energy sector in the total greenhouse gas emissions but also allows the interpretation that achieving the climate change mitigation target requires not one but a variety of different measures in all sectors. While focusing on the energy sector alone is not enough, the energy transition toward increased conversion of renewable energy to meet the higher energy demand in industry and buildings, as well as the transformation of the transportation sector, makes a significant contribution.

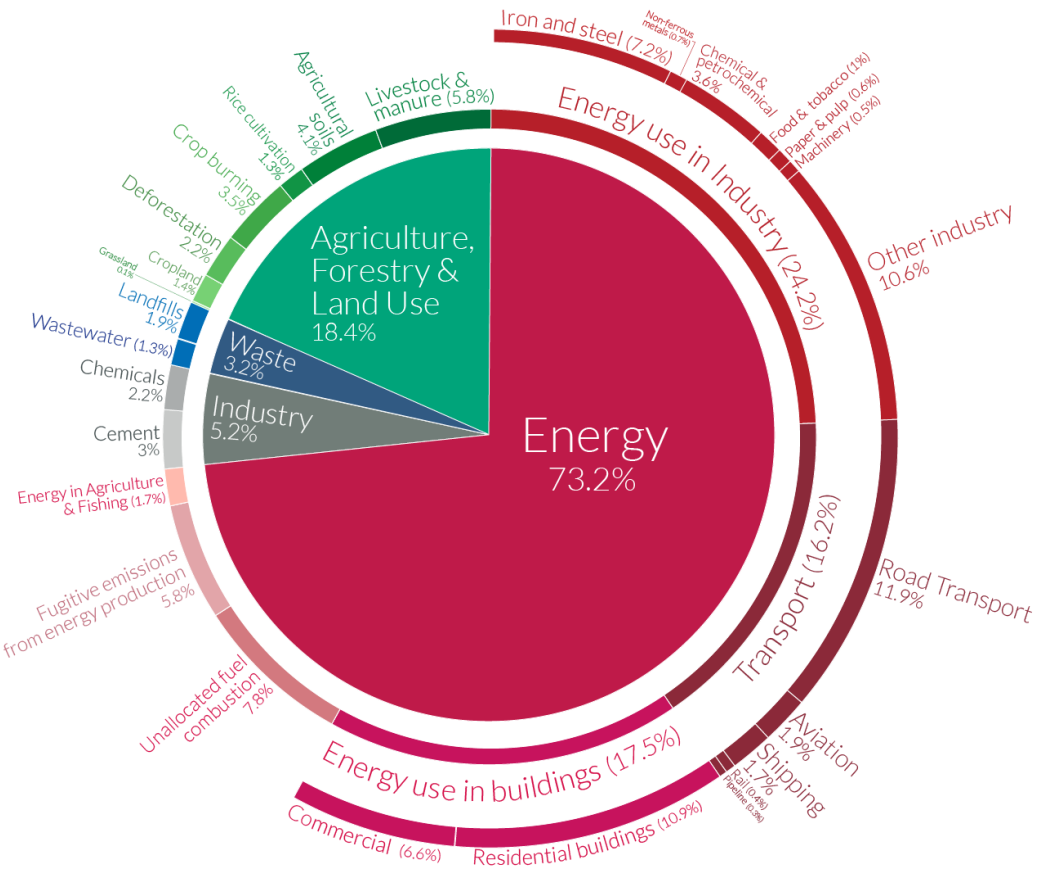

Figure 1. Sectoral breakdown of global greenhouse gas emissions in 2016 [17, 18].

Since the traded key technologies, wind and solar [3], are subject to strong fluctuations in residual loads due to their volatile generation, compensation via storage systems is inevitable [10]. The importance of using battery storage in transportation and power supply is emphasized by its projected increasing demand and broad application potential [19–22]. Battery-based energy storage at the grid level has a high potential for residual load management [23, 24]. In Europe, the transport sector accounts for a quarter of GHG emissions, which is why the EU's Green Deal envisages a 90% reduction in these emissions by 2050. Zero-emission mobility is the primary goal, which is to be achieved through the massive deployment of electric vehicles in addition to low-carbon technologies such as hydrogen or advanced biofuels [23, 25].

In addition to decarbonizing these sectors, batteries also enable decentralized and off-grid energy supply solutions, which can significantly improve the quality of life for globally 850 million people without access to electricity. This fact also considerably contributes to the United Nations SDGs (Sustainable Development Goals) [12].

This high increase in demand for battery technologies is automatically accompanied by the fact that the production of these has a significant GHG footprint depending on the energy mix in the production facilities, the contribution of which must not be disregarded under any circumstances [26]. In this respect, a functioning battery circuit is essential for a sustainable and sensible energy transition. According to forecasts, a global battery value chain enables an estimated 30% reduction in emissions in the transportation and power sectors, the idea of which is visualized in **Figure 2**. This scenario also serves as a basis until 2030 for subsequent implementation of alternative technologies such as hydrogen or power-to-liquids [12].

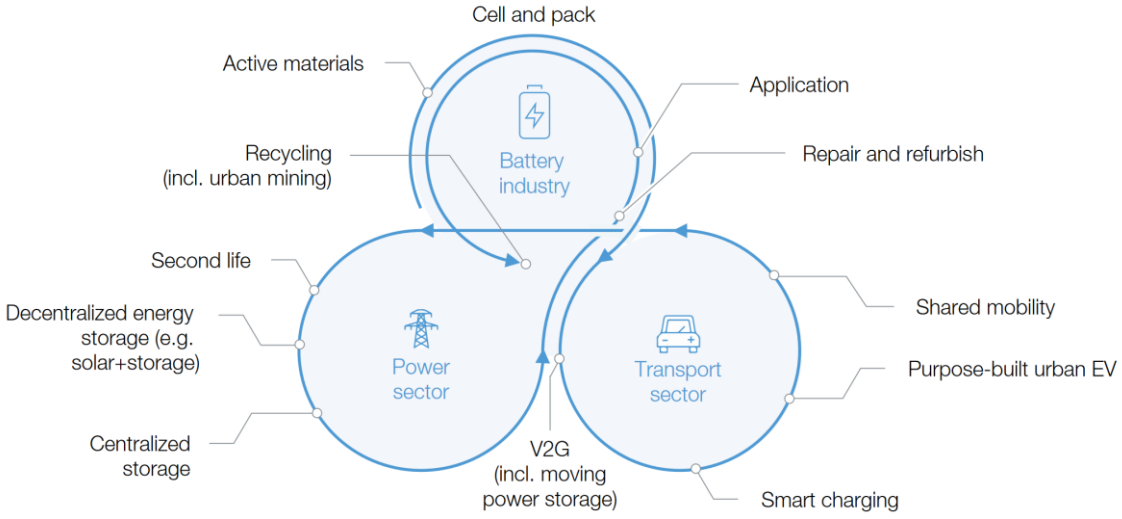

Figure 2. Idea of a global circular battery value chain by 2030 and base for additional alternative technologies (e.g., hydrogen, power-to-liquids) [12].

This visualization also confirms the statement above, that many individual measures must be taken to reduce GHG emissions. This circular approach also supports the concerns of the European Green Deal, which, in addition to reducing net greenhouse gas emissions by 55% until 2030, also aims to strengthen the circular economy and thus reduce dependence on raw materials which are acquired in third countries [1]. Recycling is also presented as a central element in **Figure 2** and can be highlighted as a key factor.

If we go a step deeper into the consideration at this point, the technology of lithium-ion batteries is currently and forecast to be the one with the largest market shares. This can mainly be attributed to the high energy density, specific energy, and good rechargeability of LIB and its high maturity [27, 28]. In addition, the projected increase in global LIB demand from 700 GWh in 2022 to 4700 GWh in 2030 [29] (01/2023 updated numbers of [12]) can be primarily attributed to electromobility with 4300 GWh, in whose application area the use of LIB dominates [29]. This also implies a corresponding growth in demand for all materials used in

these batteries. Particularly noteworthy are the cathode materials which mainly contain valuable metals. Special attention should also be paid to the anode material, which commercially consists primarily of graphite [30].

The importance of a battery circular economy becomes apparent when looking at the EU list of critical raw materials. This register includes natural graphite, phosphorus, lithium, and cobalt [31]. Comparing these raw materials with the active material used in the LIB, consisting of cathode and anode material, the economic and ecological importance of sustainable use is evident. This statement is extended by the research of Xu et al. [32], in which the cumulative primary material demand of Li, Co, and Ni from 2020-2050 is described in different scenarios, as can be seen in **Figure 3**. The scenarios are based on those of the International Energy Agency, whereby an increased development towards NCX materials - in EV, lithium nickel cobalt aluminum oxide (NCA) and lithium nickel manganese cobalt oxide (NMC) cathodes are predominant - is assumed. Thereby, the STEP represents the one based on the current governmental policies in force. Sustainable Development (SD) is the scenario based on the Paris Agreement's climate goals and considers achieving the planned 30% share of EV sales by 2030. In addition, the respective raw material reserves, the effects of recycling, and a deviation between the total use of battery electric vehicles (BEV) and plug-in hybrid electric vehicles (PHEV) are also shown.

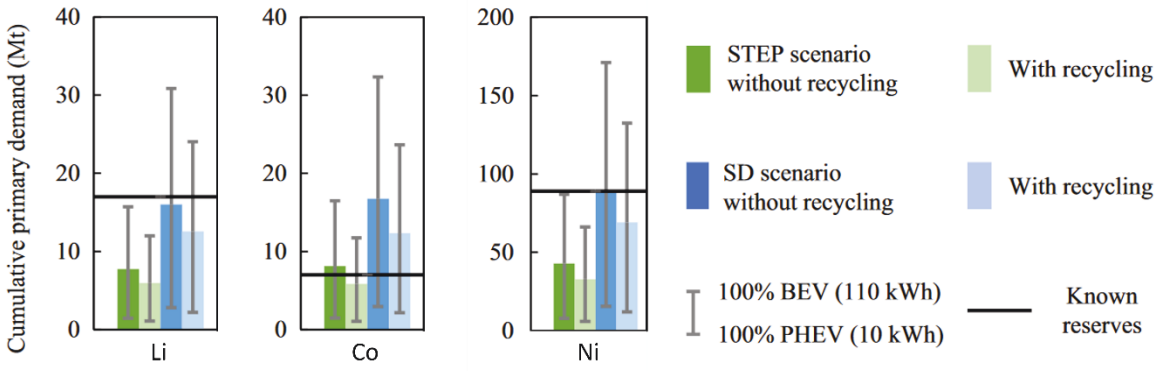

Figure 3. Visualization of the cumulative primary global material demand for 2020-2050 of Li, Co, and Ni for battery production in different scenarios [32].

The most important conclusion from **Figure 3** is that the coverage of demand in connection with the currently known global reserves of valuable metals from primary production is scenario-dependent. It is imperative to mention Co, with which it is only possible to cover the demand in the STEP scenario with recycling. It should be noted that this scenario building is always dependent on the technologies under consideration due to the current high research output and further development in the industry. For example, in the base scenario of Hanicke

et al. [29], the demand for lithium carbonate (raw material for Li in batteries), nickel, and manganese are not met by 2030, but that for cobalt is achieved because a higher proportion of low-cobalt cathode chemistries was included. Regardless of the different individual results, the sources all agree that there will be massive bottlenecks in the supply of raw materials in the future.

Finally, coming back to the forecast in **Figure 3**, it is also very interesting that in the case of the planned path of SD, it is shown that implementing 100% BEV with the currently available cathode materials is not possible from the point of view of raw materials. This also supports the parallel implementation of alternative technologies, such as hydrogen or power-to-liquid. Furthermore, this also emphasizes the statement that only a bundle of different measures can achieve the goals set by the Paris Climate Agreement.

In summary, the reduction of GHGs and the sustainable use of raw material resources are two compelling arguments that justify the EU regulations on a sustainable circular economy and the recycling ambitions described in the Introduction. The current recycling processes on the market are still subject to some drawbacks, which is why developing a holistic efficient recycling route is necessary to meet the EU targets [33].

2.2 Recycling of Lithium-Ion Batteries

The need to develop efficient recycling processes was illustrated in the previous point. In the following, the structure of LIBs is described for basic understanding, followed by the individual steps and possible process sequences in recycling.

The structure of the lithium-ion battery developed and patented by Nobel Prize winner John B. Goodenough, among others, can be seen in **Figure 4**. In a nutshell, this rechargeable cell operates by transporting lithium ions through the electrolyte via a separator from the negative to the positive electrode. Electrons travel across the external conductor to balance the charge and supply the consumer. The reverse process takes place during charging. In charged state, the positive electrode is called the cathode, and the negative is referred to as the anode. The layer applied to the negative electrode conductor foil made of Cu currently consists primarily of graphite with binding agents. The positive Al conductor foil is coated with lithium metal oxide ($LiMeO_2$). The composition of this so-called cathode material depends on the application. The currently commercially used materials are the three composed in a layer structure lithium cobalt oxide (LCO), lithium nickel cobalt aluminum oxide (NCA), and lithium nickel manganese cobalt oxide (NMC), as well as lithium iron phosphate (LFP) with its olivine structure. The electrolyte is a form of lithium salt (e.g., $LiPF_6$) dissolved in organic solvents, such as propylene

carbonate, ethylene carbonate, dimethyl carbonate, or diethyl carbonate. An electron-impermeable microporous separator isolates the two electrodes. In most applications, the various cells are combined to form modules, whereby material flows from the cell housing and electronics, such as various plastics, aluminum, steel, and cables, are also encountered during recycling [30, 34–37].

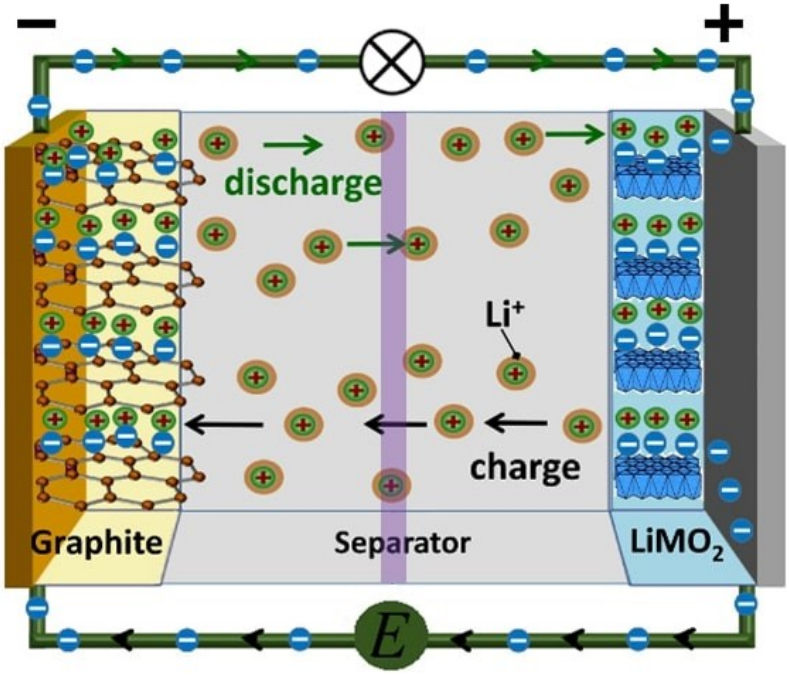

Figure 4. Schematic illustration of the lithium-ion batteries' constructional design (cf. [38]).

The different types of LIB and the resulting waste stream is likely to fluctuate in its chemical composition, therefore, the aim must be developing an insensitive overall process. In this respect, many different technologies on the market or in research can be assigned to various processing steps. A graphical representation of these with the possible process routes can be taken from **Figure 5**.

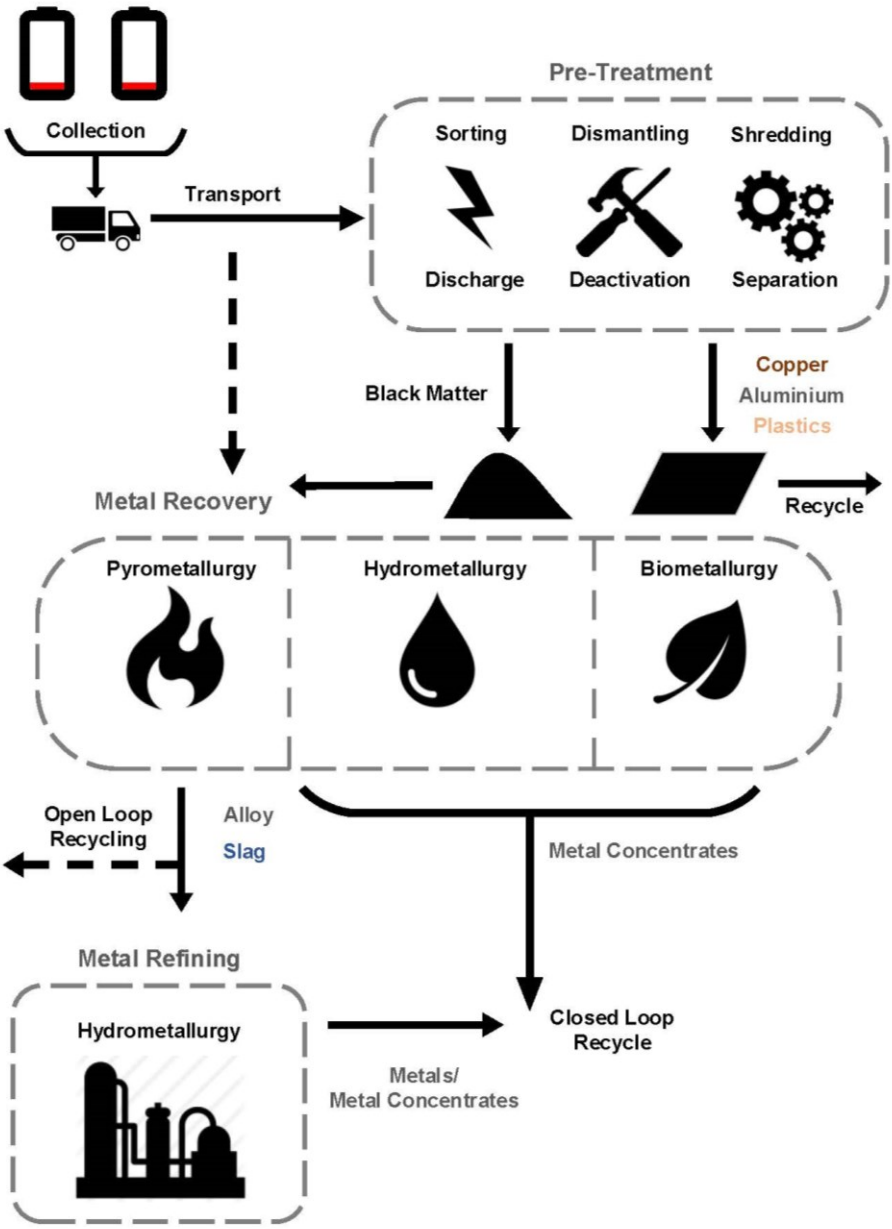

Figure 5. Schematic representation of potential technologies for recycling LIB from collection to metal recovery (cf. [39]).

At the beginning of the process chain, collection and logistics must be mentioned. Since even this step is not trivial, it is the first indication of the complexity of LIB recycling. The essential task here is the danger of a thermal runaway, which poses the highest risk of fire and release of toxic gases in the process [40–42].

The most common next step is physical treatment. This preparation can be divided into sorting based on its chemical composition, discharging, dismantling of battery packs to cell or module size, and separation of, e.g., housing components and cables. In addition, mechanical

and/or thermal pre-treatment takes place for further safe handling, resulting in deactivation, among other things. The resulting components can either be recycled directly, such as copper, aluminum, or plastics or must undergo further treatment, such as black matter. The resulting black matter - visually classified as a black powder - can be described as a mixture of anode and cathode material and battery components not wholly separated from the pretreatment, containing valuable metals [16, 37, 43].

The main recycling step is the chemical treatment, divided into pyro-, hydro- and biometallurgy, these may also be combined. Therein, the product from the valuable metal-containing black matter is either transferred to another industrial process in an open-loop or recycled as a raw material for battery production in a closed-loop [33]. Biometallurgical processes separate and recover the metals with the help of metabolic excrements of microorganisms or fungi. With this low-cost and environmentally friendly alternative to hydrometallurgy, recovery rates of more than 98% of Ni and Co and 80% of Li can be achieved. Still, due to their low kinetics, only low throughput rates are currently possible [44–52]. Hydrometallurgical technologies are highly selective, with recovery rates of up to 100% of high-purity metals. Therefore, leaching, solution extraction, chemical precipitation, or electrochemical deposition are used. Even though this process step has high potential, there are also significant limitations to be mentioned here. These include the sensitivity to a fluctuating waste stream and the resulting large number of process steps and complexity, which directly impact efficiency. In addition, the high demand for chemicals and the high volume of contaminated wastewater have to be mentioned [44, 53–56]. Pyrometallurgical processes operate at temperatures above 1400°C. This processing method is remarkably robust against impurities and accompanying organic elements. Consequently, it has a unique selling point compared to other chemical treatments, as the expected fluctuating chemical composition of the waste stream is less of a task. A significant additional advantage is that the mass of the LIB material used is reduced by approx. 50% during the process. Besides removing volatile components, the material is converted into fractions that are easier to handle than black matter, such as alloy and slag, which provides a significant advantage in a combined process connection with hydrometallurgy. The disadvantages mentioned here are the high energy requirement due to this high-temperature application, post-treatment of the process gases is indispensable, and Li is slagged in currently available processes and not returned to the cycle for economic reasons [16, 39, 57–60].

The last recycling method not yet mentioned in **Figure 5** is the immediate treatment of LIB batteries in a pyrometallurgical method, such as that developed by Umicore. Despite the advantage of the less complex process design and the industrial implementation that has

already taken place, the essential benefit of a recycling combination with pretreatment must be mentioned. In this case, by-products such as Al, Cu, casing parts, etc., can be separated in advance and returned to the cycle and are not largely found in the alloy or the slag like in this direct pyrometallurgical treatment [61–63].

2.3 InduRed Reactor Concept

The disadvantages mentioned above of pyrometallurgical processes currently available on the market were taken as an opportunity to develop a novel process approach. As a basis, the research group of the Chair of Thermal Processing Technology (TPT) at Montanuniversitaet Leoben was able to use a process developed in-house, the so-called InduRed reactor concept. The composition of the name is due to its intended function, whereby metal oxides are to be reduced in an inductively heated treatment. Research into developing this process idea dates back to 2012. Therein, the cornerstone of the technology was laid within the framework of an EU project [64], focusing on developing a process for recovering phosphorus from sewage sludge ash with the thermo-reductive RecoPhos concept. The core of this process was designed and built in collaborative work at the TPT in a continuous pilot plant with a throughput of 10 kg/h. An illustration of this pyrometallurgical site is shown in **Figure 6**.

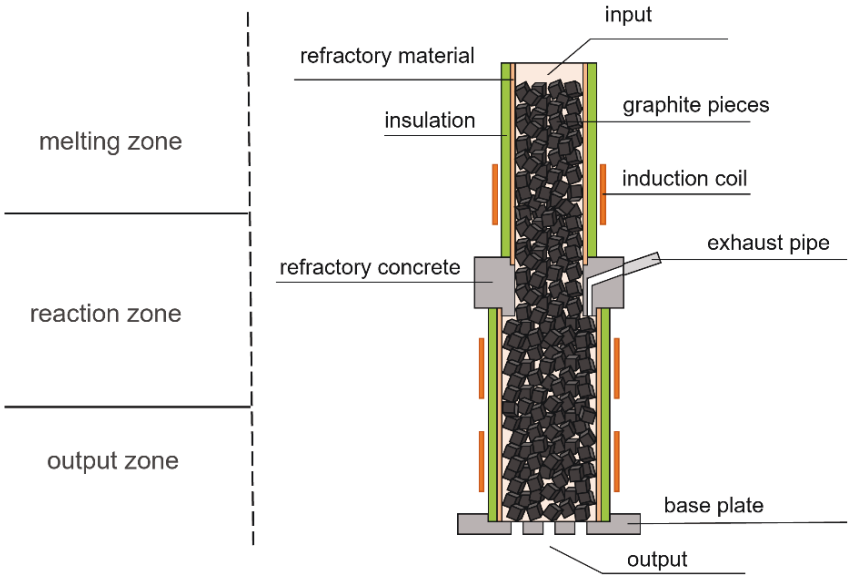

Figure 6. Conceptual illustration of the InduRed reactor concept (cf. [65, 66]).

Its principle is based on a cylindrical arrangement of refractory materials filled with graphite pieces as susceptors that allow a horizontal and radial homogeneous temperature distribution up to 1750°C. Resistance losses provide heat due to eddy currents in the susceptor material

caused by an electromagnetic field through the induction coils, which can be controlled individually. The main driver of the whole process is the highly reducing atmosphere, with a high CO-to-CO_2 ratio and low oxygen partial pressure, as well as direct reduction with carbon powder [65].

The material is fed from the top with thermal management in the first zone, forming a thin melting film or drops on the bed's large surface. The charging is carried out under inert gas purging to avoid atmospheric influence due to an undesired supply of ambient air. The formed melt migrates into the subsequent reaction zone, where the temperature is controlled, so the phosphorus is gasified. The thin melt film or drops allow short diffusion paths and, thus, a low possibility of contact between metal and gaseous product, suppressing undesirable reactions like iron phosphide formation. This avoidance of undesired liquid-gaseous reactions is the unique selling point compared to, e.g., a molten bath. Consequently, the phosphorus is extracted with other process gases through a waste gas pipe with negative pressure and further processed to phosphoric acid via post-combustion and quenching. The P-depleted melt subsequently enters the discharge zone. Herein, the lowest coil can adjust the temperature, ensuring the discharge of a liquid phase from the reactor via the inert-gas-purged bottom [65, 66].

In addition to the processing of sewage sludge ash, the applicability of this system was also successfully demonstrated for the treatment of basic oxygen furnace slag in further years of research. A pre-pilot scale was constructed in the scope of the doctoral thesis of Ponak [65] to generate a higher degree of knowledge about the high-temperature behavior of the materials used. The system shown in **Figure 7** is a single-coil system using batch operation, the so-called InduMelt plant.

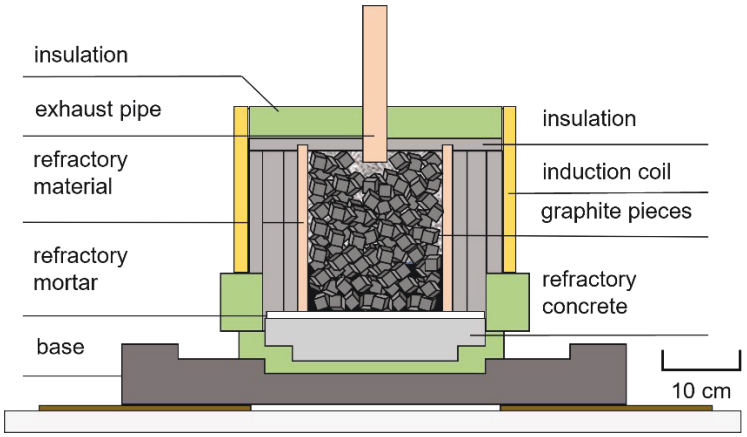

Figure 7. Illustration of the pre-pilot plant InduMelt (cf. [65, 67]).

The underlying principle based on the InduRed reactor concept of reducing metal oxides in an inductively heated packed bed reactor remains the same as in the previous application. In this original design, an alumina ring (Al_2O_3) refractory cylinder was fixed to a refractory concrete using refractory mortar. The filling is done according to the before-mentioned InduRed reactor concept with graphite pieces.

The field of application was consequently extended to valuable metal recovery from spent LIB [43, 67]. During development, a gas extraction system was integrated to identify the gas flow composition. Consequently, this status also represents the initial situation for further research activities within the scope of the present doctoral thesis.

3 Research Objectives and Methodology

As seen from the previous chapter, developing a holistic recycling process to recover all valuable metals is one of the most essential research topics in the lithium-ion battery circular economy field. However, this also means that the efficiency of the individual technologies from the physical and chemical steps and synergy effects are essential for an adequate process design. Including a pyrometallurgical process in the overall concept appears to be promising. Still, there are significant disadvantages to be considered, for example, the tendency of lithium to slag. Another critical factor is the integration into the overall process. Particularly, from a material-specific point of view, the quality of the product depends to a large extent on the input stream from the pretreatment. This also impacts plant engineering issues such as design and material use. The research questions are defined as follows, which are aimed at these tasks. Furthermore, an overview of the methodology is given.

3.1 Research Objectives

The further development of the pyrometallurgical process engineered at the Chair of Thermal Processing Technology requires a broad knowledge of the high-temperature behavior of the black matter used. This can be divided into questions regarding the material quality, the interconnectivity with the plant engineering, and the resulting design. Three more in-depth scientific questions were formulated from these overarching questions. Based on previous research on the InduRed reactor concept, further reactor design development was necessary for optimized treatment of the LIB material. This and the resulting increase in material specific knowledge is addressed in the first research question block. The next block takes an additional step towards using black matter instead of cathode material from battery production and

examines the influence of accompanying elements from pretreatment. Finally, the last block of questions deals with the use of black matter in the InduMelt plant.

1. **Optimization of the reactor design**
    - 1a. How does the new design affect productivity using commercially available LIB cathode materials? Which transfer coefficients can be achieved?
    - 1b. Is the MgO crucible material selected adequate for a future continuous process?
2. **Determining the influence of impurities on the melting ability of the black matter**
    - 2a. Which influence do incompletely separated accompanying elements from the electrode conductor foils have?
    - 2b. Does the graphite from the anode material affect the melting ability?
    - 2c. How can a quick and low-trial statement be made concerning the usability of input materials from pretreatment in the InduRed reactor concept, considering a waste stream that fluctuates in its composition?
3. **Behavior of black matter in the InduRed reactor concept**
    - 3a. What productivity results from tests with black matter from a pretreatment step in the InduMelt plant?
    - 3b. How do the results reflect the findings from using cathode material from the battery production?
    - 3c. Does the result fit with the findings from basic research? What exactly is the reaction behind lithium removal via gas flow?

In order to answer these questions, numerous experiments were designed and carried out in the InduMelt plant and the heating microscope for basic research. In addition to answering the main questions formulated here, it was also possible to gain further insights, which are also discussed in this thesis' context. In the following section, the underlying methodology is explained in detail.

3.2 Methodology

Four peer-reviewed journal articles provided detailed answers to the abovementioned questions, which can be found in Appendix A. The results obtained in these articles were generated successively, building on each other so that a thread can be drawn from the high-temperature behavior of the idealized cathode material without accompanying elements to the

use of black matter from a pretreatment step in the InduMelt system. **Figure 8** represents the overview of the research process within this thesis.

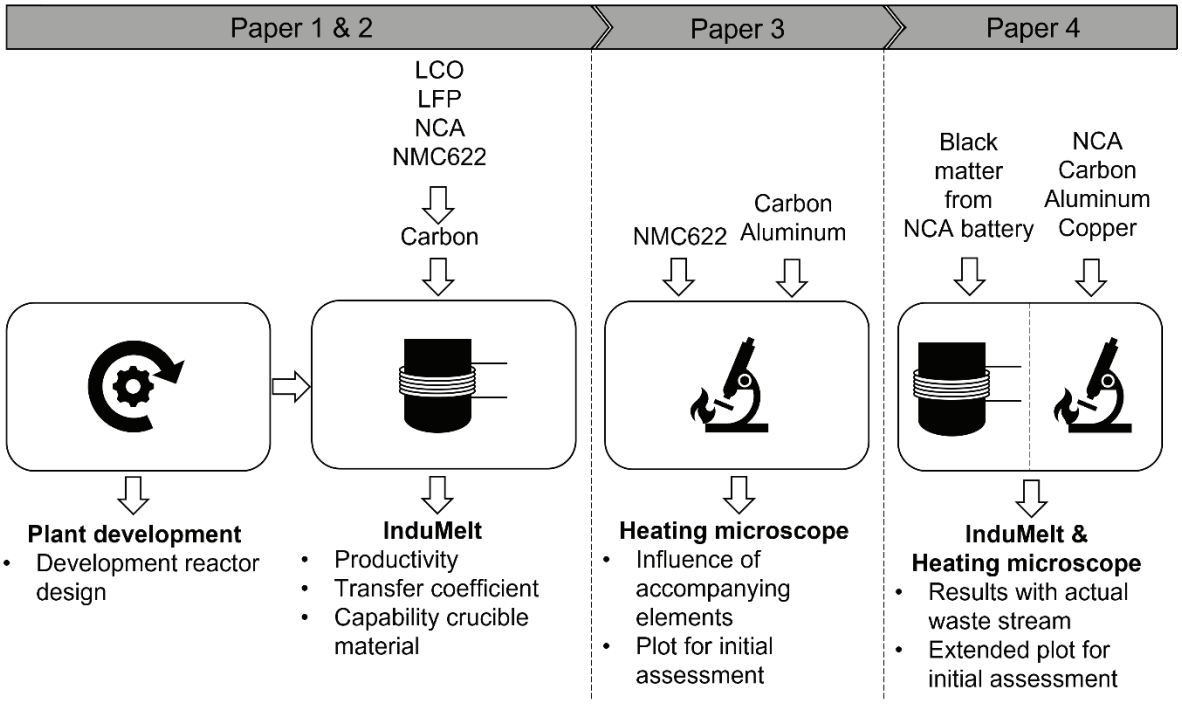

Figure 8. Graphical abstract of the present doctoral thesis.

The idealized or pure cathode materials mentioned are commercially available for battery production, obtained from Gelon Energy Corp in China. These were chosen for the basic investigations due to the scarce data in the literature to avoid influences from accompanying elements from the battery assembly. Carbon was added as a reducing agent to reduce the lithium metal oxides ($LiMeO_2$) and protect the graphite cubes acting as susceptor material during the InduMelt experiments. The detailed investigations with this standard combination enabled the determination of fundamental data on the behavior in the high-temperature range and also the generation of reference values for maximum recovery rates in the InduRed reactor concept. The cathode materials used in this work are listed in **Table 1**.

Table 1. Cathode materials used in the scope of this thesis.

Abbreviation	Chemical formula	Designation
LCO	$LiCoO_2$	Lithium cobalt oxide
LFP	$LiFePO_4$	Lithium iron phosphate
NCA	$LiNi_{0,8}Co_{0,15}Al_{0,05}O_2$	Lithium nickel cobalt aluminum oxide
NMC622	$LiNi_{0,6}Mn_{0,2}Al_{0,2}O_2$	Lithium nickel manganese aluminum oxide

An additional focus was placed on further developing the InduMelt reactor design. Therefore, the initially used alumina oxide (Al_2O_3) crucible was revised in shape and material. Instead of the structure of the Al_2O_3 ceramic ring, which is fixed to a refractory concrete bottom through refractory mortar, a cylindrical magnesium oxide (MgO) crucible with an elliptical head was chosen. In addition to increased productivity, this more straightforward and faster setup should also allow for more reproducible tests. To comparatively evaluate the new design, a series of experiments were conducted using the same feedstock in both setups. Consequently, a statement could be made about the suitability of the crucible materials for use in the continuous process and the effect on product quality for the cathode materials mentioned in **Table 1**.

Since these tests only draw an idealized picture of the input stream, the elements Cu and Al, primarily originating from the electrode conductor foils, were identified as the main accompanying elements in terms of quantity after analysis of black matter from a pretreatment step. Additionally, it was determined that a C amount above the stoichiometrically necessary for reducing the $LiMeO_2$ also influences the reduction process. Its influence on the melting ability required in the InduRed reactor concept was therefore investigated in advance by numerous tests with NMC622 under the heating microscope. This cathode material was chosen due to its use in e-mobility and its predicted strong market growth. In these heating microscope experiments, the successive change in the sample's cross-sectional area (CSA) is detected when heated to 1620°C. After an initial assessment, Al and C were found to be the factors with the most significant negative impact, so different compositions with these elements in combination with pure cathode material were subsequently investigated at temperatures up to 1700°C under argon purging. In the process, plots could be created, providing a more straightforward and faster initial assessment of the usability of black matter for the future use of the InduRed reactor concept.

Consequently, the transition to an actual LIB waste stream was accomplished in cooperation with Fraunhofer Research Institution for Materials Recycling and Resource Strategies IWKS from Hanau, Germany. The black matter was extracted from spent pedelec batteries with NCA cathode material from their hydromechanical pretreatment step. As a consequence of the experiments in the heating microscope, the excess graphite from the anode material was depleted by flotation at the Chair of Mineral Processing of the Montanuniversitaet Leoben. The resulting fraction could consequently be treated in the InduMelt plant. To better interpret the results, an additional test series was subsequently carried out in the heating microscope to analyze the influence of Al, C, and additionally of Cu. Consequently, an even more accurate plot could be created for a future initial assessment of the melting ability.

4 Results and Discussion

In the first stage of the research activities, the applicability of the InduRed reactor concept was confirmed for all commercially available cathode materials in Publication 1 [68] and Publication 2 [69]. The avoidance of Li slagging – further presented in the fraction "removed" - and the metal alloy were defined as a measurable result. In addition, concerning the "removed" fraction, it should be noted that this is the amount that was not found again in the solid fractions (metal, slag, powder smaller than 1 mm) compared to the input material. These elements were either removed from the reactor via the gas flow or entered into a compound with the crucible, which could not be separated during sampling. Detailed analyses could be realized by discharging the gas via a gas wash bottle. The generated powder was analyzed in detail, but the goal in future research activities must be the complete elimination of this fraction to increase productivity. Due to the low mass fraction of slag (or mineral phase) in all tests, this analysis can be neglected at this point. To be able to provide a reliable comparison between the original reactor design with an Al_2O_3 crucible (Design 1) and the optimized variant with a MgO crucible (Design 2) in parallel with this knowledge, all tests were carried out in both setups and compared. For evaluation and comparison, the transfer coefficient was introduced. It describes the transfer of the individual elements into the fractions by combining the analytical results from the ICP-OES - according to ÖNORM EN SIO 11885:200911 - and the respective mass of the products obtained. The resulting transfer coefficients can be found in **Table 2**. It should be mentioned that the results of NCA and NMC622 in the Al_2O_3 crucible design originate from the work of Windisch-Kern et al. [43, 70] and were processed according to the uniform calculation method. In addition, at least two tests were performed in the experiments in Design 2, so the mean values from these are given in the table below.

Table 2. Transfer coefficients to metals and removed phase from InduMelt trials with the cathode materials LCO, LFP, NCA, and NMC 622

Sample/ Element	Fraction	Design	Li	Co	Ni	Mn	Al	Fe	P
LCO	Metal	Al_2O_3 crucible	0.1%	95.2%	-	-	-	-	-
		MgO crucible	0.6%	77.1%	-	-	-	-	-
	Removed	Al_2O_3 crucible	97.5%	<0.1%	-	-	-	-	-
		MgO crucible	98.3%	6.6%	-	-	-	-	-
LFP	Metal	Al_2O_3 crucible	6.2%	-	-	-	-	44.1%	12.8%
		MgO crucible	4.4%	-	-	-	-	73.8%	30.4%
	Removed	Al_2O_3 crucible	70.0%	-	-	-	-	15.9%	66.2%
		MgO crucible	85.1%	-	-	-	-	12.2%	61.6%
NCA	Metal	Al_2O_3 crucible*	11.4%	80.4%	>95%	-	83.3%	-	-
		MgO crucible	1.2%	78.3%	93.1%	-	11.4%	-	-
	Removed	Al_2O_3 crucible*	81.4%	19.6%	3.3%	-	5.7%	-	-
		MgO crucible	90.1%	10.3%	<0.1%	-	75.6%	-	-
NMC622	Metal	Al_2O_3 crucible*	0,4%	84.2%	91.6%	83.5%	-	-	-
		MgO crucible	1.4%	83.5%	88.5%	79.7%	-	-	-
	Removed	Al_2O_3 crucible*	96,4%	6.7%	<0.1%	7.2%	-	-	-
		MgO crucible	92.2%	2.9%	<0.1%	6.7%	-	-	-

*Edited results from Windisch-Kern et al. [43, 70]

1. Optimization of the reactor design

With the results from **Table 2**, the first point in the research question block can now be answered.

1a.) How does the new design affect productivity using commercially available LIB cathode materials? Which transfer coefficients can be achieved?

As mentioned earlier, avoiding Li slagging is an essential quality factor of the InduRed reactor concept. On the one hand, this was achieved by almost completely preventing slag formation. On the other hand, the attainment of the target is reflected in a high proportion of Li in the removed fraction and a low proportion in the metal. Looking at the results of separated Li in both setups, the removal of at least about 81% in Design 1 and about 90% in Design 2 is

always evident for the cathode materials in layered structures (LCO, NCA, and NMC622). For LFP in its olivine structure, 70% of the Li could be transferred using Design 1 and around 85% utilizing Design 2. In this narrow consideration, a higher tendency for Li removal with Design 2 is evident.

The metal alloy formation of Co and Ni is similar for NCA and NMC622. The high Al and Li content in the NCA metal with Design 1 can be seen as a significant difference. However, when the alloy is used in the steel-producing industry, for example, this contamination of Co and Ni would have a disadvantageous effect. While looking at the results from LFP, a much higher transfer of iron to the metal fraction is evident in Design 2. In contrast to the other cathode materials, a higher outcome of the metal could be achieved with LCO in Design 1. In this evaluation carried out for the productivity analysis, another factor must be mentioned at this point, namely the powder content after the tests. This fraction is primarily a mixture of carbon powder and partially reduced, but not molten, metal powder. As stated at the beginning, this fraction is undesirable after the trials since it directly influences the amount of metal alloy produced. In **Table 3**, the corresponding powder fractions are listed, whereby an average value was formed in the case of multiple tests.

Table 3. Listing of the powder content (<1 mm) of the product fractions generated in the InduMelt tests in wt.%.

Design / Sample	LCO	LFP	NCA	NMC622
Design 1 (Al_2O_3 crucible)	6.8 wt.%	22.0 wt.%	3.0 wt.%	7.4 wt.%
Design 2 (MgO crucible)	10.3 wt.%	10.5 wt.%	11.1 wt.%	11.1 wt.%

By comparing the powder fractions, it can be seen that there are almost identical values in the experiments from Design 2. This, in turn, is a strong indication of higher reproducibility and confirms the successful implementation of the more straightforward reactor design for more comparable experiments. In addition, by comparing with **Table 2**, it can be seen that the metal yield is always higher in those tests with lower powder content. Conversely, this finding shows the importance of an input material adapted to the InduRed reactor concept to increase efficiency.

If these findings are thus broken down to the formulated research question, the new reactor design influences productivity in a higher average Li removal and a more stable metal yield.

The reactor concept's basic suitability and high potential could be clarified within the scope of these tests. In order to further develop the InduMelt batch plant into a continuous process,

material-specific research activities and plant engineering issues need to be clarified. These were also considered in more detail in Publication 1 [68] and Publication 2 [69] by examining the interaction of the input material with the crucible material. The underlying question was as follows:

1b. Is the crucible material selected adequate for a future continuous process?

Both preliminary tests in the heating microscope when using Al_2O_3 platelets as sample support and InduMelt tests in Design 1 in the Al_2O_3 crucible showed an interaction with the platelet and the crucible when using cobalt-containing cathode material. A blue coloration of the ceramic was immediately recognizable during an initial optical assessment. On closer inspection, an abrasive behavior was also observed, which was particularly evident in the InduMelt crucible due to deep indentations in the mantle surface. This reaction could be attributed to cobalt aluminate formation, also widely referred to as cobalt blue. Since massive abrasion of the ceramics occurred even at such low test run times as in the heating microscope or the InduMelt system, using Al_2O_3 materials in this manner was not considered optimal for continuous use. In addition to the reactor redesign, the alternative crucible material of MgO was also closely examined. From the first InduMelt tests, it could be determined that no attack on the crucible wall occurred, but adhesions were recognizable. Further detailed investigations showed an increase in the weight of the crucible during all trials. The influence of the crucible's reuse was also examined to obtain a first estimate of the interaction between feedstock and crucible material. It was found that the packings could be reduced by up to 50% in the second test. Although this would be a positive development for continuous use, it was found by chemical analysis that Li diffused or adhered to the reactor even in repeat tests.

In general, increasing adhesion in the bottom area of the reactor was detected, and a concomitant growing diffusion into the crucible wall. It was demonstrated by analysis of the crucibles over the height that a lower value of Li detection in the scrubbing liquid is associated with an increased Li occurrence in the middle to bottom region of the reactor. In contrast, a high Li content in the washing solution resulted in a more substantial presence of Li in the higher reactor area. Even if the occurrence of Li in the reactor wall is fundamentally undesirable, this effect can possibly be attributed to the removal of the element via the gas flow and contact with the crucible surface in the higher range. The metal alloy elements (Co, Ni, Fe, Mn), which are shown as "removed" in **Table 2**, tend to be found in the middle to bottom of the reactor. This can be attributed to their physical properties. Special attention also for future research activities is phosphorus. When tested once, the tendency is to find it in the upper area of the reactor, but when the crucible is used several times, it seems to form a bond with the adhering metal in the bottom area.

Based on the unique selling point of the InduRed reactor concept for Li removal via the gas flow, a statement about the functionality of the MgO crucible material has now been made from these findings. As shown in **Figure 9**, a high proportion of Li from the "removed" fraction is found in the crucible for all cathode materials. This interaction between MgO and input material turns out to be so disadvantageous that the choice of this crucible material is not advisable for a continuous process. In addition, the packings could successively reduce the reactor diameter in this mode of operation, which could subsequently cause reduced throughput or clogging.

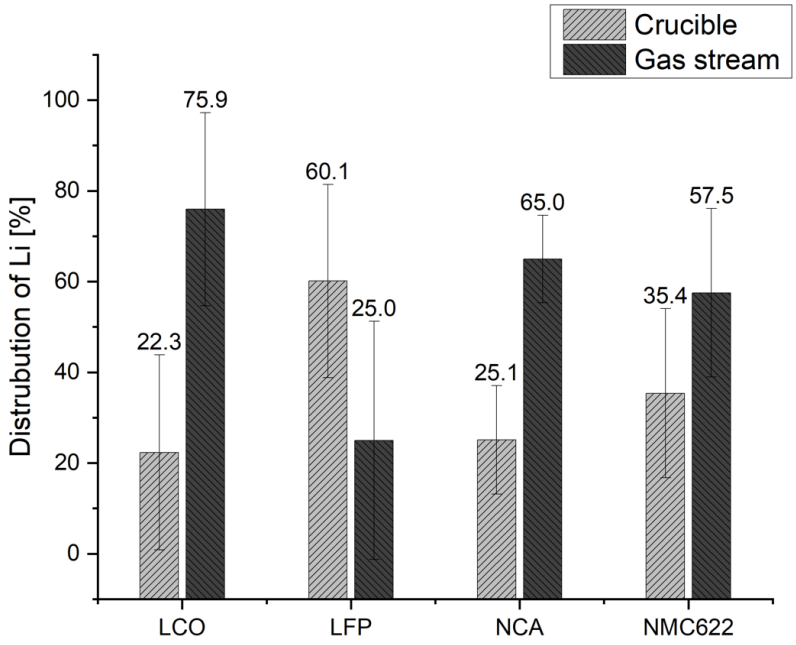

Figure 9. Illustration of the distributed Li into the crucible wall and the resulting amount potentially transferred to the gas stream during InduMelt trials in Design 2 [69].

The theoretical approach of the reaction processes up to the transfer of Li into the gas phase is discussed in more detail in Question 3b.

2. Determining the influence of impurities on the melting ability of the black matter

In the previous block of questions, the basic research was always done with cathode material from battery production to explore the high-temperature behavior. However, other accompanying elements can be found in an actual waste stream of EoL batteries after the pretreatment necessary for the InduRed reactor concept. These originate from the battery assembly and are difficult to separate in the pretreatment step due to agglomerations or very small particle sizes, for example. The type of pretreatment also plays a significant role, which has a direct impact on the chemical composition of the black matter. For example, the

electrolyte is already evaporated upstream in process routes with thermal preconditioning, so the off-gas post-treatment in the pyrometallurgical process is easier to design.

It was known from the studies of, e.g., Windisch et al. [43], that the black matter and the pure cathode material behave fundamentally differently in the heating microscope. So, how do the chemical compositions of the input materials compare? Which accompanying elements influence the high-temperature behavior most significantly? It was found that the main accompanying elements in the black matter were Cu and Al, most likely from the electrode conductor foils. Also, a significant amount of carbon greater than 30 wt.% could be detected from the anode graphite. In order to get one step closer to the use of black matter in the InduRed system, the following questions had to be answered first:

2a. What influence do incompletely separated accompanying elements from the electrode conductor foils have?

2b. Does the graphite from the anode material affect the melting ability?

To answer these questions, in-depth heating microscope experiments with argon purging were performed on the NMC622 cathode material as part of Publication 3 [71]. This cathode material was chosen because it is primarily used in electric cars, and, as explained in chapter 2, this sector is forecast to be a significant driver of future market growth.

It was shown that only in the presence of carbon as the reducing agent could produce a reduction and thus a magnetic behavior of the sample. The stoichiometric amount of carbon necessary for the complete reduction of the $LiMeO_2$ was added. In the next step, it was demonstrated that adding Al worsens the melting ability, while Cu lowers the melting temperature and hence promotes the formation of a melting phase. This was also investigated to gain insight into the influence of the over-stoichiometrically addition of carbon, as it is present in the black matter from the anode material. It could be explained that an oversupply has a significant detrimental effect on the melting ability.

The main conclusion from these results is that Al and C are the most harmful factors for a successful transfer to a melt. This also implies an increased demand for the pretreatment of black matter. Therefore, particular attention has been paid to carbon. In preliminary tests, it was clarified that graphite from the anode material has the same reducing effect as the carbon in the laboratory tests. In addition, calculations showed that for the complete reduction of the lithium metal oxide at a given atmosphere and operating parameters in the InduRed reactor concept, about 20 wt.% C is required for the layer materials and about 24 wt.% C for the olivine structure in LFP. Since the black matter, as mentioned above, contains more than 30 wt.%

graphite, an additional step in the pretreatment to remove the graphite must be considered when designing the overall process.

An additional factor that appears with the influencing elements mentioned is that Al from the electrode conductor foils also has a strong reducing effect due to its high oxygen affinity. This, therefore, directly influences the individual quantities required to provide the necessary amount of reducing agent. To consider this fact as well as the expected fluctuating waste stream and to allow a simpler estimation for the processability in the InduRed reactor concept, the following research question was defined:

> **2c. How can a quick and low-trial statement be made concerning the usability of input materials from pretreatment in the InduRed reactor concept, taking into account a waste stream that fluctuates in its composition?**

The basis for fulfilling this question was heating microscope tests with NMC622, also described in detail in Publication 3 [71]. By adding different proportions of the detected most harmful elements for the melting ability, C and Al, to the cathode material, a contour plot could be developed from the results using Matlab, as shown in **Figure 10**.

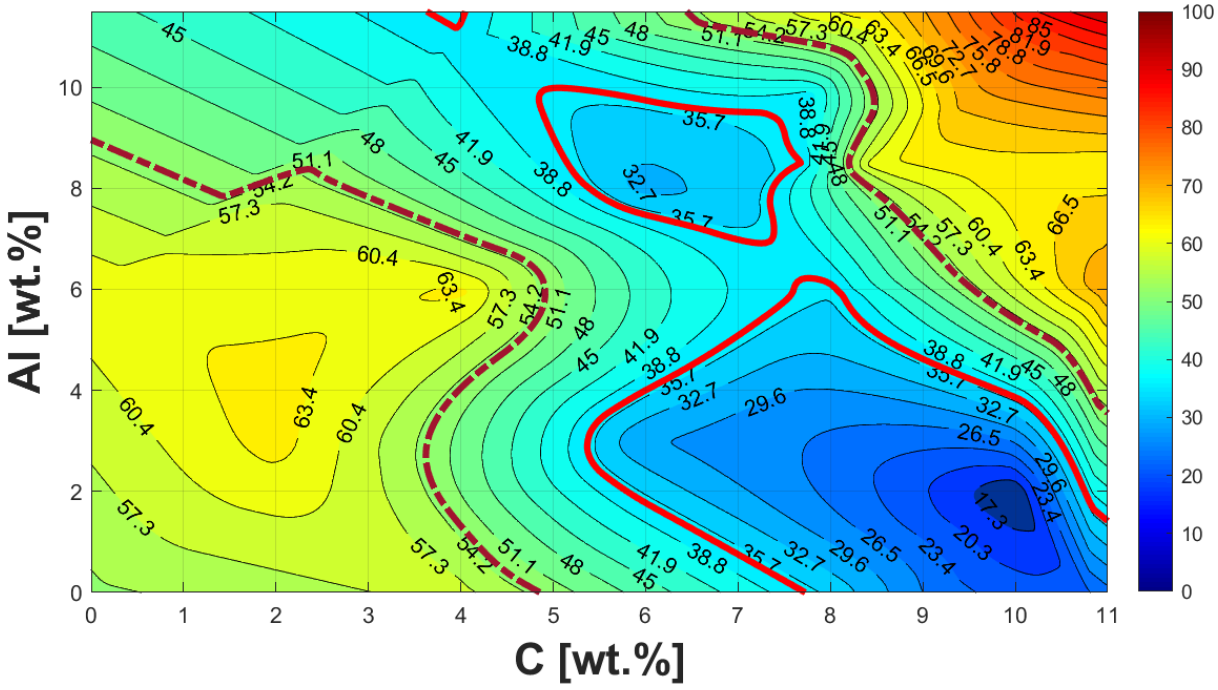

Figure 10. Contour plot of the cross-sectional area in the Al-C-NMC622 system at 1550°C through heating microscope experiments (cf. [71]).

By comparing the heating microscope data and pictures, as well as the appearance of the sample after the trial, a range of good melting ability and a transition area towards a slight melt formation were also defined. The first mentioned is marked within the red line in **Figure 10**,

and the second is between the red line and the dark red dotted border. It is important to mention at this point that, for safety reasons, the experiments in this apparatus were not carried out under the strongly reducing CO/CO_2 atmosphere that is predominantly encountered in the InduMelt. The argon purging used had the advantage that undesired reoxidation could be suppressed. Due to the resulting different reaction course, the result of the C content presented here must be converted to the process of the InduMelt plant. For example, a value of 10.0 wt.% C would yield a proportion of 18.2 wt.% in the InduMelt atmosphere. Although this simplified calculation must be made more precise in the future by further basic research, it is sufficient for an initial estimate of the behavior in the InduRed reactor concept. Regardless, based on the plot, the dependence between C and Al concerning its function as a reducing agent was made graphically apparent. The higher the C content, the lower the Al content should be, and vice versa.

In addition to the melting ability of these composition combinations, an important finding was safety-related. It was observed that with a high Al content compared to the amount of cathode material, a strongly exothermic reaction occurs, which is attributed to aluminothermy. For this reason, the Al percentage in the active material used was set at less than 6 wt.% for use in the InduRed reactor concept.

With these observations, a first estimation of the behavior of recycled material similar to black matter in high-temperature applications is possible.

3. Behavior of black matter in the InduRed reactor concept

The cited results from the various tests with pure cathode material from battery production are an indispensable basis. But how does an actual waste stream from EoL batteries behave? Are the results already generated comparable? For this purpose, the research activities on this topic were discussed in the last Publication 4 [72] of this dissertation.

3a. Which productivity results from tests with black matter from a pretreatment step in the InduMelt plant?

3b. How do the results reflect the findings from using cathode material from the battery production?

Interpreting the results from experimental work with EoL battery material in the same way as the experiments with pure cathode material, the transfer coefficients of the individual elements into the fractions obtained are shown in **Figure 11**.

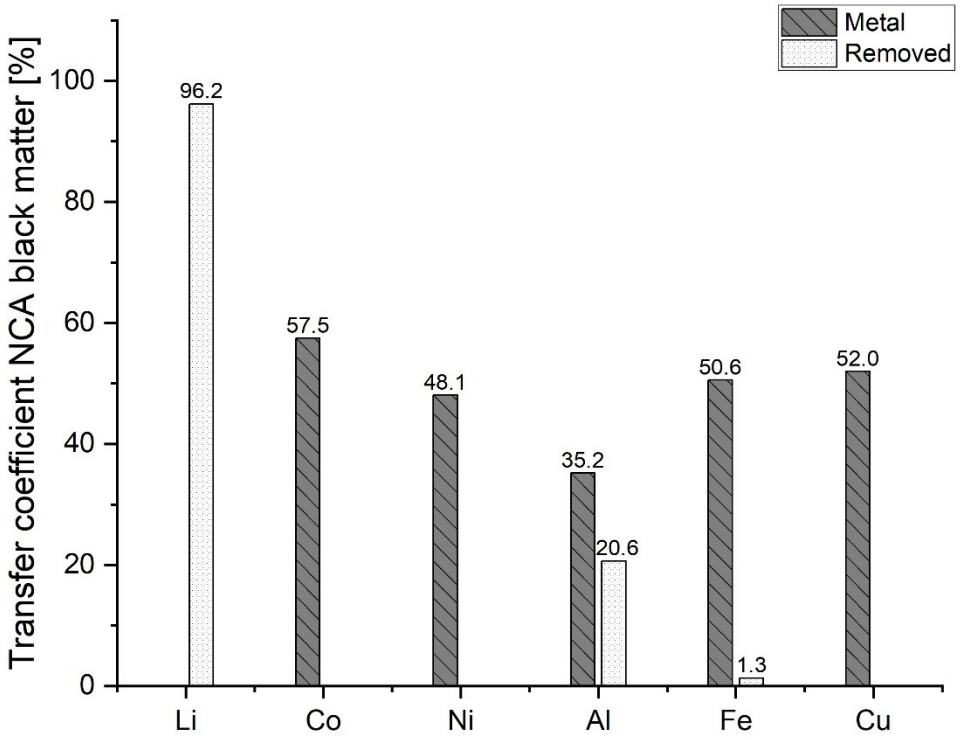

Figure 11. Illustration of the elemental transfer coefficients to the obtained fractions after InduMelt trials with NCA black matter.

The most significant finding is that the lithium removal from the hydromechanically pre-treated and floated NCA black matter used in this study affirms the high transfer rates from more than 90% into the "removed" fraction from the pure cathode material. However, the powder content of 30.75% is three times higher than that obtained from the comparative tests. This fact also explains the much lower Co and Ni transfer rates into the metal compared to the results of pure NCA in **Table 2**. It underlines the need to minimize this fraction to increase the product yield.

In addition, the visual appearance of the metal fraction showed a significant difference compared to the tests with the pure material. The formation of smaller spheres instead of metal lumps has been attributed, parallel to the higher powder content, to a lower melting ability. Therefore, a contour plot was also created for the Al-C-NCA system. By extending the system to include Cu, an increase in the good melting range was observed, and a shift in the optimum composition for maximum melt formation in the direction of lower C and higher Al content was detected. The composition of the NCA black matter was subsequently identified to be in the poor melting range of this plot, which is a possible explanation for the undesirable appearance. Another possibility is the relatively high Fe content in the input material, which has not been taken into account so far due to the negligible content in black matter from other pretreatment methods.

The use of black matter in the InduMelt also allowed the path of Cu and Fe from the battery structure to be practically demonstrated for the first time. The similar transfer rate of these elements with Co and Ni allows the assumption that by reducing the powder fraction, this fraction can also be increased towards the metal fraction. Conversely, this also means that special attention must be paid to the Cu content, especially for reusing the metal fraction in the open loop in the steel-producing industry. In secondary metallurgy, the so-called tramp element Cu is considered an undesirable impurity, which is why its use in steelmaking is limited [73]. Irrespective of the limits observed in this application area, the valuable metals contained would be removed from the battery cycle in this type of product utilization. In the case of closed-loop recycling, this result clearly shows the need for post-treatment to separate the resulting metal alloy into its individual elements. This enables the metals to be made available for the repeated production of active material for batteries.

3c. Does the result fit with the findings from basic research? What exactly is the reaction behind lithium removal via gas flow?

The InduRed reactor concept enables carbothermal reduction of the lithium metal oxide according to equation 4-1 due to its strongly reducing atmosphere and carbon content [70, 74].

$$4LiMeO_{2(s)} + 3C_{(s)} \rightarrow 2Li_2CO_{3(s)} + 4MeO_{(s)} + CO_{2(g)} \qquad \text{Eq. 4-1}$$

Considering the possible path of the resulting lithium carbonate, equation 4-2 is likely due to the permanent intentional supply of C via the graphite of the anode material or unintentionally via the graphite cube bulk [75].

$$Li_2CO_{3(s)} + 4C_{(s)} \rightarrow Li_2C_{2(s)} + 3CO_{(g)} \qquad \text{Eq. 4-2}$$

The resulting lithium carbide consequently dissociates to gaseous Li and C due to the prevailing high temperatures in the InduRed reactor, as shown in equation 4-3 [75].

$$Li_2C_{2(s)} \rightarrow 2Li_{(g)} + 2C_{(s)} \qquad \text{Eq. 4-3}$$

Small amounts of mineral phase adhesions to the metal were observed in the tests with NCA black matter. Line-point analysis in laser-induced breakdown spectroscopy, illustrated in **Figure 12**, provided evidence that there was little to no Li presence in the mineral phase adhering to the Li-free metal alloy (according to **Figure 11**). The main portion of Li could be detected in a thin layer between these two phases. With optimal process control and contact with C, it is reasonable to suspect that the reactions occur according to equations 4-2 and 4-3. However, more detailed analyses are needed to confirm this reaction sequence.

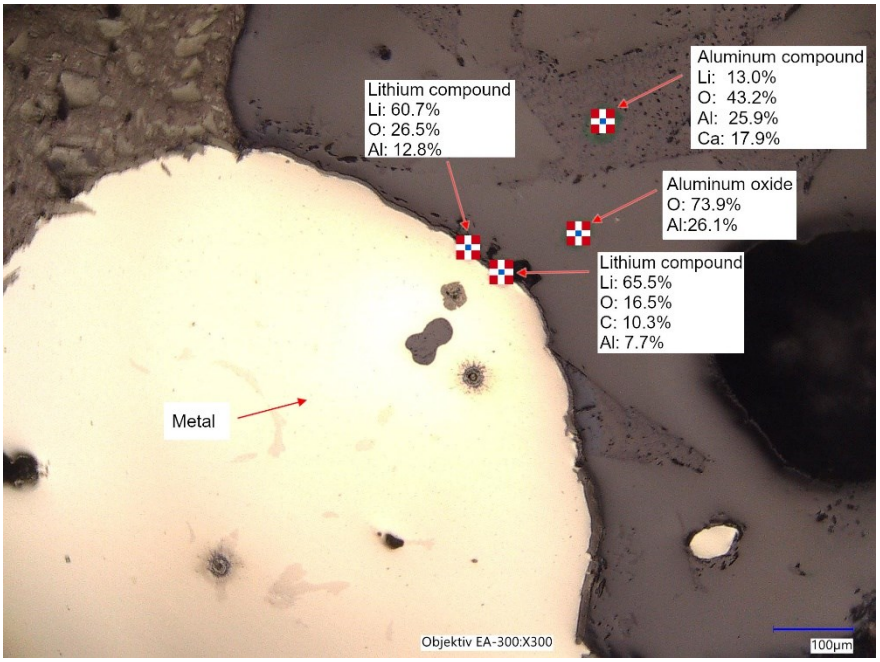

Figure 12. Digital microscope image of the metal and mineral phase transition band with laser-induced breakdown spectroscopy measurement of the product from InduMelt trial with NCA black matter (cf. [72]).

5 Conclusion

Within the scope of the present doctoral thesis, two main topics were addressed as scientific basis for the further development of the InduRed reactor concept. On the one hand, the InduMelt pre-pilot plant running in batch operation was redesigned, and its applicability with lithium-ion battery material was tested. On the other hand, the knowledge of the high-temperature behavior of pure cathode material from battery productions was stretched over the addition of companion elements to using an actual waste stream from EoL batteries.

The most significant finding from the results is that the InduRed reactor concept delivers high metal recovery rates not only when using cathode material from battery production but also when using an actual waste stream from EoL batteries. Particularly noteworthy is that Li can be removed from the input material at a rate of over 85%, with this value tending towards higher rates of up to 98%. This aspect represents a unique selling point compared to pyrometallurgical processes available on the market, in which lithium is primarily slagged. Consequently, a higher share of the recycling rate in the material cycle can be achieved, which is necessary for a sustainable circular economy, among other things, due to increased political pressure and the drive to lead Europe into increased independence from raw materials.

The basis for efficient process design is a sound knowledge of the behavior of the material used in the corresponding application. The influence of accompanying elements like Al, C, and Cu from the battery structure significantly affects the melting ability required by the InduRed reactor concept. In the sense of further development and integration into an overall recycling process, defining limit values for interfering elements is fundamental. The contour diagram developed in the course of this work will enable a low-test and rapid assessment of the usability of material from the pretreatment. This allows a more targeted adaptation of the pretreatment to work well in combination with the InduRed process. Independently of the more optimal

process control made possible by this, the generated knowledge about the LIB black matter also assists the overall process development, increasing the product quality.

For industrial applications, the batch system used must be scaled up to continuous operation. It is essential to select a reactor material that can withstand temperatures around 1700°C and does not react with the input material. Besides redesigning the batch setup for simpler and more reproducible experiments, investigating the crucible materials Al_2O_3 and MgO showed a high need for future research. Even though the temperature resistance could be confirmed with both materials, the interactions with the LIB material are not recommended for different reasons. Al_2O_3 shows a reaction with Co-rich materials to most likely cobalt aluminate. This is not acceptable, especially in long-term tests, due to the strong abrasive effect it causes. Even if this effect does not occur when MgO is used, both packing and diffusion of the elements from the black matter or cathode material could be detected. The effects of continuous operation can not only lead to high wear and tear but also have a massive impact on productivity. In particular, the high amount of Li detected in the reactor must be emphasized. This can lead to less than 40% of the Li being removed from the reactor via the gas flow. Conversely, this would also significantly lower the advantage of the InduRed reactor concept over other pyrometallurgical technologies.

6 Outlook

Even if the high potential of the InduRed reactor concept as a contribution to a sustainable circular economy emerges from the experiments conducted within the scope of this work, a large number of research activities are still required before it is ready for industrial use. These range from plant engineering issues to material science aspects. Essential next steps and the most important ideas for successfully implementing the recycling standard are discussed in this last chapter.

- **Extension of research activities on the influence of accompanying elements on high-temperature behavior**

Although the presented contour model represents a good basis for the first assessment of the usability of the InduRed reactor concept, a more in-depth research is nevertheless necessary. Currently, a model including Al, C, and Cu exists only for NCA. This must also be extended to cover the other commercially used cathode materials. In addition, further accompanying elements have to be considered in more detail. In particular, Fe is highlighted. Since its share in the black matter depends on the pretreatment efficiency and its process design, its influence on the melting ability should also be considered. As the inert atmosphere used in the heating microscope does not correspond to that in the InduRed reactor concept, the accuracy of the models must also be checked in the InduMelt plant. In order to increase productivity, care must also be taken to reduce the powder content to a minimum. Another basic research topic is the effect of pretreatment-dependent accompanying elements in pyrometallurgical processing. Electrolyte or binder can influence product quality according to the process design. Safety-related issues, such as the outgassing of toxic gases [42], are also important, which now leads to the next important topic as follows.

- **Post-treatment of the exhaust gas and utilization of the lithium**

In the field of spent LIB treatment, the occurrence of CO_2, CO, H_2, C_xH_y, or HF is possible, just to name a few [16, 42]. An extensive exhaust gas cleaning system is indispensable for safe handling. However, the composition of the resulting off-gas depends on many aspects. The cathode material, for example, is essential in this respect. LFP is to be emphasized by the contained phosphorus, which is transferred into the gas stream along with Li, as could be shown in this work. In this respect, an important step is utilizing these two critical raw materials. In addition, the pretreatment route is of great importance for the design of the off-gas treatment. The chemical composition of the gas stream can be influenced by premature separation of volatile elements, thus simplifying the process interconnection for the exhaust gas post-treatment. As a basis for implementing a safe and efficient downstream conditioning step, sound knowledge of the reaction sequence inside and, subsequently, outside the reactor is required.

- **Plant engineering optimization and gradual scale-up**

The current state of the technology is classified as TRL3-4 (Technology Readiness Level). This is defined as the confirmation of the technology concept at component level, whereby the functional proof of the technology was provided on a laboratory scale respectively in the pre-pilot plant with the help of the InduMelt system. In order to increase this level to 4, the next step is to develop the system into a continuous feeding system. This means that a feed of the EoL LIB material onto the hot bed must be realized, the exhaust gas post-treatment section and the material discharge have to be designed. Of particular scientific interest in this regard is the influence of kinetics on product quality and productivity due to hot feed versus successive heating, as in this work in batch operation. In order to operate the set-up safely in continuous operation and with a maximum product yield, detailed investigations must be carried out into an optimum crucible material.

- **Development and integration into an overall recycling process**

Even though the InduRed reactor concept shows considerable potential for high valuable metal recovery rates when using EoL battery material, the exclusive consideration of single technology development is too narrowly conceived.

In general, the investigated process interconnection between hydromechanical pretreatment, flotation, and pyrometallurgy shows the importance of a holistically thought recycling process. The fundamental question during the development must be the definition of the further use of the resulting product. The proposed EU guidelines provide percentage recovery rates for the valuable metals but do not specify the type of product utilization.

Essentially, this directive is intended to close the material loop in the EU. Conversely, this also means that the choice of overall process design to compete in the market depends largely on the economic outcome. Of course, from the point of view of a sustainable circular economy, this is not desirable. In addition to political regulations or funding, the market price of the containing valuable metals will significantly influence the choice between product recycling and closed-loop recycling in the future.

Realistically, the overall efficiency and effort required to generate a high-quality product strongly depend on the pretreatment step, regardless of the open- or closed-loop decision. The better the separation of the battery assembly to the active material operates, the less effort is needed in the chemical recycling step, which is an energy and cost-intensive step with any technology usage. Even if the theoretical approach of complete separation is desirable, the technical feasibility and, as a consequence, the economic and ecological viability must always be considered. In this context, the eco-footprint of the overall recycling process must not reasonably exceed that of primary production.

In addition to the question of open- and closed-loop recycling, it must also be defined which product qualities are acceptable and which will subsequently find a market. For this reason, it is of high priority to strive for inclusion in an overall recycling chain during the current expansion stage of the batch plant. This will enable the further development of the pyrometallurgical intermediate step to always consider the upstream and downstream processes. In this way, possible weaknesses of individual technologies can be compensated for in the overall design and immediately addressed in the individual process development. This overall view enables lower costs due to increased efficiency and faster time to market through targeted overall process development toward industrial maturity. Due to the topicality of the subject and the resulting high level of research activity worldwide, the time of market launch, in addition to cost efficiency, will be decisive for success.

References

1. European Commission (11.12.2019), The European Green Deal: COM(2019) 640 final. Available online at https://eur-lex.europa.eu/legal-content/EN/TXT/?qid=1576150542719&uri=COM%3A2019%3A640%3AFIN, checked on 15.01.2023.
2. Intergovernmental panel on climate change, Climate change 2021, IPCC, Geneva, Switzerland, 2021.
3. Intergovernmental panel on climate change, Climate Change 2022, IPCC, Cambridge, UK and New York, USA, 2022.
4. United Nations: Paris (2015), Paris agreement, revised United Nations Framework Convention of Climate Change.
5. Rhodes, C. J., The 2015 Paris Climate Change Conference: COP21, Science progress 99 (2016), Pt 1, 97–104. DOI: 10.3184/003685016X14528569315192.
6. Teske, Achieving the Paris Climate Agreement Goals, Springer International Publishing, Cham, 2019.
7. Pregger, T.; Simon, S.; Naegler, T. and Teske, S., 2019, Main Assumptions for Energy Pathways. In : Achieving the Paris Climate Agreement Goals: Springer, Cham, 93–130. Available online at https://link.springer.com/chapter/10.1007/978-3-030-05843-2_5. DOI: 10.1007/978-3-030-05843-2_5.
8. Lovins, A. B., How big is the energy efficiency resource?, Environ. Res. Lett. 13 (2018), 9, 90401. DOI: 10.1088/1748-9326/aad965.
9. Teske, S.; Pregger, T.; Simon, S.; Naegler, T.; Pagenkopf, J.; Deniz, Ö. et al., It Is Still Possible to Achieve the Paris Climate Agreement: Regional, Sectoral, and Land-Use Pathways, Energies 14 (2021), 8, 2103. DOI: 10.3390/en14082103.
10. Yang, Y.; Bremner, S.; Menictas, C. and Kay, M., Modelling and optimal energy management for battery energy storage systems in renewable energy systems: A review, Renewable and Sustainable Energy Reviews 167 (2022), 112671. DOI: 10.1016/j.rser.2022.112671.
11. Zhao, Y.; Pohl, O.; Bhatt, A. I.; Collis, G. E.; Mahon, P. J.; Rüther, T. and Hollenkamp, A. F., A Review on Battery Market Trends, Second-Life Reuse, and Recycling, Sustainable Chemistry 2 (2021), 1, 167–205. DOI: 10.3390/suschem2010011.
12. World Economic Forum and The Global Battery Alliance (Ed.), 2019, A Vision for a Sustainable Battery Value Chain in 2030: Unlocking the Full Potential to Power Sustainable Development and Climate Change Mitigation. WeForum. Cologny, Switzerland (p. 52).

13. European Parliament (26.09.2006), DIRECTIVE 2006/66/EC OF THE EUROPEAN PARLIAMENT AND OF THE COUNCIL of 6 September 2006 on batteries and accumulators and waste batteries and accumulators and repealing Directive 91/157/EEC: L 266/1. Available online at https://eur-lex.europa.eu/legal-content/EN/TXT/PDF/?uri=CELEX:32006L0066&from=DE, checked on 25.04.2022.
14. European Commission (10.12.2020), Proposal for a Regulation of the European Parliament and of the Council concerning batteries and waste batteries, repealing Directive 2006/66/EC and amending Regulation (EU) 2019/1020: SWD(2020) 334 final. Available online at https://www.parlament.gv.at/PAKT/EU/XXVII/EU/04/37/EU_43776/imfname_11029480.pdf, checked on 21.12.2020.
15. European Commission, REPORT on the proposal for a regulation of the European Parliament and of the Council concerning batteries and waste batteries, repealing Directive 2006/66/EC and amending Regulation (EU) No 2019/1020: COM(2020)0798 – C9-0400/2020 – 2020/0353(COD), revised 22.02.2022. Source: https://www.europarl.europa.eu/doceo/document/A-9-2022-0031_EN.html.
16. Sojka, R.; Pan, Q.; Billman, L. (Eds.), 2020, Comparative study of Lithium-ion battery recycling processes. 25th International Congress for Battery Recycling ICBR 2020. Salzburg, Austria, 16-18 September 2020.
17. World Resources Institute, Climate Watch Historical GHG Emissions, Available online at https://www.climatewatchdata.org/ghg-emissions, checked on 15.01.2023.
18. Hannah Ritchie et al., CO_2 and Greenhouse Gas Emissions, Our World in Data, 2020. Available online at https://ourworldindata.org/emissions-by-sector#citation., checked on 19.01.2023
19. Palacín, M. R. and Guibert, A. de, Why do batteries fail?, Science (New York, N.Y.) 351 (2016), 6273, 1253292. DOI: 10.1126/science.1253292.
20. Pillot, C., 2021, The Rechargeable Battery Market and Main Trends 2020-2030. ICBR 2019 Avicenne Energy, Geneva, 22.09.2021.
21. Martins, L. S.; Guimarães, L. F.; Botelho Junior, A. B.; Tenório, J. A. S. and Espinosa, D. C. R., Electric car battery: An overview on global demand, recycling and future approaches towards sustainability, Journal of environmental management 295 (2021), 113091. DOI: 10.1016/j.jenvman.2021.113091.
22. Lebedeva, N.; Ruiz Ruiz, V.; Bielewski, M.; Blagoeva, D. and Pilenga, A., 2020, Batteries: Technology development report Europäische Gemeinschaften, Luxembourg (Low carbon energy observatory, JRC123165).
23. European Comission, 10 trends reshaping energy and climate, Publications Office of the European Union, Brussels, 2018.
24. Lebedeva et al., Li-ion batteries for mobility and stationary storage applications, Publications Office of the European Union, Luxembourg, 2018.
25. European Commission, IN-DEPTH ANALYSIS IN SUPPORT OF THE COMMISSION COMMUNICATION COM(2018) 773: A Clean Planet for all A Clean Planet for all; A European long-term strategic vision for a prosperous, modern, competitive and climate neutral economy. Source: COM(2018) 773.
26. Degen, F. and Schütte, M., Life cycle assessment of the energy consumption and GHG emissions of state-of-the-art automotive battery cell production, Journal of Cleaner Production 330 (2022), 129798. DOI: 10.1016/j.jclepro.2021.129798.
27. Larcher, D. and Tarascon, J.-M., Towards greener and more sustainable batteries for electrical energy storage, Nature chemistry 7 (2015), 1, 19–29. DOI: 10.1038/nchem.2085.
28. Da Deng, Li-ion batteries: basics, progress, and challenges, Energy Sci Eng 3 (2015), 5, 385–418. DOI: 10.1002/ese3.95.
29. Hanicke, M.; Ibrahim, D.; van de Rijt, A.; Linder, M. and Schaufuss, P., Lithium-ion battery demand 2030: Resilient, sustainable, and circular; McKinsey, Available online at https://www.mckinsey.com/industries/automotive-and-assembly/our-insights/battery-2030-resilient-sustainable-and-circular#/, checked on 17.01.2023.

30. Berckmans, G.; Messagie, M.; Smekens, J.; Omar, N. and Vanhaverbeke, L., Cost Projection of State of the Art Lithium-Ion Batteries for Electric Vehicles Up to 2030, Energies 10 (2017), 9, 1314. DOI: 10.3390/en10091314.

31. Blengini et al., Study on the EU's list of Critical Raw Materials (2020) Final Report, 2020.

32. Xu, C.; Dai, Q.; Gaines, L.; Hu, M.; Tukker, A. and Steubing, B., Future material demand for automotive lithium-based batteries, Commun Mater 1 (2020), 1. DOI: 10.1038/s43246-020-00095-x.

33. Windisch-Kern, S.; Gerold, E.; Nigl, T.; Jandric, A.; Altendorfer, M.; Rutrecht, B. et al., Recycling chains for lithium-ion batteries: A critical examination of current challenges, opportunities and process dependencies, Waste management (New York, N.Y.) 138 (2022), 125–139. DOI: 10.1016/j.wasman.2021.11.038.

34. Korthauer, Handbuch Lithium-Ionen-Batterien, Springer Berlin Heidelberg, Berlin, Heidelberg, 2013.

35. Kurzweil and Dietlmeier, Elektrochemische Speicher, Springer Vieweg, Wiesbaden, 2015.

36. Georgi-Maschler, T.; Friedrich, B.; Weyhe, R.; Heegn, H. and Rutz, M., Development of a recycling process for Li-ion batteries, Journal of Power Sources 207 (2012), 173–182. DOI: 10.1016/j.jpowsour.2012.01.152.

37. Arnberger, A.; Coskun, E. and Rutrecht, B., 2018, Recycling von Lithium-Ionen-Batterien. In Stephanie Thiel, Elisabeth Thomé-Kozmiensky, Daniel Goldmann (Eds.): Recycling und Rohstoffe. Nietwerder: TKh2018.

38. Madian, M.; Eychmüller, A. and Giebeler, L., Current Advances in TiO2-Based Nanostructure Electrodes for High Performance Lithium Ion Batteries, Batteries 4 (2018), 1, 7. DOI: 10.3390/batteries4010007.

39. Windisch-Kern, S., Evaluation of the suitability of an inductively heated carbon bed reactor for the pyrometallurgical recycling of lithium-ion batteries, Doctoral Thesis Montanuniversitaet Leoben, Leoben, 2022.

40. Feng, X.; Ouyang, M.; Liu, X.; Lu, L.; Xia, Y. and He, X., Thermal runaway mechanism of lithium ion battery for electric vehicles: A review, Energy Storage Materials 10 (2018), 246–267. DOI: 10.1016/j.ensm.2017.05.013.

41. Pan, Q.; Weyhe, R.; Melber, A.; Klavina, I. and Friedrich, B., 2014, Packaging Materials for Li-Ion Batteries. DOI: 10.13140/RG.2.1.1607.8320

42. Diaz, F.; Wang, Y.; Weyhe, R. and Friedrich, B., Gas generation measurement and evaluation during mechanical processing and thermal treatment of spent Li-ion batteries, Waste management (New York, N.Y.) 84 (2019), 102–111. DOI: 10.1016/j.wasman.2018.11.029.

43. Windisch-Kern, S.; Holzer, A.; Ponak, C. and Raupenstrauch, H., Pyrometallurgical Lithium-Ion-Battery Recycling: Approach to Limiting Lithium Slagging with the InduRed Reactor Concept, Processes 9 (2021), 1, 84. DOI: 10.3390/pr9010084.

44. Yao, Y.; Zhu, M.; Zhao, Z.; Tong, B.; Fan, Y. and Hua, Z., Hydrometallurgical Processes for Recycling Spent Lithium-Ion Batteries: A Critical Review, ACS Sustainable Chem. Eng. 6 (2018), 11, 13611–13627. DOI: 10.1021/acssuschemeng.8b03545.

45. Meshram, P.; Abhilash; Pandey, B. D.; Mankhand, T. R. and Deveci, H., Comparision of Different Reductants in Leaching of Spent Lithium Ion Batteries, JOM 68 (2016), 10, 2613–2623. DOI: 10.1007/s11837-016-2032-9.

46. Ghassa, S.; Farzanegan, A.; Gharabaghi, M. and Abdollahi, H., Novel bioleaching of waste lithium ion batteries by mixed moderate thermophilic microorganisms, using iron scrap as energy source and reducing agent, Hydrometallurgy 197 (2020), 105465. DOI: 10.1016/j.hydromet.2020.105465.

47. Mishra, D.; Kim, D.-J.; Ralph, D. E.; Ahn, J.-G. and Rhee, Y.-H., Bioleaching of metals from spent lithium ion secondary batteries using Acidithiobacillus ferrooxidans, Waste management (New York, N.Y.) 28 (2008), 2, 333–338. DOI: 10.1016/j.wasman.2007.01.010.

48. Xin, Y.; Guo, X.; Chen, S.; Wang, J.; Wu, F. and Xin, B., Bioleaching of valuable metals Li, Co, Ni and Mn from spent electric vehicle Li-ion batteries for the purpose of recovery, Journal of Cleaner Production 116 (2016), 249–258. DOI: 10.1016/J.JCLEPRO.2016.01.001.

49. Zeng, G.; Deng, X.; Luo, S.; Luo, X. and Zou, J., A copper-catalyzed bioleaching process for enhancement of cobalt dissolution from spent lithium-ion batteries, Journal of hazardous materials 199-200 (2012), 164–169. DOI: 10.1016/j.jhazmat.2011.10.063.

50. Zeng, G.; Luo, S.; Deng, X.; Li, L. and Au, C., Influence of silver ions on bioleaching of cobalt from spent lithium batteries, Minerals Engineering 49 (2013), 40–44. DOI: 10.1016/J.MINENG.2013.04.021.

51. Bahaloo-Horeh, N.; Mousavi, S. M. and Baniasadi, M., Use of adapted metal tolerant Aspergillus niger to enhance bioleaching efficiency of valuable metals from spent lithium-ion mobile phone batteries, Journal of Cleaner Production 197 (2018), 1546–1557. DOI: 10.1016/j.jclepro.2018.06.299.

52. Heydarian, A.; Mousavi, S. M.; Vakilchap, F. and Baniasadi, M., Application of a mixed culture of adapted acidophilic bacteria in two-step bioleaching of spent lithium-ion laptop batteries, Journal of Power Sources 378 (2018), 19–30. DOI: 10.1016/J.JPOWSOUR.2017.12.009.

53. Vest, M., Weiterentwicklung des pyrometallurgischen IME Recyclingverfahrens für Li-Ionen Batterien von Elektrofahrzeugen, Dissertation RWTH Aachen; Shaker Verlag GmbH.

54. Zheng, X.; Zhu, Z.; Lin, X.; Zhang, Y.; He, Y.; Cao, H. and Sun, Z., A Mini-Review on Metal Recycling from Spent Lithium Ion Batteries, Engineering 4 (2018), 3, 361–370. DOI: 10.1016/j.eng.2018.05.018.

55. Nasser, O. A. and Petranikova, M., Review of Achieved Purities after Li-ion Batteries Hydrometallurgical Treatment and Impurities Effects on the Cathode Performance, Batteries 7 (2021), 3, 60. DOI: 10.3390/batteries7030060.

56. Nayaka, G. P.; Manjanna, J.; Pai, K. V.; Vadavi, R.; Keny, S. J. and Tripathi, V. S., Recovery of valuable metal ions from the spent lithium-ion battery using aqueous mixture of mild organic acids as alternative to mineral acids, Hydrometallurgy 151 (2015), 73–77. DOI: 10.1016/j.hydromet.2014.11.006.

57. Liu, C.; Lin, J.; Cao, H.; Zhang, Y. and Sun, Z., Recycling of spent lithium-ion batteries in view of lithium recovery: A critical review, Journal of Cleaner Production 228 (2019), 801–813. DOI: 10.1016/j.jclepro.2019.04.304.

58. Huang, B.; Pan, Z.; Su, X. and An, L., Recycling of lithium-ion batteries: Recent advances and perspectives, Journal of Power Sources 399 (2018), 274–286. DOI: 10.1016/j.jpowsour.2018.07.116.

59. Yin, H. and Xing, P., Pyrometallurgical Routes for the Recycling of Spent Lithium-Ion Batteries. Vol. 4, 57–83. DOI: 10.1007/978-3-030-31834-5_3.

60. Elwert, T. and Frank, J., 2020, Auf dem Weg zu einem geschlossenen Stoffkreislauf für Lithium-Ionen-Batterien. In Olaf Holm, Elisabeth Thomé-Kozmiensky, Daniel Goldmann, Bernd Friedrich (Eds.): Recycling und Rohstoffe. Neuruppin: Thomé-Kozmiensky Verlag GmbH, 525–530.

61. Horn, D.; Zimmermann, J.; Gassmann, A.; Stauber, R. and Gutfleisch, O., 2019, Battery Recycling: Focus on Li-ion Batteries. In Peter Birke (Ed.): Modern battery engineering. A comprehensive introduction. New Jersey, London, Singapore, Beijing, Shanghai, Hong Kong, Taipei, Chennai, Tokyo: World Scientific, 223.

62. Öhl, J.; Horn, D.; Zimmermann, J.; Stauber, R. and Gutfleisch, O., Efficient Process for Li-Ion Battery Recycling via Electrohydraulic Fragmentation, MSF 959 (2019), 74–78. DOI: 10.4028/www.scientific.net/MSF.959.74.

63. Mossali, E.; Picone, N.; Gentilini, L.; Rodrìguez, O.; Pérez, J. M. and Colledani, M., Lithium-ion batteries towards circular economy: A literature review of opportunities and issues of recycling treatments, Journal of environmental management 264 (2020), 110500. DOI: 10.1016/j.jenvman.2020.110500.

64. Cordis, Recovery of Phosphorus from Sewage Sludge and Sewage Sludge Ashes with the thermo-reductive RecoPhos-Process | RECOPHOS Project | Fact Sheet | FP7 | CORDIS | European Commission, Available online at https://cordis.europa.eu/project/id/282856, checked on 14.01.2023.

65. Ponak, C., Carbo-thermal reduction of basic oxygen furnace slags with simultaneous removal of phosphorus via the gas phase, Dissertation Montanuniversitaet Leoben, Leoben, 2019.

66. Schönberg, A., Mathematical modeling of metallurgical processes - inductive heating of a graphite packed bed, Doctoral Thesis Montanuniversitaet Leoben, Leoben, 2014.

67. Holzer, A., Pyrometallurgisches Recycling von Aktivmaterial aus der Aufbereitung von Lithium-Ionen-Batterien in einem induktiv beheizten Schüttschichtreaktor, Master Thesis Montanuniversitaet Leoben, Leoben, 2019.

68. Holzer, A.; Windisch-Kern, S.; Ponak, C. and Raupenstrauch, H., A novel pyrometallurgical recycling process for Lithium-Ion-Batteries and its use in recycling LCO and LFP, Metals 2021 (2021), 11(1), 149. DOI: 10.3390/met11010149.

69. Holzer, A.; Wiszniewski, L.; Windisch-Kern, S. and Raupenstrauch, H., Optimization of a Pyrometallurgical Process to Efficiently Recover Valuable Metals from Commercially Used Lithium-Ion Battery Cathode Materials LCO, NCA, NMC622, and LFP, Metals 12 (2022), 10, 1642. DOI: 10.3390/met12101642.

70. Windisch-Kern, S.; Holzer, A.; Wiszniewski, L. and Raupenstrauch, H., Investigation of Potential Recovery Rates of Nickel, Manganese, Cobalt, and Particularly Lithium from NMC-Type Cathode Materials (LiNixMnyCozO2) by Carbo-Thermal Reduction in an Inductively Heated Carbon Bed Reactor, Metals 11 (2021), 11, 1844. DOI: 10.3390/met11111844.

71. Holzer, A.; Baldauf, M.; Wiszniewski, L.; Windisch-Kern, S. and Raupenstrauch, H., Influence of Impurities on the High-Temperature Behavior of the Lithium-Ion Battery Cathode Material NMC Under Reducing Conditions for Use in the InduRed Reactor Concept, Detritus (2022). DOI: 10.31025/2611-4135/2022.15215.

72. Holzer, A.; Zimmermann, J.; Wiszniewski, L.; Necke, T.; Gatschlhofer, C.; Öfner, W. and Raupenstrauch, H., A Combined Hydro-Mechanical and Pyrometallurgical Recycling Approach to Recover Valuable Metals from Lithium-Ion Batteries Avoiding Lithium Slagging, Batteries 9 (2023), 1, 15. DOI: 10.3390/batteries9010015.

73. Panasiuk, D.; Daigo, I.; Hoshino, T.; Hayashi, H.; Yamasue, E.; Tran, D. H. et al., International comparison of impurities mixing and accumulation in steel scrap, J of Industrial Ecology 26 (2022), 3, 1040–1050. DOI: 10.1111/jiec.13246.

74. Kwon, O. and Sohn, I., Fundamental thermokinetic study of a sustainable lithium-ion battery pyrometallurgical recycling process, Resources, Conservation and Recycling 158 (2020), 104809. DOI: 10.1016/j.resconrec.2020.104809.

75. Abegg, R.; Auerbach, F. (Eds.), 1908, Handbuch der Anorganischen Chemie: Zweiter Band, Erste Abteilung. 4 volumes, Leipzig (2). Available online at https://archive.org/details/handbuchderanor00koppgoog/page/135/mode/1up?view=theater, checked on 27.04.2022.

Appendix A: Publications

Publication 1

A novel pyrometallurgical recycling process for Lithium-Ion-Batteries and its use in recycling LCO and LFP

Holzer, A.; Windisch-Kern, S.; Ponak, C.; Raupenstrauch, H., Metals 2021 (2021), 11(1), 149. DOI: https://doi.org/10.3390/met11010149.

Publication 2

Optimization of a Pyrometallurgical Process to Efficiently Recover Valuable Metals from Commercially Used Lithium-Ion Battery Cathode Mate-rials LCO, NCA, NMC622, and LFP

Holzer, A.; Wiszniewski, L.; Windisch-Kern, S. and Raupenstrauch, H., Metals 12 (2022), 10, 1642. DOI: https://doi.org/10.3390/met12101642.

Publication 3

Influence of Impurities on the High-Temperature Behavior of the Lithium-Ion Battery Cathode Material NMC Under Reducing Conditions for Use in the InduRed Reactor Concept

Holzer, A.; Baldauf, M.; Wiszniewski, L.; Windisch-Kern, S. and Raupenstrauch, H., Detritus (2022). DOI: https://doi.org/10.31025/2611-4135/2022.15215.

Publication 4

A Combined Hydro-Mechanical and Pyrometallurgical Recycling Approach to Recover Valuable Metals from Lithium-Ion Batteries Avoiding Lithium Slagging

Holzer, A.; Zimmermann, J.; Wiszniewski, L.; Necke, T.; Gatschlhofer, C.; Öfner, W. and Raupenstrauch, H., Batteries 9 (2023), 10. DOI: https://doi.org/10.3390/batteries9010015.

6.1 Publication 1

A novel pyrometallurgical recycling process for Lithium-Ion-Batteries and its use in recycling LCO and LFP

Holzer, A.; Windisch-Kern, S.; Ponak, C.; Raupenstrauch, H.

Article Information:

Journal	Metals, Volume 11, Issue 1
Section	Extractive Metallurgy
Special Issue	New Science Based Concepts for Increased Efficiency in Battery Recycling 2020
Pages	22
Received Date	11 December 2020
Revised Date	31 December 2020
Accepted Date	11 January 2021
Published Date	14 January 2021
DOI	https://doi.org/10.3390/met11010149

Author's contribution: Conceptualization, Methodology, Investigation, Resources, Writing – original draft preparation, Writing – review and editing, Visualization

metals

MDPI

Article

A Novel Pyrometallurgical Recycling Process for Lithium-Ion Batteries and Its Application to the Recycling of LCO and LFP

Alexandra Holzer *, Stefan Windisch-Kern, Christoph Ponak and Harald Raupenstrauch

Chair of Thermal Processing Technology, Montanuniversitaet Leoben, Franz-Josef-Strasse 18, 8700 Leoben, Austria; stefan.windisch-kern@unileoben.ac.at (S.W.-K.); christoph.ponak@unileoben.ac.at (C.P.); harald.raupenstrauch@unileoben.ac.at (H.R.)

* Correspondence: alexandra.holzer@unileoben.ac.at; Tel.: +43-3842-402-5803

Abstract: The bottleneck of recycling chains for spent lithium-ion batteries (LIBs) is the recovery of valuable metals from the black matter that remains after dismantling and deactivation in pre-treatment processes, which has to be treated in a subsequent step with pyrometallurgical and/or hydrometallurgical methods. In the course of this paper, investigations in a heating microscope were conducted to determine the high-temperature behavior of the cathode materials lithium cobalt oxide (LCO—chem., $LiCoO_2$) and lithium iron phosphate (LFP—chem., $LiFePO_4$) from LIB with carbon addition. For the purpose of continuous process development of a novel pyrometallurgical recycling process and adaptation of this to the requirements of the LIB material, two different reactor designs were examined. When treating LCO in an Al_2O_3 crucible, lithium could be removed at a rate of 76% via the gas stream, which is directly and purely available for further processing. In contrast, a removal rate of lithium of up to 97% was achieved in an MgO crucible. In addition, the basic capability of the concept for the treatment of LFP was investigated whereby a phosphorus removal rate of 64% with a simultaneous lithium removal rate of 68% was observed.

Keywords: lithium-ion batteries (LIBs); recycling; pyrometallurgy; critical raw materials; lithium removal; phosphorous removal; recovery of valuable metals

Citation: Holzer, A.; Windisch-Kern, S.; Ponak, C.; Raupenstrauch, H. A Novel Pyrometallurgical Recycling Process for Lithium-Ion Batteries and Its Application to the Recycling of LCO and LFP. *Metals* **2021**, *11*, 149. https://doi.org/10.3390/met11010149

Received: 11 December 2020
Accepted: 11 January 2021
Published: 14 January 2021

1. Introduction

The development of lithium-ion batteries (LIBs) has experienced an enormous upswing in recent years, which is, in addition to portable devices, mainly due to the steadily increasing demand in the electric vehicle (EV) sector. According to forecasts, this trend will continue in the coming years [1,2]. Further prognoses predict that sales of LIBs are expected to increase from 160 GWh in 2018 to over 1.2 TWh in 2030 [1]. Their use in electrical appliances, EVs and stationary storage is due to their advantages over other storage media, such as high energy density, long service life and high operating voltage [3,4]. Since consumed LIBs contain a large number of valuable metals, recycling has a considerable environmental impact in view of the conservation of valuable resources [5]. In addition to this idea of resource protection, waste reduction and the energy-efficient and economical treatment of hazardous substances are also driving recycling efforts [6]. The timeliness and necessity of recycling LIBs is further underlined by the 2020 list of critical raw materials published by the European Commission. Among others, cobalt, lithium and phosphorus can be found [7].

A major challenge with regard to recycling is posed by the strongly fluctuating waste stream. This is the product of the requirements of the countless applications for energy storage and the resulting multitude of electrode materials of LIBs [8]. In the respective literature there is a variety of different recycling processes, which can basically be divided into preparation for recycling, pre-treatment and main processing, including pyro- and hydro-metallurgy. In the first mentioned area, the processes of discharging and dismantling can be found [5]. The aim of the pre-treatment is to improve the recovery rate, to adapt

the waste stream to the downstream process step and to reduce the energy consumption of the following pyro- or hydro-metallurgical process [6,9]. In Europe, there are several companies that already perform the preparation and pre-treatment of spent LIBs on a larger scale, like Accurec Recycling GmbH, Duesenfeld GmbH or Redux GmbH [10–12]. The latter starts the recycling process with collection and temporary storage, followed by manual sorting. As of this point in time there is still a considerable safety risk due to the residual charge of the LIBs. They are completely discharged, and the energy gained is fed back into the operating network. Subsequently, components such as electronics, cables, plastics, aluminum, and iron are dismantled and sorted. During the subsequent deactivation, the coating of the conductor foils is dissolved and the separator as well as the electrolyte are removed. During the mechanical treatment, the remaining components such as iron, aluminum, copper and the fine material (also called active material or black matter) of cathode and anode material are separated. The separation of the individual fractions is carried out with a magnetic separator, air separator and sieving [13]. The resulting black matter can be further treated in a pyro- or hydro-metallurgical process.

In pyrometallurgical treatment of LIBs, the physiochemical transformation temperatures above 1400 °C are used to recover the valuable metals [14]. As a partial step in an overall process, pyrometallurgy is a suitable instrument for purifying the feed stream of substances undesirable for hydrometallurgy. Fluorine, chlorine, graphite, phosphorus, etc., pose a particular challenge to hydrometallurgy. Pyrometallurgical processes are generally robust against impurities and organic contaminants, because volatile components can be evaporated [5]. Graphite from the anode can be used as a reducing agent and burned in various processes in the presence of oxygen, thus helping to maintain the process temperature. Since the reaction kinetics in pyrometallurgical processes increase extremely due to the high temperatures, productivity is higher compared to hydrometallurgy [15]. Although the large number of research activities in recent years has focused on hydrometallurgy [9], there is significant scientific output in the field of pyrometallurgy, some of which is already being applied on an industrial scale. Several recent reports claim that large-scale pyrometallurgical processes have greater potentials in terms of sustainability than their hydrometallurgical counterparts [16–21]. Industrial scale processes are those that have more than 1000 t/a recycling capacity. In Europe, the companies Umicore, Accurec and Nickelhütte Aue should be mentioned here, and outside the EU, for example, SungEel, Kyoei Seiko and Dowa. The overall processes usually lead via a mechanical and/or thermal step to pyro- and hydro-metallurgy [5]. The pyrometallurgical step is typically based on shaft furnaces or electric arc furnaces for melting this feedstock [22]. A direct comparison of the recycling efficiency of the individual processes is often very difficult, since the reference basis of the values given is usually not given or only partially given. However, it can be stated that recycling routes which include a pyrometallurgical step have the highest overall recycling efficiency, in some cases exceeding 50% [5]. Since pyrometallurgical processes are operated at high temperatures, their energy requirements are correspondingly high. In addition, large quantities of waste gas are produced which have to be treated. A disadvantage of current pyrometallurgical processes is the slagging of lithium, the recovery of which in turn requires an enormous hydrometallurgical effort [9,23]. The economic efficiency of lithium recovery depends on the concentration in the slag. As a rule, in the co-processing of LIBs in metallurgical plants, the lithium is diluted to such an extent that recovery is not economically feasible [24]. In recent years, a number of advances have been made in the field of slag post-treatment. These research ventures on a non-industrial scale focus, for example, on the concentration of Li in the slag by selective addition of slag-forming agents during the pyrometallurgical process and subsequent hydrometallurgical treatment [25,26]. Recent progress has also been made in the area of early-stage lithium extraction. In this process, sulphate roasting treatment was used to convert the cathode material from NMC batteries into a water-soluble lithium sulphate (Li_2SO_4) and a water-insoluble oxide (NiCoMn-oxide) [5]. However, depending on the price of lithium, processes specially developed for LIB recycling may in future be

quite economical in terms of lithium recovery [24]. Various advantages and disadvantages also result from the different interconnection types of the overall process. For example, the primary energy consumption via pyrometallurgical routes is higher, but the resulting additional costs are more than compensated by lower operating costs in the hydrometallurgical step [5]. The recycling of P from LIBs is described in the literature in very few publications. Most of them are related to the hydrometallurgical process route, other processes deal with the regeneration of the cathode material [27].

Hydrometallurgical processes are highly selective and can therefore achieve high purities [15]. Leaching is the key process in hydrometallurgy to convert the metals to ions in a solution. This can be divided into bio leaching with metabolic excrements of microorganisms or fungi and chemical leaching with organic or inorganic acids [28–30]. Subsequently, the valuable metals are separated and recovered from the leaching solution. Since the structure of the leaching solution is complicated, it is usually necessary to use several different methods from the portfolio of solvent extraction, chemical precipitation and electrochemical deposition [28]. Hydrometallurgical methods result in extremely good recycling rates of up to 100% [28,31]. They also require a high level of equipment and a large number of process steps, which usually results in a correspondingly high volume of polluted wastewater. In order to operate the process economically, it is very important to separate and concentrate as many metals and impurities as possible in advance. For each additional metal, at least 1–2 additional process steps would be required, which is only economical if the metal value or quantity is correspondingly high [15].

Especially with regard to the raw materials contained in LIBs, which are included in the list of critical raw materials of the European Commission [7], and from an ecological point of view, a sustainable handling of spent LIBs is essential. According to Elwert et al. [32], recycling processes specialized in LIBs will gain more and more importance in the future. This is due to the increasing rate of return of spent LIBs to the waste stream, more regulations by the authorities and also decreasing amounts of valuable nickel and cobalt for direct use in nickel and cobalt producing plants. Furthermore, the growing market for LFP and the increasing interest in lithium recovery also plays a major role. Of particular importance in terms of regulation is the recently published European Commission proposal to revise EU Directive 2006/66/EC, which sets recovery rates of up to 70% for Li and 95% for other valuable metals such as Co, Ni and Cu by 2030 [33], which forces recyclers to increase recovery rates and their process efficiency.

It can be summarized that there is a multitude of different recycling processes and methods, which are characterized by their positive properties in certain areas but also have individual disadvantages. In the field of pyrometallurgy, lithium slagging and in particular the absence of possibilities to recover from the slag with reasonable effort can be identified as a bottleneck.

The novel pyrometallurgical recycling process presented in this paper is characterized by the recovery of an alloy with a simultaneous utilization of lithium and phosphorus via the gas flow. The following points provide a more detailed insight into the theoretical considerations and practical implementations for the most efficient recovery of valuable metals from LIBs using this process. Initially, appropriate analyses were carried out to better understand the behavior of cathode materials in high-temperature applications under reducing conditions. To determine the lithium removal rate without the presence of phosphorus, the cathode material lithium cobalt oxide (LCO) was examined in an experiment. In addition to the successive optimization of the reactor concept and adaptation to the waste stream from spent LIBs, another experiment with LCO in a modified setup was performed and compared to the previous one. To verify the basic suitability of the pyrometallurgical apparatus for the simultaneous removal of phosphorus and lithium via the gas flow, experiments were carried out with the cathode material lithium iron phosphate (LFP).

2. Process Concept and Methods

2.1. Used Materials

In total, three different experiments were carried out with two types of feedstock. As Windisch-Kern et al. [34] have already described, experiments with black mass from a pre-processing step have already shown that lithium could be removed to a considerable extent. As this has raised additional questions, a detailed investigation of the pure cathode materials, i.e., LCO, lithium nickel manganese cobalt oxide (NMC—chem., $LiNi_{0.33}Mn_{0.33}Co_{0.33}O_2$), lithium nickel cobalt aluminum oxide (NCA—chem., $LiNi_{0.8}Co_{0.15}Al_{0.05}O_2$) and LFP, was indispensable. For the purpose of clarifying the questions dealt with in this paper, the materials LCO and LFP were used, which were produced by the Chinese company Gelon Energy Corporation. The appearance of this feedstock can be described as a fine, black powder. Since this carbo-thermal process requires a reducing agent and the graphite bed in the reactor is only used for energy input, graphite powder from coke pellets of a steel mill is added. The graphite cubes with a side length of 2.5 cm come from electrodes of a steel mill and have an average purity of 99% with an electrical resistance of 4–8 µ Ωm and a density of 1.55–1.75 g cm^{-3}. [35] The amount of graphite powder required for the reduction was determined by stoichiometry of the respective cathode material. For this purpose, the weighed mass of the cathode material was multiplied by the molar ratio of $LiCoO_2$ or $LiFePO_4$. After determining the moles O by multiplying the mass O by the relative atomic mass of O, the necessary mass of C was calculated by using the relative mass of C and assuming that a conversion to CO takes place in the reactor. The corresponding percentage C requirement is finally obtained by a rule of three of the masses of O and C. Table 1 shows the composition of the input materials determined from their stoichiometric composition.

Table 1. Composition of the mixture of cathode material and graphite powder in wt.%.

Compound	Li	Co	Fe	P	C
LCO-C	5.67	48.17	-	-	20.00
LFP-C	3.34	-	26.90	14.92	24.00

The products obtained from the experiments were examined by ICP-OES and ICP-MS by means of aqua regia digestion according to ÖNORM EN 13657:2002-12.

2.2. Material Specific Investigations

Since the behavior of the individual cathode materials at high temperature applications is hardly or not at all described in the literature, detailed investigations were undertaken at the Chair of Thermal Processing Technology. These included analyses in a Hesse Instruments EM 201 with an HR18-1750/30 furnace heating microscope. The results should be used for planning the process control in the following experiments in the inductively heated reactor, which is presented in Section 2.3. Furthermore, a better understanding of the behavior of the cathode materials should be gained. To be able to simulate the planned process as detailed as possible, graphite powder was added to the cathode material. The addition of graphite powder was carried out to an extent of 10 wt.% under the assumption that C is converted to CO_2 and transported away via the argon-purged atmosphere. The mixture of the corresponding cathode material and graphite powder was examined with at least one reproduction experiment. For better comparability a uniform heating rate was always set, which corresponds to the maximum possible with the heating microscope used. This is primarily to ensure the shortest possible residence time in the furnace chamber since interactions of LCO with the furnace material consisting of Al_2O_3 have been determined and damage to this should be prevented as far as possible. Up to a temperature of 1350 °C, a heating rate of 80 °C/min was selected, from 1350 to 1450 °C 50 °C/min and up to 1700 °C a heating rate of 10 °C/min with a holding time of 15 min at 1700 °C was dialed. To avoid oxidation with the ambient air, the reactor was flushed with argon at a flow rate

of 2 L/min. A maximum furnace temperature of 1700 °C was chosen, which allows for an approximate sample temperature of 1630 °C.

Figure 1 illustrates the standardized sample preparation. The material is centrally positioned in a cylinder with a diameter of 3.5 mm and a height of 2.5 mm on an Al_2O_3 platelet with an approximate weight of 0.1 g.

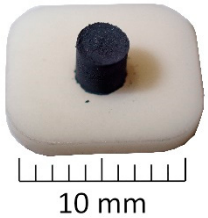

Figure 1. Structure of the sample on the white sample plate made of Al_2O_3 before the trial.

2.3. Reactor Concept

The novel reactor concept, which was constructed at the Chair of Thermal Processing Technology of the Montanuniversitaet Leoben, is based on the inductive heating of graphite pieces in a packed bed reactor. The cornerstone of knowledge generation in this field was laid at the chair already in 2012, by the EU subsidized project RecoPhos for the pyrometallurgical treatment of sewage sludge ash for simultaneous recovery of phosphorus and the contained valuable metals. Its results are described by Schönberg et al. [36] and Samiei et al. [37]. Based on this and corresponding follow-up projects, also in the field of basic oxygen furnace slag (BOFS) treatment, a batch operated post-lab-scale plant and a pilot-scale plant as a continuous process have been developed and built. This knowledge advantage was used to adapt the mechanism for pyrometallurgical recovery of valuable metals from processed LIB material in two ways. On the one hand, the theoretical idea of the continuous reactor, which should be conceptually similar to the set-up from research work in the field of sewage sludge ash and BOFS utilization, is applied. On the other hand, the post-lab-scale setup developed in the subject area mentioned above can initially be used for first experiments without further adaptations. In the long term, the realization of larger scales and corresponding throughput of recycled material as a continuous unit is planned. Intensive research activities on a small scale are indispensable for the most efficient implementation of gradual scale-ups to industrial maturity. In view of the process development as well as the knowledge gained about the input material, the previously mentioned apparatus in batch operation, the so-called InduMelt plant, is used for this purpose. These two process concepts and their respective challenges and developments are explained in detail below.

2.3.1. Continuous Reactor Concept

In order to treat the expected future waste stream from used LIBs, a technology with correspondingly high throughput rates is required. The currently pursued approach at the Chair of Thermal Processing Technology is based on a continuous reactor concept which currently exists as a pilot plant with a material throughput rate of 10 kg/h. Even if, according to initial findings from investigations of the LIB black matter, the design must differ from that used for sewage sludge ash and BOFS, the basic principle remains the same. Ponak [38] describes the so-called InduRed reactor as an cylindrical arrangement of refractory materials filled with pieces of electrode graphite which allow a horizontal and radial homogeneous temperature distribution when heated by the induction coils, as seen in Figure 2.

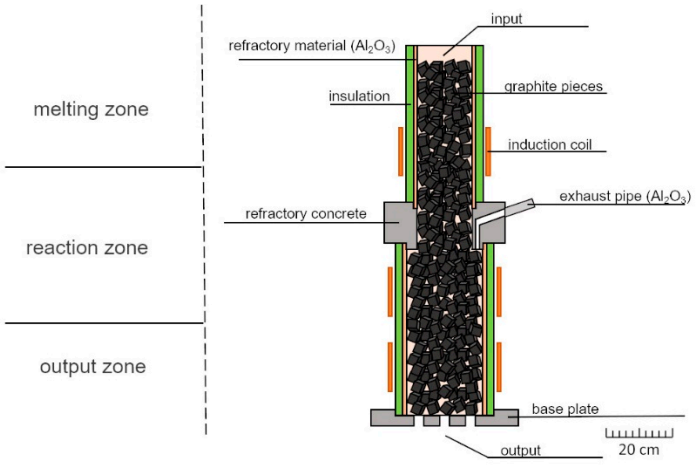

Figure 2. Schematic illustration of the InduRed reactor for the continuous treatment of sewage sludge ashes and BOFS [39].

The process starts with the material feed from a feed vessel above the reactor via a screw conveyor and a low volume of argon. Inert gas purging is highly relevant at this position, especially at higher temperatures, as the graphite bed is protected against oxidation by possible false air and, mainly, to direct small ash or black matter particles directly onto the graphite surface. In the first zone, the melting zone, the fine-grained material inserted is heated to melting temperature without reaching the reduction temperature of the critical component phosphorus. The resulting molten film then moves through the reactor to the reduction zone. In this zone the corresponding energy is induced so that the reduction temperature is reached close to the implemented gas flue. At this point, it has to be mentioned that the graphite pieces are not supposed to participate in the reduction reactions and serve only as a susceptor material. Added carbon powder functions as a reductant. Through this reaction process, phosphorus is converted into the gaseous phase and can be removed directly from the reactor via the gas flue by means of a negative pressure-generating induced draft fan. Downstream there is a post-combustion chamber in which external air or oxygen are used to convert elemental phosphorus to P_2O_5. The subsequent hydrolysis finally enables the production of phosphoric acid. The remaining material in the reactor moves on to the discharge zone, where the third and last coil provides enough energy that the phosphorus-free material does not reach the solidification temperature and finally leaves the reactor via the reactor floor. The resulting material can be divided into a metal and a slag fraction, which, however, are not yet separated from each other in the current expansion stage and are collected in a vessel below the reactor output.

The advantages of this apparatus are manifold. In comparison with an electric arc furnace (EAF), no molten bath of metal is formed so that the P_2 (g)–Fe (l) contact possibility and in further consequence the formation of iron phosphide can be decreased immensely. This fact is promoted by a thin molten film, which massively shortens the distance of mass transport. In this case it is particularly important for the diffusion of P and its removal as gas. The graphite pieces offer a large surface area for reactions and by coupling into the induction field, the heat for the endothermic reduction reactions is permanently provided directly at the respective particle surface. Even if the energy demand is increased, the main form of the reduction reaction is direct reduction, resulting in a lower carbon demand. [38] In the course of the reaction processes in the reactor, a very low oxygen partial pressure and a correspondingly high CO to CO_2 ratio is established, which in turn promotes the reduction reactions [40].

In order to use this process also for the waste stream from spent LIBs, the reactor design and the corresponding post-treatment of the output streams must be adapted. The input material for the planned continuous process comes from a pre-treatment plant, which is a fine fraction as low in Cu and Al as possible consisting of a mixture of cathode and

anode materials. After being fed into the pyrometallurgical reactor, the material should react according to the principle described above. The most important difference is that the idea of the treatment of this material is to remove not only phosphorus but also lithium from the reactor via the gas flow. An initial concept for the post-treatment of the liquid fraction, which leaves the reactor chamber via its bottom, provides for an oxygen inlet. Thus, in accordance with the different oxygen affinities, for example, the input stream of NMC, LCO, NCA and LFP should result in the purest possible CoNiFe alloy. Oxygen-affine elements such as Mn and Al, as well as the residues of P and Li that are not removed via the gas phase, are to be slagged. The resulting products can therefore either be sold on the market as raw materials as required, or further broken down into their constituent parts in further post-treatment steps, for example via the hydrometallurgical route. A further additional important step to be investigated is the post-treatment of the resulting gas fraction. In particular, it will be necessary to implement a corresponding process for the separation of Li and P and consequently to treat them further according to the resulting qualities. As the points just described show, a combination with other processes should be aimed for. With regard to the overall reactor design, an adaptation of the current development will be essential. This includes issues such as the optimal refractory material for the reactor wall or a possible need to expand the gas extraction system.

2.3.2. Batch Reactor Concept

Based on the technology described in Section 2.3.1, the process design shall be adapted to the requirements of the black matter out of LIBs. For this purpose, in-depth tests were carried out for a better understanding of the material to be processed, which are partly described in Windisch-Kern et al. [34]. Since the scale of a continuous pilot plant for experiments of this kind would firstly be too complex and secondly would not correspond to the research status at the Chair of Thermal Processing Technology in the LIB field, the experiments were carried out on a post-laboratory scale. For this purpose, the reactor concept of the unit operating in batch mode was adopted from the developments in the field of sewage sludge ash and BOFS, as shown in Figure 3a and hereinafter referred to as Design 1. The system behind it is similar to the continuous concept, with the difference that the material to be investigated is already in the reactor at the beginning of the experiment and there is no material output via the ground. Most of the material melted during the experiment is accumulated and collected at the bottom of the reactor or adheres to the cube surface as spherical formations. In addition, the gas outlet is also not subjected to negative pressure, so that the resulting gases leave the reactor without constraint. For the construction of the reactor, an Al_2O_3 ring with a diameter of 20 cm, Al_2O_3 mortar and refractory concrete were used. The graphite bed provides a cube surface of 1725 cm^2 for the transfer of the induced heat. An insulation around the reactor has the function of the protection of the induction coil, to reduce the heat losses and to enable as good a separation as possible from ambient air.

To enable a qualitative measurement of the exhaust gas flow, a gas scrubber was additionally installed at the outlet of the gas flue (Figure 3b). This was realized with a bubbling frit in which the exhaust gas is enriched in a 2.5 molar H_2SO_4 solution. The temperature was measured on the outside of the reactor by two category S-thermocouples and inside the reactor by two category K-thermocouples. Due to the expected breakage of the second mentioned thermocouples, they are only used to find a correlation between the outside temperature and the inside temperature.

Preliminary tests have shown that LCO, with its high cobalt content, is highly reactive to the crucible material of Al_2O_3. In addition, sampling proved to be particularly difficult because it was not possible to separate the black mass clearly from the mortar. This makes it almost impossible to close the mass balance in the future. Another disadvantageous fact of this reactor concept is that, due to its position, the highest induction of the current takes place in the upper part of the reactor. Because of the inevitable turbulence in the reactor during the experiment due to the gases, the material accumulates at the bottom of the

reactor, so the energy supply position is suboptimal. To take into account the mentioned disadvantages, a new design was developed, which is shown in Figure 4 and hereinafter referred to as Design 2.

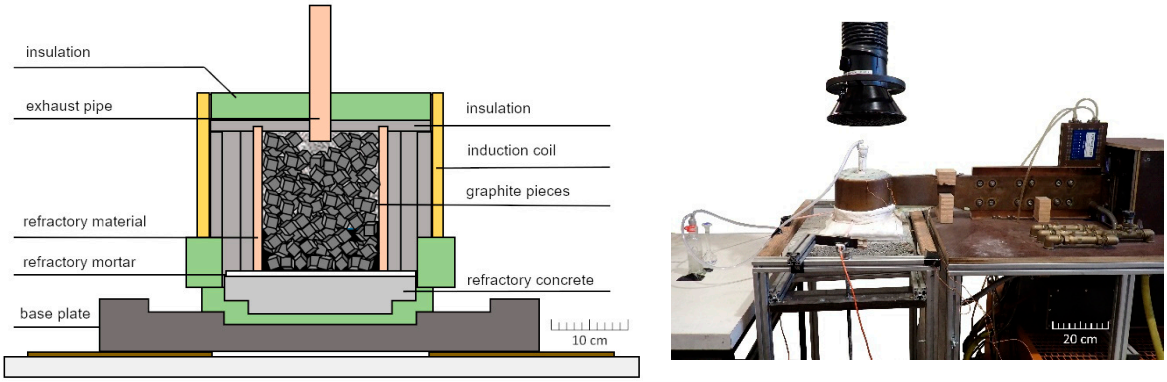

Figure 3. (**a**) Schematic representation of the original InduMelt plant (Design 1) [34]; (**b**) overall setup in test operation.

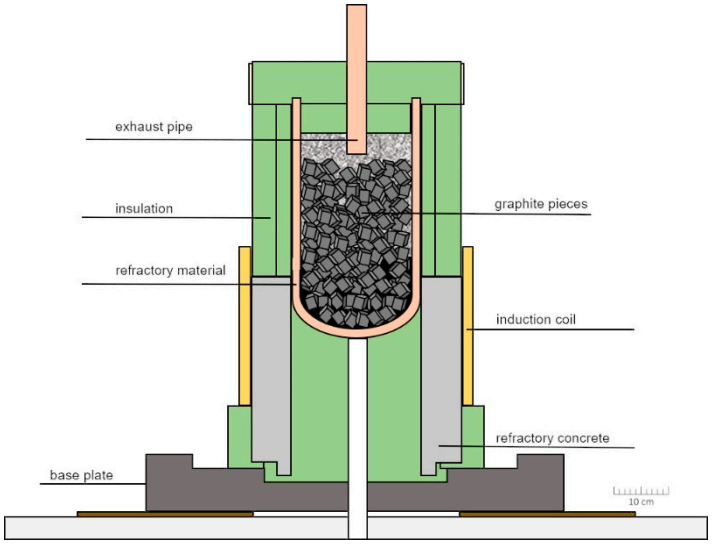

Figure 4. Schematic representation of the new reactor design (Design 2).

This is a cylindrical crucible with a half-arc bottom made of MgO. It was placed centrally on a refractory concrete structure in a way that only the lower part of the MgO crucible is within the induction coil. Appropriate insulation made of refractory matting should reduce the heat loss and thus the energy requirement and protect as far as possible against the ingress of false air from the environment. To be able to make a qualitative statement about the escaping gas during the test, an exhaust pipe made of Al_2O_3 was again implemented. The temperature was measured by a category S-thermocouple from below and in the reactor by two category K-thermocouples.

For a direct comparison of the different reactor concepts of the InduMelt plant, the same feedstock, the mixture LCO-C mentioned in Section 2.1 with a quantity of 550 g, was examined in both crucible concepts. To ensure that reproducible initial conditions prevailed in both designs, the charging of the cubes and the sample was also performed uniformly in all experiments. Thus, at the beginning, 15 cubes were positioned in the reactor and one third of the sample was charged onto them. After positioning a K-thermocouple, another 10 cubes were performed followed by addition of another third of the sample. This was repeated a second time to finally fill the reactor with 11 cubes after positioning the second

K-thermocouple. This filling quantity also represents the maximum possible capacity of Design 1. The content of Design 2 is approximately 25% larger which, however, was not utilized due to the aforementioned comparability with Design 1. After the experiment, all components of the reactor are weighed. The adhesions to the graphite cubes are removed by light mechanical processing. These adhesions are consequently separated into fractions larger and smaller than 1 mm by means of a sieve tower, together with the remaining finer fraction that may be produced. With the aid of a magnet, these are further separated into magnetic and non-magnetic, with the former finally being assigned to metal and the latter referred to as slag. Larger pieces of metal are collected together after checking with a magnet. The same is done with larger non-magnetic pieces, which are again referred to as slag. The individual fractions are finally weighed and analyzed. The main difference in sampling between Design 1 and Design 2 is the collection of the diffused areas of the grout or reactor adhesions, which will be discussed in more detail in Section 3.2.1.

The aim is to determine the interaction between the cathode material respectively the reaction products of which and the corresponding crucible material and to compare them with each other. On the other hand, the individual transfer coefficients should provide information on whether the choice of the crucible material affects the recovery rates of the individual species.

In a third trial, the basic suitability of the overall reactor concept for the treatment of LFP with the aim of removing Li and P from the material was investigated. For this purpose, Design 1 from Figure 3a was selected again in which a quantity of 394.5 g of the mixture LFP-C from Section 2.1 was charged into the reactor.

3. Results and Discussion

3.1. High-Temperature Properties of the Cathode Materials Used

In a first step to determine the behavior of cathode materials from LIBs at temperatures above 1600 °C and under reducing conditions, experiments were performed in a heating microscope. Figure 5a provides a picture of the result of the experiment with the mixture with LCO. A strong dark blue coloration was observed on the platelet. This may be due to a reaction between the Al_2O_3 platelet and cobalt to form cobalt aluminate with its typical blue appearance [41]. The product of the melting process under reducing conditions is a metal structure, which can be classified as strongly magnetic after examination with a magnet. This magnetism could also be detected in experiments with LFP, which is shown in (b). In contrast to the experiment described above, there is no blue coloration, but a brown to reddish appearance.

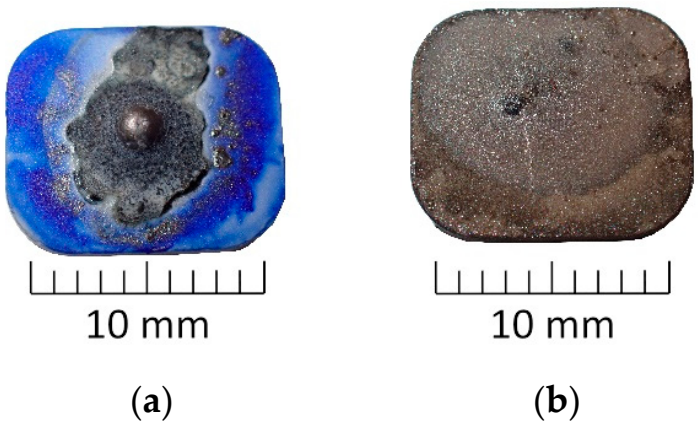

Figure 5. Condition of the sample during examination under the heating microscope: (**a**) after analysis for LCO-C; (**b**) after analysis for LFP-C.

Figure 6 displays the recording of the replication experiment LCO-C via optical measurement in the heating microscope. In Figure 6 the cross-sectional area of the exper-

iments with LCO-C (black dotted line) and its repetition LCO-C-Re (green dotted line) over temperature during the experiment is shown. This cross-sectional area is the size of the sample cylinder detected by the heating microscope respectively its change with temperature increase.

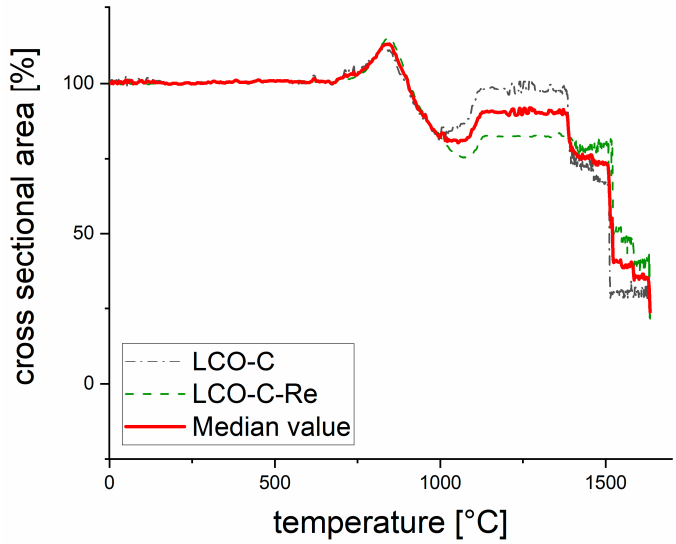

Figure 6. Results of the heating microscope of LCO-C: trend of the cross-sectional area of the experiments LCO-C and LCO-C-Re during heating and the median value of the both graphics.

It should be mentioned that by comparing the recorded images with the corresponding values of the cross-sectional area, faulty measurements caused by incorrect detection of the baseline by the heating microscope were removed from the data series. Since the basic behavior at the individual temperatures is nearly identical and differs only by different cross-sectional areas, a mean value was determined, which represents the red line. When looking at Figure 6, the first noteworthy surface changes can be observed from 675 °C onwards. From 675 °C to 845 °C a growth of the cross-sectional area was detected, which subsequently decreased again to 1054 °C with single deflections to about 80% of the original area. Up to a temperature of 1127 °C an increase in magnification was detected, which remained relatively constant with single deflections up to 1380 °C. From this temperature on, the cross-sectional area decreased continuously with a smaller slope in the range of 1393 °C to 1507 °C and a significant decrease up to 1525 °C. Up to the end there was a further decrease of the cross-sectional area, which, however, when looking at the single images from the heating microscope, can be traced back to the continuous distribution of the molten material on the platelet.

Figure 7 illustrates the results of the experiments in the heating microscope with the mixture LFP-C. The previously mentioned measurement error was particularly striking in the first experiment of LFP-C (black dotted line in Figure 7) in the range from 1163 °C to about 1400 °C. Nevertheless, a corresponding trend could be determined by correctly measuring individual values in some cases, which in turn could be confirmed by a repeated measurement of LFP-C-Re (green dotted line in Figure 7). Again, the mean value is shown in the red curve.

The results show that up to a temperature of approximately 920 °C the cross-sectional area first rises slightly and then falls back to just below 100% of the initial value. Afterwards, a pulsating enlargement of the surface takes place which decreases at about 1200 °C. After a further pulsating behavior between 1240 and 1310 °C the area is continuous again to remain relatively constant from about 1410 °C on.

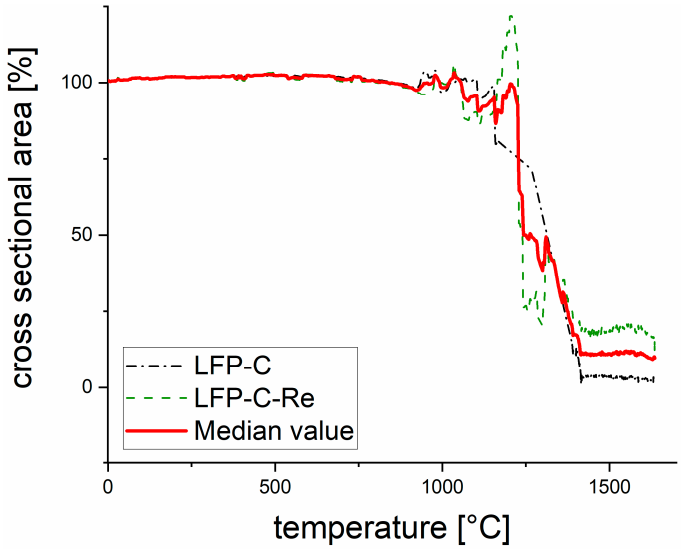

Figure 7. Results of the heating microscope of LFP-C: trend of the cross-sectional area of the experiments LFP-C and LFP-C-Re during heating and the median value of the both graphics.

3.2. InduMelt Experiments: Process Development and Suitability of the Different Reactor Concepts

The main part of the experimental investigation of LIB cathode materials was examined in the InduMelt plant. For this purpose, three experiments were carried out, which will be considered separately below according to their purpose. According to the results of the analyses, as described in Section 3.1, the maximum necessary process temperatures for the tests in the InduMelt plant were set at 1525 °C for LCO-C and 1400 °C for LFP-C. This is due to the fact that the sample material should be completely liquid at this point in time according to the heating microscope.

3.2.1. Results from Experiments with LCO-C in Both Reactor Designs

The first experiment, which is described in detail below, was carried out in Design 1. The entire experiment lasted nearly 8 h. Figure 8a shows the power input of the induction unit and the corresponding temperatures over the test time. Two type S-thermocouples (S-TC 1 and S-TC 2 in Figure 8a) were used on the reactor surface and two type K-thermocouples inside the reactor. The latter were initially installed at different heights in the reactor, one in the area of the first cube layer (K-TC bottom) and one in the upper area (K-TC top). In contrast to the S-thermocouples, the measurement results of the K-thermocouples are subject to considerable fluctuations due to melting of their insulation, influences of the material in the reactor, etc. However, an approximate temperature spread of the different thermocouple types of 500 °C could be determined up to the end.

During the process, noticeable anomalies were documented. Starting at 0.95 h and a K-TC bottom temperature of 450 °C a strong formation of condensate in the exhaust pipe to the gas scrubber was observed. This was attributed to the drying of the mortar. The temperature spread of the S-thermocouples at 1.75 h (124 °C S-TC 1) can be explained by a slight realignment of S-TC 1. Especially interesting was the continuously increasing white smoke from the exhaust pipe, which started at 5.10 h and 1180 °C internal temperature and stopped at 1341 °C. This resulted in a continuous white deposit in the exhaust pipe of the scrubber, as shown in Figure 8b. After the white smoke formation stopped, the acid in the scrubber gradually changed from transparent to a slightly yellow liquid. The assumption that the white deposits are Li or a corresponding compound could be confirmed after analysis of the liquid in the scrubber, which are summarized in Table 2.

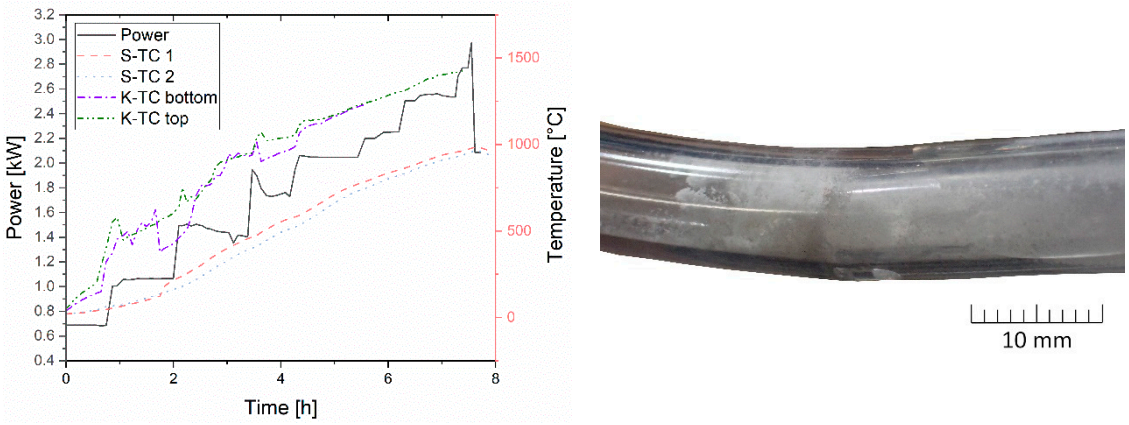

(**a**) (**b**)

Figure 8. Experimental performance of LCO-C in Design 1: (**a**) comparison of power and temperature over time; (**b**) deposits in the exhaust pipe of the gas scrubber.

Table 2. Results from the gas scrubber respectively from its frit liquid after suction of the exhaust gas in Design 1 LCO-C in mg/L.

Fraction	Li	Co
Frit liquid	1650	0.64

Sampling after the experiment revealed a total of 4 fractions, the results of which are shown in Table 3.

Table 3. Analysis results of the fractions of the experiment LCO-C in Design 1.

Fraction	Weight (g)	Li (wt.%)	Co (wt.%)
Slag	3.20	5.62	0.12
Mortar	145.60	4.52	0.12
Metal	251.70	0.01	100.00
Powder	37.30	1.49	53.4

The fraction defined therein as slag could be identified as dark to light grey non-magnetic pieces smaller than 10 mm with minimal metallic inclusions, as illustrated in Figure 9a. The mortar shown represents the part into which the test material has diffused. This is optically visible by a dark discoloration of the originally white mortar. In Figure 9b the reactor is demonstrated from below after the concrete floor has been separated. During sampling, care was taken to find the clearest possible separation between the white mortar and the diffused areas, but this proved to be very difficult. The largest product of the experiment in terms of mass was the metal fraction, which could be obtained in pieces larger than 10 mm. The metal piece shown in Figure 9c serves as an example. The analysis showed an impressive purity of 100% Co and an impurity of only 0.01% Li. It should be noted that there may be some variation in sampling and digestion errors, resulting in the overall result not reaching exactly 100%. The fourth fraction was a powder with particles smaller than 1 mm, as can be seen in Figure 9d, which was mostly magnetic. This property is also confirmed by analyses with a cobalt content of 53.4%.

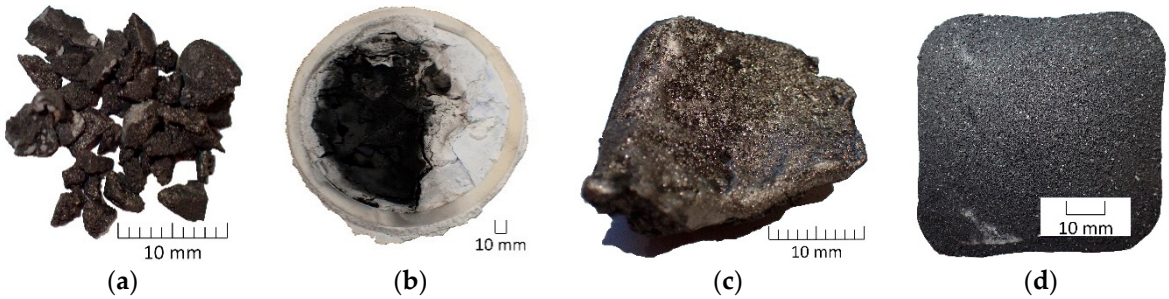

Figure 9. Products of the experiment LCO-C in Design 1: (**a**) slag; (**b**) ceramic ring and mortar seen from the bottom; (**c**) metal; (**d**) powder.

Taking into account the respective weighed masses and the analysis results, the transfer coefficients of the individual elements of the fractions were calculated. In detail, the analyses from ICP-MS and ICP-OES of the individual fractions were converted to mass percent and multiplied by the weighed mass at sampling. By adding the respective element masses, a total mass per element could be determined. This represents the amount that was still detectable in the fractions in the reactor after the test. Afterwards, a comparison of the masses before and after the experiment was carried out. The difference was assumed to be a transfer into the gas flow leaving the reactor during the experiment or a transfer into the individual solid fractions. The results of this calculation can be seen in Figure 10.

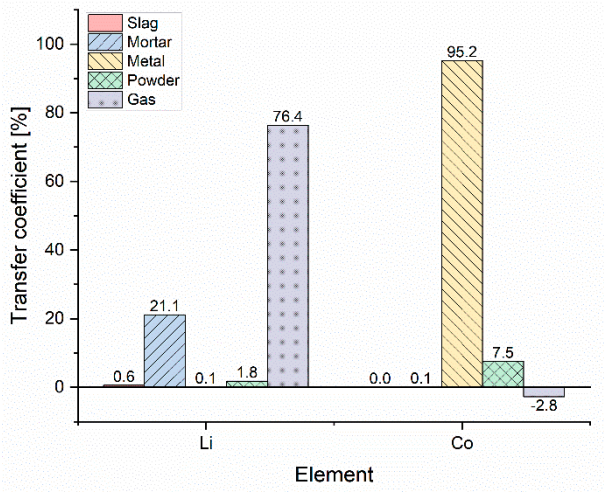

Figure 10. Transfer coefficients of the elements into the individual fractions in % of the experiment in Design 1.

At this point it should be mentioned that the transfer coefficients determined must be seen as initial guide values and internal comparison values and must be confirmed accordingly by repeated experiments in the optimum reactor setup. Nevertheless, the trend was also observed in experiments with NMC and NCA, as described in Windisch-Kern et al. [34]. The result of the transfer coefficients in Figure 10 shows a Li removal rate of over 76% into the gas stream from the cathode material used. Based on the thermokinetic consideration of LCO by Kwon et al. [16] and assuming that most of the Li has left the reactor during the phase of white smoke (approximately 1160–1340 °C), it can be assumed that it is Li_2O. The transfer of over 21% Li into the mortar can be considered as an undesirable result. The percentage of Li in the slag is not negligible in the analyses (Table 2) with 5.6%, but due to the small quantity of slag it is insignificant for the total consideration with 0.6%. The small amount of Li in the metal (0.1%) is a great result with regard to the purest possible metal fraction. A further potential for improvement can be seen when considering the Li content of 1.8% in the powder, whereby this value can possibly be lowered with a longer

holding time of the final temperature. The result of Co can be interpreted as extremely promising. Only 7.5% is found in the powder and 95.2% in the metal, which can be directly transferred for further use in the corresponding metal industry. The resulting difference to 100% can be explained by the extremely difficult sampling, especially the identification of the individual fractions and the subsequent weighing. At this point, the proportion in the slag and mortar can also be neglected with less than 0.1%. The comparison of these results with other processes is difficult at this point because the composition of the input material differs significantly from a real waste stream of LIB. Nevertheless, by using pure cathode material, without impurities such as Al or Cu, a value of the theoretically maximum possible removal rate of Li can be determined. Vest [15] describes a Li_2O transfer rate from the waste stream of LIB of 40.5% in their process based on an electric arc furnace. Even though a direct comparison with this value is not possible, the gap between Vest's result and the theoretically possible value in this method shows an enormous potential.

Much more remarkable in this context is the result of Design 2. The temperature record of the LCO-C experiment in Design 2, which can be viewed in Figure 11 in combination with the power input over time with the same naming as in the previous experiment described above, shows that the temperature is highest in the lower part of the reactor. Thus, the goal of the reactor design of a more targeted temperature provision in the lower area could be realized.

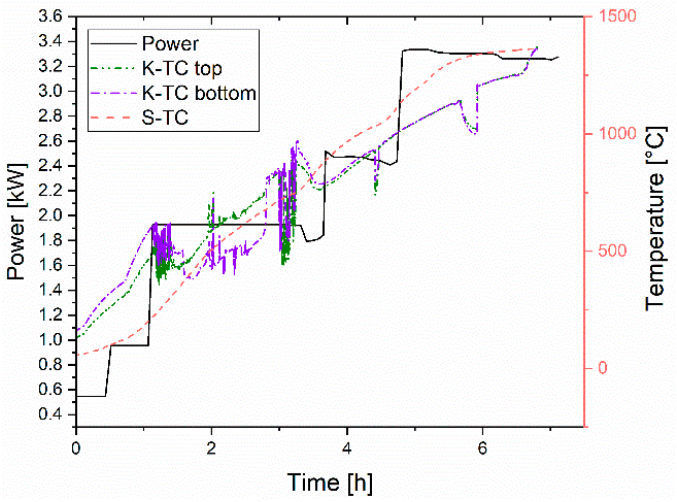

Figure 11. Experimental performance of LCO-C in Design 2, comparison of power and temperature over time.

The extreme fluctuations of the K-thermocouples between the test duration of approximately 1 to 3 h could be explained in retrospect in such a way that after the insulation around the thermocouple wires had melted, they reconnected at a higher point in the reactor. The initial theory could be confirmed when the reactor was opened after the experiment, because the thermocouples could be found in the upper part of the reactor free of cubes and no longer in the cube bed. Again, a white smoke formation with the same deposits in the exhaust pipe of the gas scrubber could be detected. This phenomenon occurred at an S-thermocouple temperature range from 1165 to 1340 °C. Again, as the smoke intensity decreased, a successive discoloration of the acid in the scrubber from transparent to a light yellow was to be determined. The results of the acid analysis from the gas scrubber can be taken from Table 4. The high value of Li confirms the impression, as already assumed in the experiment in Design 1, that Li can be removed from the reactor via the gas flow.

Table 4. Results from the frit liquid of the gas scrubber after suction of the exhaust gas in Design 2 LCO-C in mg/L.

Fraction	Li	Co
Frit liquid	1230	1.2

The results of the investigation of the test material LCO-C in Design 2 can be seen in Table 5. Essentially, the analysis differs from the experiment in Design 1 only in that there was no mortar due to the construction. When the MgO crucible was weighed after the experiment, it was found to be 81.2 g heavier than the initial weight. This could be attributed to adhesions on the crucible, which were mechanically extracted as completely as possible. The result was a fine powder. Despite considerable mechanical effort, only 3.8 g could be removed from the crucible without damage, which will be referred to as crucible adhesion in the following.

Table 5. Results from the experiment LCO-C in Design 2.

Material	Weight (g)	Li (wt.%)	Co (wt.%)
Slag	1.3	5.59	3.3
Crucible adhesion	3.8	6.29	27.2
Metal	242.2	0.12	93.9
Powder	35.2	0.69	66.6

The fractions did not differ in their appearance from those in Figure 9a,c,d. Only the metal pieces were larger, as shown in Figure 12. Analysis of the metal fraction revealed a purity of Co of 93.9% with a negligible amount of 0.12% Li.

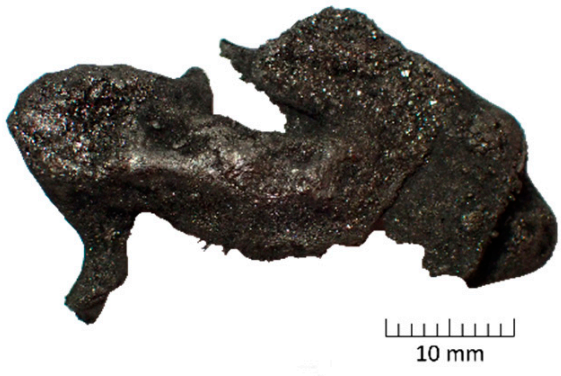

Figure 12. Metal fraction from the LCO-C experiment in Design 2.

The transfer coefficients, which are illustrated in Figure 13, were determined from the results in Table 5, taking into account the corresponding weight changes of the individual fractions during the experiment.

This result represents a unique selling point in the pyrometallurgical processing of cathode material from LIB. Compared to Design 1, even though only 85.9% of the Co was transferred to an almost pure Co-metal phase, more than 97% of the Li were removed from the material and the reactor via the gas flow. Thus, a nearly 21% higher Li removal rate could be achieved in Design 2.

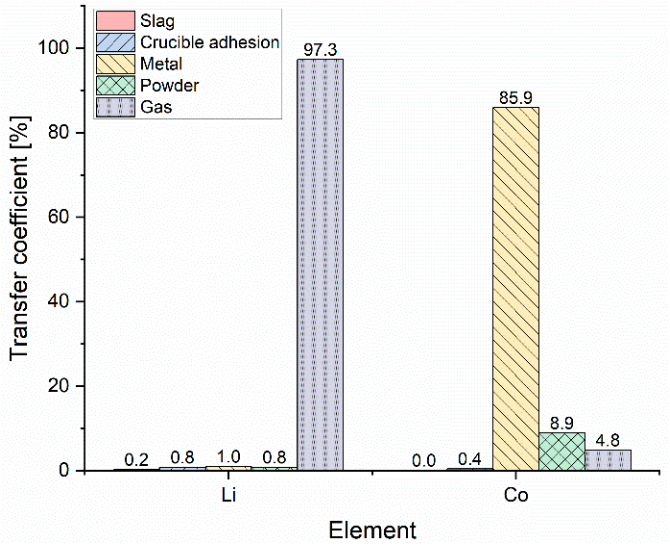

Figure 13. Transfer coefficients of the elements into the individual fractions in % of the experiment in Design 2.

Since the attribution of the Co not found to the gas phase is rather questionable to this extent and cannot be traced back exclusively to errors in sampling and analysis, a closer look at the results is necessary. In addition to the result display in Figure 13, another variant is possible. It is assumed that the difference of the weighed crucible adhesion (81.2 g) to the extracted amount (3.8 g) consists of the same composition as the extracted fraction. This results in a lithium removal rate of 81.7% with a Co value that was not found (i.e., attributed to the gas phase) of −3.12%. This variant cannot clarify the difference to 100%, but by combining the two methods, one obtains a range in which the transfer coefficients move.

Besides this result, Design 2 also turns out to be a better choice when considering the interactions between the sample material and the reactor. As shown in Figure 14a, a massive attack of the reactor wall was observed in Design 1 (Al_2O_3) with ring diameter reductions of up to 0.2 mm. On the other hand, Figure 14b shows the reactor in Design 2 (MgO) after the experiment. From the difference between the weighing before and after the test, it is known that the reactor was over 81 g heavier afterwards. The theory of adhesion to the reactor can also be seen in the illustration, whose boundary is marked with the red arrow.

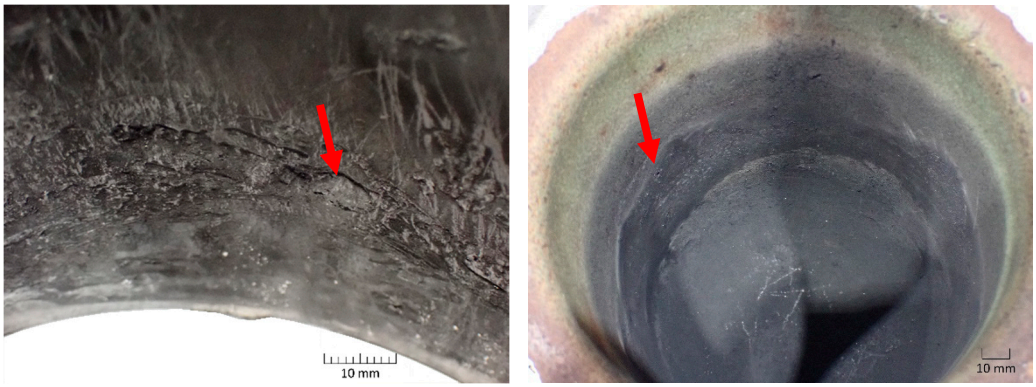

(**a**) (**b**)

Figure 14. Visual appearance of the crucibles after the experiments: (**a**) traces of attack on the Al_2O_3 crucible wall in Design 1; (**b**) appearance of the MgO crucible after experiment 2 with obvious adhesions.

This factor is particularly important for long-term experiments in a continuous set-up. If the sample material and the Al_2O_3-ceramics are in contact for a longer period of time, this attack would lead to a destruction of the reactor. In addition to the advantages already mentioned, Design 2 also features a much simpler construction and therefore easier sampling. A drawback of Design 2 is the higher energy input required, which can be seen in the comparison of the power curve of Figures 8 and 11. However, this can be solved by an improved positioning of the induction coil. Furthermore, the consequences of adhesions in continuous operation must be investigated.

Even though the target temperatures were not reached in the experiments with LCO-C, it can still be assumed that a sufficiently high temperature was reached. Firstly, the temperature in the reactor was measured in the space between the refractory mat and the graphite cubes, as mentioned above, which implies that the temperature in the cube bed must have been even higher due to the heat input in it. In addition, if the temperature was too low, the appearance of the products would be different. An example of this is the metal from Co, as shown in Figures 9c and 12, whose melting point is known to be 1495 °C.

3.2.2. Results from Experiments with LFP-C

The test with LFP-C was carried out in Design 1. Since the temperature measurement via the K-thermocouples was already faulty from the beginning of the experiment and a repair was no longer possible at this point in time, only the curves of the recordings from the S-thermocouples are visible in Figure 15. However, the delta value to the K-thermocouples should be similar to that in the LCO-C experiment in Design 1, whereby approximately 500 °C can be added to the value of the S-thermocouples to determine the internal temperature at higher temperatures.

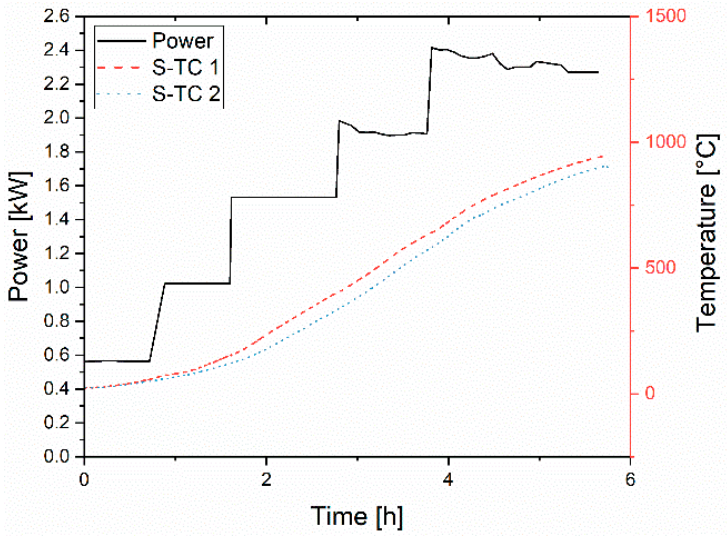

Figure 15. Experimental performance of LFP-C in Design 1, comparison of power and temperature over time.

During the heating process, smoke development was particularly noticeable at an outside temperature of approximately 750 °C (approximate internal temperature of 1210 °C), which completely ignited after a short time. This flame, which is an indication of the reaction of phosphorus with oxygen [42], could finally be detected constantly up to an outside temperature of approximately 860 °C (approximate internal temperature of 1310 °C) as shown in Figure 16a. During this time the acid in the gas scrubber changed its color to a brownish liquid. The results of the exhaust gas analysis can be taken from Table 6.

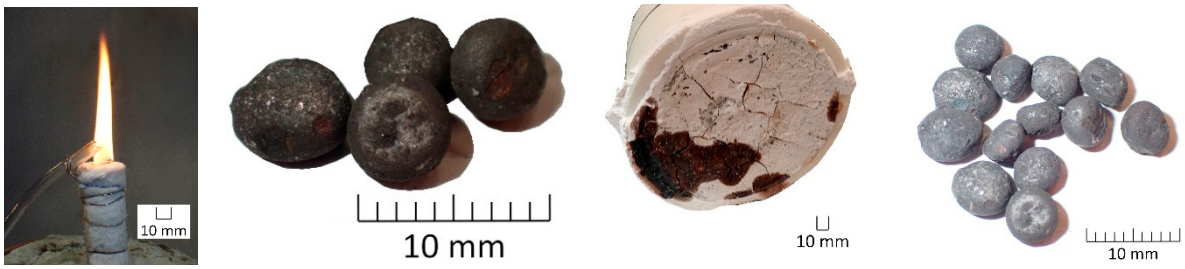

Figure 16. Products of the experiment LFP-C in Design 1: (**a**) flame formation in exhaust gas flow; (**b**) slag; (**c**) ceramic ring and mortar seen from the bottom; (**d**) metal.

Table 6. Results from the frit liquid of the gas scrubber after suction of the exhaust gas in Design 1 for LFP-C in mg/L.

Fraction	Li	Fe	P
Frit liquid	2.0	1.5	200

In the exhaust gas analysis only a small value for P and a very small amount of Li could be found, which is possibly due to the formation of a flame out of the exhaust pipe. In order to be able to make a statement about the efficiency of the reactor concept for the recycling of LFP, the results of the ICP-OES or ICP-MS must be examined more closely.

A total of 5 fractions could be detected during sampling. The appearance of the fraction classified as non-magnetic slag (Slag 1) differed significantly from that in Figure 9a. Individual spheres with a diameter of up to 5 mm were detected, as shown in Figure 16b. In comparison with the appearance of the magnetic metal fraction in Figure 16d, the difficulty of clearly classifying the individual fractions is obvious. The analysis showed that the Fe content in the slag was even higher than in the material identified as metal. In addition, however, a significant amount of Li (3.19%) and P (15.9%) was also analyzed. Slag 2 in Table 7 is a non-magnetic powder with particles smaller than 1 mm the appearance of which is the same as in Figure 9d. The same applies to the magnetic material identified as powder. In this experiment, care was again taken during sampling to separate as much diffused areas of the sample material from the mortar. These brownish areas are also visible in Figure 16c, which shows the ceramic ring with the mortar after removal of the refractory concrete. Analysis of the metal displayed in Figure 16d shows only 51 wt.% Fe and over 8 wt.% P. This low Fe content suggests that no complete reduction has occurred. A further indication for the correctness of this assumption is the fact that during mechanical processing of the fraction with a hammer, the spheres disintegrated into a powder already with a small amount of force.

Table 7. Results of the individual fractions after the experiment LFP-C in Design 1.

Fraction	Weight (g)	Li (wt.%)	Fe (wt.%)	P (wt.%)
Slag 1	36.1	3.19	53.60	15.90
Slag 2	16.3	4.95	0.61	7.89
Mortar	66.0	0.90	3.29	1.66
Metal	96.5	0.89	51.00	8.24
Powder	70.5	1.91	35.90	8.43

Referring to the respective masses of the individual fractions, the transfer coefficients can be taken from Figure 17.

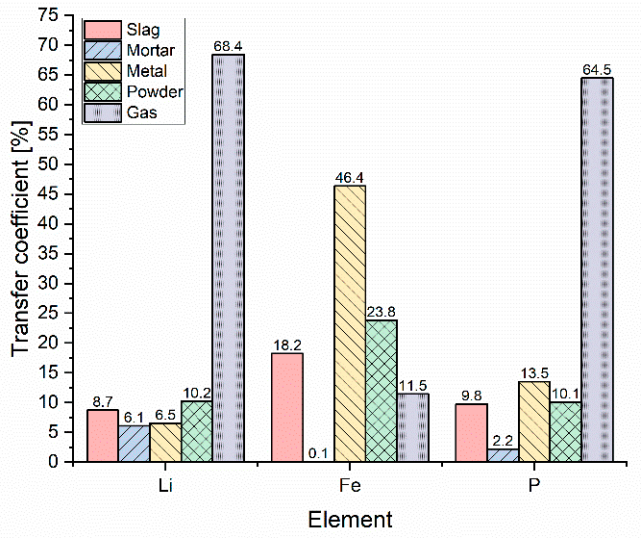

Figure 17. Transfer coefficients of the elements into the individual fractions in % of the experiment in Design 1.

Of particular interest are the removal rates of Li (68.4%) and P (64.5%) over the gas flow. The remaining amount of Li here is distributed relatively evenly among the other fractions with a slight concentration on the remaining powder. As already mentioned, it is reasonable to assume that no complete reduction of Fe has occurred. This is also reflected in a considerable value of phosphorus in the metal fraction.

A direct comparison of the experiments in Design 1 shows that the Li removal rate for LFP-C of 68.4% is 8% lower than in the experiment with LCO-C. However, the parallel removal of phosphorus of 64.5% represents a respectable result. It also can be seen that in both the LCO-C test with a transfer coefficient of 21.1% (Figure 10) for Li and the LFP-C test with 6.1% (Figure 17), a significant amount of Li was transferred to the mortar. If the results of LCO-C in Design 2 are also included, it can be assumed that gasification rates for LFP-C are better in this construction method. Looking at the transfer coefficients in Figure 17, a significant portion of the Fe (11.5%) is attributed to the gas flow. De facto, this is the amount that was not recovered during sampling compared to the input amount. The correctness or falsification of this classification and the above mentioned assumptions must be investigated in further experiments. Particular attention must be paid to safety in the pyrometallurgical removal of phosphorus from LIB, consisting of the cathode material LFP, in the exhaust gas post-processing. In addition to oxidation in the air, as shown in Figure 16a, the high toxicity [43] is also of particular importance. These factors must be given special consideration in future developments of the reactor concept presented.

4. Conclusions

Within the scope of this paper, the suitability of a new pyrometallurgical recycling process associated with materials from LIBs for the recovery of valuable metals was investigated. With the background of a continuous adaptation of the reactor concept to the waste stream from spent LIBs, two different reactor designs were used, in each of which the cathode material LCO with carbon addition was examined for better comparability. In a third trial, the basic capability of the technology for the treatment of LFP was also examined. In addition, knowledge about the behavior of the examined cathode materials used in high-temperature applications was investigated in an upstream step in a heating microscope.

The transfer coefficients determined in the experiments of the novel pyrometallurgical recycling process serve exclusively as a comparison of the efficiency of the presented reactor concepts or as a first benchmark of the basic suitability of the process for the treatment of LFP.

From the experiments in the heating microscope the maximum necessary temperatures for the transformation into a molten phase could be determined. This state of aggregation is necessary in the long run to meet the requirements of the theoretically determined principle of a continuous process. For the experiments with LCO a temperature of 1525 °C and for LFP 1400 °C could be determined.

In the trial LCO-C in Design 1, 95.2% Co of the original input fraction was converted into the metal, with a purity of Co of 100%. Due to the high Li content in the mortar, only 76.4% of the Li could be transferred into the exhaust gas flow. This contrasts with the result of the experiment with LCO-C in Design 2. Its analysis shows a metal purity of 93.9% Co and a remarkable lithium removal rate in a range from 81.7% to 97.3%. In addition to this impressive lithium removal rate, Design 2 has also proven to be the better choice for future use due to its interaction with the feed material. For example, massive interactions and attacks on the Al_2O_3 crucible have been detected in Design 1, whereas there were no physical damages with the MgO crucible in Design 2. Although the danger of destruction of the reactor wall during long-term experiments in a future continuous process has been averted, the effect of the detected adhesions on the MgO crucible still needs to be investigated in further tests. However, the initially formulated goal of a more targeted heat supply in the lower part of the crucible was achieved by Design 2.

The experiment with LFP-C was performed in Design 1 and achieved a lithium removal rate of 68.4% with parallel phosphorus removal of 64.5%. Since the results of the LCO-C experiments showed that a higher lithium removal could be achieved when using Design 2, a repetition of the LFP-C experiment in this setup can be expected to result in a higher removal rate. In addition, since sampling in this experiment has proven to be particularly difficult due to the appearance of the fractions, and since detailed examination of the results has revealed questions that need to be clarified, such as the undetectable amount of Fe, further investigations are indispensable.

Nevertheless, it can be summarized that Design 2 with its MgO crucible has proven to be a better choice with regard to its suitability for pyrometallurgical treatment of material from LIBs. This is due to its inertness to the sample material as well as the higher Li removal rate determined. In addition, it was found that the use of the technology is also suitable for the cathode material LFP and that considerable P and Li removal rates have already been achieved. However, in order to be able to treat the fluctuating waste stream from spent LIBs with an appropriate efficiency, in-depth investigations are needed beforehand to gain knowledge of the behavior of all common cathode materials. In order to increase efficiency, the fraction referred to as slag must also be subjected to more detailed investigations in the future, for example with an XRD analysis. From this, knowledge of the phases present is to be generated and the formation of these is to be suppressed with targeted measures. In the current development phase, this has not yet been the focus of research. Furthermore, it is necessary to identify the influence of additional fractions such as Cu and Al from conductor foils on the process.

Compared to commercial techniques used today for recycling spent LIBs, the simultaneous recovery of lithium and phosphorus via the process presented in this paper is its most significant advantage. This first potential assessment for pyrometallurgical recovery of Li would also theoretically meet the requirements of the proposed amendment to the EU Directive 2006/66/EC of a Li recovery up to 70% by 2030. Aspects such as the economics, energy efficiency and environmental impact of this intermediate step in the overall recycling chain, as well as possible recovery rates of a waste stream of spent LIBs in the new reactor design, need to be determined in further studies.

Author Contributions: Conceptualization, A.H. and S.W.-K.; methodology, A.H.; investigation, A.H., S.W.-K. and C.P.; resources, A.H., S.W.-K. and C.P.; writing—original draft preparation, A.H.; writing—review and editing, A.H., S.W.-K., C.P. and H.R.; visualization, A.H.; supervision, C.P. and H.R.; project administration, C.P.; funding acquisition, H.R. All authors have read and agreed to the published version of the manuscript.

Funding: This research was funded by the Zukunftsfonds Steiermark with funds from the province of Styria, Austria, grant number GZ: ABT08-189002/2020 PN:1305.

Institutional Review Board Statement: Not applicable.

Informed Consent Statement: Not applicable.

Data Availability Statement: The data presented in this study are available on request from the corresponding author.

Conflicts of Interest: The authors declare no conflict of interest.

References

1. Pillot, C. The Rechargeable Battery Market and Main Trends 2018–2030. In Proceedings of the ICBR 2019, Lyon, France, 18–20 September 2019.
2. Palacín, M.R.; de Guibert, A. Why do batteries fail? *Science* **2016**, *351*, 1253292. [CrossRef]
3. Zhang, X.; Xie, Y.; Lin, X.; Li, H.; Cao, H. An overview on the processes and technologies for recycling cathodic active materials from spent lithium-ion batteries. *J. Mater. Cycles Waste Manag.* **2013**, *15*, 420–430. [CrossRef]
4. Ordoñez, J.; Gago, E.J.; Girard, A. Processes and technologies for the recycling and recovery of spent lithium-ion batteries. *Renew. Sustain. Energy Rev.* **2016**, *60*, 195–205. [CrossRef]
5. Sojka, R.; Pan, Q.; Billman, L. Comparative Study of Lithium-Ion Battery Recycling Processes. In Proceedings of the ICBR 2020, Salzburg, Austria, 16–18 September 2020.
6. Li, L.; Zhang, X.; Li, M.; Chen, R.; Wu, F.; Amine, K.; Lu, J. The Recycling of Spent Lithium-Ion Batteries: A Review of Current Processes and Technologies. *Electrochem. Energy Rev.* **2018**, *1*, 461–482. [CrossRef]
7. Blengini, G.A.; Latunussa, C.E.; Eynard, U.; Torres de Matos, C.; Wittmer, D.; Georgitzikis, K.; Pavel, C.; Carrara, S.; Mancini, L.; Unguru, M.; et al. *Study on the EU's list of Critical Raw Materials (2020) Final Report*; Publications Office of the European Union: Luxembourg, 2020. [CrossRef]
8. Arthur D Little. Available online: https://www.adlittle.com/en/insights/viewpoints/future-batteries (accessed on 26 December 2020).
9. Huang, B.; Pan, Z.; Su, X.; An, L. Recycling of lithium-ion batteries: Recent advances and perspectives. *J. Power Sources* **2018**, *399*, 274–286. [CrossRef]
10. Duesenfeld GmbH, Ecofriendly Recycling of Lithium-Ion Batteries. Available online: https://www.duesenfeld.com/recycling_en.html (accessed on 26 December 2020).
11. Accurec Recycling GmbH, Lithium Batterie Recycling. Available online: https://accurec.de/lithium?lang=de (accessed on 26 December 2020).
12. Redux GmbH, Redux Smart Battery Recycling. Available online: https://www.redux-recycling.com/de (accessed on 26 December 2020).
13. Arnberger, A.; Coskun, E.; Rutrecht, B. Recycling von Lithium-Ionen-Batterien. In *Recycling und Rohstoffe*; Thiel, S., Thomé-Kozmiensky, E., Goldmann, D., Eds.; TK Verlag: Nietwerder, Germany, 2018.
14. Liu, C.; Lin, J.; Cao, H.; Zhang, Y.; Sun, Z. Recycling of spent lithium-ion batteries in view of lithium recovery: A critical review. *J. Clean. Prod.* **2019**, *228*, 801–813. [CrossRef]
15. Vest, M. Weiterentwicklung des pyrometallurgischen IME Recyclingverfahrens für Li-Ionen Batterien von Elektrofahrzeugen. Ph.D. Thesis, RWTH Aachen University, Aachen, Germany, 28 January 2016.
16. Kwon, O.; Sohn, I. Fundamental thermokinetic study of a sustainable lithium-ion battery pyrometallurgical recycling process. *Resour. Conserv. Recycl.* **2020**, *158*, 104809. [CrossRef]
17. Abdou, T.R.; Espinosa, D.C.R.; Tenório, J.A.S. Recovering of Carbon Fiber Present in an Industrial Polymeric Composite Waste through Pyrolysis Method while Studying the Influence of Resin Impregnation Process: Prepreg. In *REWAS 2016*; Kirchain, R.E., Blanpain, B., Meskers, C., Olivetti, E., Apelian, D., Howarter, J., Eds.; Springer International Publishing: Cham, Switzerland, 2016; pp. 313–318. [CrossRef]
18. Beheshti, R.; Tabeshian, A.; Aune, R.E. Lithium-Ion Battery Recycling Through Secondary Aluminum Production. In *Energy Technology 2017*; Zhang, L., Drelich, J.W., Neelameggham, N.R., Guillen, D.P., Haque, N., Zhu, J., Eds.; The Minerals, Metals & Materials Series; Springer International Publishing: Cham, Switzerland, 2017; Volume 135, pp. 267–274. [CrossRef]
19. Gao, R.; Xu, Z. Pyrolysis and utilization of nonmetal materials in waste printed circuit boards: Debromination pyrolysis, temperature-controlled condensation, and synthesis of oil-based resin. *J. Hazard. Mater.* **2019**, *364*, 1–10. [CrossRef]
20. Li, J.; Wang, G.; Xu, Z. Environmentally-friendly oxygen-free roasting/wet magnetic separation technology for in situ recycling cobalt, lithium carbonate and graphite from spent $LiCoO_2$/graphite lithium batteries. *J. Hazard. Mater.* **2016**, *302*, 97–104. [CrossRef]
21. Xiao, J.; Li, J.; Xu, Z. Novel Approach for in Situ Recovery of Lithium Carbonate from Spent Lithium Ion Batteries Using Vacuum Metallurgy. *Environ. Sci. Technol.* **2017**, *51*, 11960–11966. [CrossRef]
22. Werner, D.; Peuker, U.A.; Mütze, T. Recycling Chain for Spent Lithium-Ion Batteries. *Metals* **2020**, *10*, 316. [CrossRef]

23. Yin, H.; Xing, P. Pyrometallurgical Routes for the Recycling of Spent Lithium-Ion Batteries. In *Recycling of Spent Lithium-Ion Batteries*; An, L., Ed.; Springer International Publishing: Cham, Switzerland, 2019; Volume 4, pp. 57–83. [CrossRef]
24. Elwert, T.; Frank, J. Auf dem Weg zu einem geschlossenen Stoffkreislauf für Lithium-Ionen-Batterien. In *Recycling und Sekundärrohstoffe*; Thomé-Kozmiensky, E., Holm, O., Friedrich, B., Goldmann, D., Eds.; Thomé-Kozmiensky Verlag GmbH: Neuruppin, Germany, 2020.
25. Bai, Y.; Muralidharan, N.; Sun, Y.K.; Passerini, S.; Stanley Whittingham, M.; Belharouak, I. Energy and environmental aspects in recycling lithium-ion batteries: Concept of Battery Identity Global Passport. *Mater. Today* **2020**, *41*, 304–315. [CrossRef]
26. Guoxing, R.; Songwen, X.; Meiqiu, X.; Bing, P.; Youqi, F.; Fenggang, W.; Xing, X. Recovery of Valuable Metals from Spent Lithium-Ion Batteries by Smelting Reduction Process Based on MnO-SiO_2-Al_2O_3 Slag System. In *Advances in Molten Slags, Fluxes, and Salts, Proceedings of the 10th International Conference on Molten Slags, Fluxes and Salts 2016, Seattle, WA, USA, 22–25 May 2016*; Reddy, R., Chaubal, P., Pistorius, P.C., Pal, U., Eds.; Springer International Publishers: Cham, Switzerland, 2016; pp. 210–218. [CrossRef]
27. Forte, F.; Pietrantonio, M.; Pucciarmati, S.; Puzone, M.; Fontana, D. Lithium iron phosphate batteries recycling: An assessment of current status. *Crit. Rev. Environ. Sci. Technol.* **2020**. [CrossRef]
28. Yao, Y.; Zhu, M.; Zhao, Z.; Tong, B.; Fan, Y.; Hua, Z. Hydrometallurgical Processes for Recycling Spent Lithium-Ion Batteries: A Critical Review. *ACS Sustain. Chem. Eng.* **2018**, *6*, 13611–13627. [CrossRef]
29. Meshram, P.; Pandey, B.D.; Mankhand, T.R.; Deveci, H. Comparision of Different Reductants in Leaching of Spent Lithium Ion Batteries. *JOM* **2016**, *68*, 2613–2623. [CrossRef]
30. Ghassa, S.; Farzanegan, A.; Gharabaghi, M.; Abdollahi, H. Novel bioleaching of waste lithium ion batteries by mixed moderate thermophilic microorganisms, using iron scrap as energy source and reducing agent. *Hydrometallurgy* **2020**, *197*, 105465. [CrossRef]
31. Zheng, X.; Zhu, Z.; Lin, X.; Zhang, Y.; He, Y.; Cao, H.; Sun, Z. A Mini-Review on Metal Recycling from Spent Lithium Ion Batteries. *Engineering* **2018**, *4*, 361–370. [CrossRef]
32. Elwert, T.; Römer, F.; Schneider, K.; Hua, Q.; Buchert, M. Recycling of Batteries from Electric Vehicles. In *Behaviour of Lithium-Ion Batteries in Electric Vehicles. Green Energy and Technology*; Pistoia, G., Liaw, B., Eds.; Springer International Publishing AG: Cham, Switzerland, 2018; pp. 289–321. [CrossRef]
33. Republik Österreich Parlament. Available online: https://www.parlament.gv.at/PAKT/EU/XXVII/EU/04/37/EU_43776/imfname_11029480.pdf (accessed on 21 December 2020).
34. Windisch-Kern, S.; Holzer, A.; Ponak, C.; Raupenstrauch, H. Pyrometallurgical lithium-ion-battery recycling: Approach to limiting lithium slagging with the InduRed reactor concept. *Processes* **2021**, *9*, 84. [CrossRef]
35. HENSCHKE GmbH, Graphite Electrode Specification. Available online: https://henschkegmbh.de/index.php?option=com_content&view=article&id=55&Itemid=63&lang=en (accessed on 29 August 2019).
36. Schönberg, A.; Samiei, K.; Kern, H.; Raupenstrauch, H. Der RecoPhos-Prozess—Rückgewinnung von Phosphor aus Klärschlammasche. *Osterr. Wasser Abfallwirtsch.* **2014**, *66*, 403–407. [CrossRef]
37. Samiei, K.; Schönberg, A. *Basic Design of the InduCarb Reactor: Power Input for a Homogeneous Temperature Distribution*; Chair of Thermal Processing Technology (Montanuniversitaet Leoben): Leoben, Austria, 2014; unpublished.
38. Ponak, C. Carbo-Thermal Reduction of Basic Oxygen Furnace Slags with Simultaneous Removal of Phosphorus via the Gas Phase. Ph.D. Thesis, Montanuniversitaet Leoben, Leoben, Austria, 2 September 2019.
39. Ponak, C.; Windisch, S.; Mally, V.; Raupenstrauch, H. Recovery of Manganese, Chromium, Iron and Phosphorus from Basic Oxygen Furnace Slags. In *Optimum Utilization of Resources and Recycling for a Sustainable Solution*; GDMB Verlag GmbH: Clausthal-Zellerfeld, Germany, 2019; Volume 3, pp. 1311–1319.
40. Ponak, C.; Montanuniversitaet Leoben, Leoben, Austria. Personal communication, 2020.
41. Taguchi, M.; Nakane, T.; Hashi, K.; Ohki, S.; Shimizu, T.; Sakka, Y. Reaction temperature variations on the crystallographic state of spinel cobalt aluminate. *Dalton Trans.* **2013**, *42*, 7167–7176. [CrossRef]
42. Klemenc, A. *Anorganische Chemie auf Physikalisch-Chemischer Grundlage*; Springer Vienna: Vienna, Austria, 1951; pp. 201–208.
43. Sedlmeyer, J. Über Phosphorvergiftungen. *Dtsch. Z. Gesamte Gerichtl. Med.* **1932**, *19*, 365–383. [CrossRef]

6.2 Publication 2

Optimization of a Pyrometallurgical Process to Efficiently Recover Valuable Metals from Commercially Used Lithium-Ion Battery Cathode Materials LCO, NCA, NMC622, and LFP

Holzer, A.; Wiszniewski, L.; Windisch-Kern, S. and Raupenstrauch, H.

Article Information:

Journal	Metals, Volume 12, Issue 10
Section	Extractive Metallurgy
Special Issue	New Science Based Concepts for Increased Efficiency in Battery Recycling 2022
Pages	24
Received Date	21 July 2022
Revised Date	11 September 2022
Accepted Date	27 September 2022
Published Date	29 September 2022
DOI	https://doi.org/10.3390/met12101642

Author's contribution: Conceptualization, Methodology, Investigation, Resources, Writing – original draft preparation, Writing – review and editing, Visualization, Project administration

metals

MDPI

Article

Optimization of a Pyrometallurgical Process to Efficiently Recover Valuable Metals from Commercially Used Lithium-Ion Battery Cathode Materials LCO, NCA, NMC622, and LFP

Alexandra Holzer *, Lukas Wiszniewski, Stefan Windisch-Kern and Harald Raupenstrauch

Chair of Thermal Processing Technology, Montanuniversitaet Leoben, Franz-Josef-Strasse 18, 8700 Leoben, Austria

* Correspondence: alexandra.holzer@unileoben.ac.at; Tel.: +43-3842-402-5803

Abstract: With an ever-growing demand for critical raw materials for the production of lithium-ion batteries and a price increase of respective commodities, an ever louder call from the industry for efficient recycling technologies can be noticed. So far, state-of-the-art industry-scaled pyrometallurgical recycling technologies all suffer from the same bottleneck of lithium slagging. At the Chair of Thermal Processing Technology at Montanuniversitaet Leoben, a novel reactor was developed to recover lithium and phosphorus via the gas phase in a pyrometallurgical process. Critical elements such as Li, Ni, Co, and Mn of the commercially used cathode materials LCO ($LiCoO_2$), LFP ($LiFePO_4$), NCA ($LiNi_{0.8}Co_{0.15}Al_{0.05}O_2$), and NMC622 ($LiNi_{0.6}Mn_{0.2}Co_{0.2}$) were analyzed in a batch version of the so-called InduRed reactor concept. The analyses underline that the reactor concept is highly suitable for an efficient recovery for the metals Ni and Co and that slagging of Li can not only be largely prohibited, but the elements lithium and phosphorous can even be recovered from the gas phase. Plant engineering issues were also considered for further development toward a continuous process. The MgO crucible used shows significant diffusion of various elements from the battery material, which is why the choice of crucible material still requires in-depth research.

Keywords: lithium-ion battery; recycling; pyrometallurgy; critical raw materials; lithium removal; phosphorous removal; recovery of valuable metals

Citation: Holzer, A.; Wiszniewski, L.; Windisch-Kern, S.; Raupenstrauch, H. Optimization of a Pyrometallurgical Process to Efficiently Recover Valuable Metals from Commercially Used Lithium-Ion Battery Cathode Materials LCO, NCA, NMC622, and LFP. *Metals* **2022**, *12*, 1642. https://doi.org/10.3390/met12101642

Academic Editors: Bernd Friedrich and Huaiyu Shao

Received: 21 July 2022
Accepted: 27 September 2022
Published: 29 September 2022

1. Introduction

With the establishment of a green and low-carbon energy system as a central part of the 2015 Paris Agreement on Climate Change (PA), a limitation of global warming well below 2 °C above preindustrial levels has become international consensus [1]. However, it is commonly criticized that only with much higher efforts than previously anticipated can cited goals be achieved [2]. Next to the energy sector, the transport sector, with approximately 16% of global greenhouse gas (GHG) emissions [3], still takes a lion's share of the overall 52.4 gigatonnes of CO_2 equivalent annually [4]. Furthermore, the quantity of light-duty vehicles is supposed to double by 2050, even increasing the share of emissions within this sector [5]. More efficient technologies have to be introduced to the market to counteract this development and meet the PA's goals. Electric vehicles (EVs) are one possible solution to cut GHG emissions in this sector [6]. Although EVs have a better CO_2 balance than traditional vehicles with internal combustion engines (ICE), there are still parts with huge improvement potential. In particular, the production of the battery itself takes a considerable share of EVs' overall life cycle emissions, which has already been researched within several studies [6–9]. Efficient recycling technologies for batteries, and especially for the active material, the so-called black matter–consisting mainly of scrapped anodes and cathodes–could significantly reduce battery life cycle GHG emissions. This can be explained by improved carbon emissions and energy credits compared to sourcing the same raw metals from the respective primary supply chains [10]. Furthermore, since the

European Union (EU) is heavily dependent on imports from foreign markets to meet its LIB production resources, the recovery and recycling of valuable metals from spent LIBs is a cornerstone of the EU's supply independence strategy [11]. To address the sustainable use of these materials, a new proposed regulation amending EU Directive 2006/66/EC and revised version No. 2019/1020, regulating batteries and waste batteries, including recycling efficiency, was published in December 2020 [12]. The proposed regulation stipulates specific material recovery rates, namely 90% for cobalt, copper, and nickel, and 35% for lithium, to be achieved by the end of 2025. By 2030, the recovery levels are further increased, with rates of 95% for cobalt, copper, and nickel, and 70% for lithium [13].

Although several different recycling technologies are already available, ranging from mechanical pre-treatment steps to pyrolysis and metallurgical processes, all face more or less substantial bottlenecks [14]. Mechanical pre-treatment steps, as described in Windisch-Kern et al. [15], are a necessary intermediate step to separate output fractions such as Fe, Cu, and Al from the black matter. This material can then be further processed within hydro-, bio-hydro, or pyrometallurgical processes.

For hydrometallurgical recycling options, the most significant limitation is a fluctuating input material caused by different cell chemistries of used batteries. Hydrometallurgical processes are susceptible to impurities such as fluorine, chlorine, graphite, and especially phosphorus, often either part of the electrolyte or the active material [16]. Additionally, lithium partly remains in the solvent, not being considered for further recovery due to economic considerations [17,18]. Furthermore, conventional hydrometallurgical processes need an extensive amount of acidic reagents, such as HCL, HNO_3, and H_2SO_4, requiring additional disposal or recycling efforts [19]. Despite these limitations, there are already technologies that have excellent recycling efficiencies when only one cathode material is recycled on its own. One possible solution to these harsh chemicals could be ascorbic acid. Researchers have shown that in a two-molar ascorbic acid, NMC cathode material could be recovered with more than 90% efficiency for Li, Co, Ni, and Mn [20]. Another example is the RecycLib process based on hydrometallurgy, which can recycle 80–90% if LCO or NMC cathode material is processed in isolation. In this process, a very mild chemical reagent is also used consisting of magnesium sulfate heptahydrate ($MgSO_4.7H_2O$), sodium chloride (NaCl), and deionized water [21]. A more sustainable alternative to traditional hydrometallurgy, however, is bio-hydrometallurgy. One of the most promising processes, bioleaching, requires less energy, is performed at lower temperatures, and has fewer toxic gas emissions [22]. Within bioleaching, microorganisms initiate metal dissolution by using inorganic compounds such as Fe^{2+}, FeS_2, etc., as an energy resource, leading to metabolic products, which are a lot less toxic than acids used in hydrometallurgy [23]. However, compared to hydrometallurgical processes, the leaching efficiency is quite low, the leaching time is long due to slow kinetics and pulp densities, and the microorganisms are often complicated to cultivate [24].

Compared to hydro- and bio-hydrometallurgical processes, which operate at lower temperatures, the pyrometallurgical route is performed at high temperatures and, therefore, is mostly insensitive to varying input materials and impurities [25]. However, these processes are likely to face the problem of lithium slagging and metal phosphide formation [26]. Although Li and P are only present in small concentrations compared to the overall battery weight, both elements are found on the EU's list of critical raw materials with increasing economic value and therefore have to be recycled [27,28]. Next to these technical recycling options, a recycling-oriented design of LIBs, with a more rational design of the module and battery pack itself, easier to handle materials, and a better configuration, could ease the recycling process. Solid-state electrolytes, anode-free cells, or other technical revolutions could move battery technology in a more sustainable direction but have yet to be thoroughly tested [29]. Until these innovations are introduced to the market, a promising solution to these problems is a hydrometallurgical process downstream of a pyrometallurgical process [30]. With the interconnection of efficient pyro- and hydrometallurgical

recycling technologies, the advantages of both methods can be used, eliminating most of the disadvantages [31].

Therefore, a novel reactor type was developed at the Chair of Thermal Processing Technology at Montanuniversitaet Leoben to avoid the abovementioned disadvantages in the pyrometallurgical process [32]. The novelty is found in an inductively heated bed of graphite cubes. The black matter is charged continuously via a screw conveyor from above, with the possibility of removing lithium and phosphorus via the gas phase. The main advantage of the reactor concept is the possibility of horizontal and radial homogenous temperature provision, so that an optimum heat transfer to the feedstock can be provided. Furthermore, this reactor design allows the formation of a thin melt film when heated. This, in turn, enormously shortens the diffusion paths compared with, for example, a molten bath [26]. Therefore, undesirable reactions such as iron phosphide formation or lithium slagging are suppressed, and phosphorus and lithium gasification are enabled instead. Therefore, it can be recovered more easily and cost-effectively [33].

Within the scope of this paper, a batch version of this reactor type is analyzed regarding the transfer coefficients of the containing metals from different active materials, not only for lithium and phosphorus, but also for other rare critical raw materials such as nickel, manganese, and cobalt. The influences of plant engineering on recovery rates of lithium via the gas phase are discussed. In particular, the accumulation and diffusion of the elements on and in the MgO crucibles used are examined in more detail. In-depth optimization measures must be taken on the plant design as it evolves into a continuous process. The proposed reactor concept is shown to be well suited for an efficient pyrometallurgical recycling step with considerable improvements in recovery rates compared to today's BAT technologies.

2. Materials and Methods

As in previous experimental series [26,28], all tests conducted within the scope of this study strictly followed a standardized practical scheme, comprising preparation, experimental procedure, sampling, and analyzing steps. In general, it must be noted that instead of using the continuous InduRed reactor concept, a batch processing lab-scale model with almost identical properties was used. The purpose of this was to ensure comparability to previous test series and a reasonable duration of the trials, resulting in a higher number of experiments at lower costs. The mentioned lab-scale version, the so-called InduMelt reactor, developed at the Chair of Thermal Processing Technology (Montanuniversitaet Leoben, Leoben, Austria), is shown in Figure 1.

The batch version also uses the principle of inductive heating, in which graphite cubes with a side length of 2.5 cm, an electrical resistance of 4–8 $\mu\Omega$m, and a density of 1.55–1.75 gcm^{-1} are heated. The crucible, which accommodates the graphite bed, is designed as a half-arch bottom with a diameter of 20 cm and a height of 60 cm made of MgO. It is held in position by a structure of refractory concrete and entirely insulated with a high-temperature refractory mat to reduce heat losses. For temperature control, two type S thermocouples were placed on the outer surface of the reactor bottom and another on the reactor wall above the coil. Two additional type K thermocouples were positioned within the graphite bed to realize a more accurate temperature measurement during the heating phase. After the maximum operating temperature of the type K thermocouples (about 1200 °C) was exceeded, the correlation between the inner reactor and outer crucible temperature known from preliminary experiments, the latter measured by the type S thermocouple, was used for the process control.

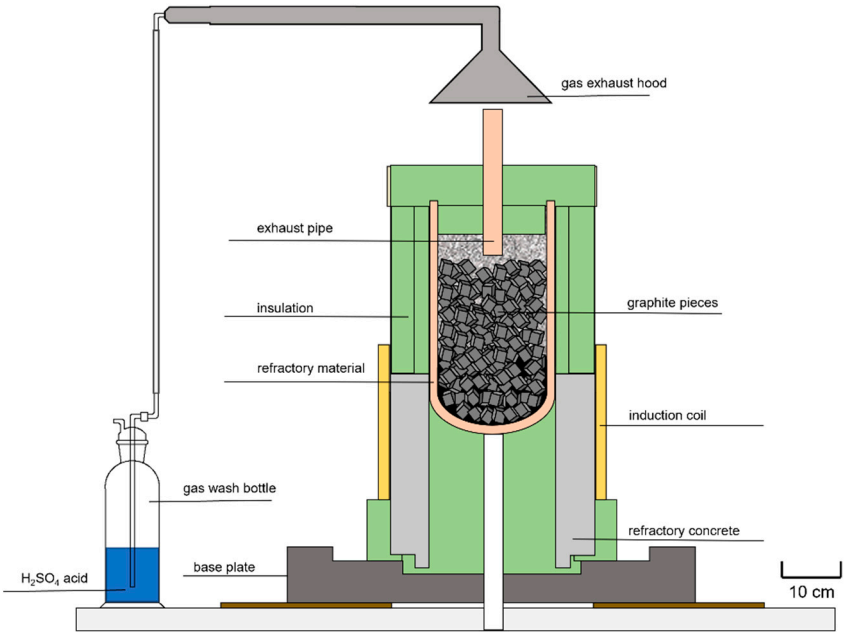

Figure 1. Schematic illustration of the so-called InduMelt crucible concept [23].

In this study, the cathode materials LCO, LFP, NCA, and NMC622, each mixed with the corresponding stoichiometrically required amount of carbon for complete reduction, were used as input material for the experiments. The reason why out of several different possible NMC chemistries only NMC622 was analyzed can be explained by today's and forecasted shares of this cathode material. In most scenarios, the NMC622 cathode chemistry takes the most significant share of up to 90% of all batteries used in electric vehicles in 2030 [34]. During preparation, a sample mass of approximately 550 g was put in the graphite bed's void fraction in each experiment. The composition of said samples can be seen in Table 1.

Table 1. Concentration of relevant elements in the samples used for the InduMelt experiments in wt.%.

Compound	Li	Co	Ni	Mn	Al	Fe	P	C
LCO_C [1]	5.67	48.17	-	-	-	-	-	20.00
LFP_C [1]	3.52	-	-	-	-	28.32	15.71	24.00
NCA_C [1]	5.88	4.99	39.76	-	2.28	-	-	20.00
NMC622_C [1]	5.73	9.73	29.07	9.07	-	-	-	20.00

[1] Difference to 100% detection rate due to the proportion of O.

The setup, test execution, and sampling were carried out in all tests according to a specified and uniform plan. It should be mentioned that the components were weighed in all the steps explained below during setup and dismantling. At the beginning, the layered loading of the MgO crucible of cubes and the individual sample material, as shown in Table 1, was performed. Two type K thermocouples were incorporated into these layers in the crucible center at different heights to ensure adequate process control in the lower temperature range up to approximately 1200 °C. For the subsequent insulation, an exhaust gas pipe made of Al_2O_3 was incorporated centrally in the lid insulation to be able to direct the gas produced during operation specifically into the gas extraction hood. After positioning the insulated crucible on the refractory concrete in the coil, one type S thermocouple each was mounted centrally on the reactor floor and one above the coil on the crucible wall. The aim is also to control the temperature above the measuring range of the type K thermocouples using known process values from preliminary tests.

Finally, the temperature was recorded during the experiments via LabVIEW with a parallel recording of the induced power data. To counteract overstressing of the crucible material due to excessive heating rates, a maximum temperature increase of 250 K/h over the experimental period of 7.5 h was selected. With a holding time of half an hour at the end of the tests, a uniform temperature of 1550 °C over the entire reactor was aimed for to always exceed the corresponding melting points of the metals contained. After the experiments, the setup was cooled for at least 24 h and consequently dismantled and unpacked in reverse order to the setup.

The experimental procedure is followed by a standardized sampling and analyzing scheme. Certain product phases, e.g., a slag or a metal alloy, were separated, weighed, and individually analyzed using ICP-OES according to ÖNORM EN ISO 11885:200911. This is performed by manually removing metal and slag depositions from the graphite cubes and the MgO crucible with subsequent magnetic separation. A fine powder phase formed due to abrasion during the removal was also sampled and analyzed separately.

Regarding the evaluation of the gas phase, an exhaust bell was positioned over the exhaust pipe, and a partial off-gas stream was passed over gas scrubbers containing a 2.5-molar H_2SO_4. To determine the actual presence of lithium or phosphorus in the exhaust stream, thus proving that a gaseous removal was achieved, said gas scrubbing medium was also analyzed using ICP-OES. All analysis results combined with the weighted samples were then used to investigate transfer coefficients of the metals of interest into the respective product phase, thus either the slag, metal, powder, or gas phase.

For a more precise statement of the results, each sample was tested at least twice. For a more straightforward assignment of the individual experiments, the respective cathode material and a consecutive numbering were used as nomenclature. For example, "LCO V1" means experiment one with a mixture of LCO with the respective carbon content from Table 1.

Regarding limitations of the overall process, the temperature is one crucial part that must be considered. Due to the thermal stability of the heating insulation material, temperatures above 1700 °C should not be exceeded. Another limitation for the batch version InduMelt is the limited power supply of 10 kW at maximum. However, for these trials, the heating rate was sufficient to prove that, at the temperature of 1550 °C, high rates of Li or P were transferred into the gas phase, which therefore proved the suitability of the reactor's core principle.

3. Results and Discussion

3.1. InduMelt Experiments

The main focus of this series of tests was to determine the quality of products that are generated during carbo-thermal reduction of the cathode materials LCO, LFP, NCA, and NMC622. In addition, attention was paid to the influence of plant engineering components on the lithium yield. A total of five fractions were identified as the resulting product streams:

- "Slag": Defined as a non-magnetic mineral phase with a grain size greater than 1 mm.
- "Powder": Particles smaller than 1 mm and categorized as close to non-magnetic.
- "Metal fraction": Defined as a magnetic alloy with a grain size larger than 1 mm.
- "Magnetic powder": Particles smaller than 1 mm obtained during magnetic separation.
- "Gas phase": Defined as the exhaust gas stream passed through the gas scrubber.

The product properties are discussed in detail in the following subsections to finally realize a comparison of all cathode materials. After the conducted series of experiments, a significant influence on the product quality could be established concerning interrupted gas stream out of the reactor due to a clogged gas pipe. In addition, it was found that the mass balance closure is not possible, mainly due to the difficulty of separating the fractions. Thus, only a qualitative consideration of the results is possible. The choice of reactor material of MgO has been found to significantly impact the transfer coefficient, which is further discussed.

3.1.1. Product Properties of LCO after the Experiments within the InduMelt Reactor

The series of tests started with experiments with LCO, with a total of two tests being carried out. Figure 2 shows examples of the resulting slag, metal, and powder.

(**a**) (**b**) (**c**)

Figure 2. Examples of the products from the InduMelt experiments with LCO: (**a**) Slag; (**b**) Metal; (**c**) Powder.

Table 2 lists both the masses of the initial input and the fractions obtained. On the one hand, it is noticeable that no sparse magnetic powder was formed and that the proportion of slag, with 0.5% and 0.8% of the total product mass, is vanishingly small compared with the magnetic fractions. Looking at the magnetic fractions, it can be seen that the transfer to the metal fraction was lower by mass in the second experiment.

Table 2. Sample mass at the beginning of the InduMelt experiment with LCO and weight of the resulting products in grams.

Trial	Input [g]	Slag [g]	Powder Sparse Magnetic [g]	Metal [g]	Powder [g]
LCO V1	549.6	1.3	-	242.3	35.2
LCO V2	551.0	2.4	-	217.1	77.5

Analyses of these three products in ICP-OES allowed the chemical composition to be determined, as shown in Table 3. It should be noted that a complete detection rate is not possible for several reasons. Firstly, in addition to the added carbon, the initial composition also contains oxygen from the lithium metal oxide, which cannot be measured via ICP. In addition, the measurement is subject to particular measurement uncertainty. The third factor is sampling. Since the fractions cannot be completely separated from each other without doubt due to their appearance, there is always a certain degree of mixing, which significantly influences the results. The phenomena mentioned must also be considered in this paper's subsequent experiments. Nevertheless, trends can be identified, allowing a statement to be made about the process.

Table 3. Content of Li and Co in the individual product phases of LCO V1 and LCO V2 in wt.%.

Element	Slag [%]	Powder Sparse Magnetic [%]	Metal [%]	Powder [%]
LCO	**V1 | V2**	**V1 | V2**	**V1 | V2**	**V1 | V2**
Li	5.59 [1] | 15.80 [2]	- [1] | - [2]	0.12 [1] | 0.03 [2]	0.69 [1] | 0.03 [2]
Co	3.30 [1] | 0.14 [2]	- [1] | - [2]	93.90 [1] | 83.50 [2]	66.60 [1] | 81.30 [2]
Sum [3]	8.89 [1] | 15.94 [2]	- [1] | - [2]	94.02 [1] | 83.53 [2]	67.29 [1] | 81.33 [2]

[1] Trial 1 (LCO V1). [2] Trial 2 (LCO V2). [3] Difference to 100% detection rate due to the proportion of C and O in the fractions or measurement uncertainties and complex sampling.

On closer inspection and direct comparison between the two tests, it can be seen that there are significant differences in product quality. The proportion of lithium in the slag is

almost three times higher in the second test. If the mass ratios in Table 2 are also considered, a higher mass proportion is recorded in the second experiment as well. However, since the proportion of slag is negligible, as already mentioned, this fact should not be overestimated. Another interesting finding is that the amount of Co in LCO V2 is lower in the metal but higher in the powder. This is also reflected in the comparison of the masses in Table 2. If the results from Tables 2 and 3 are summarized, the goal of reducing the metal oxide was basically achieved in both experiments. Even if in the second test the output into the metal fraction did not succeed to such an extent as in the first trial, the high metal content, and the quality, of the increased metal powder content again compensates for the result. However, in terms of simpler and more efficient post-treatment of the products from the InduMelt process, transfer to a metal fraction is preferable. In this application, an acceptable quality of the metal could be found. Maximizing the yield of a metal fraction should be strived for and can be considered an allowable conclusion for the above findings.

By including the results of the off-gas analysis in the interpretation of the results, as shown in Table 4, it can be seen that the lithium extraction amount of 1230 mg/L in the first test is higher than that of the second with 860 mg/L. If we now compare the removal of Li from the metal and powder with the result from the off-gas scrubber, no connection between the increased removal rate in the off-gas with an improved removal of Li in the chemical analysis can be seen.

Table 4. Results of the washing water analysis from the gas scrubber in the tests with LCO in mg/l.

Trial	Li [mg/L]
LCO V1 [1]	1230.00
LCO V2 [2]	860.00

[1] Sample quantity for analysis: 150 mL. [2] Sample quantity for analysis: 100 mL.

3.1.2. Product Properties of LFP after the Experiments within the InduMelt Reactor

In investigating the cathode material LFP, two tests were carried out in the InduMelt plant. In addition to slag and metal, both magnetic and non-magnetic powder were recovered from the reactor after the trials. Examples of the appearance of these fractions are illustrated in Figure 3.

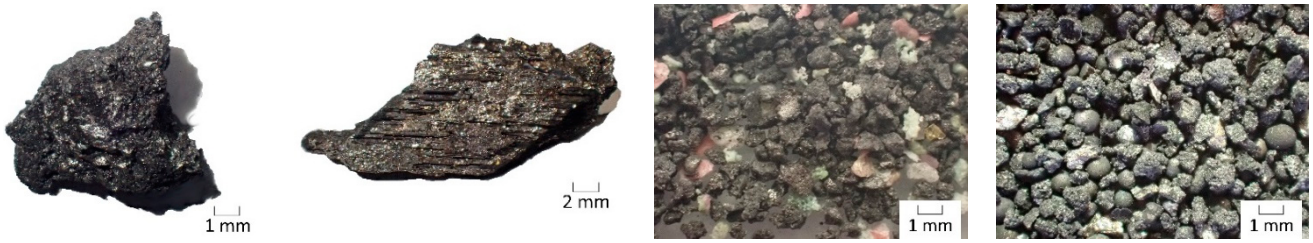

(**a**) (**b**) (**c**) (**d**)

Figure 3. Examples of the products from the InduMelt experiments with LFP: (**a**) Slag; (**b**) Metal; (**c**) Powder sparse magnetic; (**d**) Powder.

The masses of the products and the input material of the two tests can be taken from Table 5. If the masses of the two tests are compared with each other, it can be seen that in LFP V2 the proportion of metal is higher and that of slag is lower. Even if this fact indicates that the efforts towards the higher output of a metal fraction for post-treatment have been successful, the higher proportion of metal powder must be considered in more detail.

Table 5. Sample mass at the beginning of the InduMelt experiment with LFP and weight of the resulting products in grams.

Trial	Input [g]	Slag [g]	Powder Sparse Magnetic [g]	Metal [g]	Powder [g]
LFP V1	548.9	1.8	8.7	145.8	36.9
LFP V2	550.1	0.9	8.9	168.7	60.9

If the chemical composition analyses from Table 6 are included in the interpretation, the picture is entirely different from that assumed after evaluating the results with LCO. Li, Fe, and P input into the slag are many times higher in the second test than in the first, and increased values can also be found in the sparsely magnetic powder. High iron and low phosphorus content are particularly desirable in the metal fraction. This requirement is better achieved in the first test. The results in the magnetic powder also speak for the statement to be made here that the second trial, despite a better appearance of the mass ratios, delivers poorer outcomes in the product quality. Therefore, the lower P and higher Fe content in the first test are the decisive values.

Table 6. Content of Li, Fe, and P in the individual product phases of LFP V1 and LFP V2 in wt.%.

Element	Slag [%]	Powder Sparse Magnetic [%]	Metal [%]	Powder [%]
LFP	V1 | V2	V1 | V2	V1 | V2	V1 | V2
Li	0.37 [1] | 6.73 [2]	1.91 [1] | 3.62 [2]	0.22 [1] | 0.81 [2]	3.87 [1] | 3.43 [2]
Fe	0.07 [1] | 4.01 [2]	0.60 [1] | 0.70 [2]	77.10 [1] | 69.90 [2]	46.60 [1] | 43.00 [2]
P	0.07 [1] | 7.96 [2]	0.78 [1] | 1.98 [2]	14.30 [1] | 18.80 [2]	12.80 [1] | 14.40 [2]
Sum [3]	0.51 [1] | 18.70 [2]	3.29 [1] | 6.30 [2]	91.62 [1] | 89.21 [2]	63.27 [1] | 60.83 [2]

[1] Trial 1 (LFP V1). [2] Trial 2 (LFP V2). [3] Difference to 100% detection rate due to the proportion of C and O in the fractions or measurement uncertainties and complex sampling.

Looking at the analyses of the gas fraction in Table 7, it is clear that the yield of Li and P in the second trial is many times higher than in the first trial. The experiments with LFP can be summarized as follows: Either a larger fraction with lower metal quality but a higher yield of Li and P is recovered via the gas stream or a smaller fraction with opposite properties to the former. A comparison of the results of the trials with LCO and LFP is difficult to perform, since the two differ fundamentally in their structural makeup. While LCO, NCA, and NMC are layered oxides, LFP is built up as a three-dimensional olivine structure [35,36].

Table 7. Results of the washing water analysis from the gas scrubber in the tests with LFP in mg/L.

Trial	Li [mg/L]	P [mg/L]
LFP V1 [1]	7.60	87.00
LFP V2 [2]	310.00	3130.00

[1] Sample quantity for analysis: 100 mL. [2] Sample quantity for analysis: 250 mL.

3.1.3. Product Properties of NCA after the Experiments within the InduMelt Reactor

The cathode material NCA has been tested a total of three times in this described InduMelt setup. After reviewing the first two tests, it was found that the results of the lithium extracted via the gas stream were far below the expected values in both cases. Consequently, a third attempt was carried out. Figure 4 again shows illustrative examples of the fractions obtained: slag, metal, powder with low magnetic content, and magnetic powder.

(**a**) (**b**) (**c**) (**d**)

Figure 4. Examples of the products from the InduMelt experiments with NCA: (**a**) Slag; (**b**) Metal; (**c**) Powder sparse magnetic; (**d**) Powder.

The masses of the individual fractions in Table 8 show similar ratios. However, at least a small proportion of slag was recovered in the third test, while none was found in the other two. From this representation, it is difficult to estimate the success of the experiments.

Table 8. Sample mass at the beginning of the InduMelt experiment with NCA and weight of the resulting products in grams.

Trial	Input [g]	Slag [g]	Powder Sparse Magnetic [g]	Metal [g]	Powder [g]
NCA V1	550.5	-	2.5	225.9	60.4
NCA V2	550.0	-	4.2	230.7	54.9
NCA V3	550.0	1.0	3.1	223.6	58.4

The analysis results shown in Table 9 provide a better insight into product quality. Particularly noteworthy is the third test, with its high Ni rates in the metal and powder phase and, compared with the other tests, lower values of Li in the fractions, except the slag. Although the presence of slag is not desirable, the low mass in Table 8 of only 1 g means that this fact should not be overestimated. If only the first two tests are compared, a similar composition can be seen, especially in the metal and powder fractions.

Table 9. Content of Li, Co, Ni, and Al in the individual product phases of NCA V1, NCA V2, and NCA V3 in wt.%.

Trial	Slag [%]	Powder Sparse Magnetic [%]	Metal [%]	Powder [%]
NCA	V1 | V2 | V3	V1 | V2 | V3	V1 | V2 | V3	V1 | V2 | V3
Li	- [1] | - [2] | 12.80 [3]	13.70 [1] | 9.76 [2] | 9.20 [3]	0.20 [1] | 0.29 [2] | 0.06 [3]	4.39 [1] | 5.26 [2] | 3.28 [3]
Co	- [1] | - [2] | 0.10 [3]	0.19 [1] | 0.09 [2] | 0.10 [3]	9.54 [1] | 9.13 [2] | 9.81 [3]	5.07 [1] | 4.78 [2] | 6.20 [3]
Ni	- [1] | - [2] | 1.17 [3]	4.78 [1] | 2.42 [2] | 1.55 [3]	86.90 [1] | 89.60 [2] | 94.30 [3]	47.30 [1] | 43.30 [2] | 61.40 [3]
Al	- [1] | - [2] | 2.49 [3]	2.06 [1] | 1.72 [2] | 1.85 [3]	0.63 [1] | 0.48 [2] | 0.79 [3]	2.14 [1] | 1.96 [2] | 3.48 [3]
Sum [4]	- [1] | - [2] | 16.56 [3]	20.73 [1] | 13.99 [2] | 12.70 [3]	97.26 [1] | 99.49 [2] | 104.96 [3]	58.90 [1] | 55.30 [2] | 74.36 [3]

[1] Trial 1 (NCA V1). [2] Trial 2 (NCA V2). [3] Trial 3 (NCA V3). [4] Difference to 100% detection rate due to the proportion of C and O in the fractions or measurement uncertainties and complex sampling.

The above findings are also supported by the analyses of the gas flow, which can be seen in Table 10. Thus, an identical amount of 65 mg/L Li was detected in the wash water in the first two tests. The good result of the solid fractions in the third test can also be

confirmed by the high Li content of 960 mg/L. In this series of experiments, a positive effect on product quality and yield of Li from the solid fraction can be observed with increased transfer to the wash water.

Table 10. Results of the washing water analysis from the gas scrubber in the tests with NCA in mg/L.

Trial	Li [mg/L]
NCA V1 [1]	65.00
NCA V2 [2]	65.00
NCA V3 [3]	960.00

[1] Sample quantity for analysis: 200 mL. [2] Sample quantity for analysis: 200 mL. [3] Sample quantity for analysis: 100 mL.

3.1.4. Product Properties of NMC622 after the Experiments within the InduMelt Reactor

Three tests were carried out with NMC622. Here, similar to the test series with NCA, the wash water analysis of the exhaust gas stream was also far below that expected in the first two trials. The four fractions obtained, slag, metal, barely magnetic powder, and magnetic powder, are exemplified in Figure 5.

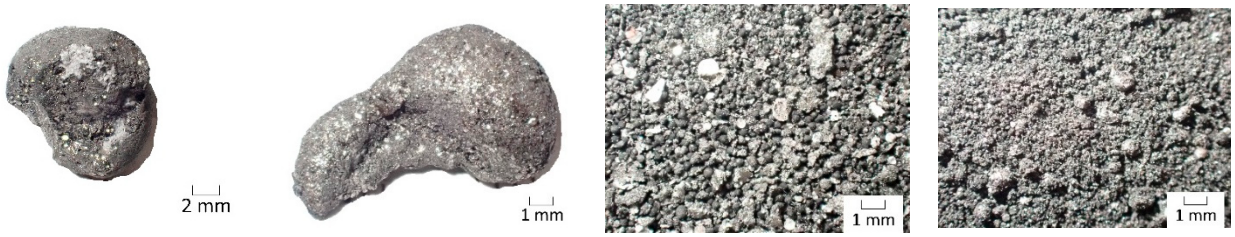

(**a**) (**b**) (**c**) (**d**)

Figure 5. Examples of the products from the InduMelt experiments with NMC622: (**a**) Slag; (**b**) Metal; (**c**) Powder sparse magnetic; (**d**) Powder.

In terms of the mass ratios in Table 11, NMC622 V3 with a higher metal and lower powder content than the other two trials, is worth highlighting. The higher proportion of barely magnetic powder or the presence of slag can be classified as more negative. As with the other test series comments, the significance of this weight in terms of test evaluation is subordinate.

Table 11. Sample mass at the beginning of the InduMelt experiment with NMC622 and weight of the resulting products in grams.

Trial	Input [g]	Slag [g]	Powder Sparse Magnetic [g]	Metal [g]	Powder [g]
NMC622 V1	550.2	-	3.4	225.7	54.3
NMC622 V2	550.2	-	4.2	220.1	60.5
NMC622 V3	549.4	3.0	10.9	231.6	49.2

However, the results of the chemical analysis given in Table 12 allow the conclusion that NMC622 V3 was more successful than the other two in terms of the product quality obtained. NMC622 V3 is convincing, with higher values for Co, Ni, and Mn, as well as lower values for Li. Although the extraction of a slag fraction is not desired in terms of maximum Li recovery, this is negligible in this consideration due to the low mass fraction of 3 g.

Table 12. Content of Li, Co, Ni, and Mn in the individual product phases of NMC622 V1, NMC622 V2, and NMC622 V3 in wt.%.

Trial	Slag [%]	Powder Sparse Magnetic [%]	Metal [%]	Powder [%]
NMC622	**V1 | V2 | V3**	**V1 | V2 | V3**	**V1 | V2 | V3**	**V1 | V2 | V3**
Li	- [1] | - [2] | 11.00 [3]	8.26 [1] | 6.95 [2] | 5.50 [3]	0.17 [1] | 0.29 [2] | 0.10 [3]	2.95 [1] | 2.88 [2] | 2.16 [3]
Co	- [1] | - [2] | 0.01 [3]	0.26 [1] | 0.12 [2] | 0.61 [3]	18.30 [1] | 18.70 [2] | 20.80 [3]	13.20 [1] | 11.90 [2] | 14.80 [3]
Ni	- [1] | - [2] | 0.06 [3]	1.52 [1] | 0.45 [2] | 1.94 [3]	57.90 [1] | 58.80 [2] | 66.30 [3]	34.50 [1] | 32.20 [2] | 46.00 [3]
Mn	- [1] | - [2] | 0.12 [3]	0.31 [1] | 0.18 [2] | 0.76 [3]	16.70 [1] | 16.20 [2] | 18.90 [3]	12.40 [1] | 11.00 [2] | 14.00 [3]
Sum [4]	- [1] | - [2] | 11.20 [3]	10.35 [1] | 7.69 [2] | 8.81 [3]	93.07 [1] | 93.99 [2] | 106.10 [3]	63.05 [1] | 57.98 [2] | 76.96 [3]

[1] Trial 1 (NMC622 V1). [2] Trial 2 (NMC622 V2). [3] Trial 3 (NMC622 V3). [4] Difference to 100% detection rate due to the proportion of C and O in the fractions or measurement uncertainties and complex sampling.

In addition to the chemical analysis of the solid fraction, the hypothesis that NMC622 V3 was the most successful among all NMC622 tests is confirmed by the analyses of the gas stream, shown in Table 13. While NMC622 V1 and V2 have low values of 32 mg/L and 20 mg/L, respectively, NMC622 V3, with 980 mg/L, can be considered successful.

Table 13. Results of the washing water analysis from the gas scrubber in the tests with NMC622 in mg/L.

Trial	Li [mg/L]
NMC622 V1 [1]	32.00
NMC622 V2 [2]	20.00
NMC622 V3 [3]	980.0

[1] Sample quantity for analysis: 200 mL. [2] Sample quantity for analysis: 200 mL. [3] Sample quantity for analysis: 100 mL.

3.1.5. Transfer Coefficient of the Elements to the Individual Fractions

To better illustrate and compare the previously described results, Figure 6 presents them as individual transfer coefficients of the metals of interest into obtained product phases. Thus, the distribution of the elements into the resulting solid fractions is visualized. For this purpose, the quantities of the individual elements were compared with those from the analysis results. Since each cathode material was repeated at least once, the transfer rates obtained in the individual tests were averaged. For a complete presentation of the results, an error bar was also integrated to show the deviations in the tests. Based on the analyses of the gas scrubber in the individual tests, there was at least one utterly successful test per cathode material and at least one unsuccessful experiment. Therefore, this circumstance allows the absolute lower and upper limits of the transfer coefficients to be achieved to be shown with this display variant. Since this is a process aimed at discharging Li and P from the reactor compartment, an additional phase, referred to as "removed", has been added to the solid fractions in the presentation, which indicates the number of individual elements not found in the overall output material compared to the input material. The material removed from the solid fractions can be found in the gas stream but also in the reactor, depending on the element. At this point, it is essential to mention again that the aim is to create a reference to make experiments in this apparatus comparable with each other via trends. This, in turn, aims to make visible the influence and effectiveness of changed adjusting screws in the course of successive optimization of the design and process control.

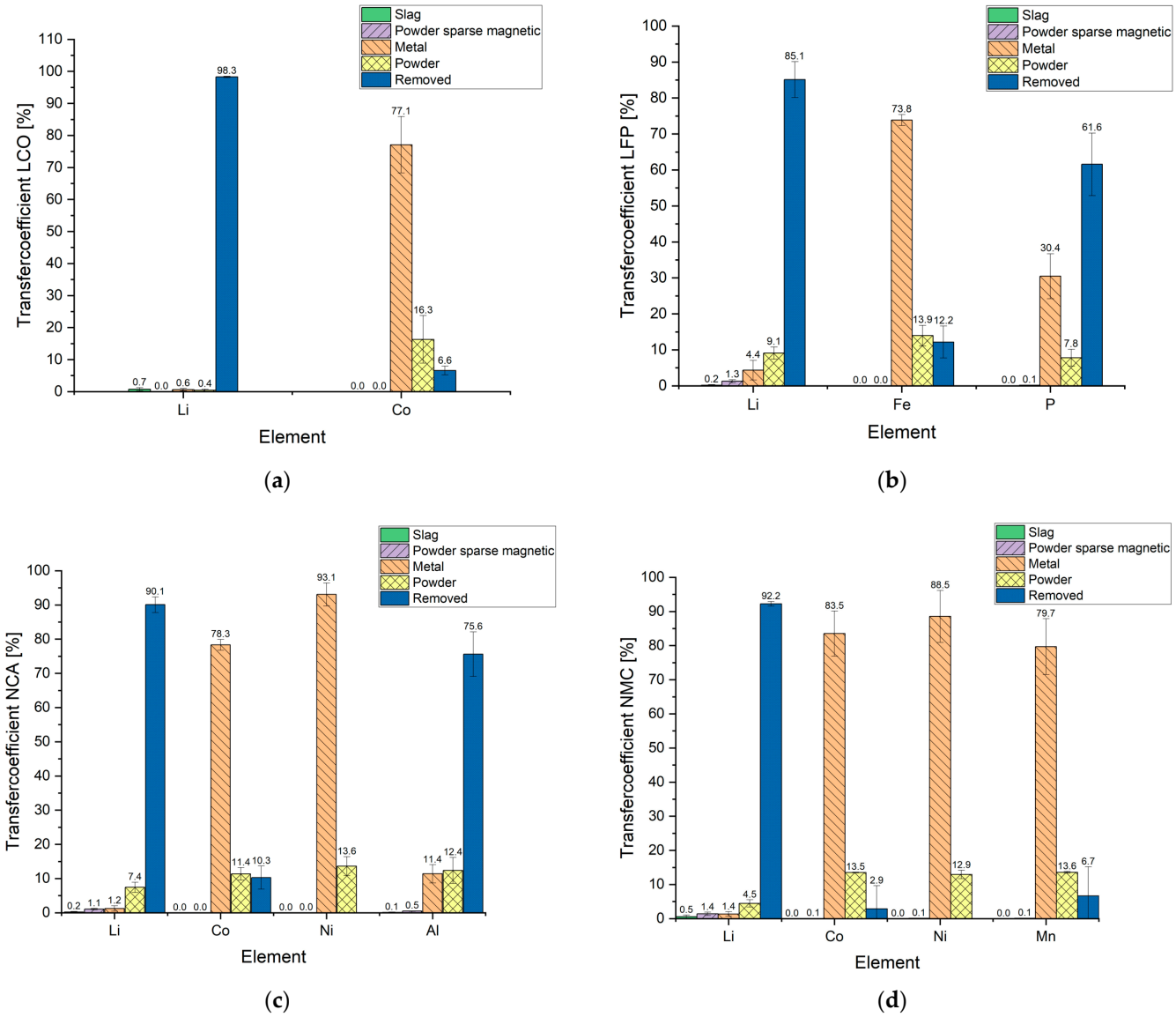

Figure 6. Transfer coefficients of the individual elements including variance because of disturbed exhaust gas discharge: InduMelt experiments with (**a**) LCO, (**b**) LFP, (**c**) NCA, and (**d**) NMC.

Figure 6a shows the transfer coefficients of LCO. Here, a removal rate for Li of more than 98% has been achieved. Most of the Co is located in the metal. The portion in the "removed" section can be assumed to be packing at the bottom of the reactor. A discharge on this scale via the gas stream is unlikely due to the chemical properties of Co.

The transfer coefficients of LFP are presented in Figure 6b. It should be emphasized that about 85% of the lithium, but also more than 60% of the P, could be removed. When considering the metal phase, the proportion of P is to be classified as disadvantageous, since a downstream oxidation step is necessary for phosphorus-free iron recovery, whereby the phosphorus is slagged [32].

The transfer coefficients of the nickel-rich cathode materials NCA and NMC622 in Figure 6c,d are extremely interesting from a process-engineering point of view. Although Li removal of over 90% could be achieved in both series of experiments, the coefficients of Co, Ni, and Mn require closer examination.

Starting with NCA, it should be noted that the value of Co removed is present as reactor attachment and has not left the reactor chamber. Due to the high oxygen affinity of Al, it is reasonable to assume that this was either partially discharged in particle form via the gas stream or entered into a compound with the crucible material. A special feature can be

seen in the case of Ni. Here, the sum of the transfer coefficient of metal and powder exceeds the 100% mark. This can be attributed in part to the difficult sampling, the division of the individual fractions, and the subsequent weighing but also measurement inaccuracies of the analyses. A complete separation into the fractions by sieving and magnetic separation is impossible due to inclusions or adhesions of unreduced active material or reducing agent. The subsequent weighing of the individual fractions finally results in a value that may deviate from the actual mass. As a result, the mass balance of the individual elements cannot be concluded after considering the analysis results. Nevertheless, this representation variant is permissible, since the trend is quite evident. The plot of the removed fraction has been omitted from the graph because a negative value, thus implying a theoretical production of Co, defies all logic and is not practically possible in this context.

The same line of reasoning Is valid when considering NMC622. In this case, there is also a clear trend toward transferring Co, Ni, and Mn to the metal fraction. The resulting negative bar for Ni was omitted for the same reasoning as Co for NCA. However, the error bars for Co and Mn in the negative range were omitted.

Comparing the tests of all cathode materials, it can be stated that, as the number of elements in the starting materials increases, closing the mass balance becomes more difficult.

3.2. Experimental and Plant Engineering-Based Influences on Product Qualities and Transfer Coefficients

The decisive factor for a successful future upscaling of the InduRed reactor concept towards industrial scale is a high product quality of the solid fraction and a maximum output of Li from the reactor. At this point, from a process-engineering point of view and as an understanding of the overall concept, it is crucial to take a closer look at the reactions that are likely to take place. At this point, it should be mentioned again that in the InduRed reactor concept, and consequently also in the InduMelt system presented here, a high CO/CO_2 value and low pO_2 partial pressure prevail due to the high C content and the resulting reactions.

Windisch-Kern et al. [28] argued, on thermokinetic studies by Kwon and Sohn [37], that the reaction of lithium metal oxide in the presence of C produces lithium carbonate, as presented in Equation (1).

$$4LiMeO_{2(s)} + 3C_{(s)} \rightarrow 2Li_2CO_{3(s)} + 4MeO_{(s)} + CO_{2(g)} \quad (1)$$

Considering the results of the transfer coefficients shown in Figure 6, it can be seen that more than 85% Li cannot be found in the fractions investigated anymore in comparison to the input amount. Based on this finding, a discharge via the gas phase is likely. This is also underlined by the presence of Li in the gas scrubbing liquid. Suppose the cross-reactions of the impurity elements are disregarded and a simplified consideration of the existing lithium carbonate is made. In that case, a possible reaction sequence to gaseous lithium can be derived from the experimental determination by Abegg et al. [38], demonstrated in Equations (2) and (3).

$$Li_2CO_{3(s)} + 4C_{(s)} \rightarrow Li_2C_{2(s)} + 3CO_{(g)} \quad (2)$$

$$Li_2C_{2(s)} \rightarrow 2Li_{(g)} + 2C_{(s)} \quad (3)$$

In addition to the stochiometric, necessary amount of carbon added to the cathode materials, the graphite bed ensures a huge excess supply of carbon at any time, as mentioned before. Therefore, the formation of Li_2C_2 is enabled according to Equation (2). Li_2C_2 is subsequently decomposed (Equation (3)) into its elements at the prevalent temperatures, with Li being transferred to the gaseous state. This provides a unique opportunity to separate Li from the other metals, limiting its slagging while recovering it. In addition, the reactor's low pO_2 and high CO/CO_2 value allow the assumption that reoxidation of the Li can probably only be expected outside this zone. As a result of this process of lithium

removal, due to its known reactivity and oxygen affinity, the earliest possible removal of the gas from the reactor must occur to increase the removal rate.

To complete the reaction sequence, the reactions of the possible direct or indirect reduction of the metal oxide follow in Equations (4) and (5) [28,39].

$$MeO_{(s/l)} + C_{(s)} \rightarrow Me_{(s/l)} + CO_{(g)} \quad (4)$$

$$MeO_{(s/l)} + CO_{(g)} \rightarrow Me_{(s/l)} + CO_{2(g)} \quad (5)$$

To determine the successful implementation of this Li removal and identify the composition of other possible adhesions on and in the crucible material, the crucibles used were analyzed before and after the experiment.

Table 11 illustrates the individual reactor weight before and after the test, as well as the resulting difference. It can be seen that the weight of the MgO crucible increases in all experiments, suggesting that packing has occurred. The mentioned adhesion comprises sample material that cannot be separated from the reactor wall by diffusion or clogging to the wall, but also residues from the structure, such as incompletely separated insulation material. In order to obtain a more precise statement about the distribution of the individual elements in and on the crucible, the reactor was analyzed by ICP-OES. To simplify the presentation, the analyses in mg/kg are converted to percentages and multiplied by the mass of the crucible. In turn, the mass of the individual elements is calculated from this. It should be mentioned that the following results have been corrected for the value of the original composition of the crucible. Including the weight, it was consequently possible to determine the proportion of the individual elements to the entire crucible.

In the beginning, the influence of double use of the crucible with different cathode materials was considered. For this purpose, the first test was performed with LFP (LFP V1). In the experiment LFP V2, the crucible was previously used in the LCO V2 test. Table 14 illustrates the values for Fe and P. The reason for not showing Li is that a clear allocation of Li in the LFP V2 experiment to LFP is not possible, since this could theoretically also originate entirely from the first experiment with LCO. The mass of Fe was significantly reduced by more than 85%, that of P by almost 76%. Taking the findings of the weighing from Table 15 into account, it can be seen that between the tests with one-time and two-time use of the crucible, the mass increase during the test was reduced by half. This result suggests that some sort of passivation layer reduces both the accumulation of Fe on the crucible and the increase in total weight by a preliminary test.

Table 14. Mass distribution of Fe and P in the reactor for the InduMelt experiments with LFP.

Trial	LFP V1 [g]	LFP V2 [g]	Difference [%]
Fe	17.8	2.6	−85.4
P	26.0	6.3	−75.7

This finding was subsequently extended to include whether such passivation is also successful with the same cathode material. For this purpose, the nickel-rich materials NCA and NMC622 were examined in more detail.

Table 16 shows the results from the test series with NCA. As with the tests with LFP, it can be concluded here that the deposition of the metals can be reduced when the crucible is used several times. In this case, there is more than 65% less adhesion of Ni in the second test than in the first, and no adherence of Co. However, a disadvantage is undoubtably that, from these results, the assumption can also be made that Li diffuses into the reactor material or adheres to it, even if the crucible is used repeatedly. However, it is worth mentioning here that from the analysis results in Section 3.1.3, Table 10, it was clarified that the removal of Li from the reactor in the first and second experiments was much worse than in the third experiment. Suggesting that due to the reduced removal of the gas flow from the reactor, it accumulated in the reactor chamber, favoring diffusion or adhesion to the crucible and

thus affecting the result in Table 16. However, the lower mass gains in the second trial compared to the first trial is already evident with the inclusion of Table 15. The finding of this effect from the experimental series with LFP, as mentioned earlier, can therefore also be confirmed.

Table 15. Weight difference of the reactor before and after the individual InduMelt trials.

Trial	Weight Reactor before Trial [g]	Weight Reactor after Trial [g]	Difference [g]
LCO V1	4655.0	4766.2	111.2
LCO V2 [1]	4761.5	4828.9	67.4
LFP V1	4650.2	4813.6	163.4
LFP V2 [1,2]	4829.2	4911.0	81.8
NCA V1 [1]	5083.9	5161.7	77.8
NCA V2 [1,2]	5161.7	5219.5	57.8
NCA V3	5011.2	5091.1	79.9
NMC V1 [1]	4786.8	4885.1	98.3
NMC V2 [1,2]	4885.1	4947.0	61.9
NMC V3	5071.8	5154.1	82.3

[1] Dual use. [2] Second experiment with the reactor.

Table 16. Mass distribution of the elements in the reactor for the InduMelt experiments with NCA.

Trial	NCA V3 [g]	NCA V1/V2 [g]	Difference [%]
Li	11.7	32.7	64.2
Co	0.6	0.0	−100
Ni	7.1	2.5	−65.2
Al	-	-	-

For the continuous process, the question now arises as to whether a kind of saturation state of Li occurs at a certain point, and the removal of this can be increased via the gas flow.

The results presented in Table 17 show those from the test series with NMC622. Compared with those from the NCA trials, a similar percentage difference for Li of just over 60% can be seen. A significant difference in comparison with the test series with LFP and NCA are the results of the other metals, which are the main components of the solid fraction. It is evident that there is no reduction, but rather a massive increase in diffusion or adhesion. The line of argument can be continued in parallel, as before, when including the higher Li yield in the third experiment to the other two from Section 3.1.4, Table 13. Even if, in principle, the proportion of the masses of Co, Ni, and Mn is negligible concerning the feed quantity of 550 g, these adhesions must be taken into account, especially for further development into a continuous process. In the future, this can lead to a successive reduction in the size of the reactor chamber. This can cause, in addition to reduced product output, also problems in terms of plant engineering.

Table 17. Mass distribution of the elements in the reactor for the InduMelt experiments with NMC622.

Trial	NMC622 V3 [g]	NMC622 V1/V2 [g]	Difference [%]
Li	17.0	44.1	61.4
Co	0.2	0.9	82.3
Ni	1.3	2.9	54.4
Mn	2.2	7.6	71.7

Especially as a knowledge base for the plant design of the continuous concept, the location of these processes in the reactor or distribution of the elements over the crucible

height is of particular interest in connection with the diffusion and adhesion of the sample material. For this purpose, the crucibles were divided into three sub-areas, each after the corresponding tests during sampling and analyzed by ICP-MS after weighing the individual fractions. Figure 7 shows the reactor from the LFP V2 experiment during this process as a representative example for all experiments. The end of the measuring tape in Figure 7a marks the dividing line between the base and the middle section, since, at this point, a higher packing was found to merge into the base area. The second dividing line between the middle and upper parts was selected 9 cm above it. This can be explained by the optical difference between these parts, i.e., a brown–black or greenish area. In Figure 7b–d, the appearance of the divided sectors can be seen. Figure 7b illustrates the upper sector, where only a thin area on the inside of the crucible shows a color change indicating a reaction with the sample material. The situation is different in Figure 7c, which symbolizes the middle section as an example. Here, a massive diffusion of the samples into the crucible material is evident. In Figure 7d, a part of the bottom is shown in which, in addition to a recognizable diffusion, a massive adhesion to the inside of the reactor can be seen.

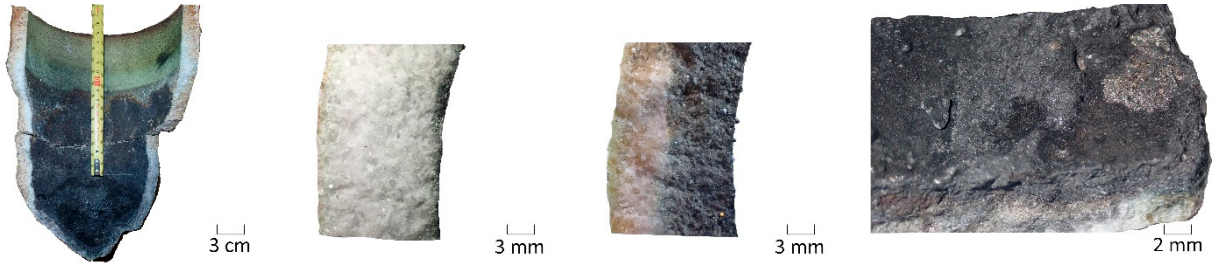

Figure 7. Example of the crucible appearance after trial LFP V2 during sampling for analyses: (**a**) Crucible over the height; (**b**) Top part; (**c**) Middle area; (**d**) Bottom.

Of particular interest was the distribution of the individual elements over the height of the reactor, but also the differences between using the crucibles once or twice. This was implemented graphically in Figure 8. It should be mentioned here that the analyses of the crucible areas were corrected for the composition of the crucible before the test to obtain a veritable result. The diffused and adhering mass of the individual elements was divided up as a percentage over the height according to the analyses of the particular areas.

Figure 8a shows the results of the series of experiments with LFP. As mentioned earlier, a crucible was used for LFP V2, which was previously used for the LCO V2 experiment. For this reason, its results are also shown for the sake of completeness in the area of the elements Li and Co. If the results from Section 3.1.2 are also taken into account, the increased proportion of Li removal from the solid fractions in the first test may indicate the increased entry of gaseous Li into the crucible wall. Since a relatively large proportion is found in the lower region of the crucible, it is reasonable to assume that a considerable amount of the Li diffused into the crucible instead of migrating through the bed into the gas space above it and then leaving the reactor chamber via the gas outlet. Comparing the experiments from LFP with already used or new reactor material, it can be seen that the entry of Li in the second experiment moves in the direction of higher layers. This, in turn, leads to the assumption that the motivation of the Li here was on the side of migration through the packed bed and possibly saturation of the crucible material occurred in the first experiment, or some passivation occurred by the Co from the first experiment with this crucible. The accumulation of Fe in the lower region can be argued to be due to the surfaces of the crucible in contact with the sample material.

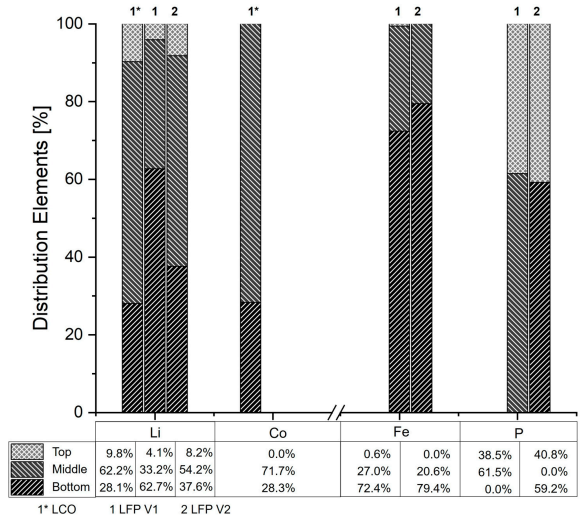

(**a**)

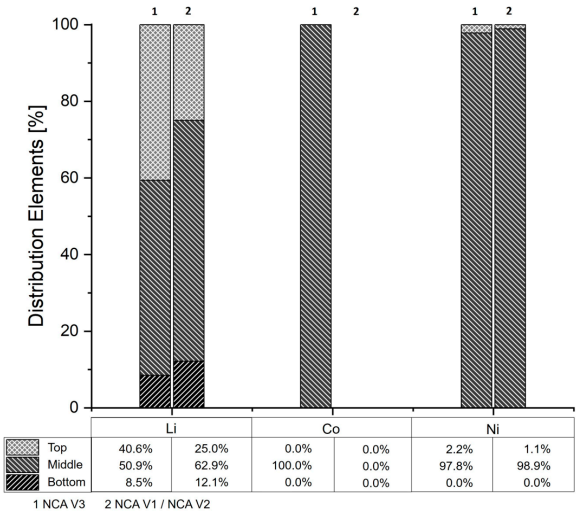

(**b**)

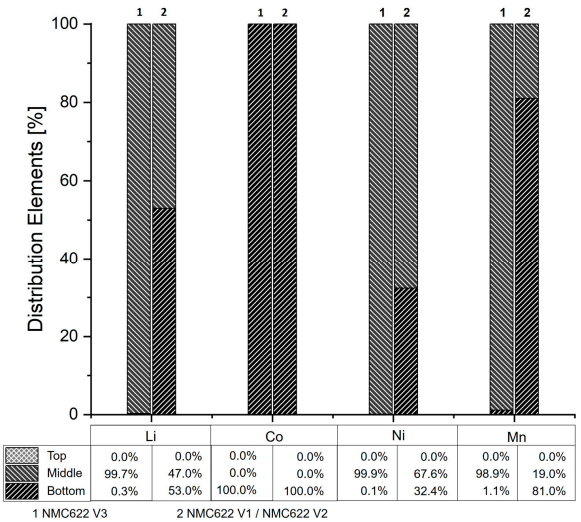

(**c**)

Figure 8. Mass distribution of adhesion to and absorption into the reactor wall of the respective elements: (**a**) Alteration in the trial with LCO and LFP, (**b**) NCA, and (**c**) NMC622.

Following this explanation, the P also tends to be removed via the gas stream, which is also supported by the results of the exhaust gas analysis in Section 3.1.2. However, for continuous operation, careful consideration of the P take-off in the plant design must be carried out, in any case, to keep the contact between liquid Fe and gaseous P as low as possible and thus suppress the undesirable iron phosphide formation [40].

The insertion of NCA elements over the crucible height shown in Figure 8b can again be explained by the results from Section 3.1.3. The columns numbered 1 indicate the results after a single use. In this case NCA V3, the numbering represents the results after two tests, i.e., NCA V1 and NCA V2 combined. The higher removal of Li from both the solid fractions and the reactor setup also argues for this element's presence, especially in the upper crucible region. The poorer removal in V1 and V2 also explains why the Li fraction is found in the middle to lower region compared when using the crucible twice. The Co and Ni content in the lower range can be attributed to their physical properties.

The results from Figure 8c, in contrast to the others in this section, do not allow for such a simple explanation. In the single test with the crucible in NMC V3 (numbering 1), lithium is primarily found in the middle area; double use with NMC V1 and NMC V2 tends to shift towards the bottom. This can be attributed to the poorer recovery, as seen in Section 3.1.4, from the solid fraction and the presence in the gas scrubber. However, the fact that Li was not found in the upper section can be argued following the previous correction of the results for the crucible input analysis that there may not only be Li transport into the crucible material, but also out of it. Further argumentation must be elicited in more detail in subsequent investigations. The position of the other elements in the lower to the middle range can again be attributed to the contact surface with the crucible or its physical properties.

Combining the findings from the analyses of the products in Section 3.1 and those of the crucibles, the transfer coefficient of Li can be considered one level deeper. Figure 9 shows the distribution of Li in the reactor and the gas stream. It should be said in advance that an average value of the results was also formed here, and the fluctuation range of this average value is shown with error bars. It can be seen that, apart from the test series with LFP, the majority of the Li could be removed via the gas flow for all other cathode materials. In the result of the LFP test series, the parallel removal of Li and P from the reactor should be emphasized. In Holzer et al. [26], experiments in a similar setup showed the formation of a flame from the exhaust tube, which was attributed to the reaction of elemental phosphorus with atmospheric oxygen. Possibly, the resulting increase in flow velocity allows a correlation to be found that explains the higher amount of Li in the reactor. Although the results of the other cathode materials are fundamentally better, to achieve the highest and most efficient output of Li from the process, the amount in the reactor must be kept to an absolute minimum in the future. Nevertheless, these results also underline the possible reactions in Equations (2) and (3) for conversion to gaseous lithium leaving the reactor chamber.

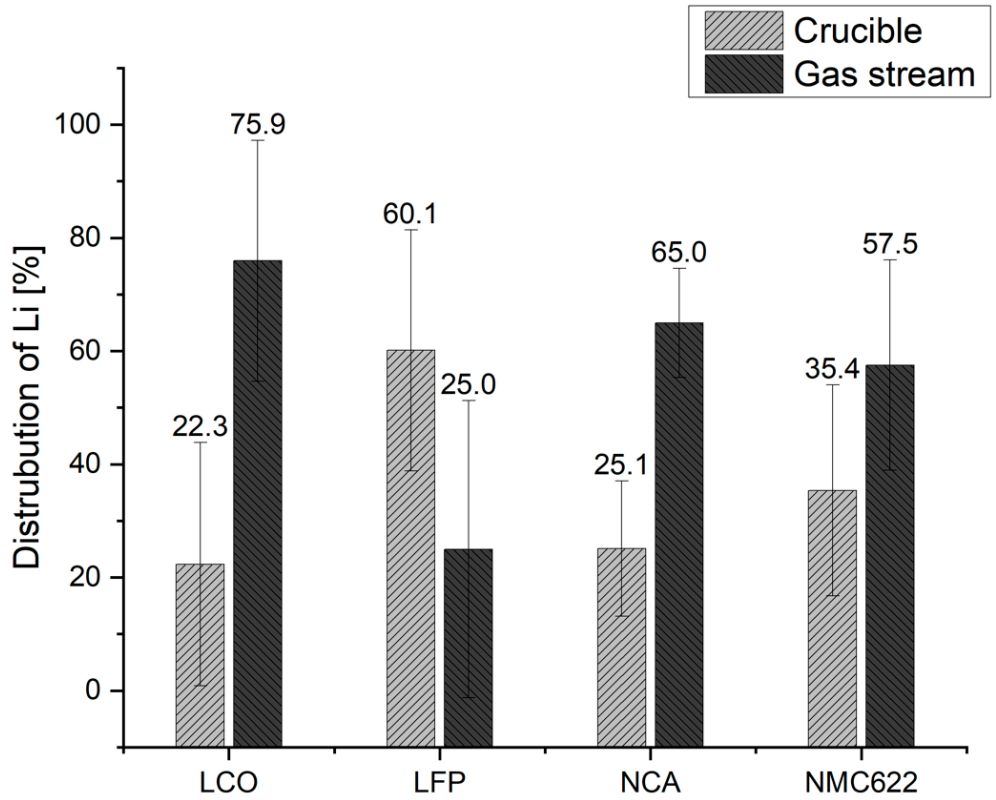

Figure 9. Mass distribution of adhesion to and absorption into the reactor wall of the respective elements.

3.3. Discussion and Comparison with Previous Experiments

As mentioned above, detailed investigations of the process have already been carried out in another reactor design, discussed in detail in Holzer et al. [26] and Windisch-Kern et al. [28,41]. The reactor design was an Al_2O_3 ceramic ring attached to a refractory concrete floor with a refractory mortar. The system with the graphite filling and the basic plant design was identical to the one used in the test described in this paper. Figure 10 shows the results of lithium removal from the solid fractions in the different reactor designs using distinct cathode materials. It should be mentioned that neither the crucible material in contact with the cathode material nor, to some extent, the refractory mortar were analyzed during the tests in the setup with the Al_2O_3 design. Thus, no statement can be made as to what percentage of the Li removed from the solid fraction could be removed from the reactor or was deposited in the reactor components. Therefore, the experimental data and results from Windisch-Kern et al. [26,30] and Holzer et al. [23] were supplemented by those extensive considerations, as described in the Section 3.1 InduMelt experiments and inserted into the following plot.

Nevertheless, the trend of high lithium removal from the solid products shown in Figure 6 is confirmed by the results in the other publications. While the results for LCO and NMC622 are consistently above 90%, and similar values for both the Al_2O_3 build-up and the MgO design, there are several percentage points in between for LFP and NCA. However, for the latter cathode materials, the difference shows a positive trend toward even higher removal rates, which is an interesting finding, especially for the further development of the reactor design toward the continuous process. In this first development step, which essentially consists of a fitting with fewer components in contact with the cathode material, an improvement in lithium removal could already be achieved.

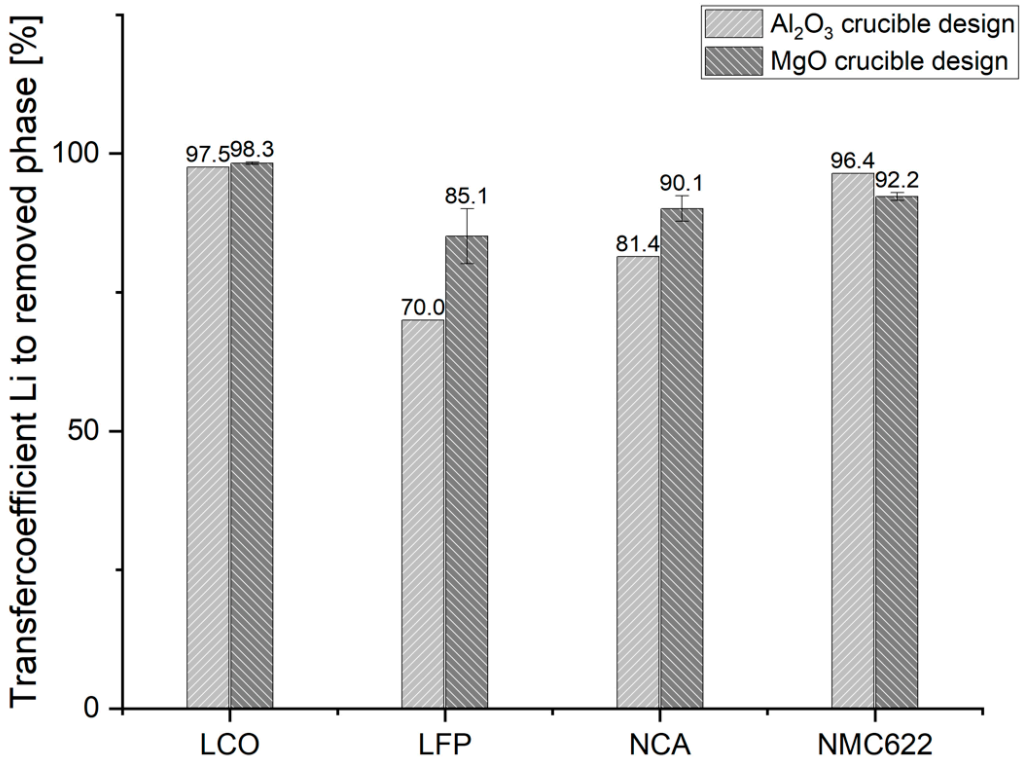

Figure 10. Comparison of Li removal from solid fractions in InduMelt experiments in the Al_2O_3 crucible design [26,28,41] and that with MgO.

In the following, the targets for Li recovery of 35% by 2025 and 70% by 2030 published in the 2020 proposal for the amendment of battery regulation EU Directive 2006/66/EC [12] are included in the consideration. These goals are not only achieved in all tests, but, in some cases, could have been far exceeded. However, further influencing factors must be included in interpreting these results to ensure the final comparability of the results achieved in the tests with the EU specifications.

Let the most important point be taken as a starting point: We are not talking about an industrial process with the InduMelt system presented here, but about a pre-pilot system in batch operation. This fact must always be taken into account when considering the results demonstrated. Compared to a continuous process, the refractory material's limited thermomechanical properties only allow low heating rates of the cathode material. On an industrial scale, running in a batch process is not feasible, and continuous feeding is indispensable. Continuous operation automatically implies that the waste stream is fed onto the hot bed, which is why the reactions, depending on the process control, may possibly already lead to partial outgassing of elements at this point due to accelerated kinetics. Therefore, the positioning of the gas vent and optimized temperature control can have a significantly favorable effect on more efficient Li removal from the reactor. The same is applicable for an adequate position of the P removal. As shown in Section 3.2, the Li reaction route is highly likely to be argued from $LiMeO_2$ to Li_2CO_3 and, due to the excess C, to Li_2C_2. Latter consequently dissociates to gaseous Li and solid C. Taking into account the boiling point of elemental Li of 1342 °C [42], it can be assumed with the knowledge provided in the Materials and Methods section that the estimated 1550 °C process temperature for the liquefaction of the metals Co and Ni is not necessary for the recovery of Li. This subsequently influences the process design of the continuous reactor setup. In this respect, a multi-zone system with different temperature profiles can be considered for energy-efficient operation.

However, the results of this series of experiments, whereby diffusion of Li into the crucible material has occurred, have additionally shown that the selection of the crucible

material contributes significantly to Lithium's output rate. Even though the results in the MgO crucible largely showed higher potential than in the Al_2O_3 crucible, the high degree of diffusion of different elements from the battery material into the crucible wall means that this reactor material should not be used for a continuous process. An adequate choice of crucible constituents should be made in the subsequent research activities, for example, through intensive trials with different crucible materials. In this respect, other points of research activity are the behavior of crucible materials under continuous loading and the influence of coatings on the crucible surface. This research must subsequently also consider the caking on the crucible, which was consistently observed in these test series and may gradually reduce the reactor diameter in continuous operation. Another possible approach to avoid packing, but also to reduce the contact area between waste gases and the refractory and thus prevent the above-mentioned diffusion of Li into the reactor, is the ratio of the reactor diameter to the material feed area.

Referring to the results in the presence of P in LFP, for the continuous process, care should be taken to minimize the contact time or area between iron and phosphorus to prevent iron phosphide formation, as previously described by Ponak [32]. The migration of the gas through the packed bed and the sample material must be prevented. In this case, gas removal close to the point of origin would be appropriate.

Beyond these plant engineering improvements, the post-treatment of the removed gas stream is of crucial importance from an overall process perspective. The future design of this process step is essential for the efficient recovery of Li and, subsequently, the balance concerning the actual recovery rate of Li from the overall process. However, this requires in-depth experimental research steps to describe the kinetics of the reaction mechanisms of complex lithium metal oxides that actually take place. From the point of view of a future industrial application, additional attention must be paid to safety aspects, such as possible toxicity or corrosive properties. Especially due to the large number of additional elements in a waste stream from spent LIB compared to the pure cathode material used here, this issue is of immense importance for all further development steps. In this context, especially noted must be aluminum from the conductor foils. Due to the ignoble properties of Al, oxidation of Al happens once a contact between the metal and oxygen occurs. Since the active material mainly consists of metal oxides, it is very likely that Al is either oxidized or not being reduced and, therefore, slagged. This mechanism's highly exothermic property, called aluminothermic reaction, is a safety issue and thermodynamic limitation. Thus, the process is capped to a specific amount of Al [43]. This critical category of future research topics also includes the post-treatment route of the resulting solid fraction, preferably the metal alloy, and the slag phase's separated treatment. The removal of oxygen, lithium, and carbon during the reduction process results in a mass loss of up to 50%. Thus, the described pyrometallurgical process significantly lowers the number of intermediate products (i.e., the metal alloy) and, consequently, also the effort in downstream hydrometallurgical refining processes. This, in turn, conserves resources and increases the efficiency of the entire recycling process.

As can be seen from these explanations, many research questions need to be solved before the system is ready for industrial use, which are only the most obvious ones at this point, and others will be added in the course of the ongoing R&D work. Due to TRL3, the results presented here cannot be used as comparative data with industrial plants. Particularly noteworthy is the current relatively high fluctuation range of the results in the repeat tests. On the one hand, there are a lot of adjustment screws up to TRL9, but above all, the continuous feeding and dimensional scaling will provide more stable results over a more extensive flow rate range. Nevertheless, as mentioned previously, it was qualitatively established at this point over several trials and different cathode materials that Li and P can be extracted via the gas phase, and low lithium and low phosphorus alloy can be obtained.

In general, a special requirement for the overall process's design process chain, but also as an issue in the further development of the InduMelt plant, is the waste stream, which fluctuates in its composition. In detail, this involves how the recycling process,

i.e., from collection to metallurgy, must be designed and interconnected to deal with the different battery types. As in many metallurgical processes, the more homogeneous the input stream, the easier an optimum product quality can be achieved. In this respect, the sorting of the different types already sets the course for how the downstream steps must look and what compositions they must be able to handle. For this reason, a key success factor in designing an efficient recycling system is that the individual process steps are coordinated at each stage of further engineering. In the future, this will be one of the primary considerations in developing the InduMelt plant.

Finally, it should be noted that for future comparison of the achieved recovery with the EU requirements, such issues as the technical implementation of a post-treatment route have to be clarified. The resulting products are only comparable after implementing the pyrometallurgical process used here into an overall strategy.

Author Contributions: Conceptualization, A.H.; methodology, A.H.; investigation, A.H. and S.W.-K.; resources, A.H., S.W.-K. and L.W.; writing—original draft preparation, A.H.; writing—review and editing, A.H., L.W., S.W.-K. and H.R.; visualization, A.H.; supervision, H.R.; project administration, A.H.; funding acquisition, H.R. All authors have read and agreed to the published version of the manuscript.

Funding: This paper is supported by the Zukunftsfonds Steiermark with funds from the province of Styria, Austria, grant number GZ: ABT08-189002/2020 PN:1305.

Data Availability Statement: The data presented in this study are available upon request from the corresponding author.

Conflicts of Interest: The authors declare no conflict of interest. The funders had no role in the design of the study; in the collection, analyses, or interpretation of data; in the writing of the manuscript, or in the decision to publish the results.

References

1. Doukas, H.; Nikas, A.; González-Eguino, M.; Arto, I.; Anger-Kraavi, A. From Integrated to Integrative: Delivering on the Paris Agreement. *Sustainability* **2018**, *7*, 2299. [CrossRef]
2. Dimitrov, R.; Hovi, J.; Sprinz, D.F.; Sælen, H.; Underdal, A. Institutional and environmental effectiveness: Will the Paris Agreement work? *WIREs Clim. Change* **2019**, *10*, e583. [CrossRef]
3. IEA. Emissions by Sector—Greenhouse Gas Emissions from Energy: Overview—Analysis—IEA. Available online: https://www.iea.org/reports/greenhouse-gas-emissions-from-energy-overview/emissions-by-sector (accessed on 25 April 2022).
4. PBL Netherlands Environmental Assessment Agency. *Trends in Global CO_2 and Total Greenhouse Gas Emissions: 2020 Report*; PBL Netherlands Environmental Assessment Agency: The Hague, The Netherlands, 2020.
5. Martins, L.S.; Guimarães, L.F.; Botelho Junior, A.B.; Tenório, J.A.S.; Espinosa, D.C.R. Electric car battery: An overview on global demand, recycling and future approaches towards sustainability. *J. Environ. Manag.* **2021**, *295*, 113091. [CrossRef]
6. Verma, S.; Dwivedi, G.; Verma, P. Life cycle assessment of electric vehicles in comparison to combustion engine vehicles: A review. *Mater. Today* **2022**, *49*, 217–222. [CrossRef]
7. Chordia, M.; Nordelöf, A.; Ellingsen, L.A.-W. Environmental life cycle implications of upscaling lithium-ion battery production. *Int. J. Life Cycle Assess.* **2021**, *26*, 2024–2039. [CrossRef]
8. Ellingsen, L.A.-W.; Singh, B.; Strømman, A.H. The size and range effect: Lifecycle greenhouse gas emissions of electric vehicles. *Environ. Res. Lett.* **2016**, *11*, 54010. [CrossRef]
9. Nordelöf, A.; Messagie, M.; Tillman, A.-M.; Ljunggren Söderman, M.; van Mierlo, J. Environmental impacts of hybrid, plug-in hybrid, and battery electric vehicles—What can we learn from life cycle assessment? *Int. J. Life Cycle Assess.* **2014**, *19*, 1866–1890. [CrossRef]
10. Rajaeifar, M.A.; Raugei, M.; Steubing, B.; Hartwell, A.; Anderson, P.A.; Heidrich, O. Life cycle assessment of lithium-ion battery recycling using pyrometallurgical technologies. *J. Ind. Ecol.* **2021**, *25*, 1560–1571. [CrossRef]
11. European Commission. Strategic Dependencies and Capacities: SWD (2021) 352 Final. 2021. Available online: https://ec.europa.eu/info/sites/default/files/swd-strategic-dependencies-capacities_en.pdf (accessed on 25 April 2022).
12. European Parliament. DIRECTIVE 2006/66/EC OF THE EUROPEAN PARLIAMENT AND OF THE COUNCIL of 6 September 2006 on Batteries and Accumulators and Waste Batteries and Accumulators and Re-Pealing Directive 91/157/EEC: L 266/1. 2006. Available online: https://eur-lex.europa.eu/legal-content/EN/TXT/PDF/?uri=CELEX:32006L0066&from=DE (accessed on 25 April 2022).
13. European Commission. *Critical Raw Materials for Strategic Technologies and Sectors in the EU: A Foresight Study*; European Commission: Brussels, Belgium; Luxembourg, 2020. [CrossRef]

14. Sojka, R.; Pan, Q.; Billman, L. Comparative study of lithium-ion battery recycling processes. In Proceedings of the 25th International Congress for Battery Recycling ICBR 2020, Salzburg, Austria, 16–18 September 2020.
15. Windisch-Kern, S.; Gerold, E.; Nigl, T.; Jandric, A.; Altendorfer, M.; Rutrecht, B.; Scherhaufer, S.; Raupenstrauch, H.; Pomberger, R.; Antrekowitsch, H. Recycling chains for lithium-ion batteries: A critical examination of current challenges, opportunities and process dependencies. *Waste Manag.* **2022**, *138*, 125–139. [CrossRef]
16. Nasser, O.A.; Petranikova, M. Review of Achieved Purities after Li-ion Batteries Hydrometallurgical Treatment and Impurities Effects on the Cathode Performance. *Batteries* **2021**, *7*, 60. [CrossRef]
17. Wesselborg, T.; Virolainen, S.; Sainio, T. Recovery of lithium from leach solutions of battery waste using direct solvent extraction with TBP and FeCl3. *Hydrometallurgy* **2021**, *202*, 105593. [CrossRef]
18. Sattar, R.; Ilyas, S.; Kousar, S.; Khalid, A.; Sajid, M.; Bukhari, S.I. Recycling of end-of-life LiNixCoyMnzO2 batteries for rare metals recovery. *Environ. Eng. Res.* **2020**, *25*, 88–95. [CrossRef]
19. Lv, W.; Wang, Z.; Cao, H.; Sun, Y.; Zhang, Y.; Sun, Z. A Critical Review and Analysis on the Recycling of Spent Lithium-Ion Batteries. *ACS Sustain. Chem. Eng.* **2018**, *6*, 1504–1521. [CrossRef]
20. Munir, H.; Srivastava, R.R.; Kim, H.; Ilyas, S.; Khosa, M.K.; Yameen, B. Leaching of exhausted LNCM cathode batteries in ascorbic acid lixiviant: A green recycling approach, reaction kinetics and process mechanism. *J. Chem. Technol. Biotechnol.* **2020**, *95*, 2286–2294. [CrossRef]
21. Santos, M.D.; Garde, I.A.A.; Ronchini, C.M.B.; Filho, L.C.; de Souza, G.B.M.; Abbade, M.L.F.; Regone, N.N.; Jegatheesan, V.; de Oliviera, J.A. A technology for recycling lithium-ion batteries promoting the circular economy: The RecycLib, Resources. *Conserv. Recycl.* **2021**, *175*, 105863. [CrossRef]
22. Kaksonen, A.H.; Boxall, N.J.; Gumulya, Y.; Khaleque, H.N.; Morris, C.; Bohu, T.; Cheng, K.Y.; Usher, K.M.; Lakaniemi, A.-M. Recent progress in biohydrometallurgy and microbial characterization. *Hydrometallurgy* **2018**, *180*, 7–25. [CrossRef]
23. Baniasadi, M.; Vakilchap, F.; Bahaloo-Horeh, N.; Mousavi, S.M.; Farnaud, S. Advances in bioleaching as a sustainable method for metal recovery from e-waste: A review. *J. Ind. Eng. Chem.* **2019**, *76*, 75–90. [CrossRef]
24. Zheng, X.; Zhu, Z.; Lin, X.; Zhang, Y.; He, Y.; Cao, H.; Sun, Z. A Mini-Review on Metal Recycling from Spent Lithium Ion Batteries. *Engineering* **2018**, *4*, 361–370. [CrossRef]
25. Nakajima, K.; Takeda, O.; Miki, T.; Matsubae, K.; Nagasaka, T. Thermodynamic analysis for the controllability of elements in the recycling process of metals. *Environ. Sci. Technol.* **2011**, *11*, 4929–4936. [CrossRef]
26. Holzer, A.; Windisch-Kern, S.; Ponak, C.; Raupenstrauch, H. A novel pyrometallurgical recycling process for Lithium-Ion-Batteries and its use in recycling LCO and LFP. *Metals* **2021**, *2021*, 149. [CrossRef]
27. European Comission. COM(2020)474—Critical Raw Materials Resilience: Charting a Path towards Greater Security and Sustainability. Available online: https://ec.europa.eu/transparency/documents-register/detail?ref=COM (accessed on 16 August 2022).
28. Windisch-Kern, S.; Holzer, A.; Wiszniewski, L.; Raupenstrauch, H. Investigation of Potential Recovery Rates of Nickel, Manganese, Cobalt, and Particularly Lithium from NMC-Type Cathode Materials (LiNixMnyCozO2) by Carbo-Thermal Reduction in an Inductively Heated Carbon Bed Reactor. *Metals* **2021**, *11*, 1844. [CrossRef]
29. Mao, J.; Ye, C.; Zhang, S.; Xie, F.; Zeng, R.; Davey, K.; Guo, Z.; Qiao, S. Toward practical lithium-ion battery recycling: Adding value, tackling circularity and recycling-oriented design. *Energy Environ. Sci.* **2022**, *15*, 2732–2752. [CrossRef]
30. Sommerville, R.; Zhu, P.; Rajaeifar, M.A.; Heidrich, O.; Goodship, V.; Kendrick, E. A qualitative assessment of lithium ion battery recycling processes. *Resour. Conserv. Recycl.* **2021**, *165*, 105219. [CrossRef]
31. Mossali, E.; Picone, N.; Gentilini, L.; Rodrìguez, O.; Pérez, J.M.; Colledani, M. Lithium-ion batteries towards circular economy: A literature review of opportunities and issues of recycling treatments. *J. Environ. Manag.* **2020**, *264*, 110500. [CrossRef] [PubMed]
32. Ponak, C. Carbo-Thermal Reduction of Basic Oxygen Furnace Slags with Simultaneous Removal of Phosphorus via the Gas Phase. Master's Thesis, Montanuniversitaet Leoben, Leoben, Austria, 2019.
33. Ponak, C.; Mally, V.; Windisch, S.; Holzer, A.; Raupenstrauch, H. Phosphorus Gasification during the Re-duction of basic Oxygen Furnace Slags in a Novel Reactor Concept. *Adv. Mater. Lett.* **2020**, *11*, 1–7. [CrossRef]
34. Seck, G.S.; Hache, E.; Barnet, C. Potential bottleneck in the energy transition: The case of cobalt in an accelerating electro-mobility world. *Resour. Policy* **2022**, *75*, 102516. [CrossRef]
35. Liu, K.; Liu, Y.; Lin, D.; Pei, A.; Cui, Y. Materials for lithium-ion battery safety. *Sci. Adv.* **2018**, *4*, eaas9820. [CrossRef]
36. Chen, Y.; Kang, Y.; Zhao, Y.; Wang, L.; Liu, J.; Li, Y.; Liang, Z.; He, X.; Li, X.; Tavajohi, N.; et al. A review of lithium-ion battery safety concerns: The issues, strategies, and testing standards. *J. Energy Chem.* **2021**, *59*, 83–99. [CrossRef]
37. Kwon, O.; Sohn, I. Fundamental thermokinetic study of a sustainable lithium-ion battery pyrometallurgical recycling process, Resources. *Conserv. Recycl.* **2020**, *158*, 104809. [CrossRef]
38. Abegg, R.; Auerbach, F. *Handbuch der Anorganischen Chemie: Zweiter Band, Erste Abteilung*; S. Hirzel Verlag: Leipzig, Germany, 1908. Available online: https://archive.org/details/handbuchderanor00koppgoog/page/135/mode/1up?view=theater (accessed on 27 April 2022).
39. Makuza, B.; Tian, Q.; Guo, X.; Chattopadhyay, K.; Yu, D. Pyrometallurgical options for recycling spent lithium-ion batteries: A comprehensive review. *J. Power Source* **2021**, *491*, 229622. [CrossRef]
40. Schlesinger, M.E. The thermodynamic properties of phosphorus and solid binary phosphides. *Chem. Rev.* **2002**, *102*, 4267–4301. [CrossRef] [PubMed]

41. Windisch-Kern, S.; Holzer, A.; Ponak, C.; Raupenstrauch, H. Pyrometallurgical Lithium-Ion-Battery Recycling: Approach to Limiting Lithium Slagging with the InduRed Reactor Concept. *Processes* **2021**, *9*, 84. [CrossRef]
42. Outotec Research Center; Roine, A. *HSC Chemistry 7*; Outotec: Espoo, Finland, 2009.
43. Holzer, A.; Baldauf, M.; Wiszniewski, L.; Windisch-Kern, S.; Raupenstrauch, H. Influence of Impurities on the High-Temperature Behavior of the Lithium-Ion Battery Cathode Material NMC Under Reducing Conditions for Use in the InduRed Reactor Concept. *Detritus* **2022**, *in press*. [CrossRef]

6.3 Publication 3

Influence of Impurities on the High-Temperature Behavior of the Lithium-Ion Battery Cathode Material NMC Under Reducing Conditions for Use in the InduRed Reactor Concept

Holzer, A.; Baldauf, M.; Wiszniewski, L.; Windisch-Kern, S. and Raupenstrauch, H.

Article Information:

Journal	Detritus, Volume 20 - 2022
Pages	7
Received Date	20 June 2022
Revised Date	5 August 2022
Accepted Date	29 August 2022
Published Date	14 September 2022
DOI	https://doi.org/10.31025/2611-4135/2022.15215

Author's contribution: Conceptualization, Methodology, Investigation, Resources, Writing – original draft preparation, Writing – review and editing, Visualization

detritus | Multidisciplinary Journal for Waste Resources & Residues

CISA

INFLUENCE OF IMPURITIES ON THE HIGH-TEMPERATURE BEHAVIOR OF THE LITHIUM-ION BATTERY CATHODE MATERIAL NMC UNDER REDUCING CONDITIONS FOR USE IN THE INDURED REACTOR CONCEPT

Alexandra Holzer *, Mathias Baldauf, Lukas Wiszniewski, Stefan Windisch-Kern and Harald Raupenstrauch

Montanuniversitaet Leoben, Chair of Thermal Processing Technology - Franz-Josef Straße 18, 8700, Austria

Article Info:
Received:
20 June 2022
Revised:
5 August 2022
Accepted:
29 August 2022
Available online:
14 September 2022

Keywords:
Recycling
Pyrometallurgy
Carbo-thermal reduction
Lithium removal
Reducing conditions

ABSTRACT

In terms of an efficient circular economy in the field of the steadily increasing use of lithium-ion batteries, sustainable recycling methods are of fundamental importance. Therefore, the Chair of Thermal Processing Technology at Montanuniversitaet Leoben has developed the so-called InduRed reactor, a carbo-thermal concept to recover valuable metals from this waste stream. For optimization and further development of this technology, it is essential to have a sound knowledge of the cathode materials' behavior in combination with various impurities in the high-temperature range under reducing conditions. Detailed experiments were carried out in a heating microscope at temperatures up to 1620°C and argon purge. Aluminum from the electrode conductor foils and an excessive proportion of graphite from the anode were identified as the impurities with the most significant negative influence on the process. An optimum melting behavior was found during the tests at an admixture of 10 wt. % C and 1.95 wt. % Al to the cathode material NMC622 ($LiNi_{0.6}Mn_{0.2}Co_{0.2}O_2$).

1. INTRODUCTION

The main objective of the international climate policy agreed upon the Paris Climate Conference in 2015 is to limit global warming to below 1.5°C compared to the pre-industrial era. To achieve this goal, industrialized countries must reduce their consumption of fossil fuels and aim for a zero-emissions target by the middle of this century. Concerning the period 2021 to 2030, an overall reduction of 30% on average per country must be achieved in the non-emissions trading scheme (ETS) sectors (Anderl et al., 2019).

A decisive element of the measures to curb climate-damaging emissions is the rapid expansion of renewable energies. A major technical challenge in this respect is the storage of the converted energy. Electricity from renewable energy sources is subject to certain seasonal, regional, and weather-related fluctuations, which is why storage is necessary to implement a sustainable energy economy. In addition to various other technologies, such as Power to Gas and Power to X, battery storage systems will play an increasingly important role (Altmann-Mavaddat et al.; Thielmann et al., 2017).

As part of the European Green Deal, a modernization of the existing battery legislation was proposed at the end of 2020 (European Commission, 2020). With this proposal, the European Union is trying to form a strengthened circular economy to conserve resources and efficiently decouple economic growth from resource dependency. As of July 1, 2024, only batteries for which a CO_2 footprint declaration has been made may be used in the European Union. Furthermore, new targets are set for the content of recycled materials along the entire value chain. To reach these targets, efficient recycling processes are needed that allow most materials to re-enter the material cycle (European Commission, 2020).

Due to the cathode materials' complex structure and chemical composition, the complete recycling process is typically composed of two process steps, one physical and one chemical. The physical process includes pre-treatment steps such as disassembly, crushing, screening, magnetic separation, and thermal pre-treatment. This step significantly reduces the waste's mass and volume in downstream recycling processes, which focus on recovering the valuable metals from the residual stream consisting of active material (or black matter). The black matter

* Corresponding author:
Alexandra Holzer
email: alexandra.holzer@unileoben.ac.at

Detritus / Volume 20 - 2022 / pages 22-28
https://doi.org/10.31025/2611-4135/2022.15215

is composed of anode and cathode material and other components of the LIB structure like electrode conductor foil, which could not be separated completely. The black matter to be treated has the visual appearance of a fine black powder. The following procedure is a chemical process step classified as a pyrometallurgical or a hydrometallurgical process. However, hybrid processes also utilize both pyrometallurgical and hydrometallurgical methods. The hydrometallurgical process typically includes leaching, separation, extraction, and chemical or electrochemical precipitation (Holzer, 2019; Holzer et al., 2021; Huang et al., 2018; Kwon & Sohn, 2020; Swain, 2017). Although this process generally achieves high purities and requires lower energy input, the sensitivity on a fluctuating waste stream composition is a considerable disadvantage compared to pyrometallurgical methods (Holzer et al., 2021).

For industrial-scale applications, processes with pyrometallurgical steps are considered to have higher potential than those with a purely hydrometallurgical approach. This statement is also underlined by the fact that promising pyrometallurgical approaches are already being used in industry (Abdou et al., 2016; Beheshti et al., 2017; Gao & Xu, 2019; Kwon & Sohn, 2020; Li et al., 2016; Sojka et al., 2020; Xiao et al., 2017). However, the considerable need for more optimal process design research is reflected in the disadvantages of pyrometallurgical processes. Since temperatures above 1400°C are necessary for the recovery of the valuable metals, correspondingly high energy input is required. In addition, considerable amounts of waste gas are generated during the process, which must be subjected to downstream waste gas purification. The resulting metal alloy additionally requires a downstream process for use in a closed loop in battery production. However, the most significant disadvantage is that lithium is transferred to the slag phase in currently used methods, from which it is not recovered for functional recycling. (Elwert & Frank, 2020; Huang et al., 2018; Liu et al., 2019; Makuza et al., 2021; Yin & Xing, 2019).

A novel reactor design was developed at the Chair of Thermal Processing Technology at the Montanuniversitaet Leoben to circumvent this significant issue (Holzer et al., 2021). The process idea is based on the principle of carbo-thermal reduction of the LIB black matter from a pre-treatment process. For the further development of the process, in-depth fundamental research is required. The fluctuating waste stream and the associated varying chemical composition of the input material pose a particular challenge. Knowledge about the influence of certain impurities on the high-temperature behavior of black matter is of great importance to take optimal advantage of the developed approach. The impurities are residuals that were not separated during the upstream pre treatment procedures. These are mainly non-volatile components such as aluminum, copper, and graphite from the LIB structure. For the investigations presented in this paper, the cathode material NMC622 ($LiNi_{0.6}Mn_{0.2}Co_{0.2}O_2$) was chosen. This is one of the currently preferred materials for use in e-mobility (Windisch-Kern, Holzer, Ponak, Hochsteiner, & Raupenstrauch, 2021), with this sector forecast to be and remain a key driver of the technology (Pillot, 2019). A limit value determination of the mentioned interfering substances for optimized use in the InduRed concept is explained in the following. For this purpose, the influences of Al, Cu and C on the cathode material in high-temperature applications under reducing conditions are examined in more detail. Consequently, the behavior in different mixtures is determined.

2. INDURED REACTOR AND ITS REQUIREMENTS

Fundamental knowledge about the desired reactor's properties, benefits, and drawbacks is a prerequisite for comprehending the scope of the presented work. Thus, this part of the paper briefly introduces the InduRed reactor concept, focusing on its potential application for LIBs.

2.1 InduRed reactor scheme

Originally designed and developed to enable superior phosphorus recovery rates from sewage sludge ashes, the InduRed reactor concept, shown in Figure 1, proved itself a promising alternative for several industrial and municipal wastes.

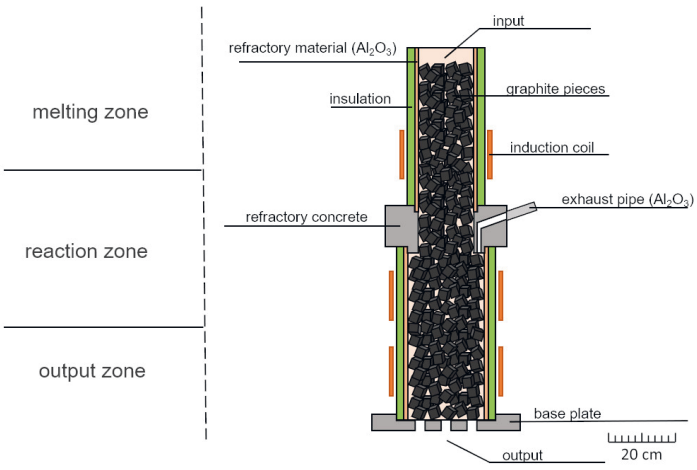

FIGURE 1: Schematic illustration of the continuously charged, fixed carbon bed reactor referred to as InduRed concept (Ponak, 2019).

The InduRed reactor consists of a stack of aluminium oxide rings filled with a fixed bed of graphite pieces and surrounded by three induction coils. An electromagnetic field generated by the induction coils induces a current in the graphite pieces heated to up to 1750°C. It should be noted that the graphite pieces in the reactor serve only as a susceptor material for the inductive heat input, and C powder is added to the feedstock as a reducing agent. The metal oxides containing feed are continuously charged from the top, melt, move downwards, and constantly discharge at the reactor's bottom. Reduction reactions in the reaction zone are particularly promoted due to high CO/CO_2 ratios, a significant reaction surface and a sufficient supply of carbon. The exhaust gas pipe gives the unique opportunity to remove gaseous reaction products directly and thus limit undesired reactions between the gaseous and the liquid phase.

Regarding LIB recycling, the concept should enable the simultaneous recovery of all cathodic metals, including lithium. This is intended to be achieved by separating Li via the gas stream instead of being undesired slagged as in conventional pyrometallurgical procedures.

So far, experiments with pure cathode material from battery production with the addition of carbon in a lab-scale model of the InduRed reactor have already revealed promising results, in which up to 95% of the initial Li was removed from the residual material. In addition, initial results from the investigation of the phosphorus-containing cathode material LFP (LiFePO4) have also shown that over 64% phosphorus could be removed (Holzer et al., 2021; Windisch-Kern, Holzer, Ponak, Hochsteiner, & Raupenstrauch, 2021; Windisch-Kern, Holzer, Ponak, & Raupenstrauch, 2021; Windisch-Kern, Holzer, Wiszniewski, & Raupenstrauch, 2021).

3. DETERMINATION OF MATERIAL BEHAVIOR IN HIGH-TEMPERATURE APPLICATIONS

For the further development of the InduRed concept towards the waste stream from LIBs, specific knowledge of the material used is the basis for efficient upscaling. Although the InduRed reactor concept presented is capable of withstanding temperatures of up to 1750°C, the target temperature set for using materials from LIBs is about 1550°C. This temperature was chosen because the melting temperatures of the reduced metals contained in the reactor are below 1500°C and a safety margin had to be included due to possible local temperature differences. Thus, in-depth investigations of the material to be utilized in the high-temperature area of 1550° are necessary. The material used as well as the methods are explained in detail below.

3.1 Materials and Methods

To extend the investigations of the high-temperature behavior of the cathode material NMC622 under reducing conditions published by Windisch-Kern et al. (2021) by thermogravimetric analysis and differential scanning calorimetry, experiments in the heating microscope were carried out within the scope of this work. For this purpose, the Hesse Instruments EM 201 with an HR18-1750/30 furnace was deployed. The cathode materials used in the tests are manufactured by and purchased from Gelon Energy Corporation in Linyi, China. These experiments aimed to visualize the changes of the cross-sectional area of the samples over temperature, thus allowing conclusions about the melting ability, which is a requirement of the InduRed concept. To extend these findings towards expected waste stream compositions, additional investigations must be carried out in which possible impurities are added.

TABLE 1: Heating program in the heating microscope to perform the tests with NMC622 and addition of different additives.

Temperature range	Heating rate
Start - 1350°C	80°C/min
1350 - 1450°C	50°C/min
1450 - 1700°C	10°C/min
1700°C	5 min holding time

For this purpose, different extents of aluminum, copper and carbon were added to the cathode material NMC622. The sample was then pressed in a standardized cylindrical form with an approximate mass of 0.1 g and placed on an Al_2O_3 analysis plate. It should be mentioned that carbon or graphite is used as a reducing agent for the reduction reaction.

For safety reasons, the experiments were not carried out under a CO atmosphere, which would better fit to the actual conditions provided by the InduRed concept. However, since it is primarily essential to prevent oxidation reactions, purging with 2.5 l/min argon was applied instead. Accordingly, the C demand was calculated considering a conversion to CO_2 instead of CO.

Finally, the sample was heated in the heating microscope to an oven temperature of 1700°C, corresponding to approximately 1620°C sample temperature.

The heating program, which can be taken from Table 1, corresponds to the maximum possible rate of the heating microscope used, approximating the range of application in the InduRed concept.

3.2 Experimental approach

The experiments were carried out in two phases to determine the influence of the substances Al, Cu, and C on the melting ability. Firstly, the cathode material was mixed with the elements mentioned above and examined under a heating microscope to assess the behavior. This allowed an estimation of the most significant negative influencing factors. To gain quick information about the successful reduction process without further analysis in the laboratory, the magnetic behavior of all samples was subsequently examined using a neodymium magnet. It should be noted that the stoichiometric carbon demand for complete reduction of NMC622 in inert atmosphere and assuming a conversion to CO_2 is 11 wt. %, rounded. This ratio was taken as the baseline for this series of experiments.

The next phase aimed on determining the limits of elements interfering the InduRed concept requirements of a melting phase. For this purpose, a total of 26 tests were

carried out with different mixing ratios, as shown by the green dots in Figure 2. A specified mass fraction of Al and/or C calculated on the total mass was added to the resulting mass fraction of NMC622 and examined under the heating microscope (Baldauf, 2022).

To be able to make a statement on the change in the cross-sectional area of samples or mixtures other than those investigated and to optimize the number of experiments, an interpolation network was designed, which is shown as a black dotted grid in Figure 2 (Baldauf, 2022).

To evaluate the resulting data quantity of approx. 1500 data points per test accordingly reliable, additional effort is required. Oscillating data areas, which can occur due to optical measurement errors, are corrected by smoothing over a polynomial. Oscillation can also be caused by incorrect detection by the heating microscope due to focusing problems over a more comprehensive temperature range than that. The accrued data gap can be corrected by comparing the last measured values with the stored images and the following linear correlation of the corrected values. Because of the reaction kinetics as well as the adjustment of the temperature ramp of the heating microscope, a specific temperature can address several data points. However, data points may not be available for every temperature, further data processing is necessary. This problem may be overcome by the processing and output of the arithmetic mean of the data of the same temperature values or by a logical continuation of the temperature (Baldauf, 2022).

4. RESULTS AND DISCUSSION

As explained in point 3.2 Experimental approach, the experimental procedure was divided into two parts. A preliminary series of tests was conducted under a heating microscope to determine the basic influence of different impurities. Based on this, a limit value determination of impurities for further pyrometallurgical recovery of valuable metals in the InduRed concept was carried out.

4.1 Basic influence of different impurities

The representation of the cross-sectional area in Figure 3 shows the most important tests in this series. The terminology in the legend, as NMC622_C11_Al10, specifies 11 wt. % C and 10 wt. % Al beeing added to the resulting proportion of NMC622.

Significant findings can be deduced from Figure 3 comparing the change in cross-sectional area over temperature. Thus, in comparison with NMC622 without addition of C, Al or Cu to the test with the admixture of the stoichiometrically necessary C for complete reduction (NMC622_C11), a significant difference can be seen in the cross-sectional area reduction and in the final area. In addition, the examination of the magnetic behavior showed that only those samples with the addition of C are magnetic. The comparison between NMC622_C11 and those with the addition of Al and Cu is particularly interesting. It can be seen that the end surface of NMC622_C11_Cu10 intersects with the sample without Cu addition. Thus, it can be concluded that the addition of Cu has less a negative influence on the melting behavior since the final surface already develops at lower temperatures, in this case, approx. 1250°C instead of 1450°C. The situation is different for the addition of Al. The essential reduction in the surface area takes place earlier. Still, the final surface is considerably

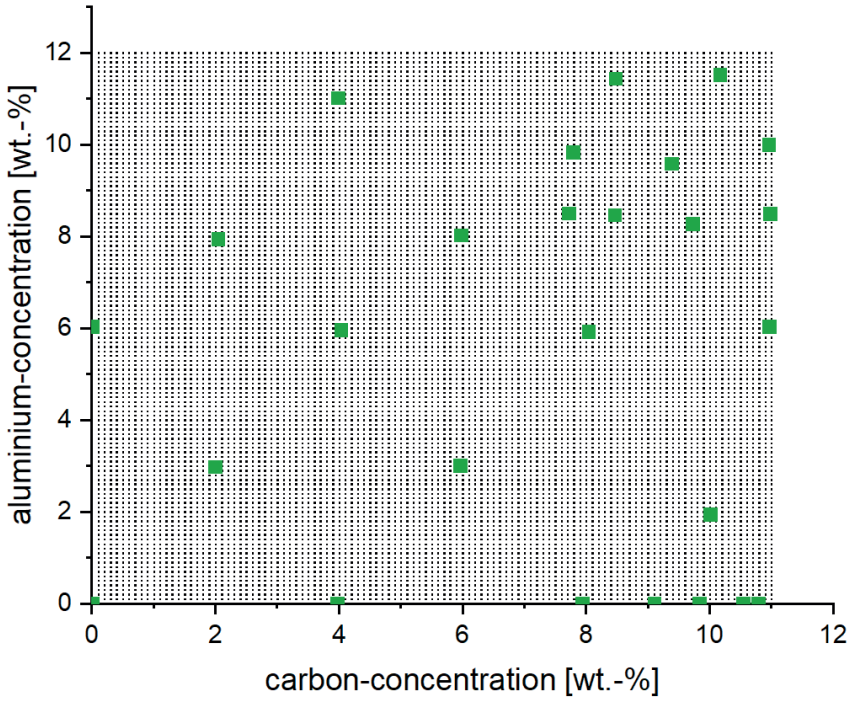

FIGURE 2: Measured points (green points) in the heating microscope depending on the corresponding proportions of aluminum and carbon to NMC622 and the interpolation network (black dotted grid) (Baldauf, 2022).

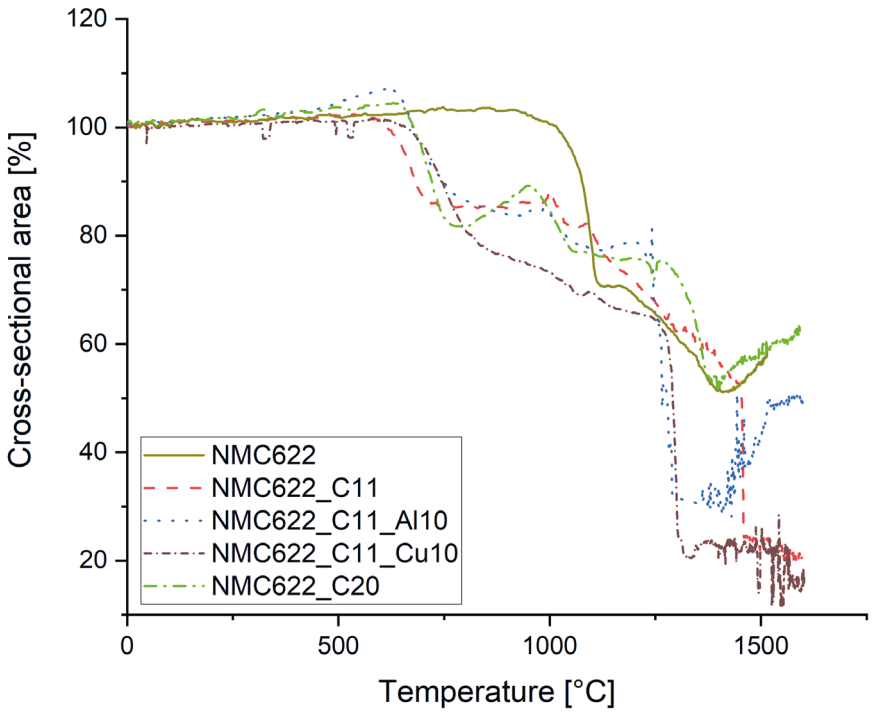

FIGURE 3: Comparison of the change in cross-sectional area in the heating microscope as a function of temperature of NMC622 without and with the addition of Al, Cu and/or C.

higher than that without additives. To gain results on the behavior with the addition of C above the stoichiometrically necessary amount, investigations were carried out with a C content of 20 wt. %. The cross-sectional area's behaviour is considerably worse compared to 10 wt. %. For further detailed studies, it can be deduced that the proportion of Al and C in the mixture has the most significant influence on the melting ability, suggesting intensification of research in this field.

4.2 Limit value determination of interfering substances

Since the rigid two-dimensional view of the cross-sectional area versus temperature for a system of Al/C/NMC622 entails a considerable loss of information, and since it is also possible to represent the high-temperature behavior for other variants of the composition without conducting experiments using the generated data, the vectorial view in three-dimensional space was chosen as the representation variant.

The mesh shown in Figure 4 represents the change in the cross-sectional area of NMC622 in combination with Al and/or C. It can be seen that the area moves towards a composition of 10 wt. % C and 1.95 wt. % Al to an absolute area minimum of 13.59%. To apply this finding to the InduRed reactor, a conversion is necessary, assuming a reaction to mainly form CO instead of CO_2. This results in a C content of 18.20 wt. % to achieve the absolute area minimum.

By comparing the images of the heating microscope and the photos of the sample after the test, it was found that there is a transition range from a slightly melting fraction to a minimal melting fraction at ranges between 36.6% and 53.3%. Consequently, from the 53.3% mentioned, no more continuous melt was formed. In order to always be able to generate a molten phase in the process, mix ratios should be selected that are in the range of less than 36.6% (Baldauf, 2022).

Resulting from this fact, the data were plotted in a height stratification in a 2-D plot, as shown in Figure 5. A diagonal band from the upper left to the lower right is visible, in which the desired area of less than 36.6% is partially included.

It can be seen that while higher proportions of Al are in principle possible in smaller areas, this is accompanied by lower proportions of C. One possible reason for this is that Al has a higher affinity for oxygen than C, as can be seen in the Richardson-Ellingham diagram (Biswas, 1981). This means that Al acts as a reducing agent (Makuza et al., 2021), which implies that an excess of C inhibits melting. However, it is additionally evident from the figure that the higher melting ability is in the range of lower Al values and C contents towards the stoichiometrically calculated value of 11 wt. % for a complete reduction of the oxides contained in NMC622.

As can be seen in Figure 5, extrapolations were used in the range greater than 6 wt. % Al and 0 wt. % C to 11 wt. % Al and 4 wt. % C. Experiments in this area were not carried out in the present series of tests for safety reasons. This is because of the risk of an aluminothermic reaction observed in parallel trials.

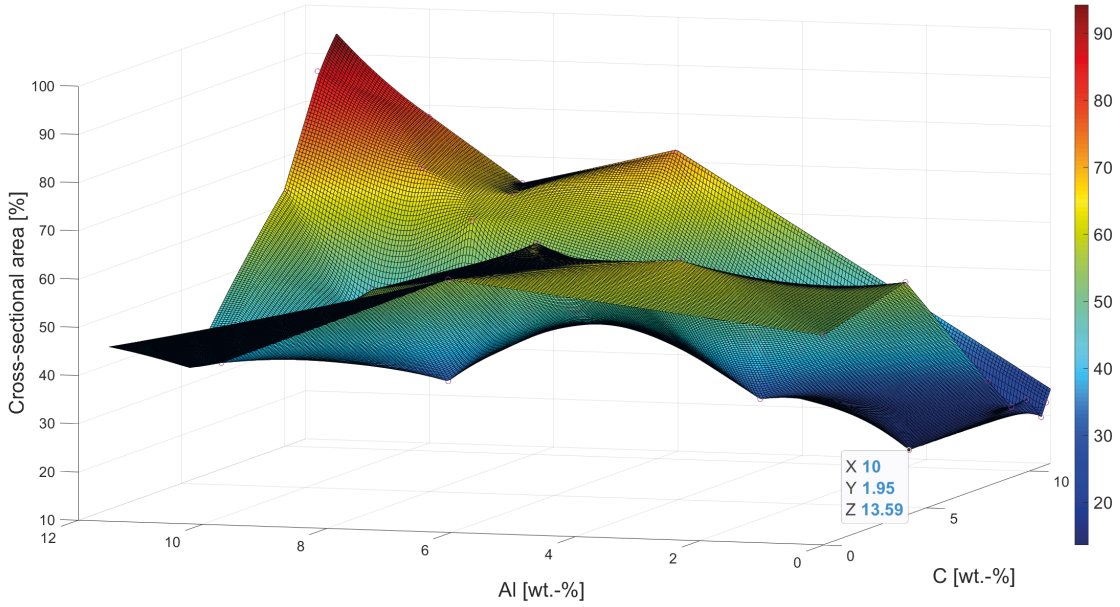

FIGURE 4: 3-D mesh plot of the measured points (blend NMC622 with/without Al or C) in the heating microscope as a function of the cross-sectional area acquired at 1550°C.

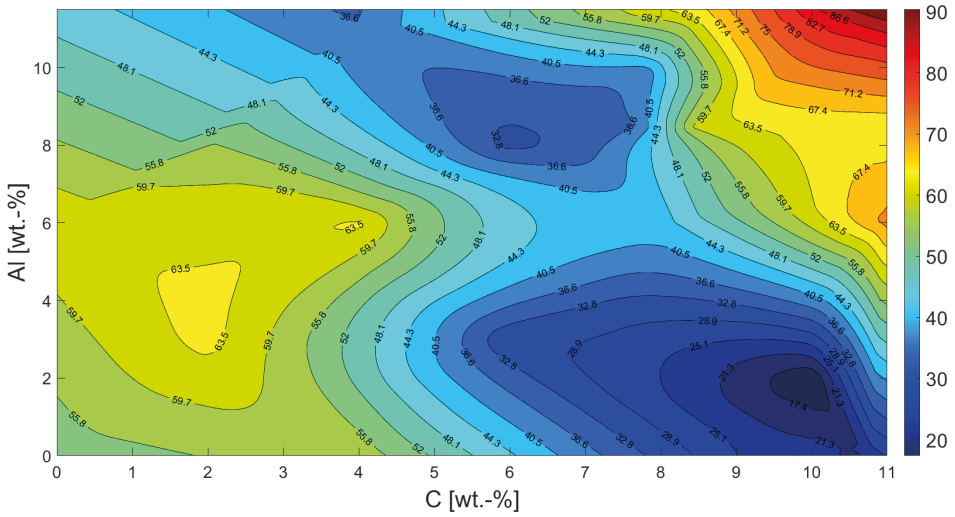

FIGURE 5: Schematic representation of the change in cross-sectional area of the cathode material NMC622 when combined with varying C and Al additions ratios over a height stratification at 1550°C.

5. CONCLUSIONS

In the context of this publication, the compositional requirements of black matter from lithium-ion batteries (LIB) for a pyrometallurgical recycling approach were investigated.

In this respect, it was determined in a heating microscope that the main factors negatively influencing the required melting ability are the elements Al and C. Cu even positively affects the melting temperature in the experimental setup.

Subsequently, the focus was on Al and C. Thus, the change in the cross-sectional area (CSA) at 1550°C with a varying NMC622-Al-C system was investigated. It was found that mixtures with a final cross-sectional area (CSA) of less than 36.6% should be aimed for. Finally, a composition of 10 wt. % C, 1.95 wt. % Al and the resulting amount of NMC622 with a cross-sectional area of 13.59% was found to be the optimum blend. Considering the reaction sequences in the InduRed reactor, a C content of 18.20 wt. % would be necessary for this respect. In addition, it was recognized that attention must also be paid to the Al/C ratio. Due to their property in terms of oxygen affinity, care must be taken not to result in excess of C, which negatively affects the melting ability. However, even a bunch of Al can cause significant safety and process engineering difficulties with respect to a possible aluminothermic reaction and its strongly exothermic behavior. For this reason, according to initial findings, Al contents of less than 6 wt. % should generally be aimed for, which must be investigated in more detail in further trials.

As an outlook for future research activities, the determination of the properties of all commercially used cathode materials such as NMC, LCO, NCA, and LFP with additional Cu from the electrode conductor foils can be mentioned here. From this knowledge, pyrometallurgical processes can consequently be better adapted to the expected waste stream. An essential point in pyrometallurgy is also the optimization of the resulting products, such as the value-added metal alloy. Attention must be paid to this in the adaptation of input flows, process design, and post-treatment processes development, where in-depth knowledge of high-temperature behavior can significantly contribute.

ACKNOWLEDGEMENTS

This paper is supported by the Zukunftsfonds Steiermark with funds from the province of Styria, Austria, grant number GZ: ABT08-189002/2020 PN:1305.

REFERENCES

Abdou, T. R., Espinosa, D. C. R., & Tenório, J. A. S. (2016). Recovering of Carbon Fiber Present in an Industrial Polymeric Composite Waste through Pyrolysis Method while Studying the Influence of Resin Impregnation Process: Prepreg. In R. E. Kirchain, B. Blanpain, C. Meskers, E. Olivetti, D. Apelian, J. Howarter, A. Kvithyld, B. Mishra, N. R. Neelameggham, & J. Spangenberger (Eds.), REWAS 2016 (pp. 313–318). Springer International Publishing. https://doi.org/10.1007/978-3-319-48768-7_49

Altmann-Mavaddat, N., Athavale, S., Baumann, M., Bogner, T., Bürbaumer, H., Hirtl, A., Höher, M., Indinger, A., Kalt, G., Knaus, K., Lackner, P., Reidlinger, B., Raimund, W., Schilcher, K., Thenius, G., Tretter, H., Wanjek, M., & Zelalic, A. Klima und Energie: Wissen kompakt. Vienna. https://www.klimafonds.gv.at/wp-content/uploads/sites/16/Klima-und-Energie-Wissen-kompakt-final.pdf

Anderl, M., Zechmeister, A., Geiger, K., Gugele, B., Gössl, M., & Haider, S. (2019). Klimaschutzbericht 2019 (Report / Umweltbundesamt REP-0702). Wien. https://www.umweltbundesamt.at/studien-reports/publikationsdetail?pub_id=2279&cHash=b58b3e425d-78c6778b8d595035962135

Baldauf, M. (2022). Grenzwertbestimmung und Analyse von Aluminium- und Kohlenstoffzuschlägen zu Kathodenmaterial aus Lithium-Ionen-Batterien für die Wertmetallrückgewinnung im pyrometallurgischen Reaktorkonzept InduRed [Master thesis]. Montanuniversitaet Leoben, Leoben.

Beheshti, R., Tabeshian, A., & Aune, R. E. (2017). Lithium-Ion Battery Recycling Through Secondary Aluminum Production. In L. Zhang, J. W. Drelich, N. R. Neelameggham, D. P. Guillen, N. Haque, J. Zhu, Z. Sun, T. Wang, J. A. Howarter, F. Tesfaye, S. Ikhmayies, E. Olivetti, & M. W. Kennedy (Eds.), The Minerals, Metals & Materials Series. Energy Technology 2017 (pp. 267–274). Springer International Publishing. https://doi.org/10.1007/978-3-319-52192-3_26

Biswas, A. K. (1981). Principles of blast furnace ironmaking: Theory and practice. Cootha Publ. House.

Elwert, T., & Frank, J. (2020). Auf dem Weg zu einem geschlossenen Stoffkreislauf für Lithium-Ionen-Batterien: Towards a Closed Loop for Lithium-Ion Batteries. In E. Thomé-Kozmiensky, O. Holm, B. Friedrich, & D. Goldmann (Eds.), Recycling und Sekundärrohstoffe (pp. 525–530). Thomé-Kozmiensky Verlag GmbH.

European Commission. (2020, December 10). Green Deal: Sustainable batteries for a circular and climate neutral economy [Press release]. https://ec.europa.eu/commission/presscorner/detail/en/ip_20_2312

Gao, R., & Xu, Z. (2019). Pyrolysis and utilization of nonmetal materials in waste printed circuit boards: Debromination pyrolysis, temperature-controlled condensation, and synthesis of oil-based resin. Journal of Hazardous Materials, 364, 1–10. https://doi.org/10.1016/j.jhazmat.2018.09.096

Holzer, A. (2019). Pyrometallurgisches Recycling von Aktivmaterial aus der Aufbereitung von Lithium-Ionen-Batterien in einem induktiv beheizten Schüttschichtreaktor [Master Thesis]. Montanuniversitaet Leoben, Leoben.

Holzer, A., Windisch-Kern, S., Ponak, C., & Raupenstrauch, H. (2021). A novel pyrometallurgical recycling process for Lithium-Ion-Batteries and its use in recycling LCO and LFP. Metals, 2021(11(1), 149). https://doi.org/10.3390/met11010149

Huang, B., Pan, Z., Su, X., & An, L. (2018). Recycling of lithium-ion batteries: Recent advances and perspectives. Journal of Power Sources, 399, 274–286. https://doi.org/10.1016/j.jpowsour.2018.07.116

Kwon, O., & Sohn, I. (2020). Fundamental thermokinetic study of a sustainable lithium-ion battery pyrometallurgical recycling process. Resources, Conservation and Recycling, 158, 104809. https://doi.org/10.1016/j.resconrec.2020.104809

Li, J., Wang, G., & Xu, Z. (2016). Environmentally-friendly oxygen-free roasting/wet magnetic separation technology for in situ recycling cobalt, lithium carbonate and graphite from spent LiCoO2/graphite lithium batteries. Journal of Hazardous Materials, 302, 97–104. https://doi.org/10.1016/j.jhazmat.2015.09.050

Liu, C., Lin, J., Cao, H., Zhang, Y., & Sun, Z [Zhi] (2019). Recycling of spent lithium-ion batteries in view of lithium recovery: A critical review. Journal of Cleaner Production, 228, 801–813. https://doi.org/10.1016/j.jclepro.2019.04.304

Makuza, B., Tian, Q., Guo, X., Chattopadhyay, K., & Yu, D. (2021). Pyrometallurgical options for recycling spent lithium-ion batteries: A comprehensive review. Journal of Power Sources, 491, 229622. https://doi.org/10.1016/j.jpowsour.2021.229622

Pillot, C. (2019, September 18). The Rechargeable Battery Market and Main Trends 2018-2030. Avicenne Energy. ICM AG. ICBR 2019, Lyon.

Ponak, C. (2019). Carbo-thermal reduction of basic oxygen furnace slags with simultaneous removal of phosphorus via the gas phase [Dissertation]. Montanuniversitaet Leoben, Leoben.

Sojka, R., Pan, Q., & Billman, L. (September 2020). Comparative study of Lithium-ion battery recycling processes.

Swain, B. (2017). Recovery and recycling of lithium: A review. Separation and Purification Technology, 172, 388–403. https://doi.org/10.1016/j.seppur.2016.08.031

Thielmann, A., Neef, C., Hettesheimer, T., Döscher, H., Wietschel, M., & Tübke, J. (12 / 2017). Energiespeicher-Roadmap: Hochenergie-Batterien 2030+ und Perspektiven zukünftiger Batterietechnologien. Fraunhofer-Institut für System- und Innovationsforschung ISI. https://www.isi.fraunhofer.de/content/dam/isi/dokumente/cct/lib/Energiespeicher-Roadmap-Dezember-2017.pdf

Windisch-Kern, S., Holzer, A., Ponak, C., Hochsteiner, T., & Raupenstrauch, H. (2021). Thermal analysis of lithium ion battery cathode materials for the development of a novel pyrometallurgical recycling approach. Carbon Resources Conversion, 4, 184–189. https://doi.org/10.1016/j.crcon.2021.04.005

Windisch-Kern, S., Holzer, A., Ponak, C., & Raupenstrauch, H. (2021). Pyrometallurgical Lithium-Ion-Battery Recycling: Approach to Limiting Lithium Slagging with the InduRed Reactor Concept. Processes : Open Access Journal, 9(1), 84. https://doi.org/10.3390/pr9010084

Windisch-Kern, S., Holzer, A., Wiszniewski, L., & Raupenstrauch, H. (2021). Investigation of Potential Recovery Rates of Nickel, Manganese, Cobalt, and Particularly Lithium from NMC-Type Cathode Materials (LiNixMnyCozO2) by Carbo-Thermal Reduction in an Inductively Heated Carbon Bed Reactor. Metals, 11(11), 1844. https://doi.org/10.3390/met11111844

Xiao, J., Li, J., & Xu, Z. (2017). Novel Approach for in Situ Recovery of Lithium Carbonate from Spent Lithium Ion Batteries Using Vacuum Metallurgy. Environmental Science & Technology, 51(20), 11960–11966. https://doi.org/10.1021/acs.est.7b02561

Yin, H., & Xing, P. (2019). Pyrometallurgical Routes for the Recycling of Spent Lithium-Ion Batteries. In L. An (Ed.), Recycling of Spent Lithium-Ion Batteries (pp. 57–83). Springer International Publishing. https://doi.org/10.1007/978-3-030-31834-5_3

6.4 Publication 4

A Combined Hydro-Mechanical and Pyrometallurgical Recycling Approach to Recover Valuable Metals from Lithium-Ion Batteries Avoiding Lithium Slagging

Holzer, A.; Zimmermann, J.; Wiszniewski, L.; Necke, T.; Gatschlhofer, C.; Öfner, W. and Raupenstrauch, H.

Article Information:

Journal	Batteries, Volume 9, Issue 1
Special Issue	Circular Battery Technologies
Pages	26
Received Date	25 October 2022
Revised Date	20 December 2022
Accepted Date	21 December 2022
Published Date	26 December 2022
DOI	https://doi.org/10.3390/batteries9010015

Author's contribution: Conceptualization, Methodology, Validation, Investigation, Resources, Writing – original draft preparation, Writing – review and editing, Visualization, Supervision, Project administration, Funding aquisition

batteries

MDPI

Article

A Combined Hydro-Mechanical and Pyrometallurgical Recycling Approach to Recover Valuable Metals from Lithium-Ion Batteries Avoiding Lithium Slagging

Alexandra Holzer [1,*], Jörg Zimmermann [2], Lukas Wiszniewski [1], Tobias Necke [2], Christoph Gatschlhofer [1], Wolfgang Öfner [3] and Harald Raupenstrauch [1]

[1] Chair of Thermal Processing Technology, Montanuniversitaet Leoben, Franz-Josef-Strasse 18, 8700 Leoben, Austria
[2] Fraunhofer Research Institution for Materials Recycling and Resource Strategies IWKS, Aschaffenburger 121, 63457 Hanau, Germany
[3] Chair of Mineral Processing, Montanuniversitaet Leoben, Franz-Josef-Strasse 18, 8700 Leoben, Austria
* Correspondence: alexandra.holzer@unileoben.ac.at; Tel.: +43-3842-402-5803

Abstract: Meeting the increasing demand for energy storage based on lithium-ion batteries (LIB) is not only a question of resource availability but also an issue of resource conservation and efficient recycling management. In this respect, sustainable recycling concepts play a central role in mindful interactions with valuable materials. Based on this approach, a process interconnection of hydromechanical preparation, flotation, and pyrometallurgical treatment was investigated. The hydromechanical preparation showed promising results in achieving highly pure mixtures of LIB-active material. It was found that a pre-opening step could achieve an even better separation of impurities for downstream processes such as Cu and Al to avoid excessive particle size reduction. According to an optimized mixing stage during flotation, the C amount was reduced from 33 wt.% to 19.23 wt.%. A Li-free metal alloy was obtained through the subsequent pyrometallurgical treatment, and evidence for Li removal via the gas phase was provided. Furthermore, heating microscope trials confirmed the results of the process interconnection and showed that further optimization steps for the pre-treatment are necessary for favorable product quality. Therefore, a high-stratification plot was created, which allows a quick future statement about the suitability of the input material for use in the process.

Keywords: lithium-ion battery; recycling; hydro-mechanical preparation; flotation; pyrometallurgy

Citation: Holzer, A.; Zimmermann, J.; Wiszniewski, L.; Necke, T.; Gatschlhofer, C.; Öfner, W.; Raupenstrauch, H. A Combined Hydro-Mechanical and Pyrometallurgical Recycling Approach to Recover Valuable Metals from Lithium-Ion Batteries Avoiding Lithium Slagging. *Batteries* **2023**, *9*, 15. https://doi.org/10.3390/batteries9010015

Academic Editor: Matthieu Dubarry

Received: 25 October 2022
Revised: 20 December 2022
Accepted: 21 December 2022
Published: 26 December 2022

1. Introduction

Alternative technologies in several sectors, including energy-intensive industries [1], electrical grids [2–5], and especially within mobility [6], have been emerging all around the globe in recent years. They all try to tackle the same goal to minimize environmental impacts, reduce dependency on conventional energy sources like gas and petroleum, and diversify energy sources for the transportation sector [7]. The harsh spike in technological development ratios is based on national and international efforts to reduce global greenhouse gas emissions, resulting in a tremendous economic potential for these technologies [8–10]. One of these endeavors to limit global CO_2 emissions is the COP21, which led to the "Paris agreement" being adopted in December 2015 [11]. The aim of this agreement is to limit the rise in global temperatures to "well below" 2 °C above pre-industrial levels while striving for 1.5 °C by 2030 [12].

The electrification of these industries to replace fossil fuels with renewable electricity is essential for meeting these targets [13]. To store this energy, battery technologies are ubiquitous. With an estimated growth of 25% per year, a total capacity of up to 2.600 GWh in 2030 will be deployed [14]. With a share of 33.7% in 2018, Lithium-Ion Batteries (LIB) are

among the technologies already taking the most significant share of the overall rechargeable and non-chargeable battery market. Furthermore, it is expected that by 2024, about 82% of market growth will come from LIBs [15]. In Figure 1a, an estimation of the main drivers of demand growth is given, showing that the electrification of the transport sector is the main reason for this growth, followed by the deployment of batteries in electricity grids [14]. Each of these industries has different requirements for batteries, which can be adjusted via the chemical composition of the cathode materials. Figure 1b shows an outlook on the development of different cathode chemistries [16].

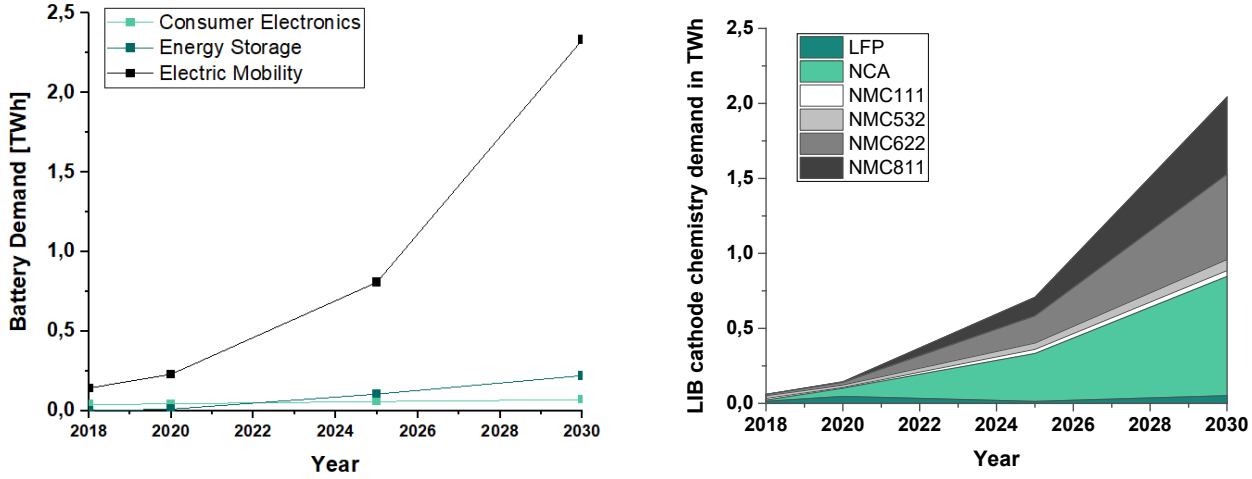

(**a**) (**b**)

Figure 1. Information about the current and future development of the battery market with a special focus on LIB: (**a**) global battery demand by application in TWh for the year 2030 (data in this figure are from WEF base case [14]); (**b**) outlook of different LIB cathode chemistries until 2030 in TWh (data in this figure are from [15,16]—the detailed calculation can be reviewed in Appendix A).

As seen in Figure 1, the forecasts for the LIB active materials show a wide variation. Hence, methods to sensitize recycling technologies towards fluctuating waste streams as well as political aspirations, and to mark batteries accordingly to their chemistry are needed. However, neither efficient recycling technologies nor legal frameworks for battery labeling are available or implemented in the primary markets [17]. The EU Commission's proposal for a regulation is considered a promising advance in this direction [18], wherein recovery rates for cobalt, copper, and nickel of 95% and 70% for lithium must be achieved by 2030. Concerning these ambitious recovery rates, and to counteract unlicensed recycling and illegal trafficking, the battery recycling chain must be revised entirely, including implementing the introduction of innovative and efficient recycling technologies. Furthermore, a complete waste battery collection system should be established to promote extended producer responsibility (EPR) [19].

State-of-the-art recycling routes for LIBs still face several dark spots, where inefficiencies or economic circumstances lead to material losses and landfilling [20]. The first operational step within the recycling chain is the pre-treatment of complete battery packs, including sorting, disassembly, and discharging. Generally, pre-treatment process steps are required to separate individual components ssuch as cables, plastics, aluminum and steel elements, and electronic components of the cooling system, etc., and the valuable remaining fractions like Fe, Cu, and Al as part of the housing or conductor foils from the cathode and anode material, the so-called black matter or active material. The dismantled parts are processed within further recycling steps; however, this is not the subject of the present work [21]. The black matter, in turn, contains the most valuable compounds, including Li, Ni, Co, Mn, and P. Next to these valuable metals, the black matter also consists of high rates of graphite (30–40% of the fines), often due to economic reasons, yet are not recycled.

However, to meet the EU's target of an overall recovery rate of 70%, it will become crucial to recover graphite in order to attain the recycling targets [22].

Within the disassembly step, shock-wave-based recycling procedures have become popular in recent years, as this technique allows a material-selective separation of complex and/or difficult-to-break composites, such as galvanized plastics [23], spark plugs [23], printed circuit boards [24], or LIBs [25,26]. Particularly in the processing of batteries, selective disintegration produces several advantageous coarse-grained by-products such as Al, Cu, and plastic foils, as well as steel housing parts, which can usually be recycled individually after further simple physical separation stages [25,26]. Furthermore, these by-products constitute a significant advantage in this pre-treatment method, especially compared to established pyrometallurgical recycling processes without further separation of battery components [27], where some of the metals, especially Al and Li, pass into the slag and are difficult or impossible to recover. The hydromechanical process enables the recovery of most of the battery cell components. However, the electrolyte remains in the process water; Li and P can at least be recovered from the water. Two of the most common alternative options for pre-treatment are mechanical shredding or crushing, including magnetic and/or density separation with or without inert atmospheres [28], and pyrolysis, a method that thermally decomposes the organic binder between conductor foils and active material [20].

Commonly, the next step in the recycling chain to recover valuable metals from the black matter consists of a pyro- and/or hydro-metallurgical process. Both of these processing routes commonly have the same goal of precious metal recovery, however, they also have to consider their individual pros and cons in combination with economic and environmental factors [20]. In downstream hydrometallurgical processes, graphite is often damaged, resulting in the unsuitability of upcycling spent anode materials [29]. Furthermore, graphite adds volume to the feed material during leaching processes, resulting in a high reagent consumption and leading to challenges in the dewatering stage [22]. In pyrometallurgical processes, graphite can be used as a reduction agent for the lithium-metal-oxides (LMO), however, it often exceeds the stoichiometrically needed content, resulting in a reduced smelting ability [30].

To separate the anode graphite and the LMO before a downstream process, froth flotation, a separation method using differences in surface wettability, might be a potential solution. The graphite particles have a size typically less than 25 µm. To achieve satisfactory separation of the graphite, the feed to the flotation stage needs to be rather fine compared to typical ore flotation [31,32]. Although the differences in wettability are pronounced, the particle size renders it an instance of fine flotation with its inherent difficulties in terms of the concentrate grade and the recovery of the valuable phase. Several approaches to improve the flotation performance, including chemical dissolution with Fenton reagent [33], thermal treatment [34], and mechanical [35] or cryogenic grinding [36], have already been tested and have shown promising results. However, they often fail when it comes to scale-up processes. Only thermal treatment at temperatures between 400–600 °C (the temperature range at which the binder starts to dissolve), ideal conditions for the flotation process, reported high graphite recovery of up to 98% in the froth product, being at the same time efficient and easy to use on an industrial scale [36]. As soon as the desired separation accuracy between the LMO and graphite has been achieved, the LMO is processed using downstream pyro-, hydro-, or bio-hydrometallurgical processes to ensure the sufficient product quality of the metals for recycling into a circular economy [37].

In order to overcome the challenges of the recycling technologies for spent LIBs currently available on the market, the scope of this paper was to investigate a novel possible interconnection between pre-treatment and pyrometallurgy. Therefore, a hydromechanical pre-treatment step with an electro-hydraulic fragmentation unit, a subsequent depletion of the graphite via flotation, and finally an inductive pyrometallurgical plant, was chosen. The pyrometallurgical plant used, the so-called InduMelt, is an inductively heated packed bed reactor in batch operations. This technology has a significant advantage over state-

of-the-art processes [27] since, in addition to the alloy, Li and P are not slagged and can be recovered via the gas phase. To explain the result from this process chain respectively and to optimize the quality of the obtained product in the future, results from further basic research on meltability and how interfering elements influence it are presented.

2. Materials and Methods

The source material for the recycling process were discharged NCA-cells (Panasonic NCR 18650A—$LiNi_{0.8}Co_{0.15}Al_{0.05}O_2$), which were obtained by manually dismantling a CUBE e-bike battery. NCA was selected as active material for this series of tests due to its expected high market share and likely its greatest impact on the fluctuating recycling stream's overall black matter chemistry, as seen in Figure 1.

The experimental series can be divided into three substeps. In the beginning, the battery cells of the NCA type are prepared in a hydromechanical pre-treatment. The resulting fine black powder containing valuable metals, consisting primarily of an anode and cathode material, in short, active material or black matter, and an electrode conductor foil made of Al and Cu, are then further processed. From previous research activities [30], it is known that for the reduction reactions in the InduRed process described in 2.3, a maximum of the stoichiometric C requirement may be present in the material since an oversupply would impair the necessary melting ability. Accordingly, in the next step, the C content was reduced via flotation from 34.57 wt.% to around 20 wt.%, corresponding to the theoretically necessary reducing agent requirement. The flotation fines were finally treated in the InduMelt plant for further valuable metal recovery. Consequently, the individual steps and the used analytical methods are described in more detail in the following subsections. In addition, the methodology for determining meltability is also discussed.

2.1. Hydromechanical Preparation

The hydromechanical processing of the battery cells was conducted at ambient conditions involving an electro-hydraulic fragmentation device (EHF-400, ImpulsTec GmbH, Germany), which was applied to produce NCA black matter. During this treatment, 40 single-round cells per batch were treated in 20 L water at a voltage of 40 kV and a frequency of 1.5 Hz within a stainless steel reactor. This procedure was conducted until all the batteries were opened and successfully disintegrated. The applied process (schematically drawn in Figure 2) is based on shock waves generated by discharges between the electrodes through the water in the reactor and targeted to separate LIBs along their weakest points, typically phase and material boundaries. At this point, it must be mentioned that in individual cases, the discharge can pass through the material (electro-dynamic fragmentation), which occurs as an undesirable side effect only to a small degree. Due to the different mechanical properties of battery materials, a high fragmentation selectivity and higher purity can be achieved via electro-hydraulic fragmentation, especially compared to conventional mechanical shredding, which is advantageous for further recycling. For more in-depth information on this technology, refer to previous publications [28–31]. After shock wave treatment, the suspension from the reactor was screened through a 500 µm sieve to separate the coarse fractions from the much finer anode and cathode particles. Subsequently, the fine fraction was vacuum filtered to separate the black matter from the water. Finally, after drying at 80 °C for 72 h, the obtained black matter was homogenized for subsequent experiments and analytics using mortar and pestle.

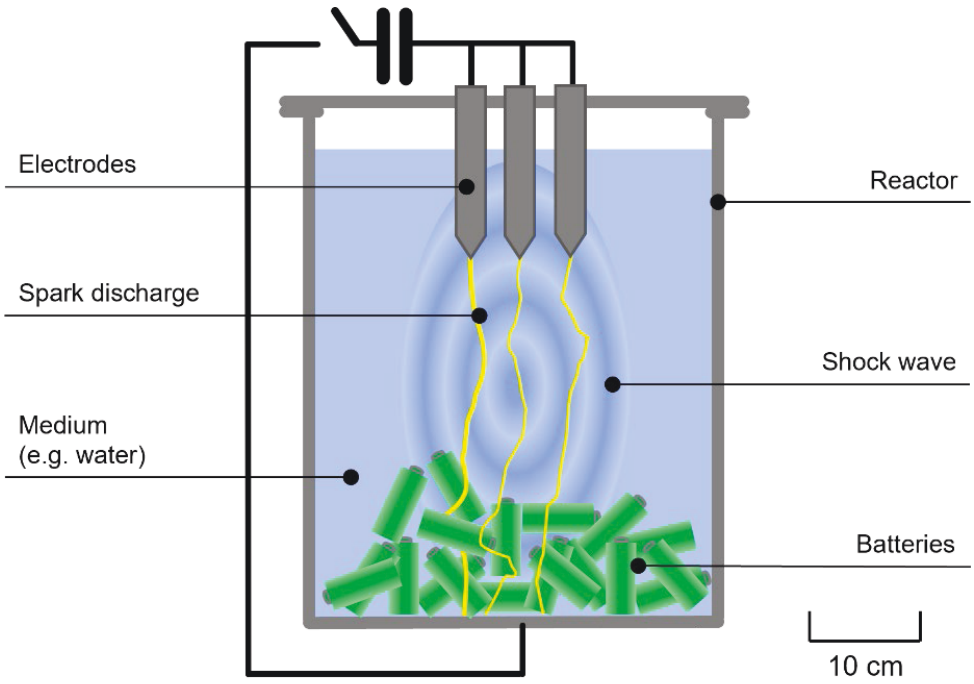

Figure 2. Schematic functional principle of electrohydraulic fragmentation.

2.2. Flotation

The flotation tests were performed in two stages. As only about 100 g of NCA was available to complete any preliminary tests, a small custom-made flotation device with a 500 mL tank size was used at this point, which is well-suited for such basic tests (Figure 3a). This device has been used at the Chair of Mineral Processing for several decades and is well-suited for such basic tests. For detection of the C amount, parallel trial with a Leco CHN 628 has been conducted. Prior checks with test tubes had shown that dispersion of the sample in water is no challenge. Furthermore, the suitability of two commercial reagent blends was confirmed for this task: Ekofol (EF) 440 and EF 452, which are sold by EKOF for the flotation of coal and graphite. They contain aliphatic alcohols, esters, and ethers; the exact composition is not disclosed. EF 452 was chosen for the tests.

To achieve good separation with the fine particle sizes present, the flotation test was performed in a rather conservative way: low solids concentration of about 5 %-vol; frother/collector EF 452 added in several increments of 200 ppm each; discharge of concentrate for as long as the froth carried particles; thick froth layer; skimming froth off only superficially; low airflow. The pulp was dispersed for 5 min at 1200 rpm prior to the first addition of EF 452 and conditioning.

When the actual NCA sample—close to 2000 g—was available, the flotation tests moved to the Denver laboratory machine D-1, with its larger working volume of either 1.2 or 2.3 L (Figure 3b). Four batches were basically treated with the same general attitude as in the preliminary test. The rotational speed of the impeller was 800 rpm. As the characteristics of the two impeller systems are different, a direct comparison with the speed of the preliminary test is not valid. In contrast to the initial examination, solids concentration was about 10%-vol for the four batches. Separation was no longer satisfactory; possible reasons will be discussed later.

The remaining six flotation tests for the Denver D-1 aimed at improving the separation result and settings varied within this series. The most important changes were a significantly more intense dispersing stage (15 min at 1200 rpm and solids concentration of up to 20 %-vol), higher reagent dosage, and a higher impeller speed (1000 rpm) during flotation.

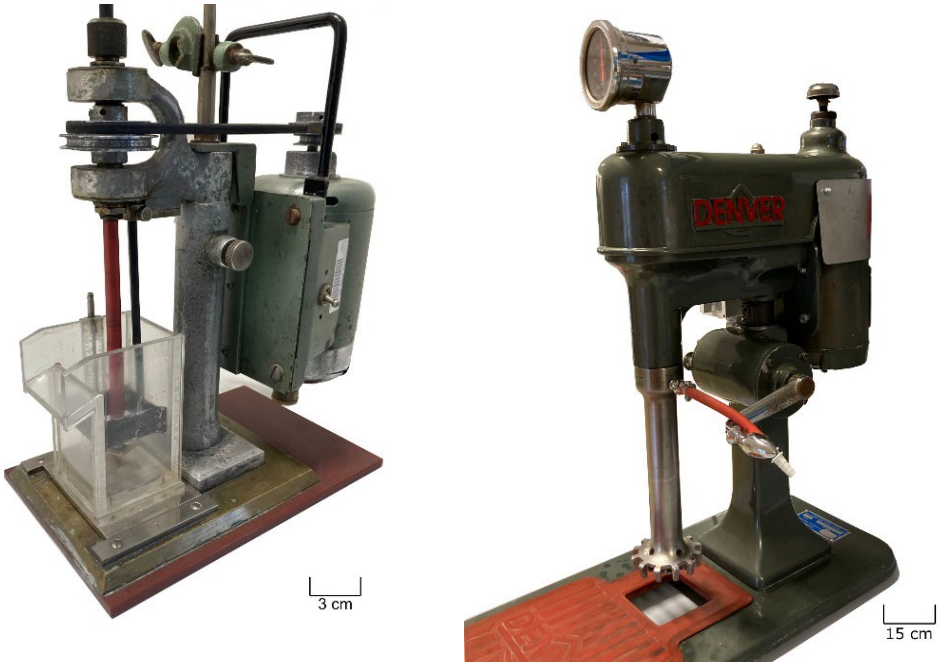

(**a**) (**b**)

Figure 3. The flotation devices used for graphite removal from NCA samples: (**a**) the custom-made cell used for the preliminary flotation test; (**b**) Denver laboratory machine D-1 used for the actual NCA sample.

2.3. Pyrometallurgical Treatment

The plant setup designed at the Chair of Thermal Processing Technology, the so-called InduMelt plant with its InduRed reactor concept, is shown schematically in Figure 4.

The main advantages of this system compared to, for example, a shaft furnace, are the high contact area between the hot graphite cubes and the active material, the homogeneous radial and horizontal heat supply, and short diffusion paths for volatile elements such as phosphorus or lithium through the resulting melt film. As a result of the engineering-related advantages of the reactor principle compared to conventional pyrometallurgical reactor concepts, valuable components like lithium are not being transferred to a mineral phase, and are thus able to be recycled. Additionally, the reactor produces a very limited amount of mineral phase, resulting almost in a closed loop process. The graphite cubes serve purely as susceptor material for providing heat on its surfaces and do not participate in the reduction reactions.

For better comparability with previous experiments, the setup, experimental procedure, and sampling are carried out precisely according to the scheme from Holzer et al. [38]. In summary, the crucible with a height of 60 cm and width of 20 cm consists of high temperature-resistant MgO. The material to be reduced in this plant was pre-treated in the hydromechanical step. Subsequently, graphite was partially separated through flotation. The crucible is filled layer by layer with 400 g of the resulting active material and the graphite cubes. The latter have a side length of 2.5 cm, an electrical resistance of 4–8 μΩm, and a density of 1.55–1.75 gcm^{-1} [38].

It should be noted that the graphite from the battery anode materials acts as a reducing agent. This creates an atmosphere in the reactor during the experiment with a high CO/CO_2 ratio and low O_2 partial pressure.

To ensure appropriate temperature control, two type-K thermocouples are placed in the bulk and one type-S in the thermocouple, each at the bottom and on the reactor wall of the outside. After insulating the wall and floor area, as shown in green in Figure 4, a ceramic pipe is installed in the lid insulation for controlled exhaust gas discharge. Above

this is the gas exhaust hood through which a water jet pump draws the gas stream over the fluid in the gas wash bottle. For this experiment, distilled water was used to avoid unwanted reactions between the fluid and the compounds in the gas stream.

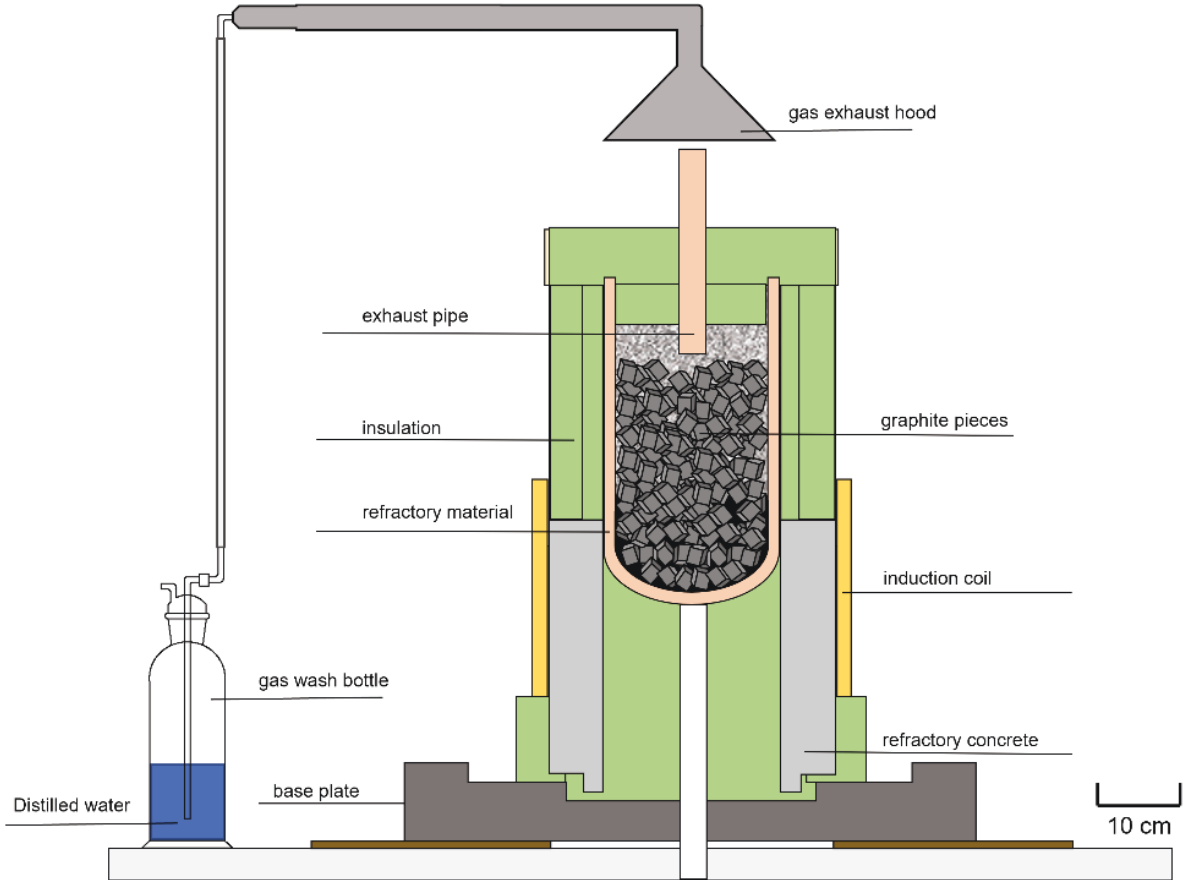

Figure 4. Schematic illustration of the InduMelt plant [38].

For the protection of the refractory material, a maximum heating rate of 250 °C/h was selected over an experimental period of 7.5 h. Consequently, the target temperature of 1550 °C was maintained for half an hour before the completion of the experiment. After a cooling phase of at least 24 h at ambient temperature, the standardized sampling was carried out. The resulting fractions (metal, powder, mineral phase) were extracted and separated via magnetic separation and sieving and finally analyzed.

2.4. Analytical Methodology for Material Characterization

In general, samples, including the floated active material and the gained fractions obtained after carbo-thermal treatment, were subjected to an SEM analysis. Except for the metal fraction embedded in an epoxy resin as a ground-glass specimen, all other specimens were prepared on self-adhesive, graphite-filled pads. In addition, the metal and mineral fractions were sputtered with gold, whereby EDX software largely corrected the gold signal. This publication's analyses were performed in the SEM of model Vega1 from Tescan (CZ) with an acceleration voltage of 0.5–30 kV from an electron source in the form of a tungsten filament. Additionally, with the aid of an energy dispersive X-ray analysis (EDX) model 5108 from Oxford Instruments type Si(Li), the elemental composition can be determined within a 10 mm^2 area of the sample with a resolution at 5.9 kV of 137 eV. Therefore, with the present instrumental setup, elements starting from atomic number 4 (i.e., carbon) can thus be detected with SEM-EDX. Since this does not allow the determination of lithium, laser-induced breakdown spectroscopy (LIBS) model EA-300 from Keyence (optics 300x,

laser–Nd: YAG 355 nm) was applied as supplementary to verify the SEM-EDX results by means of a line-point analysis. This pool of analytical methods enables the determination of elemental distribution based on mappings, point analyses of individual phases, and line spectra with SEM-EDX and LIBS.

Powder X-ray diffraction (PXRD) samples were analyzed for phase composition using an X-ray diffractometer (Empyrean, Malvern Panalytical, U.K.) within Bragg−Brentano geometry using cobalt radiation (λ = 1.789 Å) at 40 mA and 40 kV. Diffraction patterns were collected with a scan speed of 0.006°/s and a step size of 0.013° for the 2θ range from 10 to 75° and evaluated using HighScore Plus software (Malvern Panalytical, U.K.) using the inorganic crystal structure database (ICSD; FIZ Karlsruhe, Germany).

ICP-OES analyzed the chemical composition of several fractions during this investigation according to ÖNORM EN ISO 11885:200911.

2.5. Analyses Concerning High-Temperature Behavior and Influence of Impurities

For successively improving the product yield, the high-temperature behavior of the cathode material NCA was investigated under the influence of contaminants such as Cu, Al, and C. The aim was to determine the meltability of the cathode material by measuring the sample's change in cross-sectional area (CSA) during heating. For this purpose, a series of tests were carried out using a Hesse Instruments EM 201 heating microscope with an HR18-1750/30 furnace with cathode material from battery production and varying amounts of Cu, Al, and C. To simulate the low CO/CO_2 ratio of the InduMelt plant, the experiments in the heating microscope would have to be operated with a CO atmosphere. Since this is not possible for technical and safety reasons, the trials were performed with a 2.5 L/min argon purge to suppress undesired reoxidation reactions. Therefore, the C fraction for InduMelt has to be converted in order to simulate reactions from C to CO_2 (occurring in the heating microscope) to reactions from C to CO (occurring in the InduMelt). The cylindrical pressed samples of about 0.1 g each were positioned on an Al_2O_3 plate and heated up following the standardized heating program from Table 1. The maximum furnace temperature of 1700 °C contained therein results in a sample temperature of approximately 1620 °C. After the holding time at 1700 °C, the furnace load was switched off and the sample was left in the furnace chamber under argon purging until room temperature was reached.

Table 1. Standardized heating program in the heating microscope for investigations of the high-temperature behavior of NCA with different impurities.

Temperature Range	Heating Rate
Start–1350 °C	80 °C/min
1350–1450 °C	50 °C/min
1450–1700 °C	10 °C/min
1700 °C	5 min holding time

Subsequently, a height stratification diagram was selected to simplify the presentation of the results. The evaluation and execution of the experiments followed a consistent scheme. Essentially, a total of 42 experiments were carried out in the heating microscope with different mixing ratios. Based on the preparation of an Al-C-NCA system, these investigated mixing ratios were extended in a selected range by adding 3 wt.%, 6 wt.%, and 9 wt.% Cu in each case [39]. The selected range described above resulted from the findings of Baldauf [40], who defined the meltable zone at a minimum carbon demand of 5 wt.%. It should be mentioned at this point that the stoichiometrically necessary reducing agent required for a complete reduction of the oxide for NCA is around 11 wt.% C. Since processing and preparation of more than 1500 data points per test is relatively costly, they were processed as in Holzer et al. [30]. In essence, this was achieved via smoothing over a polynomial, comparing the measurement points with the corresponding images, the linear correlation of the corrected values, and the arithmetic mean of data with the same temperature or logical continuation [30,40].

3. Results and Discussion

3.1. Hydromechanical Preparation

In the hydromechanical processing of NCA cells, about 6000 pulses were required to achieve complete disintegration of the battery cells and to separate the active materials from the anode and cathode foils. In each batch, 40 cells with a total weight of about 1750 g were processed to produce about 1100 g of black matter and about 650 g of the coarse fraction. Since this work focused on the recovery of the cathode metals, the coarse fraction, which consists mainly of aluminum, copper, plastic foils and steel housing parts, was not investigated further in this study.

Characterization of the black matter specimens (NCA_AM_start) via ICP-OES and Leco analysis (see Table 2) revealed carbon (34.57 wt.%), nickel (31.0 wt.%), and cobalt (5.02 wt.%) as the main elements. The relatively high carbon content is attributed to anode graphite, carbon black, and possibly small residues of polyvinylidenfluoride binders. At the same time, lithium, nickel, cobalt, and aluminum are associated with the NCA cathode material (approximately $LiNi_{0.8}Co_{0.15}Al_{0.05}O_2$). The element concentrations for Cu, Fe, and partially Al are caused by small impurities of metal particles that pass into the fine fraction during processing.

Table 2. ICP-OES analysis of relevant elements in the sample after the hydromechanical preparation in wt.-%.

Compound	Li	Co	Ni	Al	Fe	Cu	C
NCA_AM_start [1]	3.38	5.02	31.00	2.37	2.65	3.64	34.57

[1] Difference to 100% detection rate, mainly due to the proportion of O; amounts of other elements are negligible, according to complete analysis via ICP-MS.

3.2. Flotation

The separation result of the preliminary test was quite good, even though only a rougher stage was performed. Three consecutive C concentrates, and the residue R were assayed for their C grade. The balance is given in Table 3.

Table 3. Balance of the preliminary flotation test. C1 to C3: carbon concentrates; R: residue.

Flotation Product	Mass Yield [%]	C Grade [%]	C Recovery [%]
C1	53.2	45.2	72.8
C2	8.6	48.2	12.6
C3	11.9	27.3	9.9
R	26.2	6.0	4.8
total	100.0	33.0	100.0

The residue yields 26% of the feed, while its C grade has been lowered from 33% in the feed to 6%. In this test, the 20% grade aimed for later on was already reached by removing the first graphite concentrate C1, while almost half of the feed mass remained available for the metallurgical tests. Terminating the separation after C2 would leave C3 and R as the combined residue with 38% of the feed mass at 13% C grade.

In comparison, when conducting the experiments on the Denver D-1, only one of the first four batches achieved some slight separation regarding C. The C grade of the remaining froth products and residues was virtually the same as that of the feed. There are two main reasons for inadequate separation in flotation: low degree of liberation, and entrainment.

The degree of liberation measures how much of a certain phase is present in pure particles. The rest of that phase is “intergrown” and is part of the compound particles. As the physical/mechanical separation methods of mineral processing can only separate particles from each other, good liberation is an essential prerequisite for any separation success. The only way to improve liberation is by making the particles smaller.

Entrainment occurs when non-hydrophobic particles report to the froth instead of the flotation residue. They may be trapped between hydrophobic particles and thus be forced into the wrong flotation product. Entrainment can be reduced by using the proper setting of the flotation parameters.

The SEM analysis (not shown) confirmed that in the present case the problem was the lack of liberation of graphite. Therefore, six more flotation tests were performed to address this problem. Adding a rather long and intense mixing stage (15 min at 1200 rpm; some tests even with about 15%-vol of solids) before flotation provided better liberation. Diluting the pulp again to the previous 5 %-vol of solids and using 1000 rpm (vs. 800 in the first four batches) during flotation, finally provided satisfactory separation results. Table 4 shows the C grades of graphite concentrates (C plus the number of trial and number of extracted sample) and the residues (R plus the number of trial) of those flotation tests where all products were assayed.

Table 4. C grades of flotation concentrates and residues after improving liberation.

Concentrates	C Grade [%]	Residue	C Grade [%]
C5	42.7	R5	25.7
C9-1	35.5	R9	13.1
C9-2	29.5		
C10-1	48.2	R10	14.9
C10-2	43.5		
C10-3	33.3		

As some intermediate residues had to be reworked several times, the C balances of the separate tests are inconclusive. Six suitable froth products and residues were blended for a combined C grade of 19.23% and yielded 710 g (34% of the entire NCA sample) to be used for the InduMelt tests.

The difference in separation quality between the preliminary (see Table 3) and the actual NCA sample is striking and demonstrates one of the frequent challenges when processing secondary raw materials. Although samples may seem to be "the same", assuming identical characteristics and compositions can be very misleading. For example, even the product line of one single producer of LIBs represents various states in its production history. The particle sizes of components, the type of binder, the electrolyte, the actual composition of NCA, etc., will all change, and such variations may impact mechanical separation processes.

The chemical composition of the NCA black matter, the NCA active material after flotation (NCA_AM), can be taken from Table 5. Compared to the material after the electrohydraulic fragmentation (EHF) treatment in Table 2, a depletion during the flotation process of mainly C and Al can be detected. The enrichment of Cu and Fe is particularly interesting in this context. One possible explanation is the larger size and higher weight of the Cu and Fe particles from the electrode conductor foil and battery assembly, compared to the C and NCA. As a result, these elements are less likely to be entrained in the froth during flotation and are concentrated in the residue. In contrast, the lighter Al from the electrode conductor foil tends to be more readily transferred into the foam product due to its low mass, the theory of which is consistent with depletion. The remaining elements are found in the NCA structure. The comparison of the ICP-OES analyses confirms the expected constant proportion of elements.

Table 5. ICP-OES analysis of relevant elements in the sample after flotation for use in downstream InduMelt experiment in wt.-%.

Compound	Li	Co	Ni	Al	Fe	Cu	C
NCA_AM [1]	3.48	5.07	30.70	1.88	3.43	6.36	19.23

[1] Difference to 100% detection rate, mainly due to the proportion of O; amounts of other elements are negligible, according to complete analysis via ICP-MS.

Figure 5 shows an SEM-EDX mapping of the material obtained from flotation, which is subsequently further processed in the InduMelt plant. The different colors are characteristic of the respective element present in the material, referring to the image of the SEM.

These microscopic investigations confirm the presence of spherical NCA particles with a diameter of about 25 µm within a carbon-rich matrix. In particular, the spherical appearance and the size of the NCA cathode particles are typical features of these materials, so it can be concluded that the EHF treatment only separates these materials from the foils but does not destroy the original microstructure. Furthermore, these observations are consistent with previous work conducted by Öhl [30] and Horn [31]. Carbonaceous particles are seen predominantly in SEM-EDS mapping (Figure 5d) and are related to anode graphite and carbon black being used as conductivity enhancers. In addition to these overall findings, minor indications of Cu and Al are visible in the SEM-EDS mappings attributed to minor contaminants from anode and cathode conductor foils. Generally, Co and Ni (Figure 5e,f) show an overlapping pattern over the whole SEM picture. As expected, the sample is rich in oxygen, which can be attributed to the oxidic components in the NCA-active material. Moreover, finely dispersed iron content is determined in the mapping with Fe-overlay (Figure 5h), which corresponds to traces of housing parts.

As expected, the PXRD pattern (see Figure 6) showed a lithium-nickel-cobalt-alumina oxide phase (PDF 98-009-8451) with space group R-3m and a graphite phase (PDF 98-007-6767) as the main components within the black matter specimens. Both phases correspond to NCA-type lithium-ion batteries' commonly used cathode and anode materials. In addition, small diffraction peaks of elemental copper (PDF 98-062-7113) were detected, corresponding to fine-anode foil particles, which pass during EHF processing into the fine fraction.

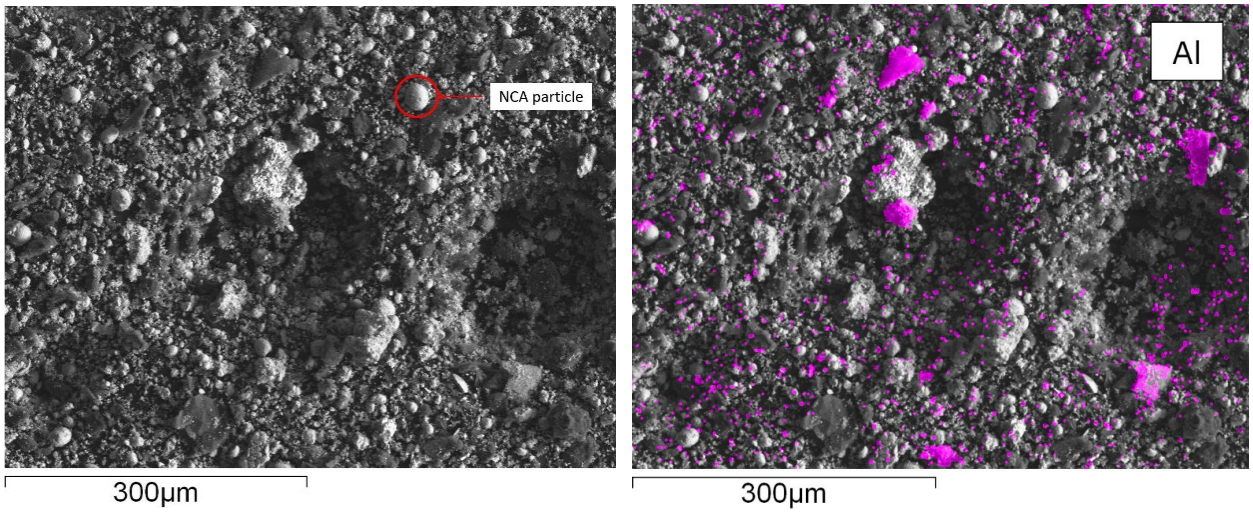

(**a**) (**b**)

Figure 5. *Cont.*

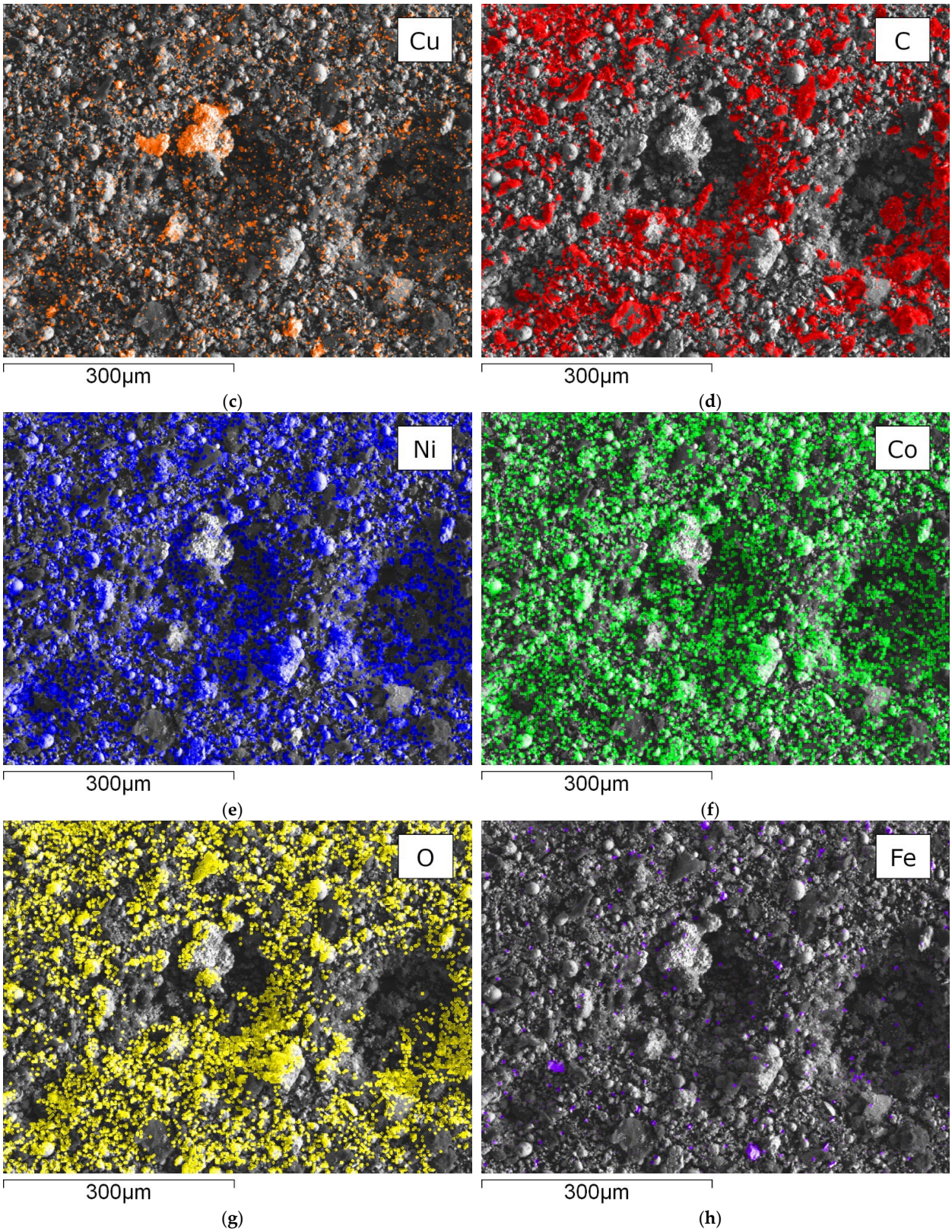

Figure 5. SEM picture and overlay of the elemental distribution of characteristic elements; (**a**) SEM picture of NCA_AM, one of the characteristic NCA agglomerates is marked in red; EDX-Mapping of (**b**) aluminum; (**c**) copper; (**d**) carbon; (**e**) nickel; (**f**) cobalt; (**g**) oxygen; (**h**) iron.

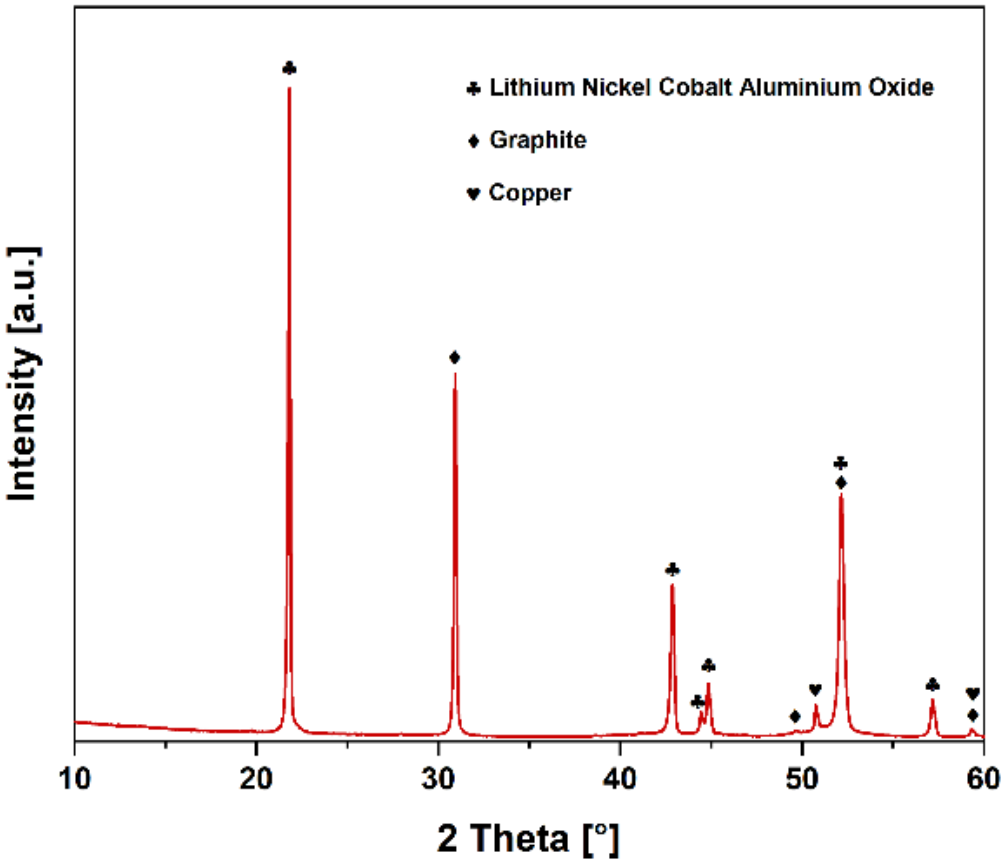

Figure 6. PXRD pattern of NCA black matter after EHF processing and flotation.

3.3. Pyrometallurgical Treatment

To determine the quality of the products from the pyrometallurgical InduRed reactor concept, the floated black matter was used in the InduMelt plant. The fractions obtained can be subdivided as follows:

- Sparse magnetic powder
- Metal fraction, with a grain size larger than 1 mm
- Powder smaller than 1 mm with magnetic properties
- Product from the gas phase, which has been deposited in the washing water or the exhaust hood

At this point, it should be mentioned that the primary objective of this process step is to obtain a fully reduced, low-lithium metal alloy. At the same time, the formation of slag or powder is not desired. For the successive optimization of the process, in addition to the knowledge of the influence of interfering elements on the product quantity, detailed analyses of the obtained fractions are necessary. Special attention is paid hereafter to the economically interesting valuable metal.

Table 6 shows the weighted masses of the individual solid fractions. When looking at these results, on the one hand, the deficient proportion of sparse magnetic powder compared to metal and powder is striking. On the other hand, it can also be seen that 56.4% of the obtained materials' mass was classified as powder and 42.4% as metal. If the results are compared with pure cathode material from battery production with the identical experimental procedure and apparatus from Holzer et al. [37], this value is about 20.1% powder and 78.8% metal. From this finding, it can be deduced in the first step that non-separated accompanying elements from the LIB, such as Cu and Al of the electrode conductor foil, harm the metal yield.

Table 6. Amount of the input and output fractions of the InduMelt experiment in grams.

Input [g]	Powder-Sparse Magnetic [g]	Metal [g]	Powder [g]
400.0	2.7	92.5	123.0

3.3.1. Analyses of the Powder Fractions

From the ICP-OES analysis of the sparse magnetic powder shown in Table 7, it can be seen that there is a significant amount of Li. Still, according to the small amount in the overall system (Table 6), this plays a minor role in the process. This fraction consists mainly of carbon, accompanied by particles in the mineral phase, both of which could be confirmed through SEM-EDX investigations.

Table 7. ICP-OES analysis of relevant elements in the produced powder fraction after the InduMelt experiment in wt.-%.

Compound	Li	Co	Ni	Al	Fe	Cu
Powder-sparse magnetic [1]	5.33	0.18	7.29	2.89	0.18	0.23
Powder [1]	0.23	9.63	56.60	2.66	5.37	11.10

[1] Difference to 100% detection rate, mainly due to the proportion of O and C or measurement uncertainties and complex sampling; amounts of other elements are negligible, according to complete analysis via ICP-MS.

If these findings are supplemented with PXRD analyses, the characteristic diffraction peaks of graphite and Li_2CO_3 in the monoclinic zabuyelite structure (PDF 98-001-6713) can be recognized, as seen in Figure 7a.

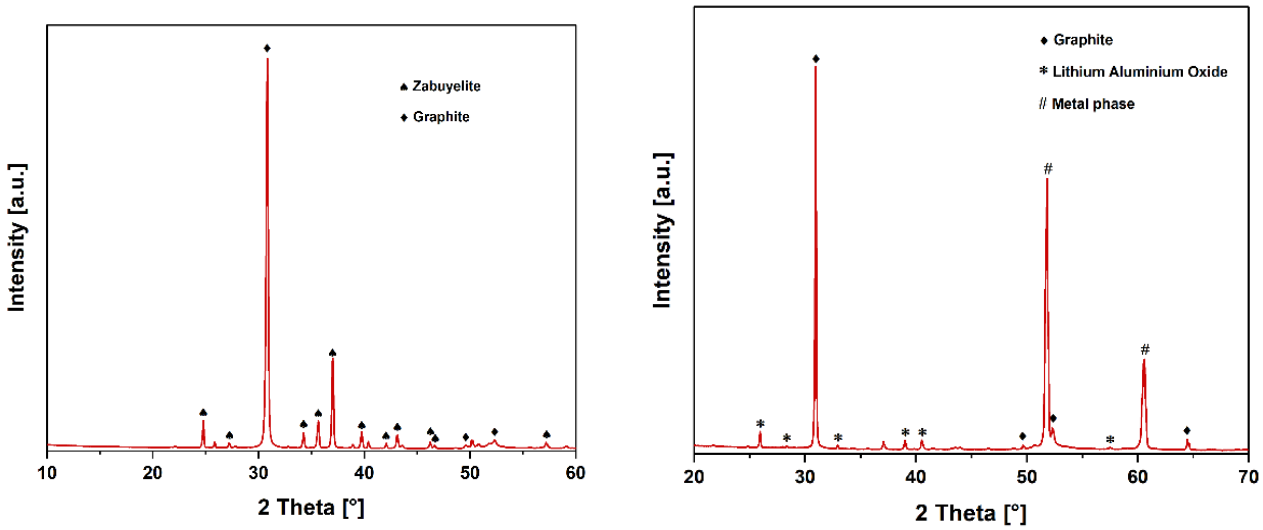

(**a**) (**b**)

Figure 7. PXRD pattern: (**a**) results of sparse magnetic powder; (**b**) results of powder.

The powder has an entirely different chemical composition compared to the less-magnetic powder. By comparing the ICP analyses of the initial NCA_AM material used from Table 5 and the powder from Table 7 and its magnetic property, it is reasonable to assume that this is partially reduced active material. The SEM and XRD show a significant amount of C, since the initial round 20 wt.% C in the NCA_AM represented the stoichiometrically necessary mass to reduce the lithium metal oxides. Its presence in the powder underscores the presumption of an incomplete reduction. The PXRD measurements could confirm these overall findings in Figure 7b, where the characteristic diffraction peaks of

gamma-$LiAlO_2$ with tetragonal symmetry could be detected in addition to the graphite. In addition, two intense diffraction peaks were detected at 51.8 and 60.0° 2 Theta, possibly corresponding to an unspecifiable cubic metal phase.

3.3.2. Analysis of the Metal Fraction

In addition to the elemental analysis using ICP-OES (Table 8), the combination with the SEM-EDX and LIBS provides comprehensive insights into the elemental assignment of existing phases. Figure 8 shows an SEM image of secondary electrons from a different ground-glass specimen compared to the metal fraction embedded in epoxy resin. The examined particles are interspersed with elongated graphite crystals (flake graphite), while shrinkage in varying degrees can also be determined. Moreover, as expected, the polished metal pieces are infiltrated with holes and show different structures, which can be attributed to the experimental setup of the non-continuous batch operation process of the InduMelt. However, according to the SEM-EDX analyses of various metal particles, the elemental composition of the metal alloy itself is consistent in a certain range.

Table 8. ICP-OES analysis of relevant elements in the produced metal fraction after the InduMelt experiment in wt.-%.

Compound	Li	Co	Ni	Al	Fe	Cu
Metal [1]	0.00	12.60	63.80	2.86	7.50	14.30

[1] Difference to 100% detection rate, mainly due to measurement uncertainties and complex sampling; amounts of other elements are negligible, according to complete analysis via ICP-MS.

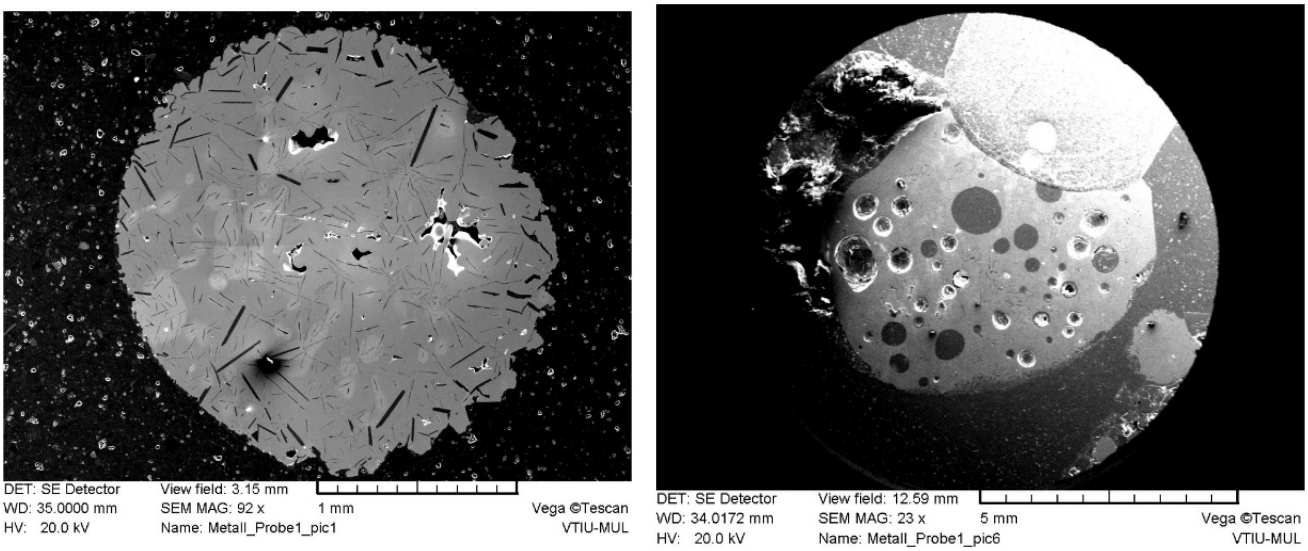

(**a**) (**b**)

Figure 8. SEM-secondary electron images of cut and polished specimens of the metal-fraction embedded in epoxy resin: (**a**) metal droplet with blowholes and elongated graphite crystallite; (**b**) metal droplet with holes and spherical inclusions.

Figure 9 shows the SEM-EDX mapping of the sample corresponding to the partial image in Figure 8b, with the metal particle mainly shown in this latter figure. Furthermore, a part of the conductor path (upper-right edge) and mineral caking can be seen at the upper-left edge. However, mineral caking represents only a small percentage of the total metal fraction mass. The metal droplet consists of a Ni-rich alloy intermixed with significant amounts of Co, Fe, and Cu. C is likely to be dissolved in the alloy, where larger accumulations in the holes come from the resin. While higher O and Al amounts in the caking indicate the primary presence of oxidic components, the remaining metal alloy is

evenly distributed with both elements. It can be assumed that Al from the conductor foil has a high affinity for oxygen and is therefore bound with the remaining oxidic Al from the active material into the mineral phase.

As previously described, numerous metal droplets show an adhesion of oxidic origin. For that reason, according to Figure 10, a line spectrum of a characteristic metallic piece with mineral caking is investigated with the SEM-EDX. Twenty measuring points assigning only a qualitative composition due to the low elemental retrieval rate are summarized in Figure 10b. The obtained results are in good accordance with the identified elements of the depicted mapping in Figure 9. In particular, two main phases could be determined: a Ni-rich metallic phase (points 1 and 9–18) with additional alloying elements such as Co, Fe, Cu, Al, and C of consistent composition; on the other hand, a mineral phase (points 2–8 and 19, 20) commonly consisting of O and Al with differing minor amounts of Mg and Ca. Moreover, points two and three are enriched with C. Comparing the results from Figure 10b with those from the chemical analysis using ICP-OES in Table 8, a good correlation can be observed.

In Figure 11, a digital microscopic image with corresponding LIBS measurements of two neighboring grains in the metallic and mineral phase is shown, whereas along the grain boundaries, higher amounts of Li combined with O, Al, and C can be proven. In some phases of the mineral caking, Li in minor amounts is also detectable. It can be assumed that Li compounds neither preferentially dissolved in the gradually formed metal nor in the separated liquefied O- and Al-rich mineral bath during high-temperature treatment. Therefore, Li species accumulate preferably at the grain boundaries before forming gaseous Li. Nevertheless, further scientific investigations should be encouraged by the outcomes of the SEM-EDX and LIBS, especially to focus on the Li behavior during carbo-thermal reduction. Again, the LIBS can verify the elements identified from the ICP-OES and SEM-EDX in a reasonable composition in both phases mentioned.

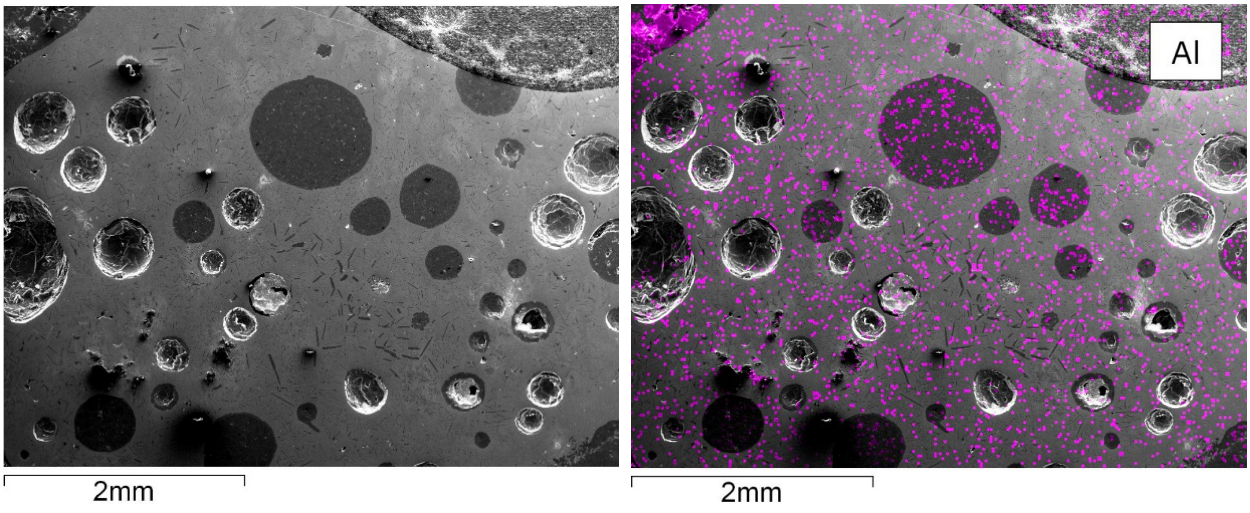

(**a**) (**b**)

Figure 9. *Cont.*

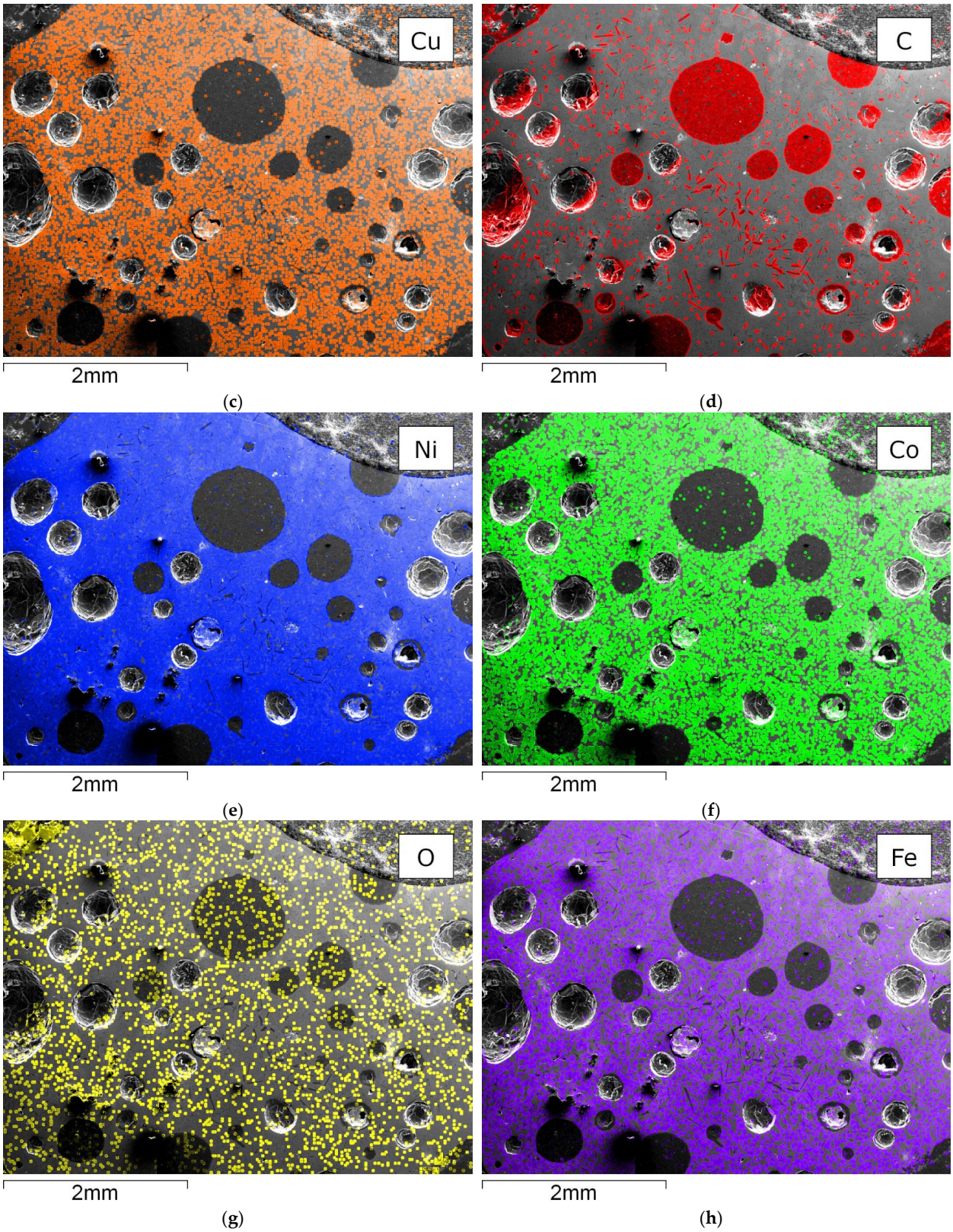

Figure 9. SEM picture and overlay of the elemental distribution of characteristic elements; (**a**) SEM picture of the metal after InduMelt experiment; SEM-EDX mapping of (**b**) aluminum; (**c**) copper; (**d**) carbon; (**e**) nickel; (**f**) cobalt; (**g**) oxygen; (**h**) iron.

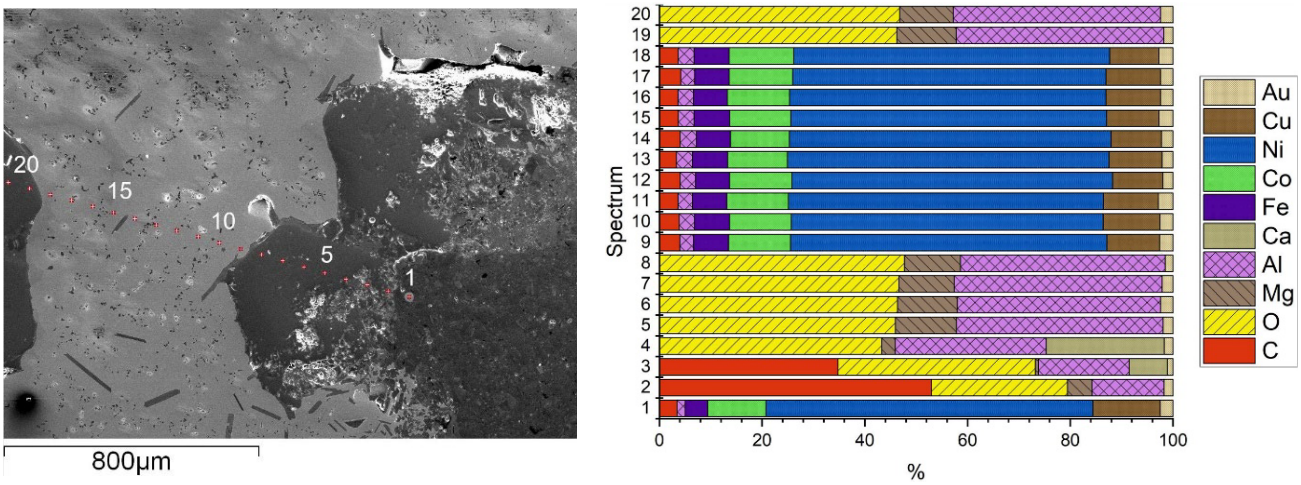

(**a**) (**b**)

Figure 10. Line spectrum through a metal piece with mineral caking; (**a**) SEM-picture of the particle with the associated analysis point position; (**b**) related composition of each analysis point from (a) using EDX analysis.

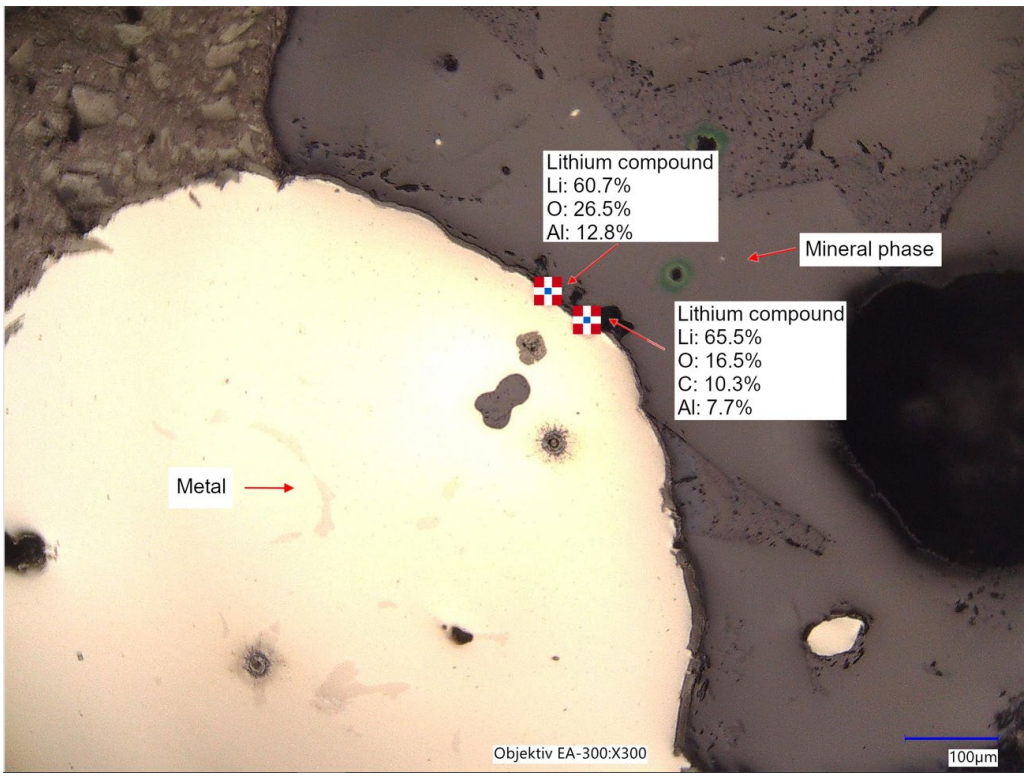

Figure 11. Digital microscopic image of the interface between metal and mineral phase with corresponding LIBS measurements.

3.3.3. Analysis of the Gaseous Fraction

The PXRD analysis of the white powder precipitated within the water-filled gas wash bottle is shown in Figure 12. Only two intense diffraction peaks were detected in the measured 2 Theta range, which generally indicates a phase with high, probably cubic, symmetry. In addition to these structural data, the ICP-OES analysis (Table 9) revealed a high lithium content of 640 mg/L in the water, so a lithium phase could also be assumed for the precipitate. After comparison with the database, only a cubic griceite-like phase

(LiF, PDF 98-005-2234) with space group *Fm*-3*m* could explain the observed diffraction peaks, which generally corresponds to the low solubility of the LiF in water (1.3 g/L at 25 °C). Slight residues of the PVDF binders in the black matter could be a likely source of the fluorine, decomposing at the high temperatures of the InduMelt process and forming the LiF together with the degassing Li.

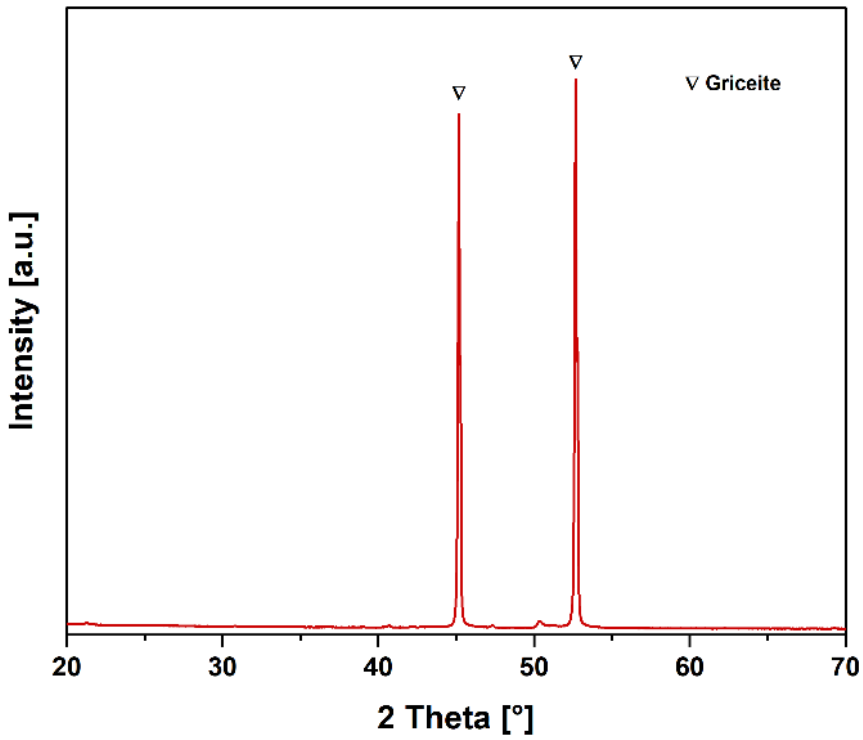

Figure 12. PXRD pattern of the filtrate of the fluid in the gas washing bottle.

Table 9. ICP-OES analysis of relevant elements in the produced gas stream after the InduMelt experiment in mg/L.

Compound	Li	Co	Ni	Al	Fe	Cu
Gas washing water [1]	640.0	0.0	2.5	0.7	0.0	9.0

[1] Analysis quantity: 50 mL.

3.4. Optimization of the Metal Amount

As discussed in Section 3.3 concerning pyrometallurgical treatment, the metal yield is subject to optimization potential. From previous experiments by Holzer et al. [30], it was found that the main factors influencing the melting ability are Al and Cu from the electrode conductor foils, as well as the C from the anode material. The influence of other possible concomitant elements was not investigated further since, from the analyses of the initial sample, a negligible value was found compared to Cu and Al. The experiments generated in the heating microscope with varying Al, Cu, and C contents can be seen in Figure 13. In the figures, different melting-ability ranges are marked, which were determined by comparing the recordings from the heating microscope with the final optical appearance. The area for good melting-ability was observed within the light red continuous line. The dark red dashed line indicates where the results deviate from the optimum range but still provide tolerable performance. Outside this range, poor-to-no melting can be assumed.

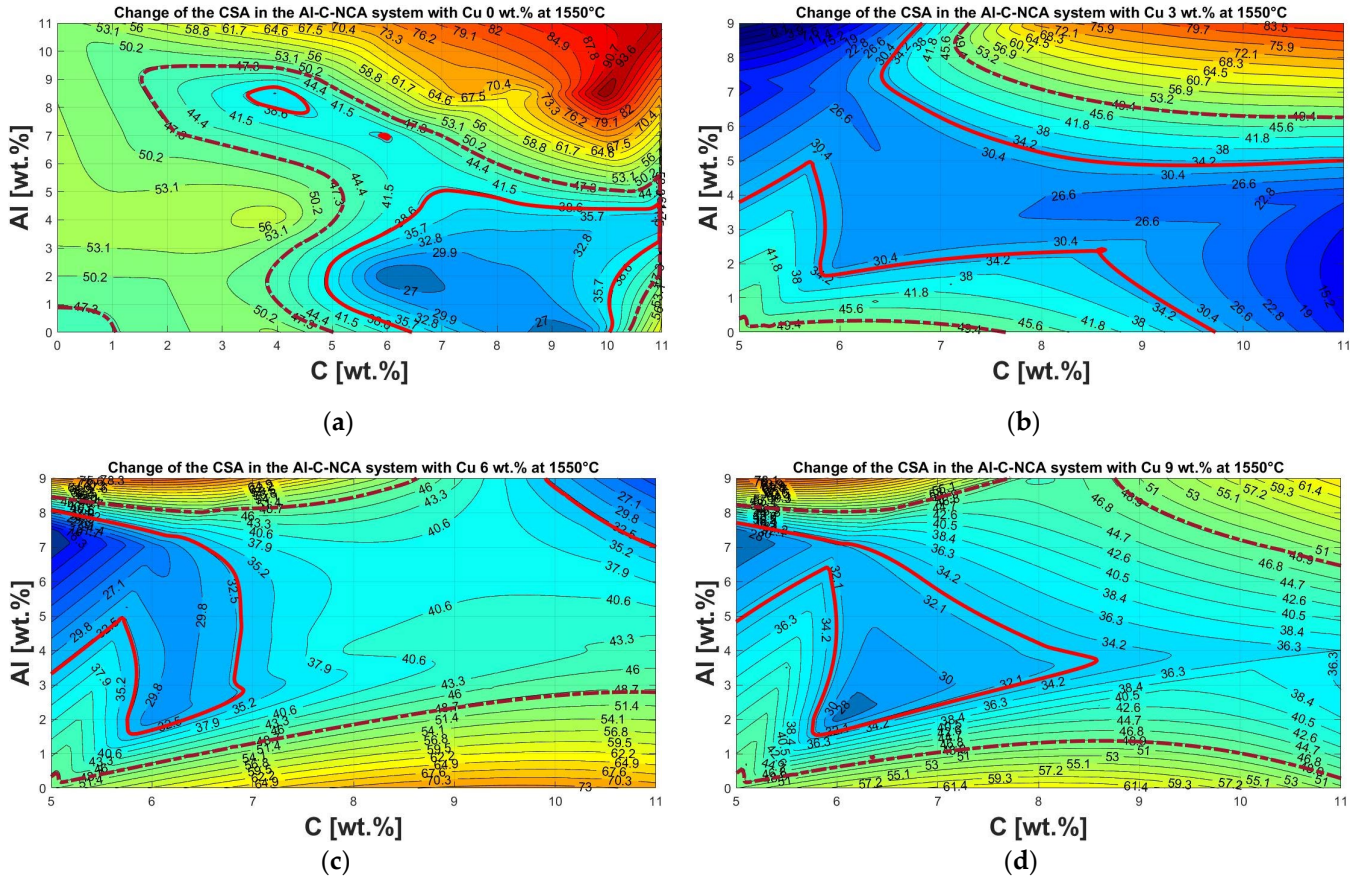

Figure 13. Representation of the change in cross-sectional area from the heating microscope with changing composition of the Al-C-NCA system at 1550 °C in a height stratification plot: (**a**) without addition of Cu; (**b**) constant Cu content of 3 wt.%; (**c**) constant Cu content of 6 wt.%; (**d**) constant Cu content of 9 wt.%.

In Figure 13a, without adding Cu, it can be seen that the optimum range is close to the stoichiometrically necessary C content of 11 wt.% for the complete reduction of the oxides mentioned at the beginning. However, its absolute optimum is in the range of between 6 and 7 wt.% C. This can be attributed to the fact that aluminum from the electrode conductor foils, with its strong oxygen affinity [41], acts as a reducing agent [27], resulting in a C excess. This, but also generally an oversupply of reducing agents, has a negative effect on meltability.

The addition of Cu to the Al-C-NCA system is shown in increasing ratios from Figure 13b–d. It can be seen that the melting range gradually increases, and that the optimum range moves in the direction of the lower C content and higher Al content.

Applying these findings to the chemical composition of the NCA material hydromechanical processing and flotation, as shown in Table 5, results in the height stratification diagram with a Cu content of 6.36 wt.%, as presented in Figure 14.

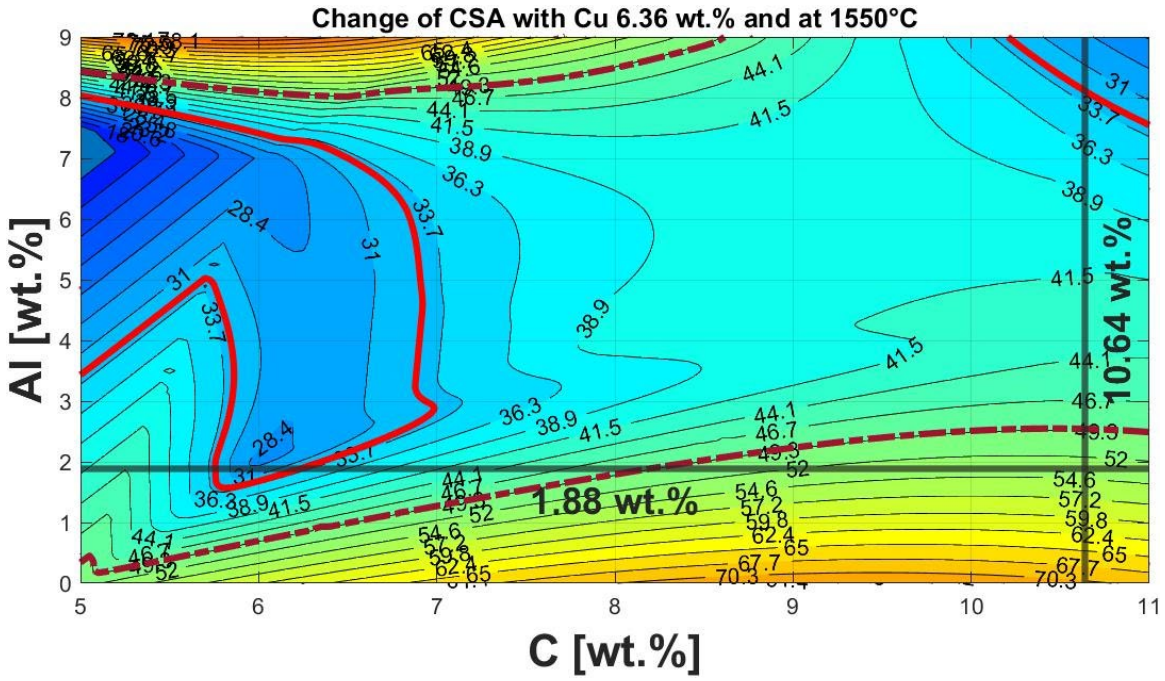

Figure 14. Height stratification diagram of the Al-C-NCA system at constant Cu content of 6.36 wt.% at 1550 °C.

Considering the argon atmosphere in the heating microscope instead of the high CO/CO_2 ratio in the InduMelt results in a comparative C content of 10.64 wt.%, instead of the 19.23 wt.% present in the material. For a more transparent representation, the 10.64 wt.% C and 1.88 wt.% Al were marked with a black line in the diagram. The intersection point consequently shows that the present mixture can be identified as not optimal for use in the InduMelt plant. This fact now coincides with the comparatively high powder content, as discussed in more detail in Section 3.3.1 concerning the analyses of the powder fractions. This is also reflected in the appearance of the metal fractions. In Figure 15, the optical difference between the metal fraction obtained from the identical experiments in Holzer et al. [37] with the material without a Cu and Al addition (Figure 15a) and that in the InduMelt series of experiments in the presented paper in Figure 15b can be seen. In Figure 15a, metal nuggets of several cm could be obtained. Figure 15b shows smaller metal spheres with various adhesions, which have already been discussed in detail in Chapter 3.3.2 concerning the nalysis of the metal fraction.

Its C grade would have to be reduced considerably to provide a more favorable composition of the InduMelt feed. As demonstrated by the subsequent concentrates in the preliminary flotation test, this can be achieved via longer flotation times, provided that the graphite is sufficiently liberated. However, mineral processing always has a trade-off between the concentrate grade and the recovery. The achievable separation results are limited by the liberation and intergrowth of the relevant phases in the feed material, so reducing the feed's C grade to InduMelt requires less feed during the metallurgical stage. If the losses of the metals are not acceptable, flotation must be assisted by some pre-treatment that improves liberation. One quite effective solution may be the removal of the binder, as indicated in the introduction.

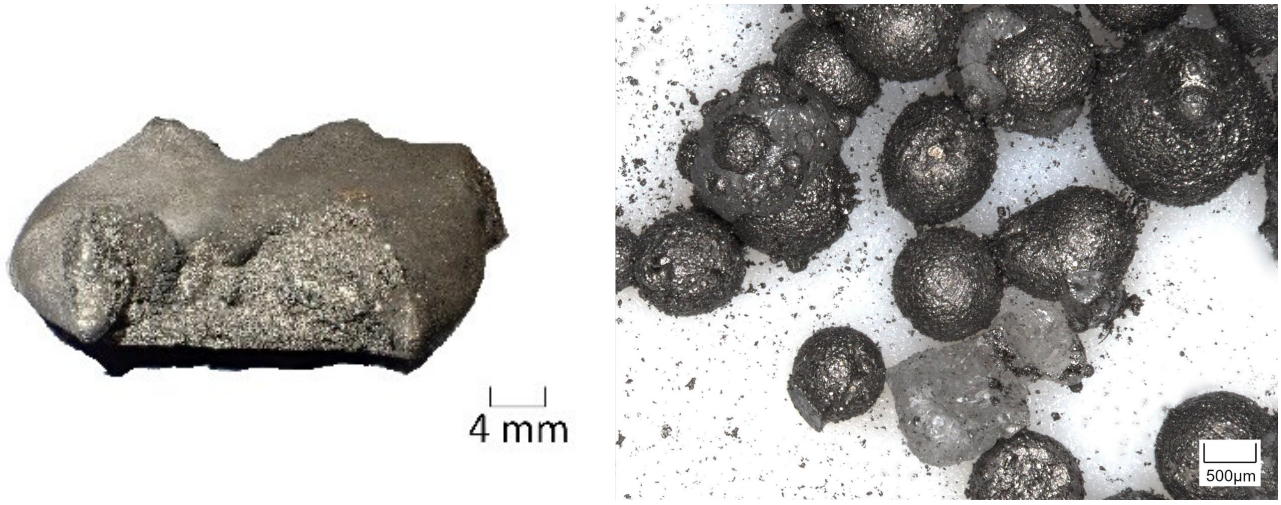

(**a**) (**b**)

Figure 15. Digital images of the metal fractions obtained from different InduMelt experiments for comparison: (**a**) trial with NCA without impurities such as Cu and Al [38]; (**b**) trial with NCA_AM.

4. Conclusions

In this work, a new combined process flow for LIB recycling has been reported, including hydromechanical pre-treatment, flotation of graphite from the anode material, and pyrometallurgical recovery of the valuable metals with the simultaneous separation of lithium via the gas phase. In addition, in-depth results from basic research were presented, which will serve future process optimization.

During these experimental investigations, it could be shown that the black matter obtained using the material-selective electro-hydraulic fragmentation after 6000 pulses fulfils the requirements for the InduRed reactor concept. Analyses confirmed that the shock wave treatment does not destroy the original microstructure and separates the NCA particles from the electrode foils, which is essential for further downstream steps. However, traces of copper and aluminum were found, which have been identified as unfavorable for the meltability. In order to improve the purity of the black matter and to reduce the number of pulses and thus the energy consumption, further studies on different pre-opening steps are currently planned to increase the overall efficiency

The flotation process needed to be modified compared to the standard procedure due to the lack of decomposition in the graphite/NCA agglomerations. This was addressed through the use of a more intense mixing phase of 15 min at 1200 rpm with approximately 15%-vol of solids in the pulp, followed by a dilution to 5%-vol, and the flotation phase being set to 1000 rpm. Consequently, a C depletion to 19.23 wt.% could be achieved, which corresponds to the approximate stoichiometrically necessary content for a complete reduction of the NCA amount within the sample.

Analytical results revealed a Li-free and Ni-Cu-Cu-rich alloy as a result of the pyrometallurgical treatment. In addition, Li and Li-compounds (e.g., Li_2CO_3 and LiF) were detected within the samples in the off-gas stream. Finally, a detected Li-rich phase (Li content up to 65.5%) at the grain boundaries between the metal and the mineral phase clearly implicates the segregation and degassing of Li at high temperatures. However, compared with preliminary tests with the pure cathode material, it was also found that much smaller amounts of metal could be recovered, and the ratio shifted toward undesirable powder, containing lithium aluminum oxide.

To improve the lithium yield via the gas phase, minimization of the powder content is fundamental, which in turn leads to an increase in Li-free alloy. For this purpose, a limit determination of the interfering elements Cu, Al, and C was carried out. The resulting height-stratification diagram enabled a quick and easy evaluation of the usability of the

black matter in the reactor, indicating poor meltability in this work. So, it can be stated that further improvements in the metallurgical stage are possible by adjusting the composition of the feedstock so that the advantages of the InduRed reactor concept can be fully utilized.

In summary, a promising future for interconnection methods concerning individual process steps for spent LIBs could be possible with the findings mentioned above, which provide great potential for further developments of holistically efficient recycling processes.

Author Contributions: Conceptualization, A.H. and J.Z.; methodology, A.H.; validation, A.H. and H.R.; investigation, A.H., J.Z., T.N. and W.Ö.; resources, A.H., H.R., J.Z. and W.Ö.; writing—original draft preparation, A.H., J.Z., C.G., T.N., L.W. and W.Ö.; writing—review and editing, A.H., J.Z., C.G., T.N., L.W., W.Ö. and H.R.; visualization, A.H.; supervision, A.H. and H.R.; project administration, A.H.; funding acquisition, A.H., H.R. and J.Z. All authors have read and agreed to the published version of the manuscript.

Funding: This paper is supported by the Zukunftsfonds Steiermark with funds from the province of Styria, Austria, grant number GZ: ABT08-189002/2020 PN:1305 and by the Hessen State Ministry for Higher Education, Research and the Arts through the Center for Dismantling and Recycling for Electromobility ZDR-EMIL®.

Data Availability Statement: The data presented in this study are available upon request from the corresponding author.

Acknowledgments: Great thanks are owed to the Chair of Process Technology and Environmental Protection at the Montanuniversitaet Leoben (in particular Simon Moll, Elias Vigl and Jan Eisbacher-Lubensky) for supporting the publication with SEM-EDX and LIBS analyses and competent advice on the evaluation of the results, as well as to Daniel Schrittwieser from the Chair of Design of Steels for preparation of the SEM samples. The authors also thank Daniel Horn, Fabian Brückner and Axel Fabian (all Fraunhofer IWKS) for their support during manual dismantling and EHF processing of battery cells.

Conflicts of Interest: The authors declare no conflict of interest. The funders had no role in the design of the study; in the collection, analyses, or interpretation of data; in the writing of the manuscript, or in the decision to publish the results.

Appendix A

The following tables and calculations shall explain Figure 1 of the introduction. The World Economic Forum (WEF) published in 2019 a report called "A Vision for a Sustainable Battery Value Chain in 2030" with data regarding the global installed battery capacity until 2030. Figure 1a with corresponding data in Table A1 shows an adapted version of this data.

Table A1. Global battery demand by application in GWh for the year 2030, WEF base case [15].

Year	2018	2020	2025	2030
Electric mobility	142	229	808	2.333
Energy storage	0	10	105	221
Consumer electronics	38	43	58	69

To draw Figure 1b based on data licensed under a Creative Commons Attribution 4.0 International License (https://creativecommons.org/licenses/by/4.0/, accessed on 21 December 2022), the following assumptions have been made: as described by Zhao et al. [15], 33.7% of the overall battery market in 2019 consited of LIBs; until 2024, the growth in the total battery sector caused by LIBs will be 81.77%; and assuming that in 2018 the share of the overall battery market was more or less the same as it was in the beginning of 2019, the following data, as seen in Table A2, have been calculated.

Table A2. Global LIB battery demand by application in GWh for the year 2030, WEF base case [14], including forecasts by Zhao et al. [15].

Year	2018	2020	2025	2030
Electric mobility	47.9	119.0	592.4	1839.4
Energy storage	0.0	8.2	85.9	180.7
Consumer electronics	12.8	16.9	29.2	28.2
SUM	60.7	144.1	707.5	2058.3

These so-calculated sums were then multiplied by the percentages of cathode chemistries published by Xu et al. [16]. In Table A3 the data for Figure 1b can be seen.

Table A3. Global LIB battery demand by cathode chemistry in GWh for the year 2030, WEF base case [14], including forecasts by Zhao et al. [15] and data from XU et al. [16].

Year	LFP	NCA	NMC111	NMC532	NMC622	NMC811
2018	14.0	7.6	10.9	18.0	9.2	1.0
2020	46.6	54.4	5.9	15.4	17.6	4.2
2025	13.4	319.1	27.6	41.7	181.1	124.5
2030	51.5	794.5	39.1	74.1	568.1	514.6

References

1. Nurdiawati, A.; Urban, F. Towards Deep Decarbonisation of Energy-Intensive Industries: A Review of Current Status, Technologies and Policies. *Energies* **2021**, *14*, 2408. [CrossRef]
2. Lamnatou, C.; Chemisana, D.; Cristofari, C. Smart grids and smart technologies in relation to photovoltaics, storage systems, buildings and the environment. *Renew. Energy* **2022**, *185*, 1376–1391. [CrossRef]
3. Borenius, S.; Hämmäinen, H.; Lehtonen, M.; Ahokangas, P. Smart grid evolution and mobile communica-tions—Scenarios on the Finnish power grid. *Electr. Power Syst. Res.* **2021**, *199*, 107367. [CrossRef]
4. Choi, D.; Shamim, N.; Crawford, A.; Huang, Q.; Vartanian, C.K.; Viswanathan, V.V.; Paiss, M.D.; Alam, M.J.E.; Reed, D.M.; Sprenkle, V.L. Li-ion battery technology for grid application. *J. Power Sources* **2021**, *511*, 230419. [CrossRef]
5. Ma, S.; Lin, M.; Lin, T.E.; Lan, T.; Liao, X.; Maréchal, F.; Yang, Y.; Dong, C.; Wang, L. Fuel cell-battery hybrid systems for mobility and off-grid applications: A review. *Renew. Sustain. Energy Rev.* **2021**, *135*, 110119. [CrossRef]
6. Nguyen, T.-V.; Schnidrig, J.; Maréchal, F. An analysis of the impacts of green mobility strategies and technologies on different European energy system. In Proceedings of the ECOS 2021, Taormina, Sicily, Italy, 28 June–2 July 2021.
7. Onat, N.C.; Kucukvar, M. A systematic review on sustainability assessment of electric vehicles: Knowledge gaps and future perspectives. *Environ. Impact Assess. Rev.* **2022**, *97*, 106867. [CrossRef]
8. Jacobson, M.Z. Review of solutions to global warming, air pollution, and energy security. *Energy Environ. Sci.* **2009**, *2*, 148–173. [CrossRef]
9. Khan, S.A.R.; Ponce, P.; Yu, Z. Technological innovation and environmental taxes toward a carbon-free eco-nomy: An empirical study in the context of COP-21. *J. Environ. Manag.* **2021**, *298*, 113418. [CrossRef]
10. Su, C.-W.; Naqvi, B.; Shao, X.-F.; Li, J.-P.; Jiao, Z. Trade and technological innovation: The catalysts for climate change and way forward for COP21. *J. Environ. Manag.* **2020**, *269*, 110774. [CrossRef]
11. Rhodes, C.J. The 2015 Paris Climate Change Conference: COP21. *Sci. Prog.* **2016**, *99*, 97–104. [CrossRef]
12. *Teske, Achieving the Paris Climate Agreement Goals*; Springer International Publishing: Cham, Switzerland, 2019.
13. Teske, S.; Pregger, T.; Simon, S.; Naegler, T.; Pagenkopf, J.; Deniz, Ö.; van den Adel, B.; Dooley, K.; Meinshausen, M. It Is Still Possible to Achieve the Paris Climate Agreement: Regional, Sectoral, and Land-Use Pathways. *Energies* **2021**, *14*, 2103. [CrossRef]
14. World Economic Forum and The Global Battery Alliance (Ed.) *A Vision for a Sustainable Battery Value Chain in 2030: Unlocking the Full Potential to Power Sustainable Development and Climate Change Mitigation*; WeForum: Cologny, Switzerland, 2019; p. 52.
15. Zhao, Y.; Pohl, O.; Bhatt, A.I.; Collis, G.E.; Mahon, P.J.; Rüther, T.; Hollenkamp, A.F. A Review on Battery Market Trends, Second-Life Reuse, and Recycling. *Sustain. Chem.* **2021**, *2*, 167–205. [CrossRef]
16. Xu, C.; Dai, Q.; Gaines, L.; Hu, M.; Tukker, A.; Steubing, B. Future material demand for automotive lithi-um-based batteries. *Commun. Mater.* **2020**, *1*, 99. [CrossRef]

17. Wang, Y.; Goikolea, E.; de Larramendi, I.R.; Lanceros-Méndez, S.; Zhang, Q. Recycling methods for different cathode chemistries–A critical review. *J. Energy Storage* **2022**, *56*, 106053. [CrossRef]
18. European Commission. Proposal for a Regulation of the European Parliament and of the Council concerning Batteries and Waste Batteries, Repealing Directive 2006/66/EC and Amending Regulation (EU) 2019/1020: SWD(2020) 334 Final. Available online: https://www.parlament.gv.at/PAKT/EU/XXVII/EU/04/37/EU_43776/imfname_11029480.pdf (accessed on 21 December 2020).
19. Zhang, W.; Xu, C.; He, W.; Li, G.; Huang, J. A review on management of spent lithium ion batteries and stra-tegy for resource recycling of all components from them, Waste management & research: The journal of the In-ternational Solid Wastes and Public Cleansing Association. *ISWA* **2018**, *36*, 99–112. [CrossRef]
20. Windisch-Kern, S.; Gerold, E.; Nigl, T.; Jandric, A.; Altendorfer, M.; Rutrecht, B.; Scherhaufer, S.; Raupenstrauch, H.; Pomberger, R.; Antrekowitsch, H.; et al. Recycling chains for lithi-um-ion batteries: A critical examination of current challenges, opportunities and process dependencies. *Waste Manag.* **2022**, *138*, 125–139. [CrossRef]
21. Arnberger, A.; Coskun, E.; Rutrecht, B. Recycling von Lithium-Ionen-Batterien. In *Recycling und Rohstoffe*; Thiel, S., Thomé-Kozmiensky, E., Goldmann, D., Eds.; Thomé-Kozmiensky Verlag GmbH: Neuruppin, Germany, 2018; Band 11.
22. Vanderbruggen, A.; Salces, A.; Ferreira, A.; Rudolph, M.; Serna-Guerrero, R. Improving Separation Efficiency in End-of-Life Lithium-Ion Batteries Flotation Using Attrition Pre-Treatment. *Minerals* **2022**, *12*, 72. [CrossRef]
23. Herdegen, J.; Benner, W.; Bokelmann, K.; Hartfeil, T.; Gellermann, C. Separationsverfahren zur Aufarbeitung von metallhaltigen Verbundwerkstoffen. In *Recycling und Rohstoffe*; Thomé-Kozmiensky, K.J., Goldmann, D., Eds.; TK Verlag Karl Thomé-Kozmiensky: Neuruppin, Germany, 2016; Band 9; pp. 601–608.
24. Bokelmann, K.; Grieger, S.; Schlummer, M.; Benner, W.; Vogelgesang, M. DISPLAY Upscaling of Material Recovery from Display Applications and Printed Circuit Boards. In *Olaf Holm*; Thomé-Kozmiensky, E., Goldmann, D., Bernd Friedrich, B., Eds.; Recycling und Rohstoffe; Thomé-Kozmiensky Verlag GmbH: Neuruppin, Germany, 2020; pp. 380–392.
25. Öhl, J.; Horn, D.; Zimmermann, J.; Stauber, R.; Gutfleisch, O. Efficient Process for Li-Ion Battery Recycling via Electrohydraulic Fragmentation. *MSF* **2019**, *959*, 74–78. [CrossRef]
26. Horn, D.; Zimmermann, J.; Gassmann, A.; Stauber, R.; Gutfleisch, O. Battery Recycling: Focus on Li-ion Batteries. In *Modern Battery Engineering. A Comprehensive Introduction*; Birke, P., Ed.; World Scientific: Hackensack, NJ, USA; London, UK; Singapore; Beijing, China; Shanghai, China; Hong Kong, China; Taipei, China; Chennai, India; Tokyo, Japan, 2019; 223p.
27. Makuza, B.; Tian, Q.; Guo, X.; Chattopadhyay, K.; Yu, D. Pyrometallurgical options for recycling spent li-thium-ion batteries: A comprehensive review. *J. Power Sources* **2021**, *491*, 229622. [CrossRef]
28. Velázquez-Martínez, O.; Valio, J.; Santasalo-Aarnio, A.; Reuter, M.; Serna-Guerrero, R. A Critical Review of Lithium-Ion Bat-tery Recycling Processes from a Circular Economy Perspective. *Batteries* **2019**, *5*, 68. [CrossRef]
29. Porvali, A.; Aaltonen, M.; Ojanen, S.; Velazquez-Martinez, O.; Eronen, E.; Liu, F.; Wilson, B.P.; Serna-Guerrero, R.; Lundström, M. Mechanical and hydrome-tallurgical processes in HCl media for the recycling of valuable metals from Li-ion battery waste. *Resour. Conserv. Recycl.* **2019**, *142*, 257–266. [CrossRef]
30. Holzer, A.; Baldauf, M.; Wiszniewski, L.; Windisch-Kern, S.; Raupenstrauch, H. Influence of Impurities on the High-Temperature Behavior of the Lithium-Ion Battery Cathode Material NMC Under Reducing Conditions for Use in the InduRed Reactor Concept. *Detritus* **2022**, *in press*. [CrossRef]
31. Feng, D.; Aldrich, C. Effect of particle size on flotation performance of complex sulphide ores. *Miner. Eng.* **1999**, *12*, 721–731. [CrossRef]
32. Derhy, M.; Taha, Y.; Hakkou, R.; Benzaazoua, M. Review of the Main Factors Affecting the Flotation of Phosphate Ores. *Minerals* **2020**, *10*, 1109. [CrossRef]
33. Zhan, R.; Yang, Z.; Bloom, I.; Pan, L. Significance of a Solid Electrolyte Interphase on Separation of Anode and Cathode Materials from Spent Li-Ion Batteries by Froth Flotation. *ACS Sustain. Chem. Eng.* **2021**, *9*, 531–540. [CrossRef]
34. Zhang, G.; He, Y.; Wang, H.; Feng, Y.; Xie, W.; Zhu, X. Application of mechanical crushing combined with pyrolysis-enhanced flotation technology to recover graphite and $LiCoO_2$ from spent lithium-ion batteries. *J. Clean. Prod.* **2019**, *231*, 1418–1427. [CrossRef]
35. Yu, J.; He, Y.; Ge, Z.; Li, H.; Xie, W.; Wang, S. A promising physical method for recovery of LiCoO 2 and graphite from spent lithium-ion batteries: Grinding flotation. *Sep. Purif. Technol.* **2018**, *190*, 45–52. [CrossRef]
36. Liu, J.; Wang, H.; Hu, T.; Bai, X.; Wang, S.; Xie, W.; Hao, J.; He, Y. Recovery of $LiCoO_2$ and graphite from spent lithium-ion batteries by cryogenic grinding and froth flotation. *Minerals Engineering* **2020**, *148*, 106223. [CrossRef]
37. Gaines, L. Lithium-ion battery recycling processes: Research towards a sustainable course. *Sustain. Mater. Technol.* **2018**, *17*, e00068. [CrossRef]
38. Holzer, A.; Wiszniewski, L.; Windisch-Kern, S.; Raupenstrauch, H. Optimization of a Pyrometallurgical Pro-cess to Efficiently Recover Valuable Metals from Commercially Used Lithium-Ion Battery Cathode Materials LCO, NCA, NMC622, and LFP. *Metals* **2022**, *12*, 1642. [CrossRef]

39. Fercher, A. Grenzwertbestimmung und Analyse von Kupfer-, Aluminium-und Kohlenstoffzuschlägen zu dem Kathodenmaterial NCA aus Lithium-Ionen-Batterien. Bachelor's Thesis, Montanuniversitaet Leoben, Leoben, Austria, 2022.
40. Baldauf, M. Grenzwertbestimmung und Analyse von Aluminium-und Kohlenstoffzuschlägen zu Kathodenma-terialien aus Lithium-Ionen Batterien für die Wertmetallrückgewinnung im pyrometallurgischen Reaktorkonzept InduRed. Master's Thesis, Montanuniversitaet Leoben, Leoben, Austria, 2022.
41. *Biswas, Principles of Blast Furnace Ironmaking*; Cootha Publishing House: Brisbane, Australia, 1981.

Appendix B: List of further publications

Peer-Reviewed Publications

- Windisch-Kern, S.; **Holzer, A.**; Wiszniewski, L.; Raupenstrauch, H. Investigation of Potential Recovery Rates of Nickel, Manganese, Cobalt, and Particularly Lithium from NMC-Type Cathode Materials (LiNixMnyCozO2) by Carbo-Thermal Reduction in an Inductively Heated Carbon Bed Reactor, Metals 11 (2021), 11, 1844. DOI: https://doi.org/10.3390/met11111844.
- Windisch-Kern, S.; **Holzer, A.**; Ponak, C.; Hochsteiner, T. and Raupenstrauch, H., Thermal analysis of lithium ion battery cathode materials for the development of a novel pyrometallurgical recycling approach, Carbon Resources Conversion. 2021, 4, S. 184-189 6 S. DOI: https://doi.org/10.1016/j.crcon.2021.04.005.
- Windisch-Kern, S.; **Holzer, A.**; Ponak, C.; Raupenstrauch, H. Pyrometallurgical Lithium-Ion-Battery Recycling: Approach to Limiting Lithium Slagging with the InduRed Reactor Concept, Processes 9 (2021), 1, 84. DOI: https://doi.org/10.3390/pr9010084.
- Windisch-Kern, S.; **Holzer, A.**; Nagovnak, P.; Ponak, C. and Raupenstrauch, H., Pyrometallurgical recycling of lithium ion batteries: Preliminary experiments to investigate the behaviour of cathode materials under reducing conditions, 16. Minisymposium der Verfahrenstechnik 2020. DOI: https://doi.org/10.34726/594.
- Ponak, C.; Mally, V.; Windisch, S.; **Holzer, A.** and Raupenstrauch, H. Phosphorus Gasification during the Reduction of basic Oxygen Furnace Slags in a Novel Reactor Concept, Advanced materials letters. 11.2020, 7, 7S. DOI: https://doi.org/10.5185/amlett.2020.071535.

Not peer reviewed Publications and Articles

- Windisch-Kern, S.; **Holzer, A.**; Ponak, C.; Nagovnak, P. and Raupenstrauch, H. Recycling von Lithium-Ionen-Batterien: Herausforderungen und aktuelle Forschungsergebnisse, Berg- und hüttenmännische Monatshefte : BHM, 166.2021(3), 150-156. DOI: https://doi.org/10.1007/s00501-021-01091-5.

- Berger, G.; **Holzer, A.** and Raupenstrauch, H. Industrielle Energietechnik, Berg- und hüttenmännische Monatshefte : BHM, 165.2020(7), 320-323. DOI: https://doi.org/10.1007/s00501-020-00994-z.

- Holzer, A.; Mally, V.; Ponak, C.; Windisch, S. and Raupenstrauch, H. Technologien zur Nutzung von Wertstoff- und Energiepotentialen in LD-Konverterschlacken, Berg- und hüttenmännische Monatshefte : BHM, 165.2020(7), 302-307. DOI: https://doi.org/10.1007/s00501-020-00992-1.

- Ponak, C.; Windisch, S.; Breuer, F.; Holzer, A.; Mally, V.; Raupenstrauch, H. and Lasser, M. Vermeidung von Calciumsilikatzerfall und Förderung der Glasbildung bei vollständiger Reduktion von Konverterschlacken, Stahl und Eisen, 18-23.

Conference Publications, Posters and Contributions

- **Holzer, A.**; Wiszniewski, L., Windisch-Kern, S. and Raupenstrauch, H., Entwicklung eines pyrometallurgischen Prozesses zur Wertmetallrückgewinnung aus Li-Ionen-Batterien, In Recy & Depotech 2022

- **Holzer, A.**; Baldauf, M.; Windisch-Kern, S.; Wiszniewski, L. and Raupenstrauch, H., New Insights into the Influence of Impurities on the High-Temperature Behavior of the LIB Cathode Material NMC622 under Reducing Conditions for Use in the InduRed Process, In 6th Symposium on Circular Economy and Urban Mining 2022

- **Holzer, A.**; Windisch-Kern, S.; Ponak, C.; Mally, V.; Stipper, P.; Wiszniewski, L. and Raupenstrauch, H., Pyrometallurgical recycling of valuable metals from the cathode material LCO of Lithium-Ion-Batteries, 12th International advanced automotive battery conference 2022

- **Holzer, A.,** Recovery of valuable metals from black matter of lithium-ion batteries in a novel pyrometallurgical reactor, In ICBR 2021

- **Holzer, A.;** Windisch, S.; Ponak, C.; Nagovnak, P. and Raupenstrauch, H., Lithium-ion batteries: Requirements for future recycling processes, In ICBR 2020

- **Holzer, A.**; Windisch-Kern, S.; Ponak, C.; Mally, V.; Stipper, P. and Raupenstrauch, H., Pyrometallurgisches Recycling der Wertmetalle aus dem Kathodenmaterial LCO aus Lithium-Ionen-Batterien, In Batterieforum Deutschland 2020

- Windisch-Kern, S.; Nagovnak, P.; **Holzer, A.**; Ponak, C. and Raupenstrauch, H., Lithium-Ionen-Batterien: Anforderungen an das Recyclingverfahren der Zukunft. In Recy & Depotech 2020

- Ponak, C.; Mally, V.; Windisch, S.; **Holzer, A.**; Raupenstrauch, H. and Schönberg, A. Rückgewinnung von Phosphor aus Klärschlammaschen - Weiterentwicklung des RecoPhos-Prozesses, In Recy & Depotech 2018

Patent

- Raupenstrauch, H.; Windisch, S.; Ponak, C.; Mally, V.; Holzer, A. and Schönberg, A. APPARATUS AND PROCESS FOR THERMAL TREATMENT OF RAW MATERIAL CONTAINING LITHIUM COMPOUNDS AND PHOSPHORUS COMPOUNDS, METHOD OF RECOVERING LITHIUM AND/OR PHOSPHORUS FROM RESIDUE MATERIAL OF LITHIUM-ION BATTERIES, IPC Nr- C22B 26/ 12 A I, Patent Nr. WO2021175703, Priority date 02.03.2020, Priority number WO2020EP55449.

Appendix C: Erratum

In Publication 2 of this thesis “Optimization of a Pyrometallurgical Process to Efficiently Recover Valuable Metals from Commercially Used Lithium-Ion Battery Cathode Materials LCO, NCA, NMC622, and LFP” [69], reference errors were found after publication:

- Page 4:

  Published: **Figure 1.** Schematic illustration of the so-called InduMelt crucible concept [23]

  Correct: **Figure 1.** Schematic illustration of the so-called InduMelt crucible concept [26]

- Page 14:
  Published: Table 11 illustrates the individual reactor weight before and after the test, as well as the resulting difference.
  Correct: Table 15 illustrates the individual reactor weight before and after the test, as well as the resulting difference.